

# **Synthesis, Characterization and Properties of Some Novel Discotic Nanocomposites**

By  
**AVINASH B. S.**

*Thesis submitted to Jawaharlal Nehru University, New  
Delhi for the award of the degree of*

**Doctor of Philosophy**  
**October 2015**



**Raman Research Institute**  
**Bangalore-560080**

**Dedicated  
to  
My beloved  
Parents**

# CERTIFICATE

This is to certify that the thesis entitled “**Synthesis, Characterization and Properties of Some Novel Discotic Nanocomposites**” submitted by **Mr. AVINASH B.S.**, for the award of the degree of DOCTOR OF PHILOSOPHY of Jawaharlal Nehru University, New Delhi, is his original experimental investigation and conclusions. The subject matter of this thesis has not been previously published or submitted to any other university for the award of any other degree or diploma.

Prof. Ravi Subrahmanyam  
Director  
Raman Research Institute  
Bangalore -560080

Prof. Sandeep Kumar  
(Thesis Supervisor)

# DECLARATION

I hereby declare that the entire work embodied in this thesis is the result of the experimental investigation carried out by me independently at Raman Research Institute, Bangalore, under the guidance and supervision of Prof. Sandeep Kumar. The experimental work and conclusions presented in this thesis work have not been previously submitted and no part of this thesis work has formed the basis for the award of any other degree, diploma, fellowship or any other similar title. Further, I declare that I have checked this thesis through the antiplagiarism software turnitin.

Prof. Sandeep Kumar  
(Thesis Supervisor)  
Raman Research Institute  
Bangalore-560080

Avinash B.S.

## **Acknowledgements**

I wish to express profound sense of gratitude to my honored supervisor Prof. Sandeep Kumar who constantly inspired me at every stage of my research. Without his serious involvement, thoughtfulness and patience, it would have been difficult for me to complete this thesis in time. It was an invaluable experience to work with him and to learn so many things from him both as a scientist and as a human being. It has been a great pleasure and I really cherished working with him. I must express my earnest gratitude to Prof. V. Lakshminarayan, for his sound guidance during the initial period of my research and constant encouragement during the entire course of the present study. I thank Prof. V. A. Raghunathan, for many valuable discussions related to the X-ray diffraction studies. I thank Prof. J. K. Vij, Prof. Shuzi Hayase, and Prof. Shyam Pandey, for allowing me to visit their labs and helping me learn new techniques. I also thank Dr. Arun Roy for helping me to carry out Raman studies, Dr. Vijayaraghavan for the help in acquiring NMR and Dr. Prathiba for providing me various facilities for conductivity studies. I would not miss this opportunity to thank all the soft condensed matter staff members for their help in various ways. I also thank Dr. Srinivas for his invaluable help in the lab, I thank Mrs. Vasudha for her help in spectroscopic measurements, Mr. Dhason for his help in SEM and AFM imaging and fabricating glass apparatus, Mr. Ram for preparing gold samples for electrochemical studies and Mr. Mani for his help in fabricating accessories for various experiments. Mr. Yatheendran for SEM and EDAX studies. I also thank Mr. K. Radhakrishna for his valuable and timely help throughout my research work. I thank my seniors in the lab Dr. Hari, Dr. Sathyam, Dr. Kavitha Dr. Mahesh, Dr. Rakesh, Dr. Nagaraju and Dr. Suresh for their friendly support and valuable inputs regarding the research work. My sincere thanks to my batch mate Mr. Swaminathan for many valuable conversations on academic and nonacademic matters. I thank all my friends at soft condensed matter student's room Dr. Jayakumar, Mr. Marichandran, Mr. Jagadeesh, Mr. Ashwath, Mr. Manish, Mrs. Supreet, Mr. Madhukar, Mr. Samim, Mrs. Radhika, Mr. Santosh, Mr. Shabeeb, Dr. Rajib,

Mr. Debashish, Mrs. Renu, Mr. Amit, Mrs. Antara, Mr. Arif, Mr. Srinivas and Mr. Shashi. I thank my seniors Dr. Radhakrishna, Dr. Santanu, Dr. Suchand, and Dr. Anantharamakrishna for many valuable discussions. I thank my hostel friends and all my badminton friends Dr. Srikanth, Dr. Mahaveer, Mr. Jagadish, Dr. Anjan, Dr. Arnab, Mr. Prasad, Mr. Chaithra, Mr. Suman, and Ms. Jyothi. I also thank all my batch mates and friends Dr. Mohit, Dr. Pawan, Dr. Sathyaprasad at RRI and other institutions of Bangalore for their valuable inputs related to my work. I thank Prof. Shukla for his invaluable help in conducting XPS studies. The library staffs of RRI have been outstanding during the course of my research work and it is a pleasure to thank all of them for their significant and timely help. I would like to thank various other departments of RRI, Administration, and Computer section, Accounts, Workshop, Transport, Canteen and Clinic for their constant support throughout my research work. I am deeply indebted to Raman Research Institute for giving me the opportunity to carry out the research work in the friendliest surroundings. It is an immense pleasure to thank all the scientific as well as supporting staff of the institute for their cooperation. Finally, I would like to mention my sincere thanks to my brother, sister-in-law, Saanvi, and all my family for being a steady source of encouragement, support and help throughout my research work. I finally wish to thank my Father and Mother for everything they have been.

## **Synopsis**

### **Synthesis, Characterization and Properties of Some Novel Discotic Nanocomposites.**

#### **Introduction**

Liquid crystals (LCs) are soft materials that show both order and mobility on a molecular, supramolecular level and as well as macroscopic level. They are well known as active components in liquid crystal displays (LCDs) but many other commercial applications have also been explored. LCs form phases that exist between crystalline phases (ordered) and the isotropic liquid phase (disordered), which is why they belong to a class of materials called mesophases. Mesophase is a thermodynamically stable state of matter, it constitutes of mesogens, the mesogens can be, organic, inorganic, or metallomesogens.

Liquid crystals are important in material science as well as in life science. Important applications of thermotropic LCs are electrooptic displays, temperature sensors and selective reflecting pigments. Lyotropic systems are used in cleaning process, and are important in cosmetic industries. Lyotropic LCs are used as templates for the preparation of mesoporous materials and serve as model systems for biomembranes. DNA can also form lyotropic mesophases. Anisotropic fluid states of rigid polymers are used for processing of high strength fibers like Kevlar. LCs are extremely diverse since they range from DNA to high strength synthetic polymers like Kevlar (used for bulletproof vests, protective clothing, high performance composites for aircraft and automotive industries) and from small organic molecules like alkyl and alkoxy cyanobiphenyls used in liquid

crystal displays (LCDs) to self-assembling amphiphilic soap molecules. Recently their biomedical applications such as in controlled drug delivery, protein binding, phospholipid labeling, and in microbe detection have been demonstrated. Apart from material science and bio-science, LCs are now playing significant role in nanoscience and nanotechnology such as synthesis of nanomaterials using LCs as template, the design of LC nanomaterials, alignment and self-assembly of nanomaterials using LC phases and so on.

Due to non-covalent interactions in functionalized disc-shaped molecules, supramolecular columnar structures are formed; these are referred to as discotic liquid crystals (DLCs). DLC's are of enormous scientific interest because of their extraordinary anisotropic charge migration properties. These systems are of great fundamental and technological importance. A majority of discotic liquid crystals are derived from polycyclic aromatic cores such as, triphenylene, anthraquinone, coronene, phthalocyanine, etc., which possess strong pi-pi interactions favouring columnar stacking of the molecules. In the columnar mesophase of DLCs, aromatic cores are oriented in columns separated by aliphatic hydrocarbon chains. The intra-columnar (core-core) separation in a columnar mesophase is usually of the order of 0.35 nm while the inter-columnar (neighbouring columns) separation is generally in the range of 2-4 nm, depending on the length of flexible chains. Therefore, intra-columnar interactions are much stronger than inter-columnar interactions.

Materials below 100 nm in one-, two- or all the three-dimensions are commonly referred to as nanomaterials; they often possess unique

properties which differ from those of bulk materials. Many one-dimensional (1-D) nanomaterials have attracted much attention of researchers due to their unique properties and potential uses in both mesoscopic research and in the development of nanodevices. In recent years, there has been tremendous development in the fields of nanostructured materials, including metallic nanoparticles and nanorods, semiconducting quantum dots, carbon nanotubes, fullerenes and graphene. The science and technology dealing with nanomaterials have received immense interest in nearly every field of science. The potential applications of nanomaterials in the fields of energy, computing, optics, catalysis, biosciences and medical sciences have been extensively discussed. Keeping pace with topical sciences, the field of liquid crystals has recently entered into the fascinating domains of nanoscience and nanotechnology. One of the current research areas worldwide in nanoscience field is to design nanomaterials that are able to self-assemble into functional superstructures in multiple directions. Nanoparticles assembly has been induced by several methods; however, using liquid crystals as an organizing medium to induce the self-assembly of nanoparticles is a powerful tool. A number of liquid crystal-nanoparticle hybrid systems have been explored. Calamitic mesogens (liquid crystals formed by rod-shape molecules) are the most commonly employed materials in the preparation of these hybrids. However, recently some efforts have been made to incorporate various nanoparticles in the supramolecular order of discotic liquid crystals.

Here in this thesis we have studied change in the mesophase behaviour of columnar liquid crystals on doping with different one

dimensional and two dimensional nanomaterials. We have also explored formation of lyotropic mesophase in CdS nanowire system. We have probed the self-assembly of thiolated graphene oxide onto gold electrodes.

## **Chapter 1**

This is an introductory chapter to liquid crystals. It touches upon history of liquid crystals in brief. This chapter includes classification of liquid crystals. A short discussion about lyotropic liquid crystals is also included which deals with the formation of lyotropic mesophase and types of phases exhibited by them. This is followed by a discussion about thermotropic liquid crystal, and classification associated with it. As this thesis deals with discotic liquid crystals mainly, discussions on calamitic and bent core liquid crystals are given in brief. The chapter discusses in greater detail about columnar liquid crystals, it discusses various types of liquid crystalline phases shown by discotic mesogens. A typical structure associated with discotic mesogen is explained, following which synthesis methods followed to obtain the discotic mesogens are shown. Characterization techniques used to probe self-assembly of discotic mesogens are elaborated upon. Applications of discotic molecules in organic electronic devices are shown. A brief introduction to nanomaterials is also included.

## **Chapter 2**

In this Chapter we have prepared octadecylamine functionalized reduced graphene (f-graphene). The f-graphene is introduced in anthraquinone based columnar liquid crystal. The influence of the functionalized graphene on mesophase is studied using polarizing optical microscopy, X-ray diffraction, differential scanning calorimetry studies, and the mutual ordering is probed using scanning electron microscope (SEM) and cryo-scanning electron microscope (Cryo-SEM) imaging. The influence of dopants on conductivity of the mesophase has also been studied.

Here we have shown that f-graphene can be efficiently dispersed in the supramolecular order of DLCs. These composites show higher transition temperatures compared to pure DLC due to enhanced ordering of discotics on the surface of reduced graphene oxide owing to strong pi-pi attraction. Cryo-SEM images of the composites show us that discotics and graphene are mutually ordered into sandwich like structures. We have also found that the composites show higher conductivity compared to pure DLC. The f-graphene fillers act as bridges across columnar defects resulting in efficient charge transport.

## **Chapter 3**

In the previous chapter we had shown that octadecylamine edge functionalized reduced graphene oxide formed an ordered sandwich like layered structure with anthraquinone discotic liquid crystal. Here in this chapter we study self-assembling behaviour of surface functionalized graphene oxide in anthraquinone discotics. Mesophase behaviour and

ordering is studied using polarizing optical microscopy, X-ray diffraction, differential scanning calorimetry studies, and the mutual ordering is probed using SEM and Cryo-SEM imaging. We also have explored self-assembly behavior of the thiolated graphene oxide on gold electrodes and have electrochemically probed the self-assembled layer.

Characterization of the thiolated graphene oxide nanocomposites in supra-molecular structures of discotic liquid crystals reveal that thiolated graphene oxide, due to its functionalization on the surface, induces destabilization in columnar mesophase. Steric hindrance caused by the functionalities present on surface of graphene oxide inhibits the columnar mesogens from having stabilizing pi-pi interaction with graphene oxide.

We have shown for the first time that graphene oxide can be functionalized with thiol, and thiolated graphene oxide can self-assemble onto gold surface. The SEM images show presence of layered graphene oxide sheets on the gold strip. This self-assembled film of graphene oxide acting as blanket on the gold surface has potential application in various devices applications such as sensors, organic electronic devices etc.

## **Chapter 4**

In this chapter we have studied the insertion of gold nanorods in the supramolecular order of discotic liquid crystals without disturbing their mesomorphism. We have tuned the surface of gold nanorods such that they self-assemble in to columnar mesophase with gold nanorods long axis aligned parallel to the long axis of columnar liquid crystal. This can be achieved by replacing the cetyltrimethylammonium bromide (CTAB) ligands

from the gold nanorods with dodecanethiol. Dodecanethiol functionalized gold nanorods align in between columns where alkyl chains of columnar liquid crystal are present, due to van der Waals attraction between the alkyl chains on gold nanorods and those surrounding triphenylene nanoribbons.

We have shown that hexpentyloxytriphenylene primarily self-assembles into hexagonal structures, which on proper solution processing can be made to grow into ribbon like secondary structures. During the growth, these supramolecular structures can trap the gold nanorods present in the solution, thus forming supramolecular nanocomposites. Insertion of gold nanorods in nanoribbons was confirmed by dark field scanning transmission electron microscope (STEM) studies. These nanocomposites show enhanced conductivity owing to insertion of nanorods in ribbon like structures. Mesophase behaviour of the nanocomposites were characterized by polarizing optical microscopy, X-ray diffraction, differential scanning calorimetry studies.

## **Chapter 5**

We demonstrate the incorporation of Cadmium sulphide nanowires in the supramolecular order of discotic liquid crystal. This was studied by polarized optical microscopy, differential scanning calorimetry, X-ray diffraction, field emission scanning electron microscope (FE-SEM) and energy-dispersive X-ray spectroscopy (EDAX). Results indicate that CdS nanowires were trapped in ribbon like structures of hexahexyloxytriphenylene discotic liquid crystals. We have also explored the formation of lyotropic phase in CdS nanoribbons, and we have characterized this self-

organization by polarized optical microscopy, differential scanning calorimetry, X-ray diffraction, Cryo-SEM techniques.

We have observed the dispersion of CdS nanowires in discotic liquid crystals. The doping of CdS nanowires into discotic liquid crystals does not disturb the nature of mesophase, but minor shift in the transition temperature is observed. These hybrids of two different classes of semiconductors makes themselves potential candidates for devices like thin film transistors, LED's, and organic solar cell.

We have also shown that CdS nanowires of various lengths form a lyotropic liquid crystalline phase, which show a lamellar ordering. We observed that these CdS nanowires aggregate in presence of cyclohexane to form rod like (Cds-50 and CdS-60) to rope like (CdS-70) supramolecular structures.

## **Chapter 6**

In this chapter we summarize the results and conclusions of the work presented in preceding chapters.

## **List of Publications.**

- 1) Gold Nanorods Embedded Discotic Nanoribbons,  
Bangalore Shivanandareddy Avinash, V Lakshminarayanan, Sandeep  
Kumar, JK Vij,  
Chemical Communications 49 (10), 978-980, 2013.
  
- 2) Mutually ordered self-assembly of discotic liquid crystal-graphene  
nanocomposites,  
Avinash B Shivanandareddy, Suvratha Krishnamurthy, V  
Lakshminarayanan, Sandeep Kumar,  
Chemical Communications 50 (6), 710-712, 2014.
  
- 3) Self-assembly of thiolated graphene oxide onto gold surface and in the  
supramolecular order of discotic liquid crystals,  
Avinash B Shivanandareddy, M Kumar, V Lakshminarayanan, Sandeep  
Kumar,  
RSC Advances, 5, 47692-47700, 2015.
  
- 4) Photoconductivity of doped hexa-alkoxy triphenylene nano composite  
structures,  
C Kavitha, Avinash B Shivanandareddy, Sandeep Kumar, V  
Lakshminarayanan,  
Materials Chemistry and Physics 133 (2), 635-641, 2012.

5) Triphenylene-based discotic liquid crystals: recent advances, Santanu K Pal, Shilpa Setia, Avinash B Shivanandareddy, Sandeep Kumar, *Liquid Crystals* 40 (12), 1769-1816, 2013.

6) Lyotropic liquid crystals of CdS nanoribbons  
Manuscript under preparation.

7) Mutual self-assembly of inorganic CdS and organic triphenylene nanoribbons.  
Manuscript under preparation.

## **List of abbreviation**

NMR	Nuclear Magnetic Resonance spectroscopy
FT-IR	Fourier transform infrared spectroscopy
UV-Vis	Ultraviolet-visible spectroscopy
POM	Polarized optical microscopy
XRD	X-ray diffraction
XPS	X-ray photoelectron spectroscopy
DSC	Differential scanning calorimetry
SEM	Scanning electron microscopy
FE-SEM	Field emission scanning electron microscopy
TEM	Transmission electron microscopy
STEM	Scanning transmission electron microscopy
EDAX	Energy-dispersive X-ray spectroscopy
SERS	Surface-enhanced Raman spectroscopy
SPR	Surface plasmon resonance
LC	Liquid Crystal
DLC	Discotic Liquid Crystal
RTAQ	1,5-dihydroxy-2,3,6,7-tetrakis(3,7-dimethyloctyloxy)-9,10-anthraquinone
HPT	2,3,6,7,10,11-hexakis(pentyloxy)triphenylene
HAT6	2,3,6,7,10,11-hexakis(hexyloxy)triphenylene
NP	Nanoparticle
GNP	Gold nanoparticles
CdS	Cadmium Sulfide

GO	Graphene oxide
f-graphene	Octadecylamine functionalized reduced graphene oxide
HDT-GO	Hexadecanethiol functionalized graphene oxide
TP-GO	Thiophenol functionalized graphene oxide
CV	Cyclic voltammetry
CTAB	Cetyltrimethylammonium bromide
GNR	Gold Nanorod
QD	Quantum dot
CNT	Carbon nanotube
HRTEM	High resolution transmission electron microscopy
SAXS	Small angle X-ray scattering
SAED	Selected area (electron) diffraction

# Table of Contents

## Chapter 1: Introduction

---

1.1 Liquid crystals.....	2
1.2 History of liquid crystals.....	3
1.3 Classification of liquid crystals.....	5
1.3.1 Lyotropic liquid crystals .....	6
1.3.2 Thermotropic liquid crystals .....	9
1.4 Calamitic liquid crystals .....	10
1.4.1 Nematic Phase .....	11
1.4.2 Smectic Phase .....	12
1.5 Banana liquid crystals .....	13
1.6 Discotic liquid crystals.....	14
1.6.1 Structure of the liquid crystalline phases formed by discotic mesogens. ....	16
1.6.2 Nematic Phases of discotic mesogens .....	17
1.6.3 Smectic phases of discotic mesogens .....	18
1.6.4 Columnar phases of discotic mesogens.....	19
1.6.4.1 The hexagonal columnar mesophase ( $Col_h$ ).....	19
1.6.4.2 The rectangular columnar mesophase ( $Col_r$ ).....	20
1.6.4.3 The columnar oblique mesophase ( $Col_{ob}$ ).....	21
1.6.4.4 The columnar plastic mesophase ( $Col_p$ ).....	22
1.6.4.5 The columnar helical (H) phase.....	23
1.6.4.6 The columnar lamellar mesophase.....	23
1.6.4.7 The columnar square (tetragonal) phase.....	24
1.6.5 Cubic phase .....	25
1.7 Structure of the discotic mesogens .....	25
1.8 Chemistry of discotic liquid crystals.....	26
1.9 Characterization of discotic liquid crystal phases.....	27
1.10 DLCs as materials for a new generation of organic electronics .....	29
1.11 Nanoparticles .....	30
1.12 Why discotics ? .....	31
1.13 Objective .....	32
1.14 References.....	34

# Chapter 2: Mutually ordered Self-assembly of Discotic Liquid Crystal-Graphene Nanocomposites

---

2.1 Introduction.....	44
2.1.1 Carbonaceous nanoparticles in columnar liquid crystals. ....	45
2.1.1.1 Zero dimensional (0-D) spherical carbon nanoparticles in columnar liquid crystals.....	45
2.1.1.2 One dimensional (1-D) carbon nanotubes in columnar liquid crystals.....	48
2.1.1.3 Two dimensional (2-D) graphene in columnar liquid crystals. ....	52
2.2 Objective .....	53
2.3 Experimental .....	53
2.3.1 Synthesis of Graphene oxide .....	53
2.3.2 Functionalisation of graphene oxide with octadecylamine.....	55
2.3.3 Synthesis of rufigallol .....	56
2.3.4 Synthesis of 1,5-dihydroxy- 2,3,6,7-tetrakis(3,7-dimethyloctyloxy)-9,10-anthraquinone .....	57
2.3.5 Preparation of composites.....	58
2.3.6 Instruments.....	59
2.3.7 Conductivity Measurements.....	60
2.4 Results and discussions.....	60
2.5 Conclusions.....	74
2.6 References.....	75

# Chapter 3: Self-assembly of Thiolated Graphene Oxide onto Gold Surface and in the Supramolecular order of Discotic Liquid Crystals

---

3.1. Introduction.....	83
3.2 Objectives .....	84
3.3. Experimental section.....	85

3.3.1. Thiolation of graphene oxide .....	85
3.3.2. Procedure to form self-assembled thiolated graphene oxide films .....	86
3.3.3. Procedure for electrochemical studies of self-assembled films .....	86
3.3.4. Synthesis of 1,5-dihydroxy- 2,3,6,7-tetrakis(3,7-dimethyloctyloxy)-9,10-anthraquinone. ....	87
3.3.5. Preparation of composites.....	88
3.4. Results and discussions.....	88
3.4.1. Characterization of functionalized graphene oxide.....	88
3.4.1.1. FT-IR spectroscopic analysis of thiolated graphene oxide.....	88
3.4.1.2. Solid state <sup>13</sup> C NMR analysis of thiolated graphene oxide.....	90
3.4.1.3. Elemental analysis of thiolated graphene oxide.....	91
3.4.1.4. X-ray diffraction patterns of functionalized and un-functionalized graphene oxide .....	92
3.4.1.5. TEM analysis.....	93
3.4.1.6. Raman spectral analysis of modified and unmodified graphene oxide.....	95
3.4.2. Characterization of modified gold electrode.....	97
3.4.2.1. X-ray photoelectron spectroscopy analysis of gold surface modified with hexadecanethiol functionalized graphene oxide.....	97
3.4.2.2. Grazing angle IR analysis on gold surface modified with hexadecanethiol functionalized graphene oxide .....	98
3.4.2.3. Electrochemical analysis of modified gold electrode with functionalized graphene oxide .....	100
3.4.2.4. FESEM images of hexadecanethiol functionalized graphene oxide self-assembled on gold surface.....	106
3.4.3. Characterization of nanocomposites of functionalized graphene oxide with anthraquinone discotic liquid crystal.....	107
3.4.3.1. Polarized Optical Microscopy (POM) .....	107
3.4.3.2. Differential scanning calorimetry (DSC).....	110
3.4.3.3. Small angle X-ray scattering (SAXS) .....	111
3.4.3.4. Cryo-SEM analysis of self-assembled discotics with thiolated graphene oxide .....	112
3.5. Conclusions.....	114
3.6. References:.....	114

## Chapter 4: Gold Nanorods Embedded Discotic Nanoribbons

---

4.1 Introduction.....	122
4.1.1 Spherical or quasi-spherical metallic nanoparticles .....	123
4.1.2 Liquid crystal-GNP hybrids.....	124
4.1.3 Gold nanoparticles in discotic liquid crystals.....	126
4.1.4 Gold nanorods.....	131
4.1.5 Organic nanoribbons.....	133
4.2 Objectives. ....	134
4.3 Experimental Methods .....	134
4.3.1 Synthesis of gold nanorods.....	134
4.3.2 Ligand exchange of gold nanorods. ....	137
4.3.3 Synthesis of 2,3,6,7,10,11-hexakis(pentyloxy)triphenylene.....	138
4.3.4 Preparation of Triphenylene Nanoribbons.....	139
4.3.5 Preparation of Composites. ....	141
4.4 Results and discussion. ....	141
4.5 Conclusion. ....	152
4.6 References.....	152

## Chapter 5: Self-assembly of CdS Nanowires into Lyotropic Lamellar Phase, and in Supramolecular Organic Nanoribbons

---

5.1 Introduction.....	160
5.1.1 Semiconducting NPs in discotic liquid crystals .....	160
5.1.1.1 CdSe Quantum dots in discotic liquid crystals .....	160
5.1.1.2 ZnO nanoparticles in discotic liquid crystals.....	162
5.1.2 Mineral based liquid crystals .....	164
5.1.2.1 Rod like particles .....	164
5.1.2.2 Plate like particles .....	166
5.1.2.3 Lath like particles .....	168
5.2 Objectives .....	169

5.3 Experimental section.....	170
5.3.1 Synthesis of 2,3,6,7,10,11-hexakis(hexyloxy)triphenylene.....	170
5.3.2 Synthesis of CdS nanowires .....	170
5.3.3 Preparation of nanocomposites. ....	171
5.3.4 Preparation of CdS based lyotropic liquid crystals. ....	171
5.4 Results and Discussion .....	173
5.4 Conclusion .....	188
5.5 References.....	189

## Chapter 6: Summary

---

6.1 Summary.....	198
6.2 Publications.....	202

# Chapter 1

---

## **Introduction**

## 1.1 Liquid crystals

Liquid crystals (LCs) are soft materials that show both order and mobility on a molecular, supramolecular and as well as macroscopic levels. They are well known as active components in liquid crystal displays (LCDs) but many other commercial applications have also been explored. LCs form phases that exist between crystalline phases (ordered) and the isotropic liquid phase (disordered), which is why they belong to a class of materials called mesophases (Figure 1). Mesophase is a thermodynamically stable state of matter, it constitutes of mesogens, the mesogens can be, organic, inorganic, or metallomesogens.

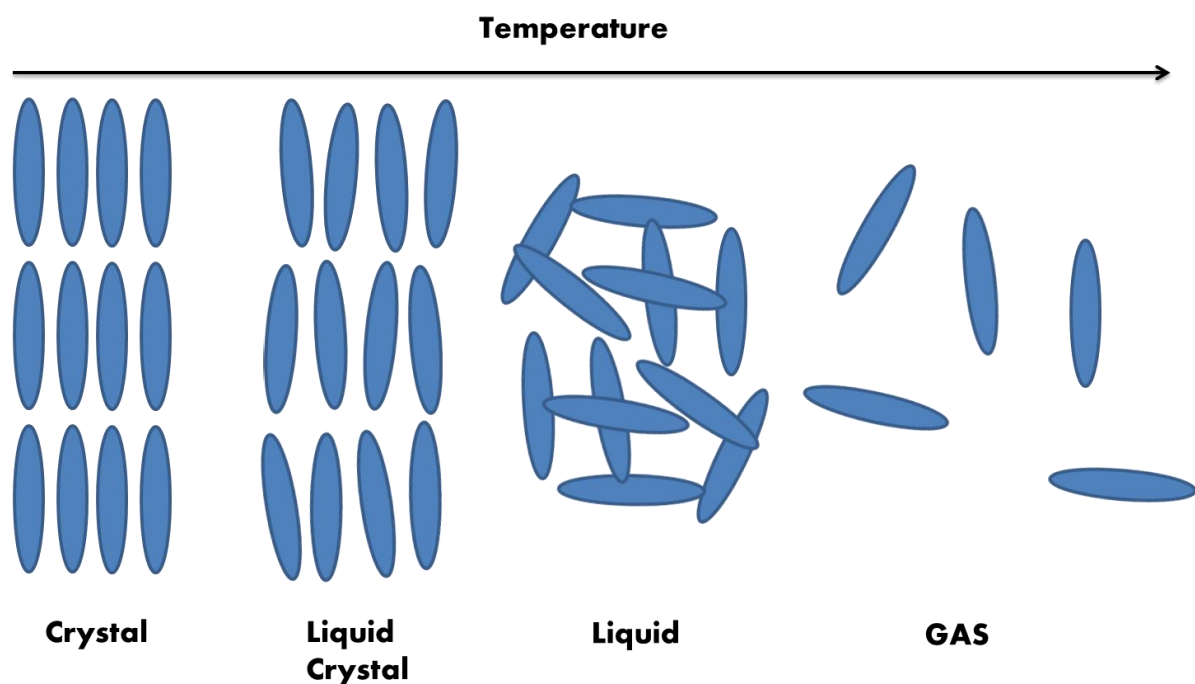


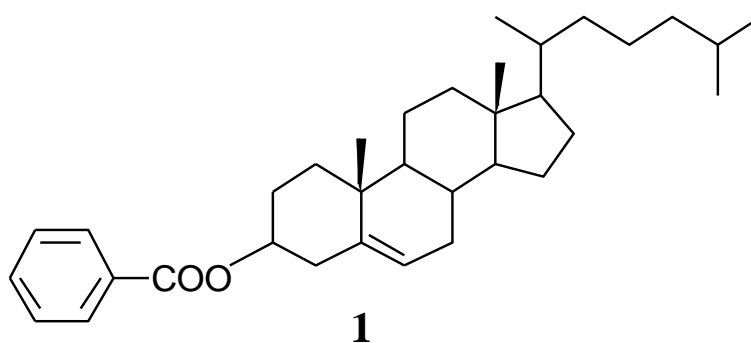
**Figure 1.** Different states of matter and ordering of molecules in those states.

In crystalline solids all molecules are arranged in a definitive pattern having long-range orientational and positional orders. In contrast, isotropic liquids have no long-range positional and orientational order. Liquid crystals have at least long range orientational order in one dimension and may or may not have long-range positional order. Consequently, the least ordered LC phase has no long-range positional order but has long-range orientational order in one dimension (nematic phase), while the most ordered LC phases have two-dimensional long range positional and orientational order.<sup>1-12</sup>

## 1.2 History of liquid crystals

Freidrich Reinitzer, in 1888, noticed a peculiar melting behavior of cholesteryl benzoate **1**, this compound melts from solid at 145.5 °C to form a cloudy liquid and at 178.5 °C it shows another transition to a clear liquid.<sup>13-14</sup> Otto Lehmann, a German physicist explained this phenomenon of “double melting”, he referred to them initially as ‘soft crystals’ and later as ‘crystalline fluids’, once he was convinced that the opaque phase was a uniform phase of matter sharing properties of both liquids and solids, he began to call them “liquid crystals”.<sup>15</sup> It has to be noted that researchers as early as 1850s actually dealt with liquid crystals but did not realize the uniqueness of the phenomena.<sup>16</sup> Daniel Vorlander a professor of chemistry, systemically studied structure-mesophase relationship and prepared 1100 liquid crystalline compounds in his laboratory.<sup>17</sup> He remarked that

mesophase are exhibited by molecules having elongated (rod-like) shape, now classified as calamitic liquid crystals. In 1965 at International Liquid Crystal Conference (ILCC), the application of cholesteric liquid crystals in thermography was shown; Heilmeyer's group presented the potential of liquid crystalline materials in electrooptical display technology. This led to an increase in interest towards liquid crystal research.



Chandrasekhar *et al.* in 1977, reported that not only rod-like (calamitic molecules), but also compounds with disc-like molecular shape are able to form mesophases.<sup>18</sup> Currently more than 3000 discotic liquid crystals are known in the literature.

Recently in 1996 it was shown that banana-shaped molecules also show liquid crystal phase. These molecules have a structure composed of three units; an angular central unit, two linear rigid cores and terminal chains. Discovery of ferroelectricity in non-chiral banana shaped molecules has led to a very intense research in this field. Several bent molecular shape compounds have been synthesized so far. Bent shaped molecules provide access to mesophases with polar order and supramolecular chirality.<sup>19-24</sup>

### 1.3 Classification of liquid crystals

There are many ways liquid crystals can be classified, such as: depending on the molar mass of the constituent molecules; low molar mass (monomeric and oligomeric), and high molar mass (polymeric) liquid crystals; depending on how the liquid crystalline phase was obtained; by varying the temperature (thermotropic) or by adding solvent (lyotropic); depending the nature of the constituent molecules (organic, inorganic and organometallic); depending on the geometrical shape of the molecules (rod-like , disc-like, bent core); depending on the arrangement of the molecules in the liquid crystalline phase (nematic, smectic, columnar, helical, B phases etc). The extensive classification of liquid crystals is shown in Figure 2.

However, the most widely used classification of liquid crystals is into two major categories;

(a) Thermotropic liquid crystals (mesophase formation is temperature dependent).

(b) Lyotropic liquid crystals (mesophase formation is solvent and concentration dependent).

If a compound displays both thermotropic and lyotropic liquid crystalline phases then it is called amphotropic liquid crystal.

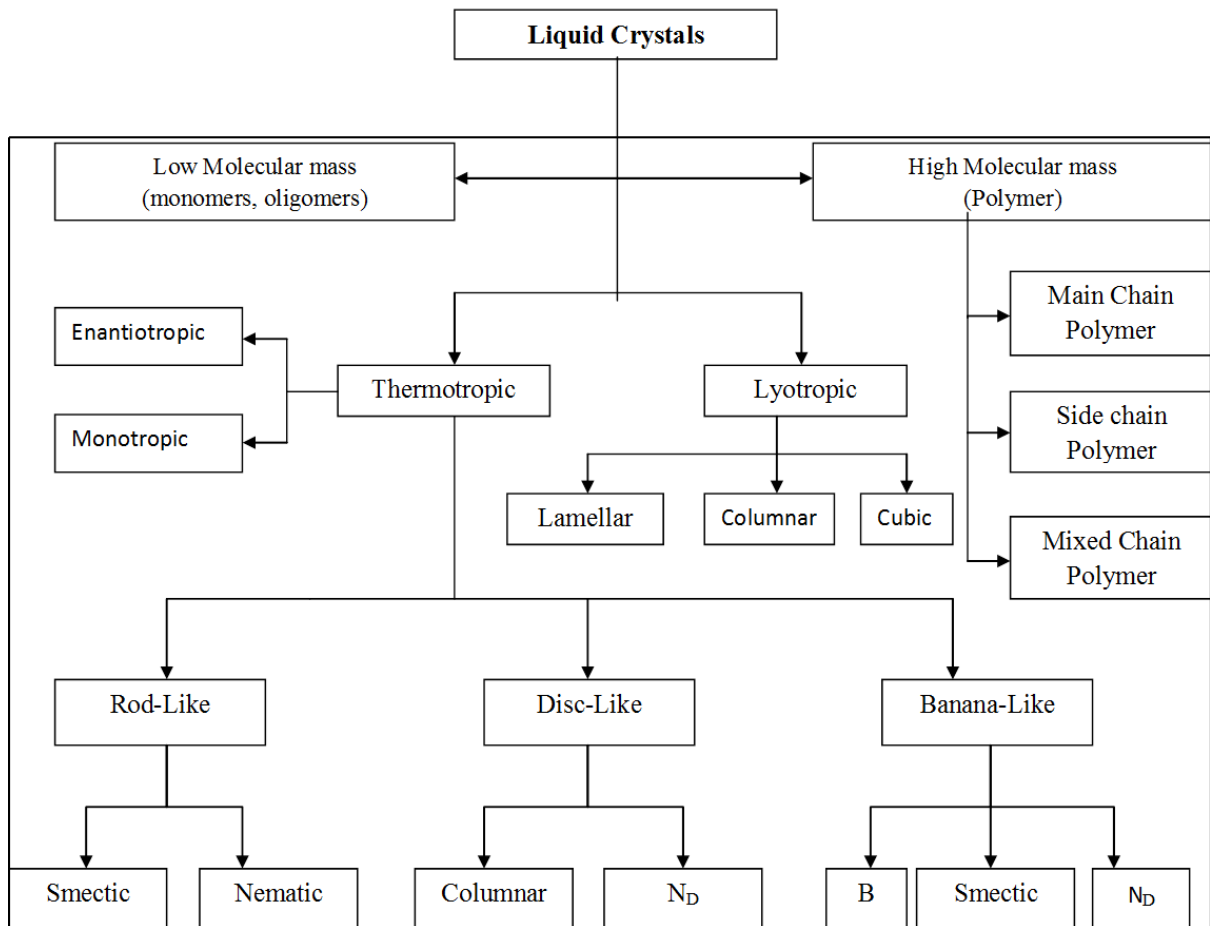


**Figure 2.** Classification of liquid crystals.

### 1.3.1 Lyotropic liquid crystals

Lyotropic liquid crystals form only on addition of a solvent, most often water (not necessarily). The building block of lyotropic liquid crystal is not one but is made of set of molecules (typically on around 100 molecules). Such lyotropic liquid crystals thus come under the category of associated liquids. The micelle formation is a result of the amphiphilic character of the

constituent molecules. Typical examples include surfactants, which have a polar (hydrophilic) head group and a nonpolar (hydrophobic) tail. Another example is amphiphilic lipids (e.g. phospho-, glyco- and sphingolipids) that build up the membranes of the cells in our own bodies. Here each polar head group normally has two or more non-polar tails, extending next to each other in the same direction. There are some examples of block co-polymers that may form liquid crystal phases in a similar way as low molar mass amphiphiles.

When amphiphilic molecules are introduced in an aqueous medium the head group is easily accommodated but the nonpolar alkyl chain disrupts the hydrogen bond network of the surrounding water molecules, thus reducing favourable interaction with their neighbours, thereby decreasing the entropy of the water.<sup>25</sup> On increasing the amphiphilic concentration, the hydrophobic effect drives the self-assembly of amphiphiles into aggregates in which the nonpolar tails are directed inwards, protected from contact with the water by the polar head groups which together form a 'shell' around the hydrophobic 'core', the entropy of the whole system is actually increased by this type of ordering. Figure 3 shows three different classes of lyotropic liquid crystal phase structures. These are the lamellar (Figure 3a), the hexagonal columnar (Figure 3b) and the cubic phases (Figure 3c). The concentration of amphiphiles molecules at which association begins is called the critical micelle concentration (CMC). Typical CMC values lie in the 1-10 mM range. At the CMC the whole medium is still similar to isotropic state in thermotropic liquid crystals. This isotropic micellar phase can be compared to the isotropic phase of a

thermotropic material above its clearing point. The main thermodynamic control parameter which determines formation of lyotropic liquid crystals is not the temperature (it is often the secondary control parameter) but the amphiphile concentration, low concentrations corresponding to high temperatures of thermotropics.

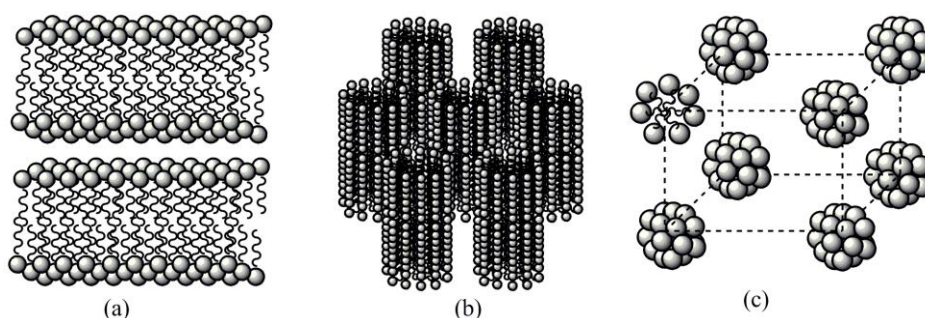


**Figure 3.** Lyotropic liquid crystalline phases.

If instead of water non-polar solvent is used then the reverse micelle structure is favourable, under such circumstances one observes inverted lyotropic phases, where the micelles have a polar interior and non-polar exterior. Often the micelles are spherical in shape and thus rather unsuitable for building liquid crystal phases, but with the right concentration of the appropriate amphiphile, sometimes with the help of an additional co-surfactant, the micelles may take a rod- or disc-like shape. Relative sizes of the hydrophilic and hydrophobic part of molecule, respectively, that dictates the shape of the micellar aggregate. The micelle in lyotropic liquid crystals plays the part of the rigid core in thermotropics, whilst the isotropic solvent takes the role of the thermotropic mesogen's flexible alkyl chains.

There are also examples of unassociated lyotropic liquid crystals. These are formed by colloidal suspensions of anisometric non-amphiphilic particles or macromolecules such as polymers, viruses or inorganic rods or discs in solution. This subclass of lyotropics, which is often ignored in basic discussions of lyotropic liquid crystals, is attracting more and more interest today.<sup>26-29</sup> Polymers that form liquid crystals of this type may be synthetic such as carbon nanotubes or the polyaramide chains that are processed via a liquid crystalline state into Kevlar fibers, or they may be biological, e.g. DNA. A somewhat intermediate position is taken by the chromonic class of lyotropic liquid crystals,<sup>30</sup> where the constituent molecules do not aggregate into micelles but instead stack up into columns of varying lengths. The molecules forming chromonic liquid crystals, which are generally dyes, and amphiphilic of different nature than the classical surfactants.

### **1.3.2 Thermotropic liquid crystals**

The term “thermotropic” arises in mesophase when transitions are induced by change in temperature. The transition temperature from the crystalline phase to the liquid crystalline phase is called the melting point, while the transition temperature from the liquid crystalline phase to the isotropic liquid is named as clearing point. When thermodynamically stable mesophases appear on both heating and cooling scans then it is called enantiotropic. If the mesophase is obtained only on while cooling from the isotropic state then it is referred to as monotropic. Generally a molecule should consist of a central rigid core (aromatic core) and a flexible peripheral

moiety (aliphatic chains) to be a thermotropic liquid crystal. Mesophase formation is also determined by geometric anisotropy, interaction anisotropy and microsegregation. Based on the shape of the mesogenic molecules, thermotropic liquid crystals are classified into three main groups:

- (a) calamitic (rod-like)
- (b) discotic (disc-like)
- (c) bent core (banana-like)

#### 1.4 Calamitic liquid crystals

Calamitic liquid crystals comprise of rod-shaped molecules, they possess a elongated shape (length of the molecule is larger than its breadth) Figure 4.

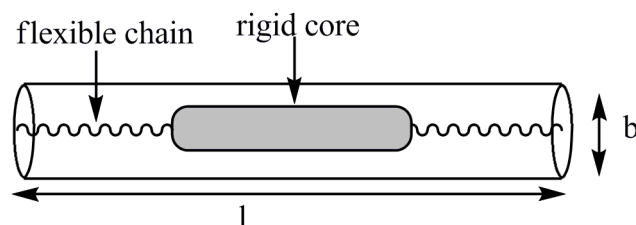


**Figure 4.** Figure representing a calamitic liquid crystal, where length  $\gg$  breadth.

Compounds showing calamitic liquid crystalline compounds consist of two or more aromatic rings, bonded together directly or via linking groups. They usually have terminal alkyl chains and sometime lateral substitutions as well. The typical chemical structure of calamitic molecules can be represented by the general template Figure 5 where A and B form aromatic

core units, R and R' are flexible alkyl Chains, M and N are generally small lateral substituents (halide, nitro, methyl, methoxy, cyano etc.). Y is a linking group connecting aromatic cores and X & Z are linking groups connecting terminal alkyl chains and aromatic cores. Lateral substituents M and N are responsible to modify the mesophase morphology and physical properties of calamitic liquid crystals.

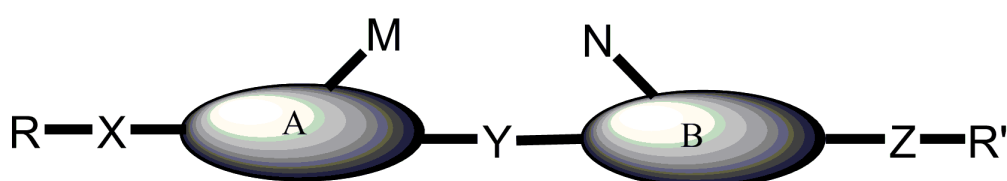


**Figure 5.** General template of calamitic liquid crystals.

Calamitic liquid crystals can be further classified based on the arrangements of mesogen in mesophase into:

- (a) Nematic (from Greek word nematos meaning “thread”)
- (b) Smectic (from the Greek word smectos meaning “soap”) etc.

### 1.4.1 Nematic Phase

The nematic phase shows high degree of long-range orientational order of the mesogens, but it lacks long-range positional order, it is the least ordered mesophase. In nematic phase mesogens are oriented with their long axes approximately parallel. The preferred axis of orientation of the molecules, depicted as a long arrow, is called the director (figure 6).

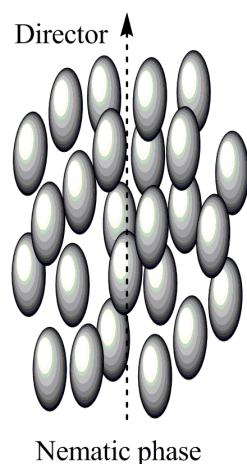


**Figure 6.** Structural representation of nematic phase formed by calamitic liquid crystal.

### 1.4.2 Smectic Phase

Rod-like molecules also form liquid crystalline phases where in addition to their orientational order, the mesogens possess positional order as well. The molecules arranged in layers have a well-defined layer spacing or periodicity. The smectic phase is denoted by the symbol Sm.

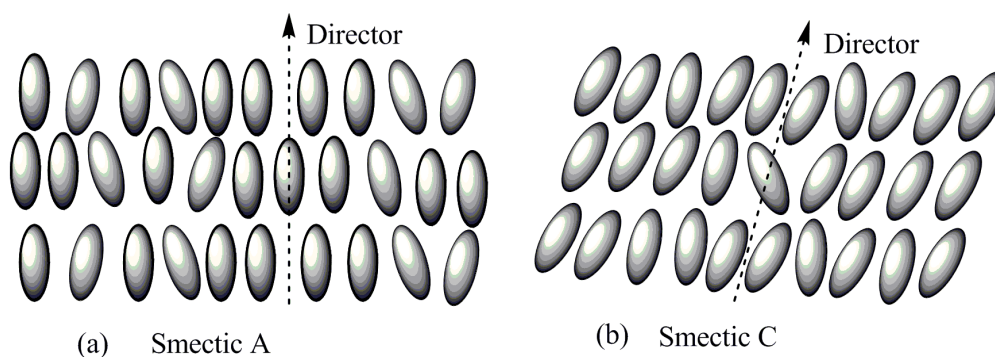


**Figure 7.** Smectic A and Smectic C liquid crystal phases.

There are various types of smectic mesophases, characterized by a variety of molecular orientation within the layers. Though the total number of smectic mesophases cannot be specified, the following types have been explored: SmA, SmB, SmC, SmF, and SmI. The SmA and SmC phases (Figure 7) are the less-ordered and more common phases. In SmA phase the mesogens form layers with their main axes parallel to the director. The SmC phase has the similar layer structure of the SmA, but the molecules are tilted at an angle respect to the layer plane. Both the phases lack positional order between molecules within the layers. SmB, SmF and SmI form more ordered smectic phases, the molecules here possess hexagonal order within the layers. They are called hexatic smectic liquid crystals. Disordered crystals having layer-like structures are often referred to as SmE, SmH, SmK, SmG and SmJ phases but they are more appropriately defined as lamellar plastic crystals. Tilted smectic mesophases formed by chiral compounds or containing chiral mixtures are designated by (\*) (eg. SmC\*, SmF\*, etc.).

## 1.5 Banana liquid crystals

Bent molecular structures form (Figure 8) a new sub-class of thermotropic liquid crystals, which can display, not just classical nematic and/or smectic phases, but also novel types of smectic-like phases called “B” phases<sup>21</sup> and are numbered according to their chronological discovery, from B<sub>1</sub> to the

most recent B<sub>8</sub>. The symbol B stands for Banana- or Bent- or Bow- shaped mesogens.

The most important thing in Banana liquid crystals is that the molecules pack along a bent direction, to constitute a polar plane which is perpendicular to the tilt plane.

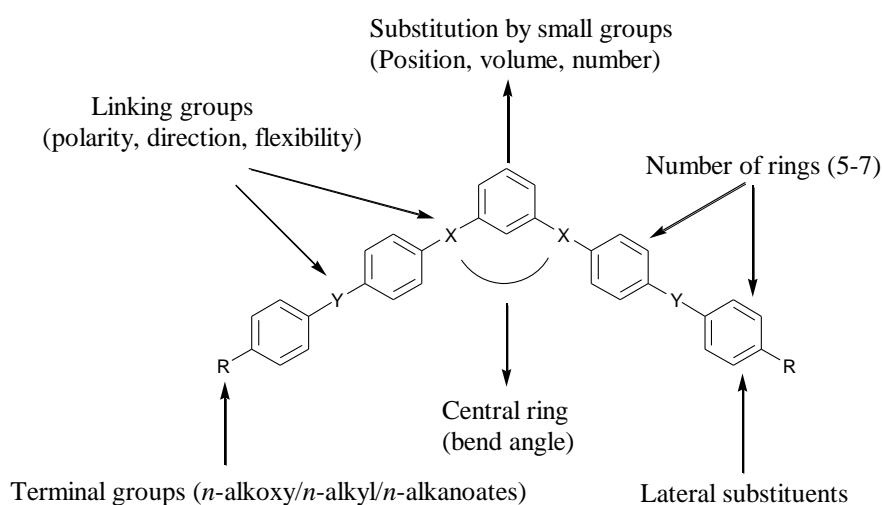
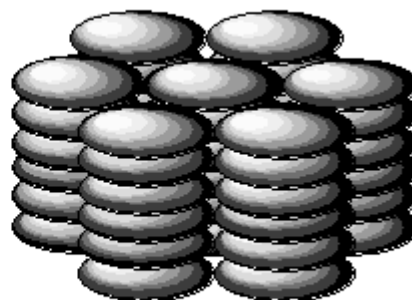
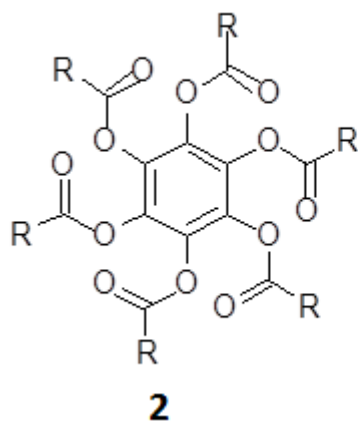


**Figure 8.** A general template of banana liquid crystals.

## 1.6 Discotic liquid crystals

S. Chandrasekhar *et al.* in 1977 reported “...what is probably the first observation of thermotropic mesomorphism in pure, single component systems of relatively simple plate like, or more appropriately disc-like molecules”.<sup>18</sup> They synthesized several benzene hexa-*n*-alkanoates (2) and from differential scanning calorimetry, polarizing optical microscopy and X-ray diffraction studies, established that these materials formed a new class of liquid crystals, in this mesophase molecules are arranged one on the top

of other to form a column like structure, columns self-assemble to form hexagonal arrangement.



Vorländer in 1924 had predicted the possibility of observing mesophases in leaf-shaped molecules<sup>31</sup> but he failed to obtain liquid crystalline behaviour in these molecules, because the molecules he studied had no peripheral alkyl chains. He thus concluded that leaf-shaped molecules did not form any liquid crystalline phases. It was later realised that the same molecules showed columnar phase on substitution with alkyl chains.

In 1960s, during pyrolysis of graphite substances Taylor *et al.* observed anisotropic mesophases with nematic texture.<sup>32-34</sup> These mesophases were thought to be made of disc-like polyaromatic molecules. Due to unstable nature of the mesophase it wasn't fully characterized.

Self-assembly of disc-shaped molecules to form columnar liquid crystals opened new class of liquid crystal, which were quite different from the classical rod-shaped liquid crystals. The discotic molecules self-

assemble in one-dimensional (1D) columns, which in turn, self-organize into various two-dimensional (2D) lattices. (Figure 9).

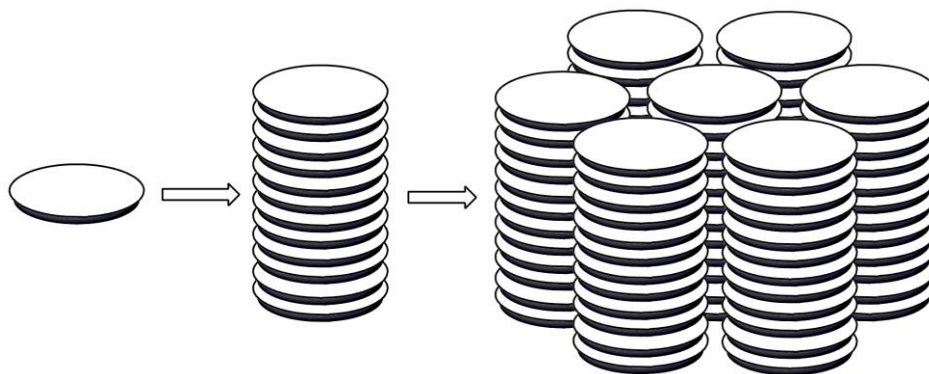


**Figure 9.** Self-assembly of discotic liquid crystals into columnar phase.

### 1.6.1 Structure of the liquid crystalline phases formed by discotic mesogens.

Most discotics molecules show only one type of mesophase but there are few examples which show polymorphism.<sup>35-48</sup> Discotic molecules primarily form four types of liquid crystals:

- (i) Nematic
- (ii) Smectic
- (iii) Columnar
- (iv) Cubic.

The columnar phase is the most commonly observed phase followed by nematic phase.

### 1.6.2 Nematic Phases of discotic mesogens

The nematic phases of disc-shaped molecules can be sub-categorised depending on the molecular arrangements. 1. Discotic nematic ( $N_D$ ), 2. Chiral nematic ( $N_{D^*}$ ), 3. Columnar nematic ( $N_{Col}$ ) and 4. Nematic lateral ( $N_L$ ). In the discotic nematic phase, the mesogens remain parallel to one another. They have orientational order but lack positional order (Figure 10a). The symmetry of the nematic phase formed by rod-shaped molecules is similar to that formed by disc-shaped molecules. But the nematic phase of discotic molecules is not miscible with the nematic phase of rod-like molecules. In discotic nematic phase the director is along the short molecular axes of the molecule since the disc normals are orientationally ordered. Discotic nematic phase is represented by the symbol ' $N_D$ '. Chiral discotic nematic mesophase  $N_{D^*}$  is obtained from either pure chiral discotic molecule or by introducing a chiral dopant in discotic nematic liquid crystals (Figure 10b). Chiral discotic nematic phase is characterized by a helical structure. The nematic columnar phase is characterized by a columnar stacking of the mesogens. But the columnar structures do not further organize into two dimensional (2D) lattice structures (Figure 10c). They display a positional short-range order and an orientational long-range order. Recently, it has been observed that discotic molecules come together to form disc shaped super structures and these aggregated superstructures show a nematic arrangement (Figure 10d). The self-assembly is driven by strong lateral interaction and thus it is called Nematic lateral phase ( $N_L$ ).<sup>42, 49</sup>

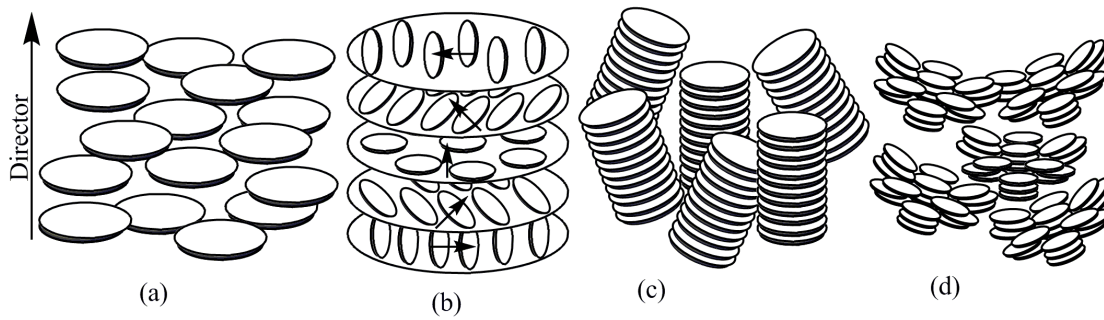


**Figure 10.** Nematic phases observed in discotic liquid crystals.

### 1.6.3 Smectic phases of discotic mesogens

The discotic mesogens exhibit smectic mesophase when there is reduced number of peripheral alkyl chains or when the distribution of peripheral alkyl chains is uneven, as shown in the Figure 11. The discs are arranged in a layered fashion in discotic smectic mesophases these layers are separated by sub layers of peripheral alkyl chains, similar to calamitic smectic mesophases.<sup>50-51</sup> They exhibit biaxial smectic phases, due to restricted molecular rotation along the long molecular axes. smectic phases are less common in discotic LCs.

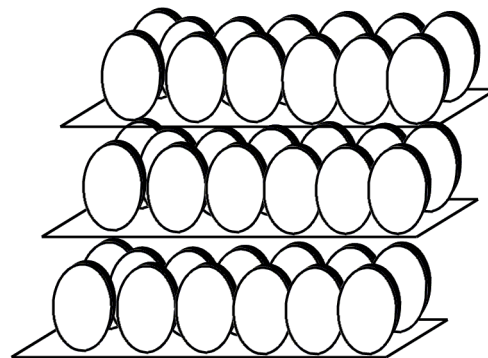


**Figure 11.** Smectic phase of discotic liquid crystals.

### 1.6.4 Columnar phases of discotic mesogens

In columnar mesophases, molecules assemble themselves on the top of each other in columns. The columns in turn self-assemble in various two-dimensional lattices. The molecules in columnar mesophases may be arranged in either disordered or ordered manner. Depending on the degree of order, orientation of the molecules, the dynamics of the molecules within the columns and the two-dimensional lattice symmetry of the columnar packing, the columnar mesophases may be classified in seven classes.

- \* Columnar hexagonal mesophase ( $\text{Col}_h$ ),
- \* Columnar rectangular mesophase ( $\text{Col}_r$ ),
- \* Columnar oblique phase ( $\text{Col}_{ob}$ ),
- \* Columnar plastic phase ( $\text{Col}_p$ ),
- \* Columnar helical phase (H),
- \* Columnar square (tetragonal) phase ( $\text{Col}_{tet}$ ), and
- \* Columnar lamellar phase ( $\text{Col}_L$ ).

#### 1.6.4.1 The hexagonal columnar mesophase ( $\text{Col}_h$ )

In columnar hexagonal mesophase, discotic columns self-assemble into hexagonal lattice. They are often denoted as  $\text{Col}_{ho}$  (Figure 12) or  $\text{Col}_{hd}$ , h here represents hexagonal phase and o and d indicate ordered or disordered stacking of the mesogens. Both the ordered or disordered phases show fluidity; the correlation lengths differ from ordered phase to disordered phase and, thus, it is advised to drop o and d subscripts. The recommended abbreviation for columnar hexagonal phase is “ $\text{Col}_h$ ”.

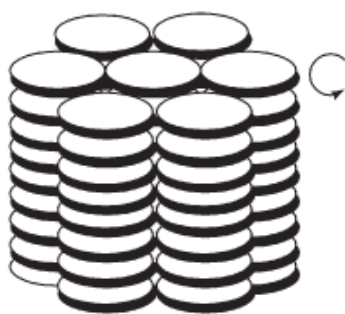


**Figure 12.** Hexagonal columnar phase.

#### 1.6.4.2 The rectangular columnar mesophase (Col<sub>r</sub>)

The molecular packing of the columns in rectangular lattice leads to the formation of columnar rectangular mesophase. Three different types of molecular ordering are observed in columnar rectangular mesophase (Figure 13 & 14). The molecules often are oriented at an angle with respect to columnar axis.<sup>52-53</sup> A orthogonal cross section to the columnar axis, is elliptic. Depending on the number of columns in a unit cell and the mutual orientation of the mesogens (ellipses), columnar rectangular phases have been sub divided into three different types. The symmetry of the 2D lattices are specified by three different planar space group i.e. P21/a, P2/a and C2/m (Figure 14 a-c) they belong to the subset of space groups which lack any translational order in the direction of the principal symmetry axis i.e. the direction of the columns. A strong core-core interactions leads to the formation of columnar rectangular phases, because the aromatic cores of one column have to 'know' how they tilt with respect to the aromatic cores of the neighbouring columns.

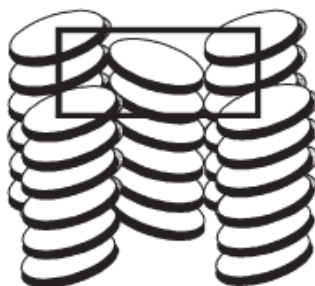


**Figure 13.** Columnar rectangular phase.

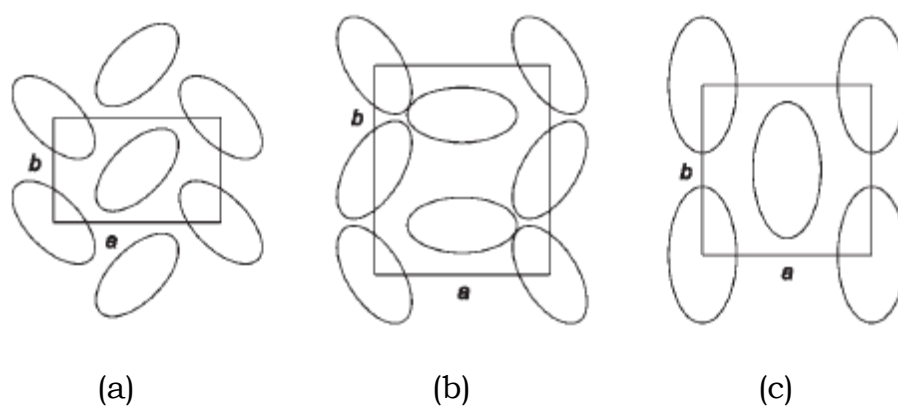


**Figure 14.** Different types of rectangular columnar phases (a) Colr (P21/a); (b) Colr (P2/a) and (c) Colr (C2/m).

#### 1.6.4.3 The columnar oblique mesophase (Col<sub>ob</sub>)

The symmetry associated with 2D lattice of columnar oblique phase matches to that of space group P1. Figure 15 shows the ordering of discotic columns in a columnar oblique mesophase, tilted columns are shown as elliptic cross sections.<sup>54-55</sup>

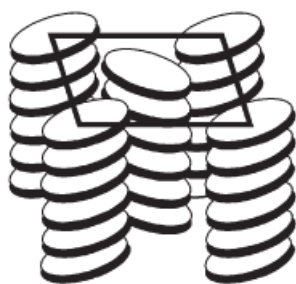


**Figure 15.** Columnar oblique phase.

#### 1.6.4.4 The columnar plastic mesophase ( $\text{Col}_p$ )

Columnar plastic phase ( $\text{Col}_p$ ), is a new addition to discotic liquid crystals.<sup>56</sup>

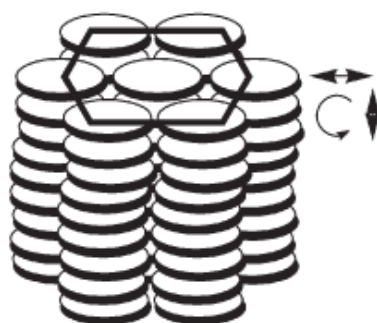


**Figure 16.** Columnar plastic phase.

This phase shows a highly ordered (crystal-like) hexagonal lattice, the aromatic discs in the columns have the freedom to rotate about their columnar axis (Figure 16). Columnar plastic phase are devoid of structural disorders like non-parallel stacking of discs, lateral or longitudinal displacements, unlike columnar hexagonal phase. The motional freedom of discs in the  $\text{Col}_p$  phase is restricted.

#### 1.6.4.5 The columnar helical (H) phase

Hexahexylthiotriphenylene (HHTT) shows a very interesting mesophase structure which shows helical order has been demonstrated.<sup>57-58</sup> In this H phase helical columns form which interdigitate in a set of three columnar stacks. The molecular ordering in H phase found is illustrated in Figure 17.

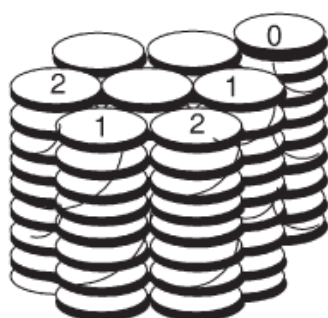


**Figure 17.** Columnar helical phase.

#### 1.6.4.6 The columnar lamellar mesophase

In this phase columnar stacks arrange themselves in layers, the columns present in lamellar layers can slide in the mesophase. The columns in layer has no positional (translational) correlation with the neighbouring layer. Lamellar structure is observed in the mesophases of certain discotic compounds e.g. bis(p-n-decylbenzoyl)methanato copper(II), some perylene derivatives, etc..<sup>59-60</sup> A columnar lamellar mesophase is assigned the symbol Col<sub>L</sub>, a layered ordering of molecules is shown in Figure 18.



**Figure 18.** Columnar lamellar phase.

#### 1.6.4.7 The columnar square (tetragonal) phase

The columnar square phases are also often referred to as the tetragonal phase ( $\text{Col}_{\text{tet}}$ ) which is shown in Figure 19. Here the columns self-assemble into square lattice. This phase shows a homeotropic alignment of the columns similar to columnar hexagonal phase. This phase is observed in certain sugar molecules, phthalocyanines and supramolecular fluorinated liquid crystals.<sup>61-65</sup>

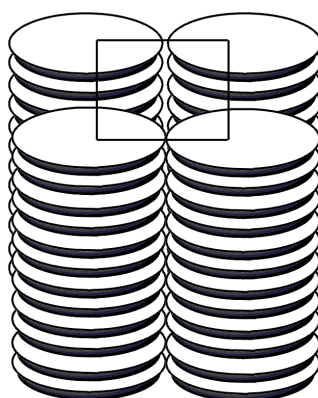


**Figure 19.** Columnar tetragonal phase.

### 1.6.5 Cubic phase

Cubic phases are very common in lyotropic liquid crystals, but some columnar phthalocyanine derivatives<sup>61-62</sup> exhibit bicontinuous cubic phase which consist of interwoven but not connected branched columns.

## 1.7 Structure of the discotic mesogens

Since the time the first discotic mesogens was discovered, scientists have explored the molecular parameters that lead to formation of columnar mesophase and further control the temperatures at which various phases appears. A central discotic aromatic core forms the backbone for the columnar phase, strong pi-pi attraction between the aromatic cores induces close stacking, and this type of arrangement provides rigidity to the mesophase. Aromatic cores are substituted with 3-8 saturated chains of three or more carbon atoms. These alkyl chains are flexible and are disordered in nature, this induces the mobility to the rigid aromatic core. Discotic materials often have two, three, four or six-fold rotational symmetry. However, there are many examples of materials with non-planar, non-aromatic core having shorter number of chains are also known to form columnar phases. The microsegregation of the two constituents induces liquid crystallinity in discotic liquid crystals. Discotic molecules self-assemble into one-dimensional columns, they possess self-healing properties, i.e. the capacity to repair the structural defects. Changing the size and type of central core alongwith different lateral alkyl chains will lead



leads to a mixture of structurally similar products, this often results in impurities having almost identical  $R_f$  values as that of pure mesogen on a chromatographic plate. Their separation is often difficult even by HPLC. In order to obtain pure product in greater yields reaction is pushed towards completion by taking small excess of the reagent and carrying out the reaction little longer. Sometimes this could lead to side reactions and further complicate the synthesis. Most important part of the synthesis is finding optimum reaction conditions. The chemistry involved in synthesis of discotic liquid crystals has been improved significantly in last two decades. Highly regio-selective and high yielding methods have been mastered particularly for the synthesis of triphenylene and anthraquinone based discotic liquid crystals.

## 1.9 Characterization of discotic liquid crystal phases

The characterization of thermotropic phase behavior of discotic liquid crystals is usually done using following techniques,

- a) differential scanning calorimetry (DSC),
- b) polarized optical microscopy (POM),
- c) X-ray scattering and
- d) solid-state NMR.<sup>44</sup>

DSC is used to determine the temperatures and enthalpy of the phase transitions. The characteristics textures of various liquid crystalline phase can be easily identified using POM. The supramolecular organization of

liquid crystalline phases into various lattice and the corresponding packing parameters in each phase can be studied in detail by X-ray diffraction. X-ray diffraction helps in probing the intra and inter-columnar order present in columnar structures. It is possible to determine core-core spacing in columnar structures, also to obtain information about the arrangement of discs within the columns, such as tilting and helical packing and also to provide much deeper insight into the various microstructures associated with the mesophase. Solid state NMR helps in studying of the molecular dynamics in liquid crystalline mesophase.<sup>66-67</sup> This technique allows one to study the rotation of the core with respect to its neighbours or about peripheral mobility of alkyl chains. The different electronic environments of the aromatic protons in the intracolumnar packing, the tilted arrangement of the discs in the solid phase can be determined as well. It is necessary to carry out all these complementary experimental methods in order to obtain a clear, comprehensive and unambiguous picture of the self-assembling behavior of discotic mesogens.

When a mesogen undergoes transition from crystalline phase to that of liquid crystalline phase it is accompanied by a surge in molecular dynamics, like axial and lateral displacement of discs and the rotation of the discs around the columnar axis etc. The centers of gravity of the mesogens in the columnar mesophases are present along the column axis, peripheral chains induce fluidity and let the column slide with respect to each other which leads to self-healing behaviour.

## 1.10 DLCs as materials for a new generation of organic electronics

In recent years, the use of conjugated organic molecules as functional components in electronic devices, has led to an increase in scientific research in this area. This field of study is referred to as Organic Electronics. This new field has led to very interesting electronic devices like, organic solar cells, organic field effect transistors (OFET), organic light-emitting diodes (OLED), sensors, memory elements, etc.<sup>35-38, 40-48, 68</sup> This has resulted in detailed studies into structure-property relationships of organic molecules, which are determined by the physical and chemical properties of these novel materials. This challenge creates the need of new novel organic materials with semiconducting properties.<sup>69-70</sup> Two of the potential systems for application in organic (opto)electronic devices are pi-conjugated conducting polymers and pi-pi stacked columnar discotic materials. Mesogens with hierarchical self-assembly into supramolecular structures, like discotic liquid crystals, which form two-dimensional ordered structures and as well has the dynamics (ability to self-healing of structural defects) are considered potential candidates for organic semiconductor devices. The low molecular weight of discotic liquid crystals allows the synthesis of defect-free chemical structures. These small molecule systems have upper hand over conducting polymers, due to the fact that very high purity low molecular mass materials can be synthesized with ease.<sup>35-38, 40-48, 68</sup>

## 1.11 Nanoparticles

Materials below 100 nm in one-, two- or all the three-dimensions are commonly referred to as nanomaterials. They often possess unique properties which differ from those of bulk material. Several phenomena become pronounced as the size of the particles decreases; for example, the conductivity of metal nanoparticles decreases significantly as their size decreases to one billionth of a meter; silver nanoparticles, show antibacterial activity, unlike that of bulk silver; bulk gold is inert and not soluble in common solvents but gold NPs exhibit catalytic properties and can be dissolved in solvents; the optical absorption and fluorescence properties of metal nanoparticles are very different than in the bulk materials, etc. <sup>71-73</sup>

Though nanomaterials are known for centuries, the field of nanoscience and nanotechnology saw explosive development during the past two decades, thanks to advancement in technology, such as scanning tunneling microscope (STM), atomic force microscope (AFM), high-resolution transmission electron microscope (HRTEM) and field emission scanning electron microscope (FESEM), scientists are able to characterize the size and shape of this nanoparticles with a very high accuracy. In recent years, there has been tremendous development in the fields of nanostructured materials, including metallic NPs and nanorods (NRs), semiconducting quantum dots (QDs), carbon nanotubes (CNTs), fullerenes and graphene. The science and technology dealing with nanomaterials have received immense interest in nearly every field of science.<sup>73</sup> Keeping pace with topical sciences, the field of

liquid crystals (LCs) has recently entered into the fascinating domains of nanoscience and nanotechnology.<sup>10, 74-78</sup>

One of the current research areas worldwide in nanoscience field is to design nanomaterials that have the potential to self-assemble into functional supramolecular structures in multiple directions. Nanoparticles assembly has been controlled by several methods; however, using liquid crystals as an anisotropic medium to induce the self-assembly of nanoparticles is a powerful tool. A number of LC-NP hybrid systems have been explored. Calamitic mesogens (liquid crystals formed by rod-shape molecules) are the most commonly employed materials in the preparation of these hybrids<sup>10, 75-78</sup> However, recently some efforts have been made to incorporate various NPs in the supramolecular order of discotic liquid crystals.<sup>79-80</sup>

Since this thesis deals with a variety of nanomaterials, they are discussed in detail in subsequent chapters.

## **1.12 Why discotics ?**

The two-dimensional chemical structure of columnar liquid crystal form a very interesting field of study. Most of discotic liquid crystals form columnar mesophases due to intense pi-pi interactions of polyaromatic cores. The core-core (intra-columnar) separation in a columnar mesophase is usually of the order of 3.6 Å this leads to a significant overlap of pi-orbitals between two neighbouring discs. Long alkyl chains surround the core which are flexible in nature, the inter-columnar distance is usually of the order of 20-

40 Å, depending on the lateral chain length and number of lateral chains. The number of alkyl chains around the aromatic core varies from 3-8 to form columnar mesophase. Therefore, interactions between neighbouring mesogens within the same column would be a lot stronger than interactions between neighbouring columns. This leads to anisotropic behaviour of liquid crystals, charge migration in these discotic materials are quasi-one-dimensional. Conductivity along the director in columnar mesophases is several orders of magnitude greater than in the perpendicular direction. Thus discotic liquid crystals or often described as molecular wires, the conducting aromatic cores are surrounded by insulating aliphatic chains in the columnar phase as shown in Figure 21.

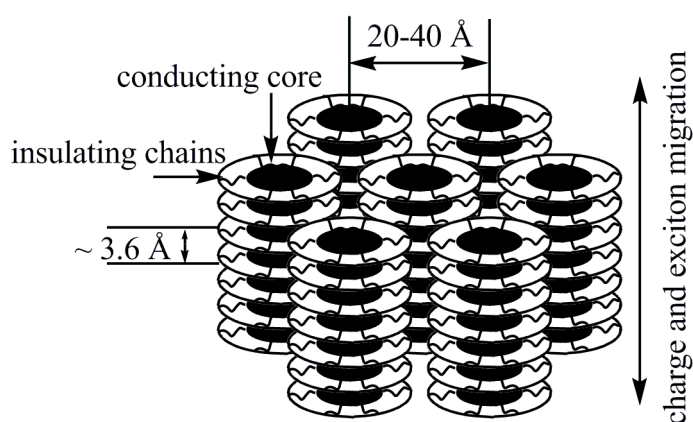


**Figure 21.** Energy and charge migration in discotic liquid crystals.

### 1.13 Objective

Studying supramolecular nanocomposites of liquid crystal and nanoparticles, is an interesting field of study. Dispersion of zero dimensional

nanomaterials in discotic liquid has been explored in detail. In this thesis we have studied dispersion of various one-dimensional (1-D) and two-dimensional (2-D) nanomaterials of different lengths and functionalities in columnar mesophase. Graphene oxide is an interesting two-dimensional nanomaterial which has gained prominence in last decade due to its high electrical and thermal conductivity. We have explored functionalizing graphene and graphene oxide systems, and introducing these functionalized nanomaterials in columnar mesophase. We wish to characterize the effect of these dopants on mesophase, and also to tune these functionalities on graphene so as to induce order or dis-order in mesophase. We have explored the self-assembling behaviour of the functionalized graphene oxide on gold surface and explore the influence of surface modification on charge transfer properties of the gold electrodes. One-dimensional nanomaterials are interesting materials as they like columnar liquid crystals are anisotropic in nature, we have tried to introduce these 1-D nanomaterials in columnar mesophase. Firstly we have introduced gold nanorods of small aspect ratio in columnar mesophase and studied how it influences mesophase behaviour, we also explored the orientation of these nanorods in ribbons formed by columnar liquid crystal. We later have tried to introduce CdS nanowires of higher aspect ratios and were able to control their self-assembly in triphenylene nanoribbons, and studied their orientation in columnar liquid crystal, we have also tried to explore the formation of lyotropic mesophase in CdS nanoribbons and have explored how the nanowires of different length lead to formation of supramolecular aggregates of different length scales.

## 1.14 References.

1. Bahadur, B., Liquid Crystals Applications and Uses. World Scientific 1991, 3, pp. 68-199.
2. Chandrasekhar, S., Liquid Crystals. Cambridge University Press 1977.
3. Collings, J., Liquid Crystals : Nature's Delicate Phase of Matter. Princeton University Press 2002.
4. Collings, J.; Hird, M., Introduction to Liquid Crystals Chemistry and Physics. Taylor & Francis 1997.
5. Collings, J.; Patel, J. S., Handbook of Liquid Crystal Research. Oxford University Press 1997.
6. Demus, D., Types and Classification of Liquid Crystals. In Liquid Crystals — Applications and Uses, WORLD SCIENTIFIC: 2012, pp 1-36.
7. Demus, D.; Goodby, J. W.; Gray, G. W., Handbook of Liquid Crystals, Handbook of Liquid Crystals: Four Volume Set. Handbook of Liquid crystals 1998.
8. Doane, J. W., Polymer Dispersed Liquid Crystal Displays. In Liquid Crystals — Applications and Uses, WORLD SCIENTIFIC: 2012, pp 361-395.
9. Gennes, P.-G., The Physics of Liquid Crystals. Clarendon Press 1974.
10. Goodby, J. W. G., Handbook of Liquid Crystals. Handbook of liquid crystals 2014.
11. Kelker, H.; Hatz, R.; Schumann, C., Handbook of Liquid Crystals. Verlag Chemie 1980.
12. Pohl, L.; MERCK, E., Physical Properties of Liquid Crystals. In Liquid Crystals — Applications and Uses, WORLD SCIENTIFIC: 2012, pp 139-170.

13. Friedrich, R., Contributions to the Knowledge of Cholesterol. *Liquid Crystals* 1989, 5.
14. Reinitzer, F., Beiträge Zur Kenntniss Des Cholesterins. *Monatshefte für Chemie* 1888, 9, 421-441.
15. Lehmann, O., On Flowing Crystals. *Zeitschrift für Physikalische Chemie* 1889, 4, 462.
16. Heintz, W., Ueber Die Fette. *Journal für Praktische Chemie* 1855, 66, 1-51
17. Vorländer, D., *Kristallinisch-Flüssige Substanzen*, 1908.
18. Chandrasekhar, S.; Sadashiva, B. K.; Suresh, K. A., Liquid Crystals of Disc-Like Molecules. *pramana* 1977, 9, 471-480.
19. Etxebarria, J.; Ros, M. B., Bent-Core Liquid Crystals in the Route to Functional Materials. *J. Mater. Chem.*, 2008, 18, 2919-2926.
20. Niori, T.; Sekine, T.; Watanabe, J.; Furukawa, T., Distinct Ferroelectric Smectic Liquid Crystals Consisting of Banana Shaped Achiral Molecules. *J. Mater. Chem.*, 1996, 6, 1231-1233.
21. Pelzl, G.; Diele, S.; Weissflog, W., Banana- Shaped Compounds—a New Field of Liquid Crystals. *Adv. Mater.* 1999, 11, No. 9.
22. Reddy, R. A.; Tschierske, C., Bent-Core Liquid Crystals: Polar Order, Superstructural Chirality and Spontaneous Desymmetrisation in Soft Matter Systems. *J. Mater. Chem.*, 2006,16, 907-961
23. Serrano, J. L.; de Fuente, L. M. R.; Folcia, C. L., Banana-Shaped Liquid Crystals: A New Field to Explore. *J. Mater. Chem.*, 2005,15, 5093-5098.

24. Takezoe, H.; Takanishi, Y., Bent-Core Liquid Crystals: Their Mysterious and Attractive World. *Japanese journal of applied physics* 2006, 25, 1.
25. Chandler, D., Interfaces and the Driving Force of Hydrophobic Assembly. *Nature* 2005, 437, 640-647.
26. Badaire, S.; Zakri, C.; Maugey, M.; Derré, A., Liquid Crystals of DNA-Stabilized Carbon Nanotubes. *Adv, Mater.* 2005, 17, 1673.
27. Dogic, Z.; Fraden, S., Ordered Phases of Filamentous Viruses. *Current Opinion in Colloid & Interface Science* 2006, 11, 47-55.
28. Mourad, M. C. D.; Wijnhoven, J., Gelation Versus Liquid Crystal Phase Transitions in Suspensions of Plate-Like Particles. *Phil. Trans. R. Soc. A* 2006 364, 2807–2816.
29. Song, W.; Kinloch, I. A.; Windle, A. H., Nematic Liquid Crystallinity of Multiwall Carbon Nanotubes. *Science* 2003, 302, 5649,1363.
30. Lydon, J., Chromonic Mesophases. *Current opinion in colloid & interface science* 2004, 8, 480.
31. Vorländer, D., *Chemische Kristallographie Der Flüssigkeiten: Kurze Anleitung Zur Synthese Und Untersuchung Polymorpher Und Kristallinflüssiger Substanzen*; Akademische Verlagsgesellschaft, 1924.
32. Brooks, J. D.; Taylor, G. H., Formation of Graphitizing Carbons from the Liquid Phase. *Nature* 1965, 206, 697-699.
33. Brooks, J. D.; Taylor, G. H., The Formation of Graphitizing Carbons from the Liquid Phase. *Carbon* 1965, 3, 185.
34. Taylor, G., Development of Optical Properties of Coke During Carbonization. *Fuel* 1961, 40, 465-472.

35. Bushby, R. J., Device Applications of Charge Transport in Discotic Liquid Crystals. *J. Mater. Chem.*, 1999, 9, 2081-2086.
36. Bushby, R. J.; Lozman, O. R., Discotic Liquid Crystals 25 Years On. *Current opinion in colloid & interface science* 2002, 7, 343.
37. Bushby, R. J.; Lozman, O. R., Photoconducting Liquid Crystals. *current Opinion in Solid State and Materials Science* 2002, 6, 769.
38. Chandrasekhar, S., Discotic Liquid Crystals. A Brief Review. *Liquid Crystals* 1993, 14, 1.
39. Chandrasekhar, S.; Ranganath, G. S., Discotic Liquid Crystals. *Recent Progress in Physics* 1990, 53, 1.
40. Kato, T.; Yasuda, T.; Kamikawa, Y.; Yoshio, M., Self-Assembly of Functional Columnar Liquid Crystals. *Chem. Commun.*, 2009, 729-739.
41. Kazuchika, O.; Kazuaki, H.; Makiko, S.; Masahiro, A.; Kazue, B.; Fumihiko, M.; Rie, N.; Kaoru, N.; Anick, M. V. d. C.; John, M. W., Discotic Liquid Crystalline Semiconductors. *Molecular Crystals and Liquid Crystals* 2003, 397.
42. Kouwer, P. H. J.; Jager, W. F.; Mijs, W. J.; Picken, S. J., The Nematic Lateral Phase: A Novel Phase in Discotic Supramolecular Assemblies. *Macromolecules* 2001, 34, 7582.
43. Kumar, S., Self-Organization of Disc-Like Molecules: Chemical Aspects. *Chemical Society reviews* 2006, 35, 83-109.
44. Laschat, S., et al., Discotic Liquid Crystals: From Tailor-Made Synthesis to Plastic Electronics. *Angew. Chemie.* 2007, 46, 4832-4887.

45. Sergeev, S.; Pisula, W.; Geerts, Y. H., Discotic Liquid Crystals: A New Generation of Organic Semiconductors. *Chem. Soc. rev.* 2007, 36, 1902-1929.
46. Shimizu, Y.; Oikawa, K.; Nakayama, K., Mesophase Semiconductors in Field Effect Transistors. *J. Mater. Chem.*, 2007,17, 4223-4229.
47. Takezoe, H.; Kishikawa, K.; Gorecka, E., Switchable Columnar Phases. *J. Mater. Chem.*, 2006,16, 2412-2416.
48. Wu, J.; Pisula, W.; Müllen, K., Graphenes as Potential Material for Electronics. *Chem. rev.* 2007, 107, 718-747.
49. Bisoyi, H. K.; Kumar, S., Discotic Nematic Liquid Crystals: Science and Technology. *Chem. Soc. rev.* 2010, 39, 264-285.
50. Alameddine, B.; Aebischer, O. F.; Amrein, W.; Donnio, B.; Deschenaux, R.; Guillon, D.; Savary, C.; Scanu, D.; Scheidegger, O.; Jenny, T. A., Mesomorphic Hexabenzocoronenes Bearing Perfluorinated Chains. *Chem. Mater.* 2005, 17, 4798-4807.
51. Bruce, D. W.; Dunmur, D. A.; Santa, L. S.; Wali, M. A., Mesomorphic Metalloporphyrins Showing Calamitic Mesophases. *J. Mater. Chem.* 1992, 2, 363-364.
52. Frank, F. C.; Chandrasekhar, S., Evidence of a Tilted Columnar Structure for Mesomorphic Phases of Benzene-Hexa-N-Alkanoates. *J. Phys. France* 1980, 41, 1285-1288.
53. Levelut, A., Structures Des Phases Mesomorphes Formée Par De Molecules Discoides. *Journal de chimie physique* 1983, 80, 149-161.
54. Destrade, C.; Foucher, P.; Gasparoux, H., Disc-Like Mesogen Polymorphism. *Molecular Crystals and Liquid Crystals*, 1984, 106.

55. Morale, F.; Guillon, D.; Bruce, D. W.; Finn, R. L., Columnar Mesomorphism from Hemi-Disklike Metallomesogens Derived from 2, 6-Bis [3', 4', 5'-Tri (Alkoxy) Phenyliminomethyl] Pyridines (L): Crystal and Molecular Structures of  $[M(L)Cl_2]$  (M=Mn, Ni, Zn), *Chemistry-A European Journal* 2003, 9, 2484.
56. Glüsen, B.; Heitz, W.; Kettner, A.; Wendorff, J. H., A Plastic Columnar Discotic Phase Dp. *Liquid crystals* 1996, 20, 5.
57. Fontes, E.; Heiney, P. A.; de Jeu, W. H., Liquid-Crystalline and Helical Order in a Discotic Mesophase. *Phys. Rev. Lett.* 1988, 61, 1202.
58. Heiney, P. A.; Fontes, E.; Jeu, D. W. H., Frustration and Helicity in the Ordered Phases of a Discotic Compound. *J. Phys. France*, 1989, 50, 461-483.
59. Nishitani, A.; Sumiya, Y.; Terauchi, H.; Ohta, K., X-Ray Diffraction Study on Discotic Lamellar Phase in Bis (1, 3-Di (Pn-Alkoxyphenyl) Propane-1, 3-Dionato) Copper (II). *Molecular Crystals and Liquid Crystals Incorporating Nonlinear Optics*, 1988, 163, 1, 211-219.
60. Takagi, A.; Hatada, K. I.; Ema, H.; Yamamoto, I., Discotic Liquid Crystals of Transition Metal Complexes, 3: The First-Established Discotic Lamellar Phase in Bis [1, 3-Di (Pn-Alkoxyphenyl) Propane-1, 3-Dionato] Copper (II). *Molecular Crystals and Liquid Crystals*, 1986, 140, 2, 131-152.
61. Hatsusaka, K.; Ohta, K.; Yamamoto, I., Discotic Liquid Crystals of Transition Metal Complexes, Part 30: Part 29: Ref. 1 Spontaneous Uniform Homeotropic Alignment of Octakis (Dialkoxyphenoxy). *J. Mater. Chem.*, 2001, 11, 423-433.

62. Ichihara, M.; Suzuki, A.; Hatsusaka, K.; Ohta, K., Discotic Liquid Crystals of Transition Metal Complexes 37\*: A Thermotropic Cubic Mesophase Having Pn M Symmetry Exhibited by Phthalocyanine Based Derivatives. *Liquid Crystals* 2007, 34, 555.
63. Praefcke, K.; Marquardt, P.; Kohne, B., Inositol Liquid Crystals, X-Ray Diffraction Studies of Their Hydrogen-Bond Supported Supramolecular Mesophases1. ... *Mol. Crystals and Liquid Cryst.* 1991, 203, 149.
64. Vlad-Bubulak, T.; Buchs, J.; Kohlmeier, A., Mesophase Morphologies of Hydrogen-Bonded Complexes of Biphenyl-Substituted Diamino-1, 3, 5-Triazines with Semiperfluorinated Benzoic Acids. *Chem. Mater.*, 2007, 19 (18), 4460–4466
65. Watanabe, T.; Hasebe, H.; Morizumi, Y., Discotic Liquid Crystals of Transition Metal Complexes 9: Synthesis and Properties of Discotic Liquid Crystals of Tetrapyrazinoporphyrazine Derivatives. *Mol. Cryst. and Liquid Cryst.* 1991, 196, 13-26.
66. Fischbach, I.; Ebert, F.; Spiess, H. W.; Schnell, I., Rotor Modulations and Recoupling Strategies in  $^{13}\text{C}$  SolidState Magic Angle Spinning Nmr Spectroscopy: Probing Molecular Orientation and Dynamics. *ChemPhysChem* 2004, 5, 895 - 908.
67. Lehmann, M.; Fischbach, I.; Spiess, H. W., Photochemistry and Mobility of Stilbenoid Dendrimers in Their Neat Phases. *J. Am. Chem. Soc.*, 2004, 126 (3), pp 772–784.
68. Chandrasekhar, S.; Ranganath, G. S., Discotic Liquid Crystals. *Rep. Prog. Phys.*, 1990, 53, 57-84.

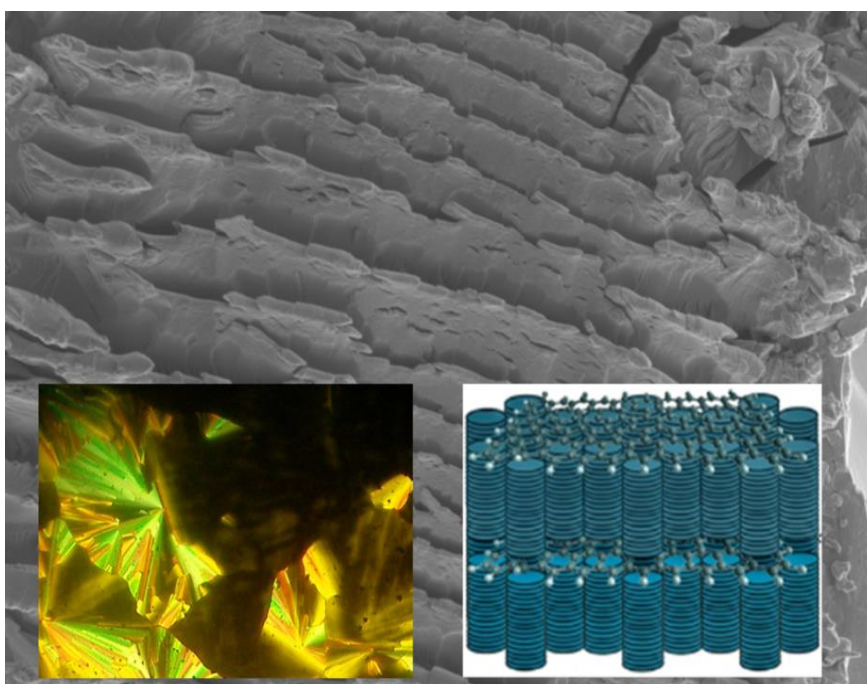
69. Hadziioannou, G.; Hutten, P. F. v., *Semiconducting Polymers : Chemistry, Physics and Engineering*; Wiley-VCH: Weinheim; New York, 2000.
70. Müllen, K.; Wegner, G., *Electronic Materials : The Oligomer Approach*; Wiley-VCH: Weinheim; New-York, 1998.
71. Daniel, M. C.; Astruc, D., *Gold Nanoparticles: Assembly, Supramolecular Chemistry, Quantum-Size-Related Properties, and Applications toward Biology, Catalysis, and Nanotechnology*. *Chem. Rev.* 2004, 104, 293–346.
72. Burda, C.; Chen, X.; Narayanan, R.; El-Sayed, M. A., *Chemistry and Properties of Nanocrystals of Different Shapes*. *Chem. Rev.*, 2005, 105 (4), pp 1025–1102.
73. Rao, C. N. R.; Müller, A.; Cheetham, A. K., *The Chemistry of Nanomaterials : Synthesis, Properties and Applications in 2 Volumes*; Wiley-VCH: Weinheim, 2004.
74. Garbovskiy, Y. A.; Glushchenko, A. V., *Liquid Crystalline Colloids of Nanoparticles: Preparation, Properties, and Applications*. *Solid state physics*. 2011, 62, 1-75.
75. Bisoyi, H. K.; Kumar, S., *Liquid-Crystal Nanoscience: An Emerging Avenue of Soft Self-Assembly*. *Chem. Soc. rev.* 2011, 40, 306-319.
76. Lagerwall, J. P. F.; Scalia, G., *A New Era for Liquid Crystal Research: Applications of Liquid Crystals in Soft Matter Nano-, Bio-and Microtechnology*. *Current Applied Physics* 2012.

77. Nealon, G. L.; Greget, R.; Dominguez, C., Liquid-Crystalline Nanoparticles: Hybrid Design and Mesophase Structures. *Beilstein J. Org. Chem.* 2012, 8, 349–370.
78. Stamatoiu, O.; Mirzaei, J.; Feng, X.; Hegmann, T., Nanoparticles in Liquid Crystals and Liquid Crystalline Nanoparticles. *Liquid Crystals* 2012, 318, 331.
79. Kumar, S., Discotic Liquid Crystal-Nanoparticle Hybrid Systems. *NPG Asia Materials* 2014, 6.
80. Kumar, S., Nanoparticles in the Supramolecular Order of Discotic Liquid Crystals. *Liquid Crystals* 2014, 41, 353.

# CHAPTER 2

---

## **Mutually ordered Self-assembly of Discotic Liquid Crystal- Graphene Nanocomposites**



We have observed that room temperature anthraquinone discotic 1,5-dihydroxy-2,3,6,7-tetrakis(3,7-dimethyloctyloxy)-9,10-anthraquinone (RTAQ) self assembles in presence of octadecylamine functionalized graphene (f-graphene) into a ordered sandwich like structure, where the discotic molecules forms columnar structures on graphene sheets. Cryo-SEM and SEM images provide evidence for this ordering. This behaviour is also supported by polarizing optical microscopy, differential scanning calorimetry, X-ray diffraction and conductivity studies of nanocomposite.

## 2.1 Introduction.

Carbon is an essential part of life. It is the sixth element of the periodic table, it has ability to form covalent bonds with the same (catenation) and other elements of the periodic table in many ways.<sup>1</sup> Carbon occurs in all forms; zero-, one-, two- and three-dimensional geometry with insulating to conducting properties. While 2-D graphite and 3-D diamond are the known naturally occurring allotropes; 0-D fullerene and 1-D nanotubes can be synthesized. Carbon allotropes possess many exciting superlative properties, such as, diamond is the hardest substance, CNTs are the mechanically strongest materials, graphite exhibits the highest electric and heat conductivities, etc. Recently, synthetic nanocarbons (fullerene, CNTs and graphene) have received much attention in materials science due to their fascinating properties.<sup>1</sup> All the three types of carbon nanomaterials (zero-dimensional fullerene, one-dimensional CNTs and two-dimensional graphene) have been coupled with LCs to hybridize their properties.

Graphene, the one-atom-thick, two-dimensional (2D) carbon allotrope is the most well-known nanomaterial with exotic optical and electronic properties.<sup>2</sup> Graphite can be chemically oxidized to obtain graphene oxide (GO),<sup>3</sup> which unlike graphene is non-conducting, but has the potential to find wider applications thanks to relative ease in synthesis and solution processability. Graphene oxide suspension when reduced using hydrazine, sodium borohydride, ascorbic acid, etc., forms reduced graphene oxide, which shows high charge mobility and therefore can be used in device applications.<sup>4</sup>

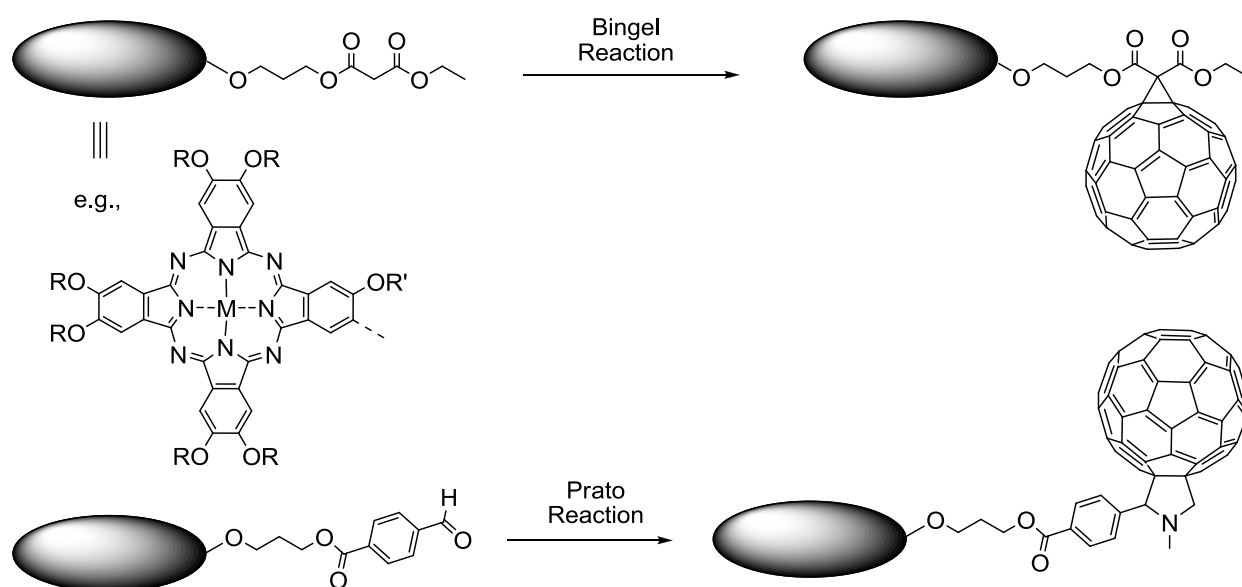
## 2.1.1 Carbonaceous nanoparticles in columnar liquid crystals.

### 2.1.1.1 Zero dimensional (0-D) spherical carbon nanoparticles in columnar liquid crystals.

Spherical carbon nanoparticles, commonly known as fullerenes, are hollow spheres composed of carbon atoms. After the discovery of this new allotrope of carbon in 1985, a huge amount of work has been carried out on fullerenes in the fields of supramolecular chemistry and materials science. Among the various fullerenes, such as  $C_{60}$ ,  $C_{70}$ , and  $C_{76}$ , the  $C_{60}$  has been studied extensively. The  $C_{60}$  molecule is a strong electron acceptor capable of accepting from one to six electrons to form the corresponding anions. The donor-acceptor conjugates of  $C_{60}$  with various organic donors have recently been extensively studied as photo-induced electron and/or energy transfer systems, and highly efficient photovoltaic cells have been prepared from these conjugates.<sup>5-6</sup> Fullerenes can be easily functionalized to yield various organic soluble  $C_{60}$  derivatives. To improve the physical properties of various thermotropic liquid crystals, efforts have been made to attach  $C_{60}$  covalently to mesogens as well as to disperse in liquid crystalline media. Both calamitic and discotic liquid crystals have been used to study the effects of  $C_{60}$  doping on phase behavior. Here we review briefly the dispersion of fullerenes in discotic liquid crystals and their covalent attachment with discotic mesogens is also discussed.

To attach  $C_{60}$  covalently with discotic molecules, primarily two synthetic routes have been explored. The first involves the Bingel reaction in which various discotic malonate derivatives are used. The Prato reaction,

using 1,3-dipolar cycloaddition reaction of  $C_{60}$  with an aldehyde terminated discotic molecule, is the other route to functionalize discotics with fullerenes (Scheme 1). A number of  $C_{60}$ -discotic adducts involving either one mesogen or two mesogens attached to a  $C_{60}$  molecule or two  $C_{60}$  molecules attached to one discotic molecule have been synthesized and studied for various properties.<sup>7-20</sup> Some representative examples are shown in Figure 1.



**Scheme 1.** Functionalization of discotic molecules with  $C_{60}$  via Bingel and Prato reactions.

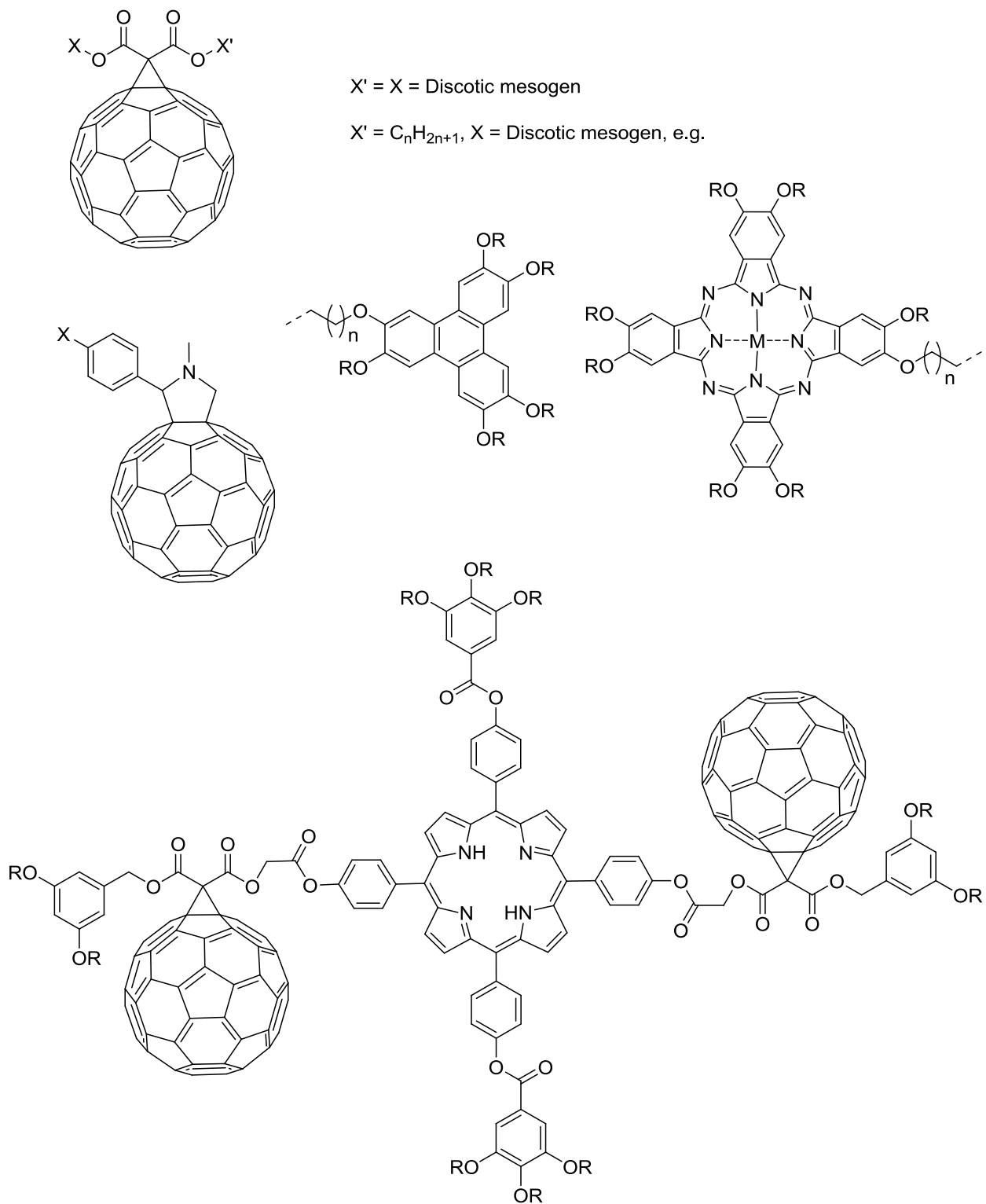


**Figure 1.** Some representative examples of discotic- $\text{C}_{60}$  adducts.

While a few C<sub>60</sub>-discotic adducts were reported to be liquid crystalline in virgin state, other can be dispersed in a columnar matrix without disturbing the mesophase behavior of the host. Bushby and co-workers observed a two-dimensional hexagonal superlattice from the ordering of fullerenes within the hexagonal columnar liquid-crystal matrix formed by a fullerene derivative and a hexaphenyl hexaazatriphenylene discotic. It is proposed that to maximize fullerene–fullerene contact, the fullerenes form chains that wrap around the central column in every group of seven columns.<sup>7</sup> A few C<sub>60</sub>-discotic nanocomposites have been successfully used to fabricate efficient solar cells.<sup>8, 14, 17</sup>

#### 2.1.1.2 One dimensional (1-D) carbon nanotubes in columnar liquid crystals.

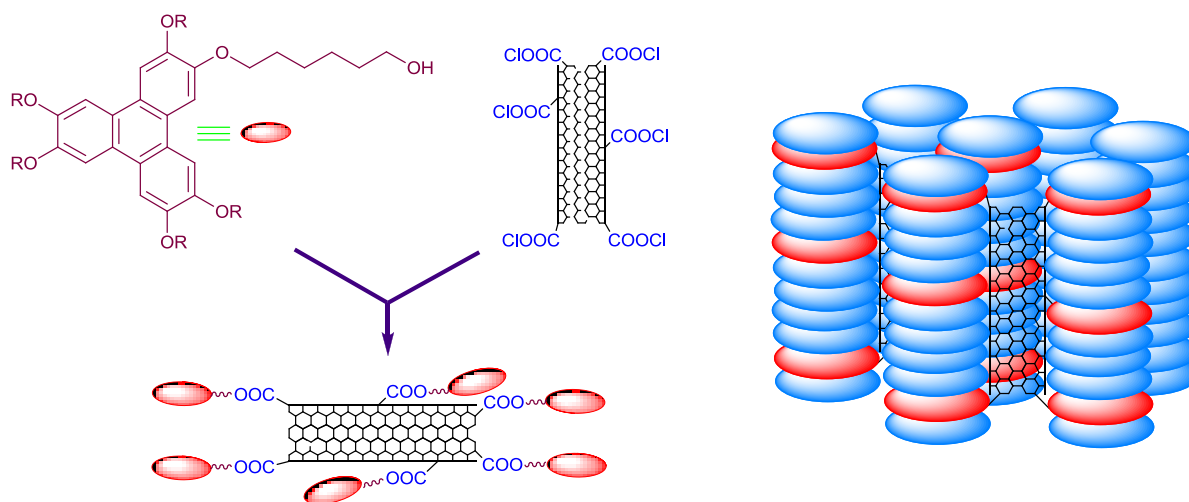
After the discovery of spherical synthetic carbon allotrope, fullerene, the existence of quasi-one-dimensional carbon nanotubes was reported by Iijima in the early 1990s.<sup>21</sup> Carbon nanotubes are seamless hollow cylinders of graphite with a high aspect ratio. Carbon nanotube formed by rolling up a single graphene sheet is called as single wall carbon nanotubes (SWNTs), while nanotubes formed by several graphene layers are defined as multi wall carbon nanotubes (MWNTs). Carbon nanotubes are either metallic or semiconducting, depending on their helicity. Accordingly their applications in the field of molecular electronics have been sought. Mechanically carbon nanotubes have been reported to be strongest material. Due to their remarkable electrical, mechanical and thermal properties, carbon nanotubes

have emerged as one of the most widely studied nanomaterials during the past two decades.

Both, SWNTs and MWNTs have been dispersed in many LCs and their effects on the electro-optical properties of LCs are extensively studied by several researchers.<sup>22-29</sup> DLCs and CNTs exhibit many similarities, e.g., both are anisotropic materials which self-assemble into hexagonal aggregates and exhibit 1D conducting properties. With the idea that cylindrical CNTs can be aligned in the cylindrical columns of discotic molecule (columnar mesophase), acid-purified SWNTs were tried to disperse into the columnar matrix of a triphenylene-based DLC.<sup>30</sup> However, it was observed that these purified SWNTs form aggregates in liquid crystal medium even in a very small concentration. This could be due to chemical noncompatibility (DLCs are non-polar hydrophobic molecules while acid-purified SWNTs are polar hydrophilic materials).

SWNTs were covalently coupled with hexaalkoxytriphenylene mesogens.<sup>30</sup> Carboxylic acid functionalities of acid-purified SWNTs were first converted to reactive acid chlorides which on classical esterification with a hydroxyl functionalized triphenylene derivative yields discotic-functionalized nanotubes (f-SWNTs) (Scheme 2). Spectral and thermal analysis confirmed the formation of discotic-functionalized nanotubes. The number of discotic molecules attached to CNTs were not sufficient to induce liquid crystallinity, however, these f-SWNTs were freely soluble in common organic solvents and therefore, they could be easily dispersed in organic-soluble DLCs. Accordingly, several composites of f-SWNTs and H4TP (having 1-10% of f-SWNTs in H4TP) were prepared and analyzed using POM, DSC

and XRD. Results indicate insertion of the f-SWNTs in the columnar matrix occupying the space between the disc columns (Scheme 2).



**Scheme 2.** Functionalization of SWNTs with discotics and their dispersion in a columnar matrix.

Organic soluble CNTs can also be prepared by attaching simple long aliphatic chains with acid functionalized CNTs. Octadecylamine (ODA)-functionalized SWNTs soluble in common organic solvents are now commercially available. Their dispersion in columnar phases of triphenylene and rufigallol-based discotic monomers and polymers was looked by Kumar and Bisoyi.<sup>31</sup> However, unlike discotic-functionalized SWNTs, which are more compatible with a discotic columnar phase, only a maximum of 2 wt.% of SWNTs could be homogeneously dispersed in the columnar matrix of these room-temperature DLCs. The pi-pi interactions of triphenylene molecules surrounding the SWNTs with the columnar phase forming triphenylene molecules will stabilize the dispersion of f-SWNTs. As the columnar phase of DLCs can be aligned parallel or perpendicular to the surface, the CNTs present in the composites would also be oriented in the

desired direction. It has recently been reported by Lee *et al.* that discotic ionic liquid crystals derived from triphenylene core can serve as excellent dispersants for pristine SWNTs.<sup>32</sup> These nanocomposites exhibit anisotropic conducting properties upon shearing the sample, and the shear-induced orientation of the SWNTs was maintained for a long period at room temperature. Kilinc *et al.* studied electrical properties of mesomorphic bis[tetrakis(alkylthio)phthalocyaninato]lutetium(III) double decker complexes [(CnS)<sub>4</sub>Pc]<sub>2</sub>Lu(III) doped with SWNTs.<sup>33</sup> The conductivities of [(CnS)<sub>4</sub>Pc]<sub>2</sub>Lu(III)-SWNT composites increased in the order of 10<sup>1</sup> to 10<sup>4</sup> and the conduction mechanism also changed from ohmic to space charge limited conduction. Zilberman *et al.* prepared discotic hexa-peri-hexabenzocoronene-functionalized CNTs based sensors for the analysis of volatile organic compounds, useful for detecting cancer.<sup>34-35</sup>

MWNTs have been mixed with naphthalene polymer based mesophase pitch.<sup>36</sup> Cho *et al.* mixed MWNTs with mesophase pitch (in the molten state) and successfully melt-spun into fibers containing 0.1 and 0.3 wt.% MWNTs. Microstructural examination reveals that whereas the carbon fibers obtained from pure mesophase pitch had a radial texture of graphene layers, the nanotube-modified fibers had a random texture. Crawford and co-workers looked the capillary infiltration of naphthalene polymer, which exhibits a discotic nematic liquid crystal phase at elevated temperature, into multiwall carbon nanotubes.<sup>37</sup> The MWNTs were first oxidized at 700 °C to open the nanotube tips. When a mixture of tip-opened MWNTs and finely ground solid naphthalene polymer were heated to 300 °C, the polymer in the discotic nematic phase infiltrates into the nanotube cavities. High resolution

transmission electron microscopy (HR-TEM) was used to visualize the director profile inside the 5 nm cavity of a multiwall carbon nanotube. The discotic planes lie approximately parallel to the tube sidewalls due to strong pi-pi interactions at the interface.

### 2.1.1.3 Two dimensional (2-D) graphene in columnar liquid crystals.

Though the presence of graphene layers in graphite is known for a long time, its synthesis and characterization could be achieved only recently. Graphene, the two-dimensional allotrope of carbon, is a monolayer of carbon atoms arranged in a honeycomb lattice. This nanomaterial has recently been found to display outstanding electrical, optical, mechanical, charge transport and thermal properties and, therefore, its applications in many devices has been sought.<sup>38-39</sup> Most of the discotic liquid crystals are derived from polycyclic aromatic hydrocarbon (PAH) cores. Benzene is the first and smallest PAH core, while graphene may be considered as the ultimate member. In between them, there exist several PAH cores such as, naphthalene, phenanthrene, pyrene, triphenylene, perylene, dibenzopyrene, truxene, decacyclene, hexabenzocoronene, etc., which form discotic liquid crystals on appropriate peripheral substitution.<sup>40</sup> As graphene is a sheet-like nano-object with very high aspect ratio, it was anticipated that upon dispersion in sufficiently high concentrations it would exhibit liquid crystalline behavior. This has indeed been proved by Pasquali and co-workers.<sup>41</sup> Graphite spontaneously exfoliates into single-layer graphene in chlorosulphonic acid and dissolves at isotropic concentrations as high as 2

mg/ml. When the precipitated soluble graphene powder was re-dispersed in about 20 mg/ml concentration and centrifuged, the spontaneous formation of liquid crystalline phase was observed. The observed liquid crystalline Schlieren texture was very similar to typical discotic nematic mesophase texture. A number of studies have been carried out to prepare discotic lyotropic liquid crystals from graphene oxide.<sup>42-44</sup> Gao *et al.* have shown that discotic chromonic liquid crystals can be used to prepare graphene sheets.<sup>45</sup>

## 2.2 Objective

In this work we have prepared octadecylamine functionalized reduced graphene oxide, this functionalized graphene is introduced in anthraquinone based columnar liquid crystal, influence of the functionalized graphene on mesophase is studied using POM, XRD, DSC studies, and the mutual ordering is probed using SEM and Cryo-SEM imaging. The influence of dopants on conductivity of the mesophase has also been studied.

## 2.3 Experimental

### 2.3.1 Synthesis of Graphene oxide

Graphene oxide is synthesized from graphite by the Hummers method.<sup>3</sup> A round bottom flask was maintained in an ice bath to control sudden change in temperature, 10g of graphite powder was taken in this round

bottom flask, to which 5g of sodium nitrate was added and stirred after adding 250 ml of Conc.  $\text{H}_2\text{SO}_4$ . To this, 30g of  $\text{KMnO}_4$  is added slowly taking into care that temperature of the suspension does not exceed  $20^\circ\text{C}$ . The ice bath is then removed and temperature was maintained at  $35^\circ\text{C}$  for 30 minutes. After which 460 ml of water was added slowly. The temperature increases to  $98^\circ\text{C}$ . It was maintained at this temperature for 15 minutes, after which it was diluted with 1500ml of Millipore water treated with 3% hydrogen peroxide and filtered when it was still warm. The graphite oxide flakes were re-dispersed in water by sonication. Finally graphene oxide was obtained after centrifugation at 5000 rpm and air drying.

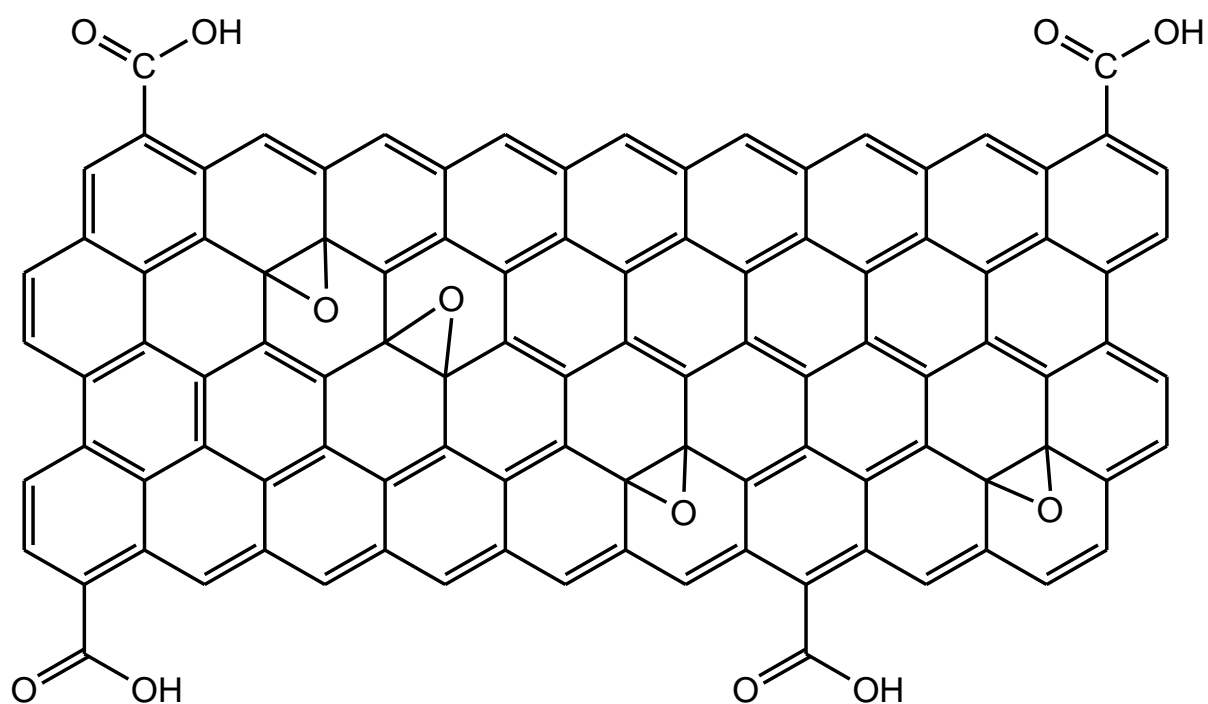
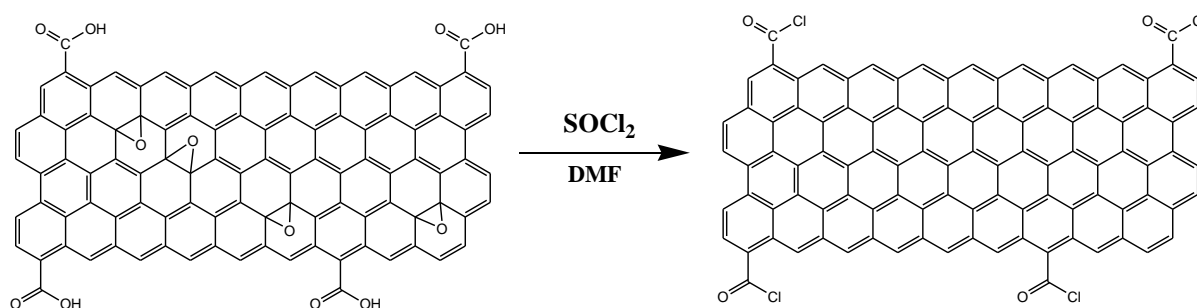


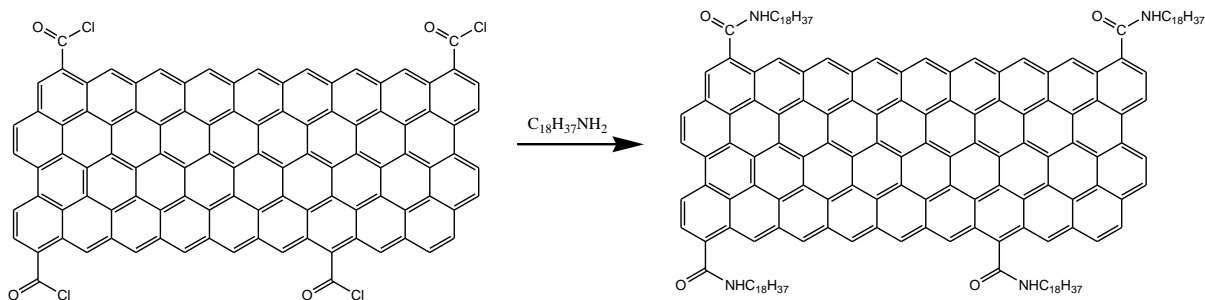
**Figure 2.** Chemical representation of graphene oxide sheet.

### 2.3.2 Functionalisation of graphene oxide with octadecylamine

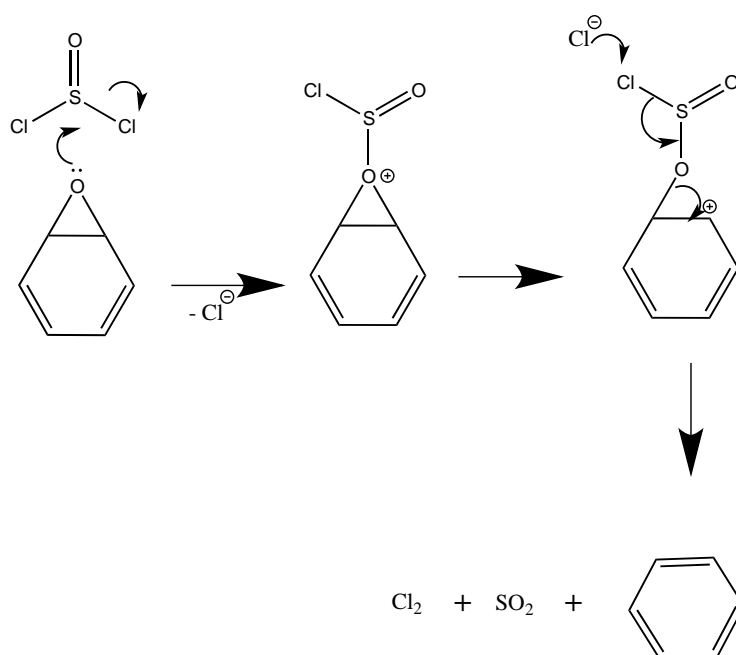
Graphene oxide obtained was functionalized with octadecylamine by following the procedure opted by Haddon *et al.*<sup>46</sup> Graphite oxide (500 mg) obtained from the Hummers method was added to 2.5 ml of N,N-dimethylformamide (DMF) and refluxed in 100ml of  $\text{SOCl}_2$ , at 70 °C for 24 hours, under anhydrous condition. The excess thionyl chloride was distilled off after the reaction (Scheme 3). The acylated graphene oxide was allowed to react with 2.7 g of octadecylamine at 120 °C for 4 days (Scheme 4). The resultant product was dissolved in hot ethanol and filtered through 0.2  $\mu\text{m}$  (PTFE) membrane and washed well with hot ethanol to remove unreacted impurities. The final product octadecylamine functionalized graphene oxide (f-graphene) was dispersed in AR grade chloroform. Functionalization of graphene oxide with octadecylamine in the presence of thionyl chloride leads simultaneously to the reduction of graphene oxide (Scheme 5).



**Scheme 3.** Converting the acid groups in graphene oxide into acid chlorides.



**Scheme 4.** Converting the graphene acid chlorides into amides with octadecylamine.



**Scheme 5.** Mechanism explaining reduction of epoxide.

The characterization of f-graphene is presented in the results and discussion part.

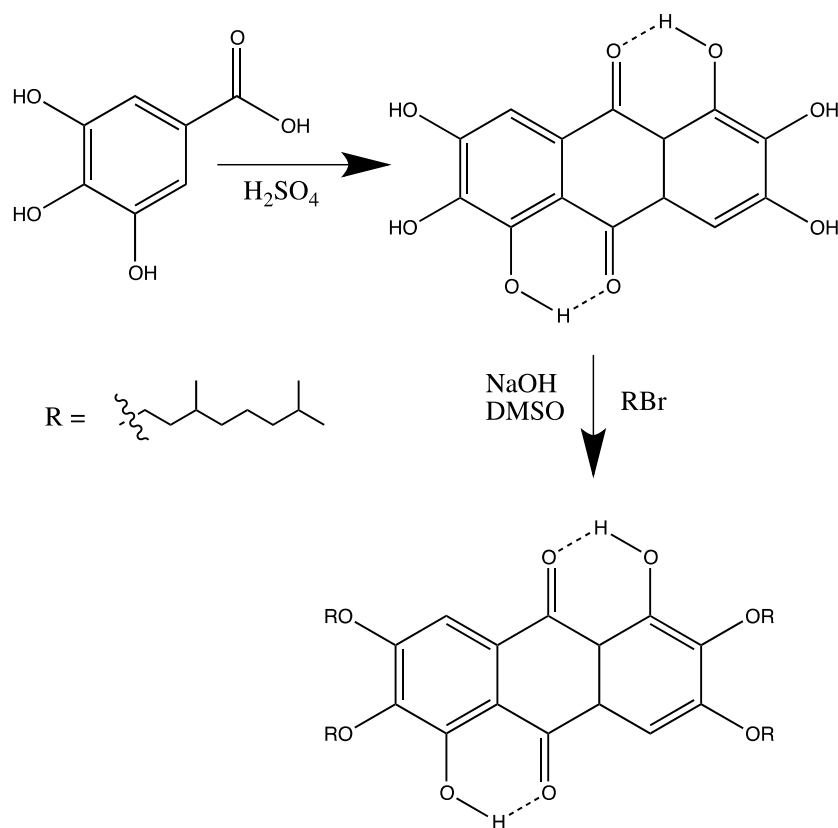
### 2.3.3 Synthesis of rufigallol

Rufigallol was prepared using the synthetic procedure developed by Grimshaw *et al.*<sup>47</sup> Anhydrous gallic acid (5 g) was dissolved in 98% sulphuric

acid (15 mL) and heated with stirring at 100 °C for 2 hrs, the resultant mixture was cooled, and poured into excess of water. The resulting orange precipitate was washed well with water, and then dried. In order to enhance purity, the precipitate was acetylated by refluxing with acetic anhydride (15 mL) and sulphuric acid (3 drops) for 2 hrs. On cooling, the hexa-acetate, separated as yellow plates and it was recrystallized from acetic anhydride. For hydrolysis, the crystallised acetate (1 g) was dissolved in boiling pyridine (20 mL), and acetic acid (25 mL) was added; a deep purple solution resulted. When concentrated hydrochloric acid (20 mL) was added down the condenser, the mixture became orange and deposited rufigallol as a scarlet powder which was collected when cold.

#### **2.3.4 Synthesis of 1,5-dihydroxy- 2,3,6,7-tetrakis(3,7-dimethyloctyloxy)-9,10-anthraquinone**

Synthetic procedure established by Kumar *et al.* was followed to synthesize 1,5-dihydroxy- 2,3,6,7-tetrakis(3,7-dimethyloctyloxy)-9,10-anthraquinone.<sup>31</sup> To a solution of rufigallol (1.52 g), 3,7-dimethyloctylbromide (4.86 g) in DMSO (10 mL) was added NaOH (0.8 g) and the mixture was stirred for about 20 hrs at 90 °C. After cooling the reaction mixture, water was added and the aqueous solution was extracted with chloroform. After solvent evaporation the product was precipitated from chloroform into methanol several times to obtain the pure product.



**Scheme 6.** Synthesis route to obtain 1,5-dihydroxy- 2,3,6,7-tetrakis(3,7-dimethyloctyloxy)-9,10-anthraquinone.

### 2.3.5 Preparation of composites.

1,5-dihydroxy-2,3,6,7-tetrakis(3,7-dimethyloctyloxy)-9,10-anthraquinone (RTAQ) used as the host liquid crystal. Two composites 1GrAQ and 5GrAQ are prepared for studies. 1GrAQ is prepared by taking 99 mg of RTAQ and adding 1mg of f-graphene, both are dissolved in chloroform and sonicated for one hour, after which solvent is removed by heating (under sonication). Similarly 5GrAQ is prepared by mixing 95mg of RTAQ and 5mg of f-graphene.

**Table 1.** Describes the composition of 1GrAQ and 5GrAQ

Sample	RTAQ (mg)	f-graphene (mg)	Doping percentage
1GrAQ	99	1	1%
5GrAQ	95	5	5%

### 2.3.6 Instruments

Fourier transform infrared (FT-IR) spectra were recorded as KBr discs on Shimadzu FTIR-8400. X-Ray diffraction studies (XRD) were carried out on unoriented samples using Cu-K $\alpha$  ( $\lambda = 1.54 \text{ \AA}$ ) radiation from a Rigaku Ultrax 18 rotating anode generator (5.4 kW) monochromated with a graphite crystal. The samples were held in sealed Lindemann capillary tubes (0.7 mm diameter) and the diffraction patterns were collected on a two-dimensional Mar research image plate. Elemental analysis was performed on Carlo-Erba Flash 1112 analyser. High Resolution Transmission Electron Microscope images of samples were recorded with JEOL JEM 2100 HRTEM. SEM images were recorded with Ultra plus FE-SEM. XPS of the samples were recorded in an ESCA-3 Mark II spectrometer (VG Scientific Ltd., England). Raman spectra were recorded with LabRAM HR High Resolution Raman spectrometer (Horiba Jobin Yvon, USA), using a He-Ne Laser ( $\lambda=632.8 \text{ nm}$ ). DSC of Liquid crystals and Composites were taken at the temperature range of 5 °C to 150 °C using Parkin-Elmer Pyris-1 DSC. Optical textures of mesophases were observed using Olympus-POM-018 Polarized Optical

Microscope.<sup>1</sup>H NMR and <sup>13</sup>C NMR were recorded on Bruker 500 MHz machine using deuterated chloroform (CDCl<sub>3</sub>) as solvent and tetramethylsilane as internal standard.

### **2.3.7 Conductivity Measurements**

The conductivity of the samples were measured in a indium tin oxide coated glass sandwich cells (10mm X 5mm) of 10 micron thickness and the sample were filled into the cells by heating to isotropic phase. The cell was heated and the temperature was recorded with resistance temperature detector (RTD). A voltage of 1V was applied from a standard voltage source. The current measurements were carried out using a Keithley picoammeter under ambient conditions.

## **2.4 Results and discussions.**

The functionalization and reduction of graphene oxide is confirmed by IR spectroscopy, elemental analysis, and X-ray diffraction analysis. IR Spectra of f-graphene (Figure 3) shows peaks at 3728 cm<sup>-1</sup> and 1690 cm<sup>-1</sup> which correspond to amide NH and amide carbonyl stretching respectively these peaks are absent in the IR Spectra of graphene oxide. The absence of peaks around 1200 cm<sup>-1</sup> and 850 cm<sup>-1</sup> in f-graphene shows absence of epoxy groups.

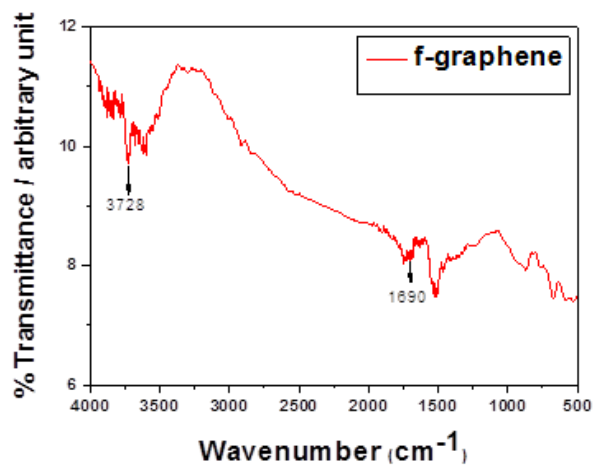


**Figure 3.** IR spectra of octadecylamine functionalized reduced graphene oxide.

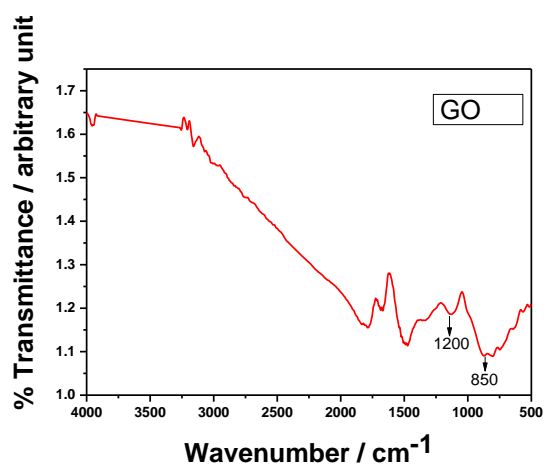


**Figure 4.** IR spectra of graphene oxide

Elemental analysis of f-graphene (Table 2) shows a marked increase in carbon content of graphene oxide after functionalization and reduction. The measured values are similar to that of reduced graphene oxide.<sup>48</sup>

**Table 2.** Elemental analysis data of graphene oxide (GO) and octadecylamine functionalized graphene oxide (f-graphene).

Sample	C (%)	H (%)	N (%)
GO	46.43	2.12	0
f-graphene	73.37	4.63	5.42

The XRD intensity vs.  $2\theta$  plot of GO (Figure 5) showed a peak at 11 degrees which corresponds to the spacing between two graphene oxide sheets of 8 Å. After the functionalization (and reduction) of graphene oxide the peak shifted to 23.8 degrees, which corresponds to a spacing of 3.3 Å (Figure 6). This confirms the reduction of graphene oxide leading to the formation of closely spaced layers of reduced graphene oxide. Raman spectra of GO (Figure 7) shows D bands at  $1340\text{ cm}^{-1}$  and G band at  $1592\text{ cm}^{-1}$ . The f-graphene shows D band at  $1337\text{ cm}^{-1}$  and G band at  $1591\text{ cm}^{-1}$ . The intensity of D band is higher compared to G band in both GO and f-graphene, this is due to increase in deformation due to oxidation.

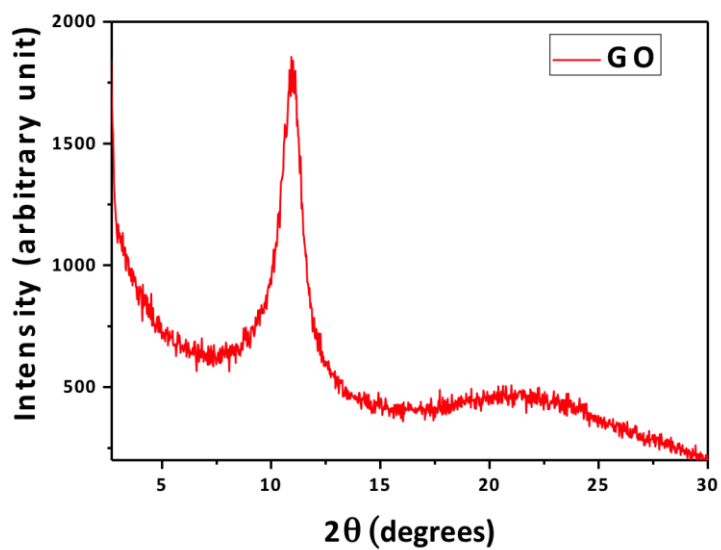


**Figure 5.** One dimensional intensity vs.  $2\theta$  plot of graphene oxide.

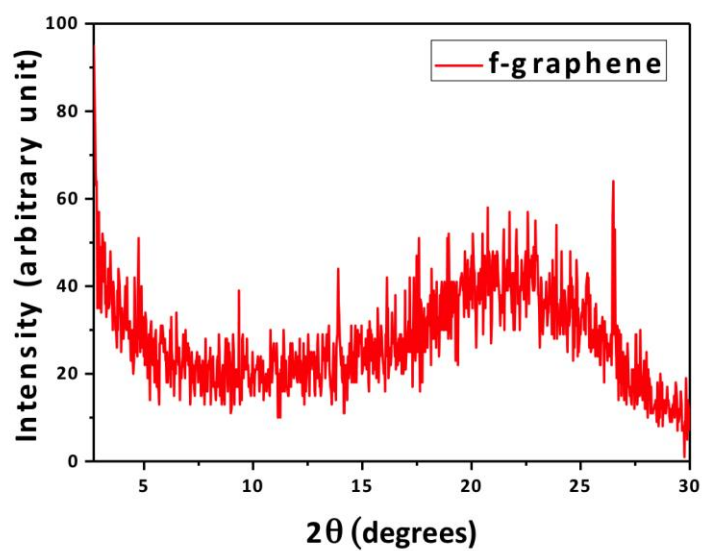


**Figure 6.** One dimensional intensity vs.  $2\theta$  plot of octadecylamine functionalized reduced graphene oxide.

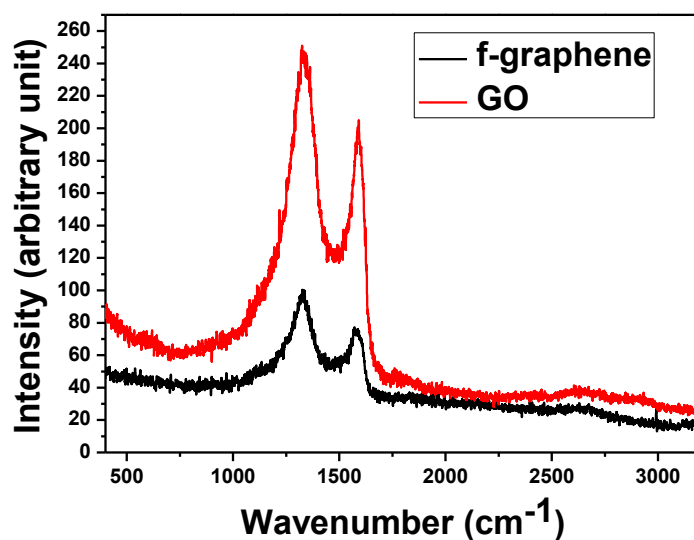


**Figure 7.** Raman spectra of graphene oxide (red), and octadecylamine functionalized reduced graphene oxide (black).

The chemical structure and purity of 1,5-dihydroxy-2,3,6,7-tetrakis(3,7-dimethyloctyloxy)-9,10-anthraquinone were established by FT-IR,  $^1\text{H}$  NMR and elemental analysis. The IR spectra showed an absorption peak at  $1616\text{ cm}^{-1}$ , characteristic of an intra-molecular hydrogen-bonded anthraquinone carbonyl moiety in addition to other aromatic, methylene and methyl absorption peaks. The  $^1\text{H}$  NMR (Figure 8) showed a singlet resonance at  $\delta$  12.7 ppm integrating for two protons, characteristic of an intra-molecular hydrogen-bonded phenoxy hydrogen and another singlet resonance at  $\delta$  7.4 ppm corresponding to the two aromatic protons in addition to the methylene and methyl resonances.

**<sup>1</sup>H NMR** (500 MHz; CDCl<sub>3</sub>) δ = 12.71 (2H, Ar-OH), 7.36 (2H, Ar-H), 4.13 (8H, ArOCH<sub>2</sub>), 1.86-1.13 (40 H, aliphatic protons); 1.09-0.91 (36 H, aliphatic CH<sub>3</sub>).

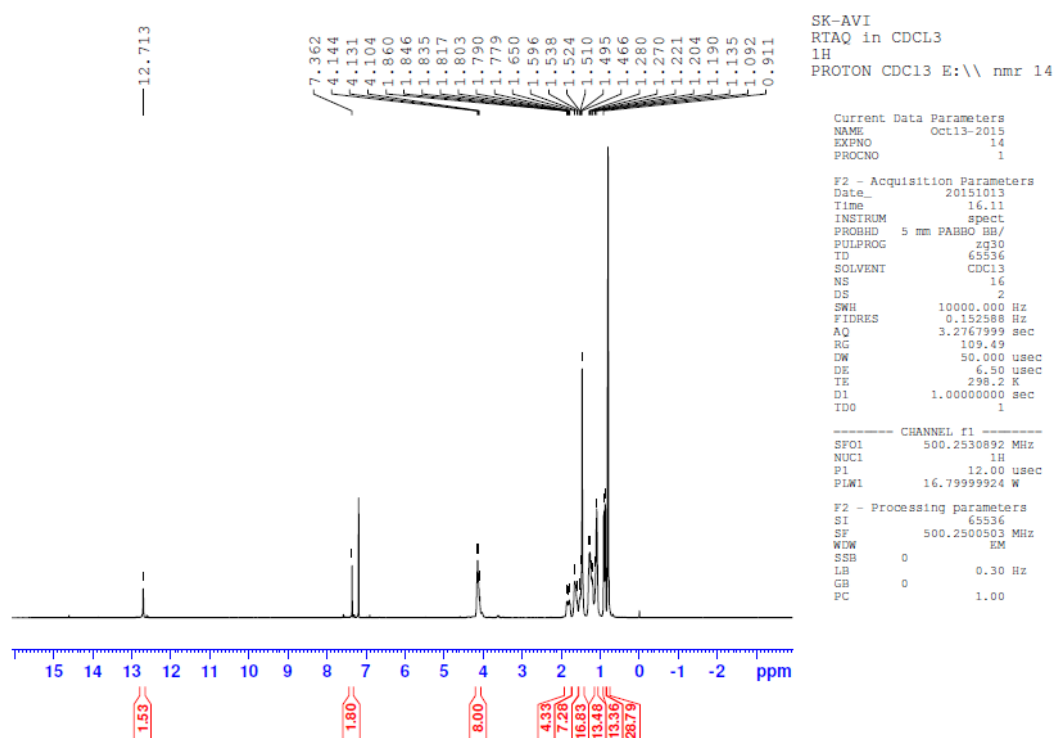


**Figure 8.** <sup>1</sup>H NMR spectrum of 1,5-dihydroxy-2,3,6,7-tetrakis(3,7-dimethyloctyloxy)-9,10-anthraquinone

These DLC-graphene nanocomposites (1GrAQ and 5GrAQ) were analysed by UV-Vis, POM, DSC, XRD, Raman spectroscopy, and conductivity studies. UV-Vis spectra of the RTAQ is compared with

composites 1GrAQ and 5GrAQ respectively (Figure 9). Both the pure and doped samples exhibit peaks at the same wavelength, indicating the absence of any strong charge transfer complex formation between f-graphene and RTAQ.

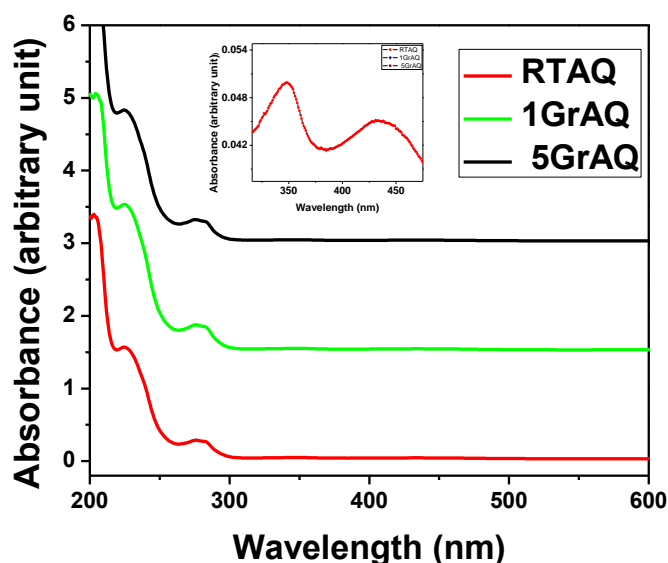


**Figure 9.** UV-Vis spectra of RTAQ (red), 1GrAQ (green), 5GrAQ (black) all recorded by spin coating respective solution in chloroform on a quartz slide. Inset shows the expanded region of RTAQ spectra between 300nm – 500nm.

The XRD patterns of all the compounds are recorded at room temperature and the intensity vs.  $2\theta$  derived from diffraction pattern is shown in (Figure 10). In the small angle region four peaks in the ratio of  $1 : 1/\sqrt{3} : 1/2 : 1/\sqrt{7}$  are seen with strong first peak while the rest three are weak. The ratios validate columnar hexagonal ordering. In wide angle region there are two broad peaks with the one centered at  $4.8\text{\AA}$  is due to liquid like

branched chains found on the periphery of discotics. The other one is a small peak at 3.34 Å corresponding to core – core separation of discotic molecules within the column of mesophase. The doping of octadecylamine functionalized reduced graphene oxide does not change the order, with both the composites retaining mesomorphic nature.

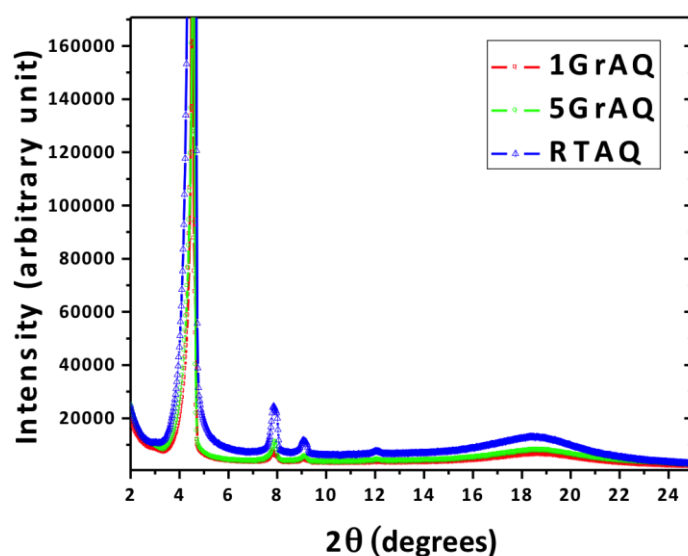


**Figure 10.** One dimensional intensity vs.  $2\theta$  and XRD pattern of RTAQ (blue), 1GrAQ (red), 5GrAQ (green)

Both composites exhibit optical texture typical of columnar hexagonal mesophase similar to RTAQ (Figure 11) under polarized optical microscope (POM), at lower concentration (1%) aggregates of reduced graphene oxide sheets are not visible in the POM, but at higher concentration (5%) these aggregates are evident, indicating that f-graphene is not uniformly distributed in the discotic system.

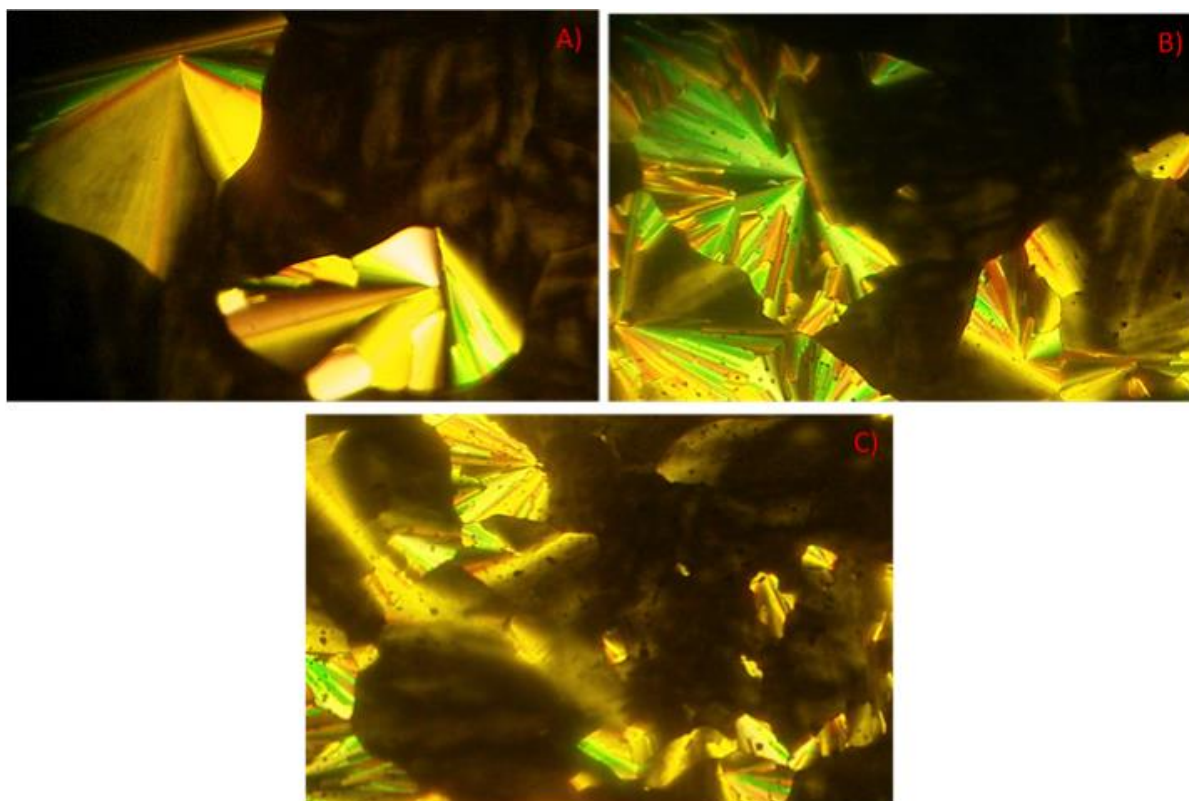


**Figure 11.** Polarizing Optical Microscope image of A) RTAQ, B) 1GrAQ, C) 5GrAQ (at 70 °C crossed polarizers, 50 X magnification).

Differential scanning calorimetry (DSC) of RTAQ, 1GrAQ and 5GrAQ are recorded at a rate of 10 °C/min to find transition temperature and enthalpy associated with it (Figure 12). The parent RTAQ compound shows a sharp clearing peak at 115.6 °C. The composites 1GrAQ and 5GrAQ show a relatively broad clearing peak at 117.3 °C and 116.7 °C respectively. The increase in clearing temperature indicates that the doping of f-graphene stabilizes the discotic mesophase. This is due to enhanced local ordering of discotics on the surface of f-graphene owing to the pi-pi stacking between their aromatic cores.

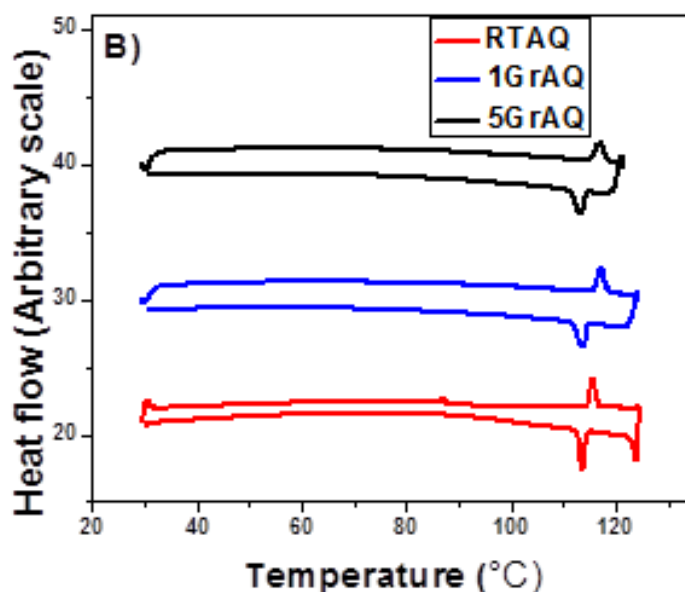


**Figure 12.** Differential Scanning calorimetry of RTAQ (red), 1GrAQ (blue), 5GrAQ (black) all recorded at scan rate of  $10\text{ }^{\circ}\text{C min}^{-1}$

To further understand the ordering of f-graphene in columnar structures Cryo-SEM of RTAQ, 1GrAQ and 5GrAQ were recorded. The Cryo-SEM images of RTAQ showed spherical structures (Figure 13a) no layered structure was present throughout the image, while SEM image of f-graphene show crumpled sheets (Figure 13b) on closer observation (Figure 13c), one can see layered structure of the graphene sheets, these structures are similar to images obtained for reduced graphene oxide.<sup>49-50</sup> The Cryo-SEM images of composite 1GrAQ (Figure 13d&13e) surprisingly showed a layered structure unlike that of pure RTAQ, though the amount of f-graphene doped was only 1%. Layers observed in Cryo-SEM images of 1GrAQ are more ordered than that of f-graphene. Discotic liquid crystals acts like glue binding to f-graphene due to pi-pi interaction between aromatic cores, thus leading to ordered arrangement of deformed f-graphene sheets. On closely

observing the Cryo-SEM images of 1GrAQ composites, one can see domains of liquid crystals present on f-graphene layers (Figure 13f), which are absent in f-graphene SEM images.

Based on the Cryo-SEM images, DSC and POM results. We propose a sandwich like structure, where discotics arrange themselves in between f-graphene sheets as shown in the model (Scheme 7), arrangement of discotics in between these layers gives rise to dark domains (aggregates) in 5GrAQ when observed under POM.

The conductivity measurements of the pure compound and composites were carried out to see the effects of f-graphene doping on anthraquinone based discotic liquid crystal. RTAQ sample showed conductivity of  $3.43 \times 10^{-8} \text{ Sm}^{-1}$  at  $41^\circ\text{C}$ . The doped samples show much higher conductivity. The sample 1GrAQ showed a conductivity of  $6.8 \times 10^{-5} \text{ Sm}^{-1}$  at  $41^\circ\text{C}$ . In this case as well the conductivity decreased with increase in temperature and finally reached a value of  $2.98 \times 10^{-7} \text{ Sm}^{-1}$  at isotropic phase. Sample 5GrAQ shows a conductivity of  $1.9 \times 10^{-4} \text{ Sm}^{-1}$  at  $41^\circ\text{C}$  which decreases to about  $10^{-5} \text{ Sm}^{-1}$  at lower temperature (Figure 14).

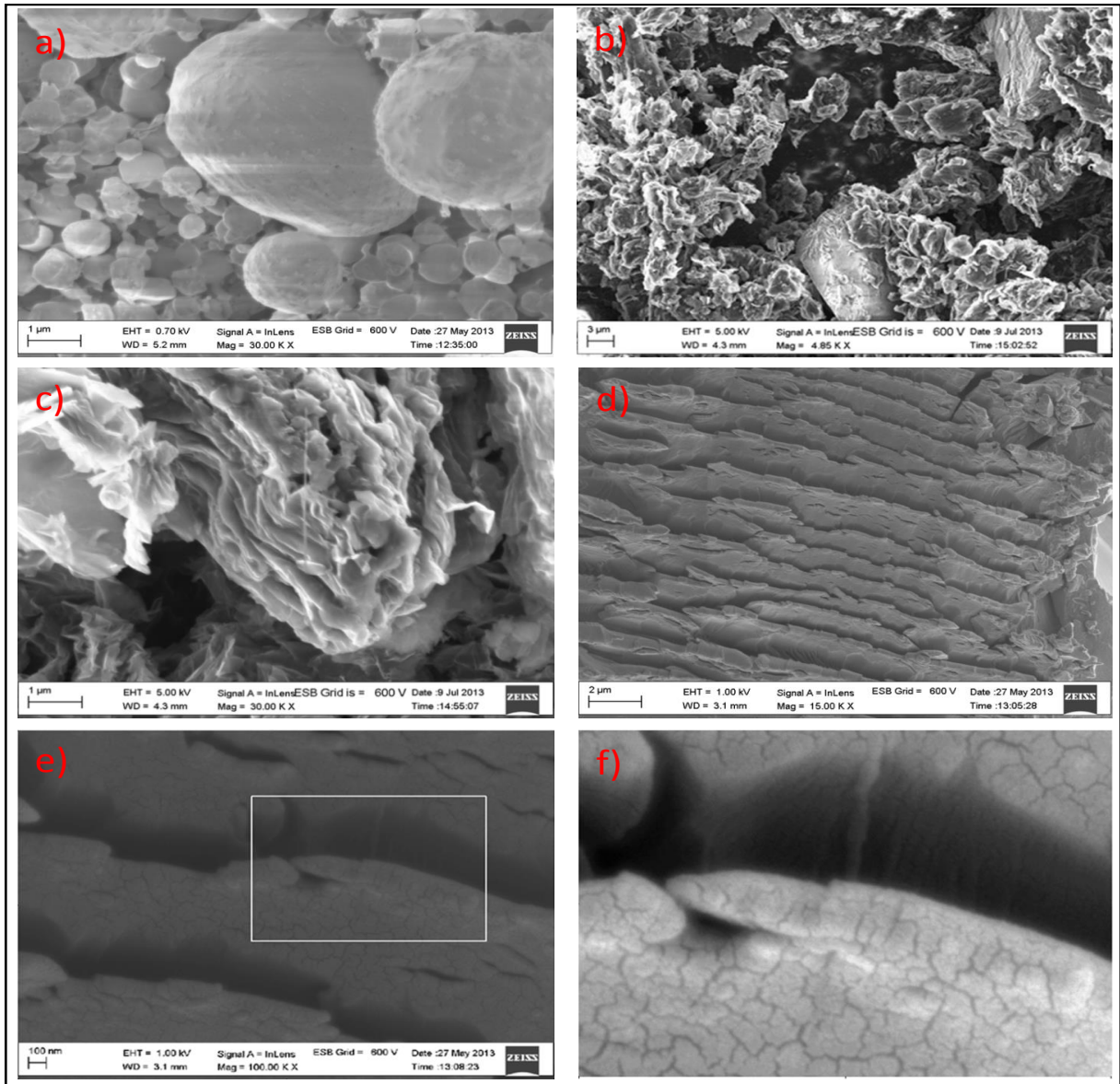


**Figure 13.** (A) Cryo-SEM image of RTAQ (B & C) SEM images of f-Graphene showing layered structure forming crumpled bundles. (D & E) 1GrAQ composite is showing a layered structure. (F) Enlarged portion of (E) shows graphene layers covered by layer of Discotics.

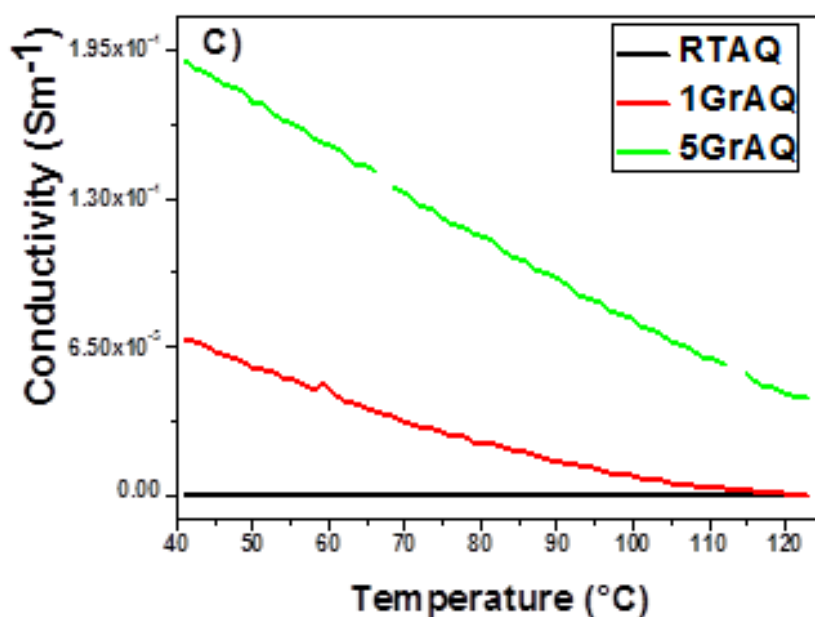


**Figure 14.** The variation of measured DC conductivity values as a function of temperature for RTAQ (black), 1GrAQ (red), 5GrAQ (green).

The enhancement of conductivity can be ascribed to ordered arrangement of discotic and f-graphene, f-graphene acts as conductive fillers which bridge the defects within the columnar matrix thus enhancing the conductivity by three to four orders of magnitude. In order to explain the decrease in conductivity with temperature, we recorded the XRD of the RTAQ as a function of temperature (Figure 15). The core-core distance increases (from 3.37 Å to 3.44 Å) as the temperature increases from room temperature to 80 °C. This change in the core to core distance leads to a decreased overlap between discotic cores, which results in decrease of conductivity with increase in temperature.

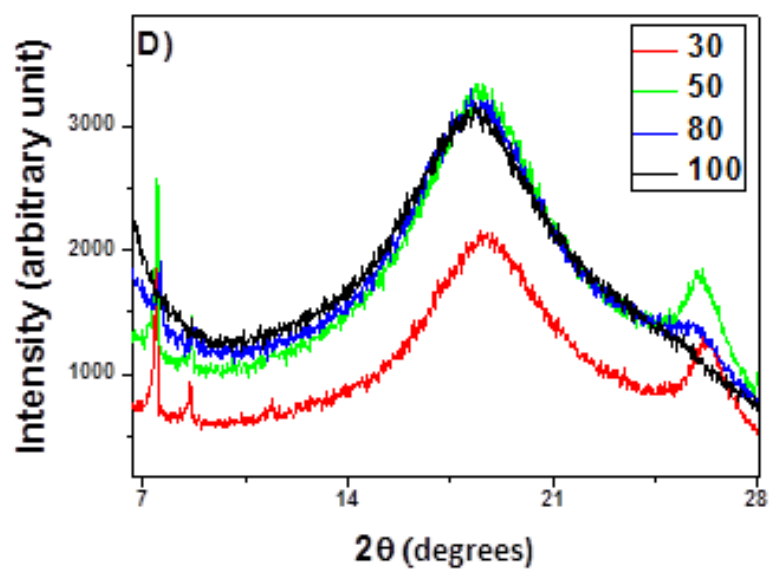
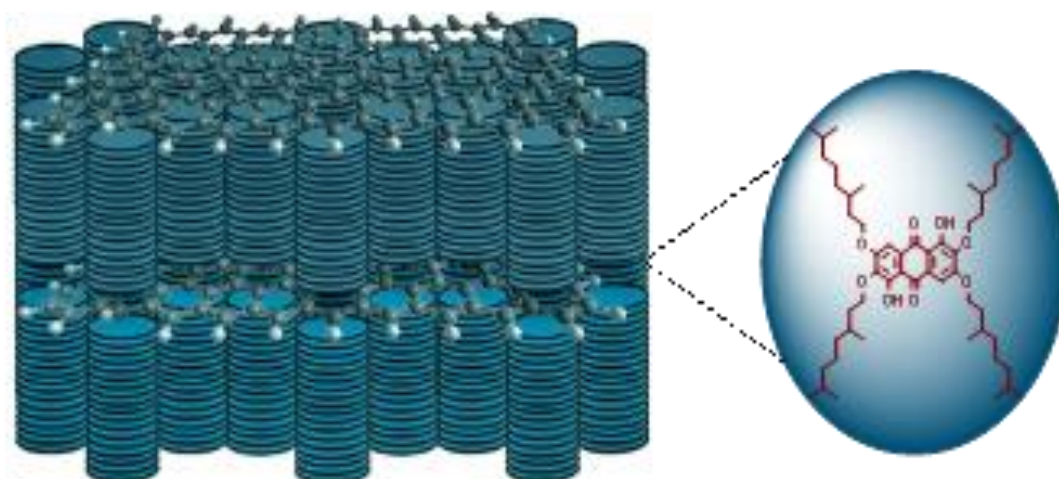


**Figure 15.** One dimensional intensity vs.  $2\theta$  plot of RTAQ recorded as a function of temperature 30°C (red), 50°C (green), 80°C (blue), 100°C (black).



**Scheme. 7** Schematic illustration of sandwich like self-assembly of discotic liquid crystal-graphene nanocomposite.

## 2.5 Conclusions

In conclusion, we have shown that f-graphene can be efficiently dispersed in the supramolecular order of DLCs. These composites show higher transition temperatures compared to pure DLC due to enhanced ordering of discotics on the surface of reduced graphene oxide owing to strong pi-pi attraction. Cryo-SEM images of the composites show us that discotics and graphene are mutually ordered into sandwich like structures. We have also found that these composites show higher conductivity compared to pure DLC. The f-graphene fillers act as bridges across columnar defects resulting in efficient charge transport. The creation of sandwich like self-assembly with DLCs may widen the applicability of these graphene derivatives in materials science. Ordered structures can be simply achieved through self-organization of a variety of interacting molecular components. The creation of such molecular buildings via self-assembly of LCs may lead to the induction of dynamically functional properties such as facile charge and energy migration in self-organized systems. The construction of such ordered molecular architectures is essential for the realization of next-generation electronic devices.

## 2.6 References

1. Hirsch, A., The Era of Carbon Allotropes. *Nat. mat.* 2010, 9, 868-871.
2. Novoselov, K. S.; Geim, A. K.; Morozov, S. V.; Jiang, D.; Zhang, Y.; Dubonos, S. V.; Grigorieva, I. V.; Firsov, A. A., Electric Field Effect in Atomically Thin Carbon Films. *Science* 2004, 306, 666-669.
3. Jr, H. W. S.; Offeman, R. E., Preparation of Graphitic Oxide. *J. Am. Chem. Soc.*, 1958, 80 (6), pp 1339–1339.
4. Chen, D.; Feng, H.; Li, J., Graphene Oxide: Preparation, Functionalization, and Electrochemical Applications. *Chem. rev.* 2012, 112(11), 6027-6053.
5. Li, C.-Z.; Yip, H.-L.; Jen, A., Functional Fullerenes for Organic Photovoltaics. *J. Mat. Chem.* 2012, 22, 4161-4177.
6. Shrestha, L. K.; Ji, Q.; Mori, T.; Miyazawa, K., Fullerene Nanoarchitectonics: From Zero to Higher Dimensions. *Chem. Asian Journal* 2013, 8, 1662.
7. Bushby, R. J.; Hamley, I. W.; Liu, Q.; Lozman, O. R., Self-Assembled Columns of Fullerene. *J. Mater. Chem.*, 2005, 15, 4429-4434.
8. Dao, Q. D.; Hori, T.; Fukumura, K.; Masuda, T., Efficiency Enhancement in Mesogenic-Phthalocyanine-Based Solar Cells with Processing Additives. *Appl. Phys. Lett.*, 2012, 101, 263301.

9. de la Escosura, A.; Martínez-Díaz, M. V., Self-Organization of Phthalocyanine-[60] Fullerene Dyads in Liquid Crystals. *J. Org. Chem.*, 2008, 73 (4), pp 1475–1480
10. Deschenaux, R.; Donnio, B.; Guillon, D., Liquid-Crystalline Fullerodendrimers. *New J. Chem.* 2007,31, 1064-1073.
11. Geerts, Y. H.; Debever, O.; Amato, C., Synthesis of Mesogenic Phthalocyanine-C60 Donor–Acceptor Dyads Designed for Molecular Heterojunction Photovoltaic Devices. *Beilstein J. Org. Chem.* 2009, 5, No. 49.
12. Hayashi, H.; Nihashi, W.; Umeyama, T., Segregated Donor–Acceptor Columns in Liquid Crystals That Exhibit Highly Efficient Ambipolar Charge Transport. *J. Am. Chem. Soc.* 2011, 133 (28), pp 10736–10739.
13. Ince, M.; Martínez-Díaz, M. V.; Barberá, J., Liquid Crystalline Phthalocyanine–Fullerene Dyads. *Mater. Chem.* 2011, 21, 1531-1536.
14. Jurow, M. J.; Hageman, B. A.; DiMasi, E.; Nam, C. Y., Controlling Morphology and Molecular Packing of Alkane Substituted Phthalocyanine Blend Bulk Heterojunction Solar Cells. *J. Mater. Chem. A*, 2013, 1, 1557-1565.
15. Kamei, T.; Kato, T.; Itoh, E.; Ohta, K., Discotic Liquid Crystals of Transition Metal Complexes 47: Synthesis of Phthalocyanine-Fullerene Dyads Showing Spontaneous Homeotropic Alignment. *J. Porphyrins Phthalocyanines*, 2012, 16, 1261.

16. Manickam, M.; Smith, A.; Belloni, M.; Shelley, E. J., Introduction of Bis-Discotic and Bis-Calamitic Mesogenic Addends to C 60. *Liq. Crystal.* 2002, Vol. 29, No. 4, 497±504.
17. Sun, Q.; Dai, L.; Zhou, X.; Li, L.; Li, Q., Bilayer-and Bulk-Heterojunction Solar Cells Using Liquid Crystalline Porphyrins as Donors by Solution Processing. *Appl. Phys. Lett.* 2007, 91, 253505.
18. Wang, C. L.; Zhang, W. B.; Hsu, C. H.; Sun, H. J.; Horn, V. R. M., A Supramolecular Structure with an Alternating Arrangement of Donors and Acceptors Constructed by a Trans-Di-C 60-Substituted Zn Porphyrin Derivative in the Solid. *Soft Matter*, 2011, 7, 6135-6143.
19. Wang, C. L.; Zhang, W. B.; Sun, H. J., A Supramolecular “Double Cable” Structure with a 12944 Helix in a Columnar Porphyrin C60 Dyad and Its Application in Polymer Solar Cells. *Advanced Energy Materials* 2011, 2(11), 1375-1382.
20. Yang, F.; Guo, H.; Xie, J.; Liu, Z.; Xu, B., Synthesis and Mesomorphic Property of Novel Discotic C60-Triphenylene Derivative. *Letters in Organic Chemistry*, 2011, 8, 599-602(4).
21. Iijima, S., Helical Microtubules of Graphitic Carbon. *Nature* 1991, 357.
22. Dhar, R.; Pandey, A. S.; Pandey, M. B.; Kumar, S., Optimization of the Display Parameters of a Room Temperature Twisted Nematic Display Material by Doping Single-Wall Carbon Nanotubes. *Appl. Phys. Exp.* 2008, 1, 121501.

23. Jan, P. F. L.; Giusy, S., Carbon Nanotubes in Liquid Crystals. *J. Mater. Chem.*, 2008, 18, 2890-2898.
24. Jeon, S. Y.; Park, K. A.; Baik, I. S.; Jeong, S. J.; Jeong, S. H.; An, K. H., Dynamic Response of Carbon Nanotubes Dispersed in Nematic Liquid Crystal. *Nano* 2007, 02, 41.
25. Manjuladevi, V.; Gupta, R. K.; Kumar, S., Effect of Functionalized Carbon Nanotube on Electro-Optic and Dielectric Properties of a Liquid Crystal. *Journal of Molecular Liquids* 2012, 171, 60.
26. Mutsumi, K.; Noritoshi, M.; Naoya, A.; Yoko, T.; Kazuchika, O.; Hirofusa, S., Organization of Single-Walled Carbon Nanotubes Wrapped with Liquid-Crystalline  $\Pi$ -Conjugated Oligomers. *J. Mater. Chem.*, 2009, 19, 1086-1092.
27. Sureshkumar, P.; Srivastava, A. K., Anomalous Electrokinetic Dispersion of Carbon Nanotube Clusters in Liquid Crystal under Electric Field. *Journal of Nanoscience and Nanotechnology* 2009, 9, 4741-4746(6).
28. Trushkevych, O.; Collings, N.; Hasan, T., Characterization of Carbon Nanotube-Thermotropic Nematic Liquid Crystal Composites. *Journal of Physics D: Applied Physics*, 2008, 41(12)
29. van der Schoot, P.; Popa-Nita, V.; Kralj, S., Alignment of Carbon Nanotubes in Nematic Liquid Crystals. *J. Phys. Chem. B*, 2008, 112 (15), pp 4512-4518.

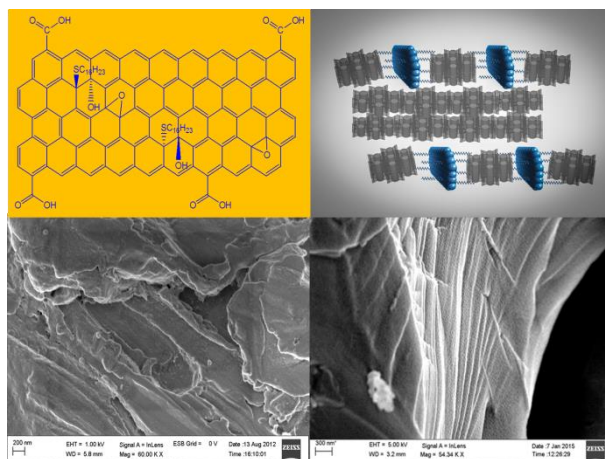
30. Kumar, S.; Bisoyi, H. K., Aligned Carbon Nanotubes in the Supramolecular Order of Discotic Liquid Crystals. *Angew. Chemie.* 2007, 46, 1501-1503.
31. Hari Krishna, B.; Sandeep, K., Carbon Nanotubes in Triphenylene and Rufigallol-Based Room Temperature Monomeric and Polymeric Discotic Liquid Crystals. *J. Mater. Chem.*, 2008, 18, 3032-3039.
32. Lee, J. J.; Yamaguchi, A.; Alam, M. A.; Yamamoto, Y.; Fukushima, T.; Kato, K.; Takata, M.; Fujita, N.; Aida, T., Discotic Ionic Liquid Crystals of Triphenylene as Dispersants for Orienting Single-Walled Carbon Nanotubes. *Angew. Chem. Int. Ed.* 2012, 51, 8490 –8494
33. Kılınç, N.; Ahsen, A.; Atilla, D.; Gürek, A. G.; San, S. E., Electrical Properties of Mesomorphic Phthalocyanine-Carbon Nanotube Composites. *Sensor Letters* 2008, 6, 607-612(6).
34. Zilberman, Y.; Tisch, U.; Pisula, W.; Feng, X.; Müllen, K., Spongelike Structures of Hexa-Peri-Hexabenzocoronene Derivatives Enhance the Sensitivity of Chemiresistive Carbon Nanotubes to Nonpolar Volatile Organic *Langmuir*, 2009, 25 (9), pp 5411–5416.
35. Zilberman, Y.; Tisch, U.; Shuster, G.; Pisula, W., Carbon Nanotube/Hexa-Peri-Hexabenzocoronene Bilayers for Discrimination between Nonpolar Volatile Organic Compounds of Cancer and Humid Atmospheres. *Adv. Mat.* 2010, 22, 4317–4320.

36. Park, J. G.; Yun, N. G.; Park, Y. B.; Liang, R.; Lumata, L., Single-Walled Carbon Nanotube Buckypaper and Mesophase Pitch Carbon/Carbon Composites. *Carbon* 2010, 48, 4276–4282.
37. Jian, K.; Hurt, R. H.; Sheldon, B. W., Visualization of Liquid Crystal Director Fields within Carbon Nanotube Cavities. *Appl. Phys. Lett.*, 2010 88, 163110.
38. Georgakilas, V.; Otyepka, M.; Bourlinos, A. B., Functionalization of Graphene: Covalent and Non-Covalent Approaches, Derivatives and Applications. *Chem. Rev.*, 2012, 112 (11), pp 6156–6214.
39. Hasobe, T.; Sakai, H., About the Cover. *J. Porphyrins Phthalocyanines* 2011, 15, 301–479
40. Kumar, S., Chemistry of Discotic Liquid Crystals: From Monomers to Polymers. *Chemistry of discotic liquid crystals: from monomers to polymers* 2010.
41. Behabtu, N., et al., Spontaneous High-Concentration Dispersions and Liquid Crystals of Graphene. *Nat. nanotech.* 2010, 5, 406-411.
42. Kim, J.; Han, T.; Lee, S.; Kim, J.; Ahn, C.; Yun, J.; Kim, S., Graphene Oxide Liquid Crystals. *Angew Chemie* 2011, 50, 3043-3050.
43. Dan, B.; Behabtu, N.; Martinez, A.; Evans, J. S.; Kosynkin, D. V.; Tour, J. M.; Pasquali, M.; Smalyukh, II, Liquid Crystals of Aqueous, Giant Graphene Oxide Flakes. *Soft Matter* 2011, 7, 11154-11159.

44. Xu, Z.; Gao, C., Graphene Chiral Liquid Crystals and Macroscopic Assembled Fibres. *Nat. commun.* 2011, 2, 571.
45. Guo, F.; Mukhopadhyay, A.; Sheldon, B. W.; Hurt, R. H., Vertically Aligned Graphene Layer Arrays from Chromonic Liquid Crystal Precursors. *Adv. Mat.* 2011, 23, 508-513.
46. Niyogi, S.; Bekyarova, E.; Itkis, M. E.; McWilliams, J. L.; Hamon, M. A.; Haddon, R. C., Solution Properties of Graphite and Graphene. *Journal of the American Chemical Society* 2006, 128, 7720-7721.
47. Grimshaw, J.; Haworth, R. D., 813. Flavogallol. *J. Chem. Soc.*, 1956, 4225-4232.
48. Moon, I.; Lee, J.; Ruoff, R.; Lee, H., Reduced Graphene Oxide by Chemical Graphitization. *Nat. commun.* 2010, 1, 73.
49. Dreyer, D. R.; Park, S.; Bielawski, C. W., The Chemistry of Graphene Oxide. *Chem. Soc. Rev.*, 2010, 39, 228-240.
50. Piner, R. D.; Kohlhaas, K. A.; Kleinhammes, A.; Jia, Y.; Wu, Y., Synthesis of Graphene-Based Nanosheets Via Chemical Reduction of Exfoliated Graphite Oxide. *Carbon* 2007, 45, 1558-1565.

# CHAPTER 3

## Self-assembly of Thiolated Graphene oxide onto Gold Surface and in the Supramolecular order of Discotic Liquid Crystals



### Abstract

Graphene oxide can be covalently functionalized with thiol molecules to produce thiolated graphene oxide which shows interesting behaviour of self-assembly on gold surfaces and in the supramolecular structures of discotic liquid crystals. The formation of self-assembled monolayer on the gold surface was confirmed by electrochemical, XPS, SEM, grazing angle IR studies. Supramolecular nanocomposites of anthraquinone based discotic liquid crystal with thiolated graphene oxide were characterized using SAXS, POM, DSC and Cryo-SEM. Such self-assembling supramolecular nanocomposites open up new and interesting possibilities for fundamental studies as well as for optoelectronic applications.

### 3.1. Introduction

Graphene, with its two-dimensional structure and fascinating physical properties, is emerging as a potential candidate for various device applications.<sup>1-5</sup> The chemical route to the preparation of graphene is by chemical exfoliation of graphite to graphene oxide by oxidation followed by the reduction of exfoliated graphene oxide with hydrazine. Interestingly, in recent times the graphene oxide is also gaining wide attention owing to its special physical and chemical properties and the ease with which it can be prepared and processed in solution. This is partly due the structure of graphene oxide with oxygen functionalities such as epoxy, hydroxyl and carboxyl groups on the basal plane and edges hinders the close stacking of layers,<sup>6-7</sup> this prevents the sheets from aggregating and makes them easily dispersible in aqueous medium and this makes the individual layers to behave like macromolecules in solution. Graphene oxide has been shown to have the potential for device applications such as in organic solar cells<sup>8-9</sup> and organic light-emitting diodes.<sup>10</sup> It is also examined as a saturable absorber in ultrafast lasers, fluorescent biosensor, cellular imaging and a drug delivery agent in cancer therapeutics.<sup>11-15</sup> The functional groups present on the surface and edges of graphene oxide viz. epoxy, hydroxyl, carbonyl and carboxyl, can be used to further modify the electronic properties of graphene oxide<sup>16-17</sup> and also to improve processability of graphene oxide sheets.<sup>18</sup>

Self-assembled graphene oxide layers on gold surface may open up several interesting possibilities for physical studies, including potential

device applications in organic electronics and for biosensing. It was recently reported that it is possible to reduce graphene oxide immobilized on the surfaces by chemical treatment with hydrazine or by heat treatment, leading to the formation of graphene films.<sup>19</sup> Graphene oxide have high surface area; therefore, they are often used as electrode materials in batteries and double-layered capacitors.<sup>20-21</sup> Ability of graphene and graphene oxide to store hydrogen<sup>22-23</sup> will be very useful for application in hydrogen fuel cells. Nanocomposites of graphene oxide and metal oxide nanoparticles have been used for high capacity energy storage in lithium ion batteries.<sup>24-28</sup> Zhu *et al.* synthesized reduced graphene oxide with high surface area using microwave assisted exfoliation, and used it in fabricating super-capacitors.<sup>20-21, 29</sup> It may be pointed out that all the previous reports were aimed at adsorption of graphene oxide onto alkanethiol monolayers and their electrochemical studies.<sup>30</sup> For example, ionic self-assembly of negatively charged graphene oxide onto oppositely charged self-assembled monolayers (SAM)<sup>31-32</sup> and self-assembly of graphene oxide at water-air interface<sup>33</sup> have been demonstrated in literature.

### 3.2 Objectives

In the previous chapter, we had shown that octadecylamine edge functionalized reduced graphene oxide formed an ordered sandwich like layered structure with anthraquinone discotic liquid crystal.<sup>34</sup> Here in this chapter we study self-assembling behaviour of surface functionalized

graphene oxide on gold surfaces and also characterize its behavior in anthraquinone discotics. We also have explored self-assembly behavior of the thiolated graphene oxide on gold electrodes and have electrochemically probed the self-assembled layer.

### **3.3. Experimental section**

#### **3.3.1. Thiolation of graphene oxide**

The graphite oxide (200 mg) obtained by the Hummers method (as presented in Chapter 2) is powdered and added to a mixture of thiol (taken in excess to ensure complete functionalization) and potassium tert-butoxide in a molar ratio of 1: 1.2. N-Methyl-2-pyrrolidone (NMP) (200 ml) was added to above mixture and maintained at 50°C for 15 minutes accompanied with stirring to ensure deprotonation. This mixture is sonicated for 5 minutes to disperse the graphene oxide in the reaction medium. The reaction is carried out at 50°C accompanied by vigorous stirring for an hour. After the reaction, the unreacted thiolate ions are neutralized by treating with dilute H<sub>2</sub>SO<sub>4</sub>. The reaction mixture is taken in a separating funnel with water and dichloromethane mixture. The thiolated graphene oxide gets suspended between the water and dichloromethane bilayer, the water and dichloromethane are separated. The thiolated graphene oxide present at the interface is collected and is filtered and washed with plenty of water and dichloromethane to remove ionic impurities and unreacted thiol. Thiolated graphene oxide was then dispersed in dichloromethane by sonication and

this was centrifuged at 5000 rpm, the top solution is decanted. The resultant thiolated graphene oxide is dried and re-dispersed in water by sonication. The dispersion is centrifuged at 5000 rpm and the thiolated graphene oxide is collected and dried. Two thiol compounds, thiophenol and hexadecanethiol are used separately for functionalization of graphene oxide.

### **3.3.2. Procedure to form self-assembled thiolated graphene oxide films**

The gold strip on which monolayer is to be formed is sonicated multiple times in millipore water and acetone for cleaning and then is immersed in the solution of thiolated graphene oxide dispersed in ethanol by sonication and kept for monolayer formation for 24 hours, with the solution being frequently sonicated to ensure that dispersed thiolated graphene oxide does not settle down.

### **3.3.3. Procedure for electrochemical studies of self-assembled films**

The gold disc electrode of area  $0.008 \text{ cm}^2$  sealed in glass is used for the formation of monolayer. The electrode preparation and surface pre-treatment are carried out as followed by Ganesh *et al.*,<sup>35</sup> the gold electrode was polished with emery paper of grade 800 and 1500, followed by polishing in aqueous slurries of progressively finer alumina (1.0, 0.3, and  $0.05 \mu\text{m}$  sizes), and ultrasonicated to remove alumina particles. Then, it was cleaned in a “piranha” solution (a mixture of 30%  $\text{H}_2\text{O}_2$  and concentrated  $\text{H}_2\text{SO}_4$  in a 1:3 ratio). Finally, it was rinsed in distilled water thoroughly, followed by

rinsing in Millipore water before SAM formation. The electrochemical gold oxidation and reduction are carried out in 0.1M HClO<sub>4</sub> solution by cycling the potential between 0V – 1.4V. Reductive stripping of thiolated graphene oxide modified gold electrode in 0.5 M KOH solution is carried out by cycling the potential between 0V and -1.4V. Electrochemical characterizations are performed in a solution of 1 mM potassium ferrocyanide and 1 mM potassium ferricyanide with 1 M sodium fluoride as a supporting electrolyte. A conventional three-electrode electrochemical cell is used for cyclic voltammetry (CV) and impedance studies. A platinum foil of large surface area is used as the counter electrode and a saturated calomel electrode (SCE) as reference electrode. The cell is cleaned thoroughly before each experiment and kept in a hot air oven at 100 °C for at least 1 h before the start of the experiment. Cyclic voltammetry study is carried out by scanning the potential between -100 to 500 mV vs. SCE. The impedance measurements are carried out by applying an AC voltage of 10 mV amplitude at the formal potential of the redox couple. A frequency range of 100 kHz to 100 mHz is used for impedance measurements.

#### **3.3.4. Synthesis of 1,5-dihydroxy- 2,3,6,7-tetrakis(3,7-dimethyloctyloxy)-9,10-anthraquinone.**

Synthesis of 1,5-dihydroxy- 2,3,6,7-tetrakis(3,7-dimethyloctyloxy)-9,10-anthraquinone,<sup>36</sup> is discussed in detail in Chapter 2.

### 3.3.5. Preparation of composites

The rufigallol-based room temperature DLC namely 1,5-dihydroxy-2,3,6,7-tetrakis(3,7-dimethyloctyloxy)-9,10-anthraquinone (RTAQ) was used as discotic host molecule to disperse the thiol functionalized graphene oxide. Dispersion was carried out by sonicating a dichloromethane solution of RTAQ and thiolated graphene oxide for 30 min followed by removal of the solvent under vacuum. The dried composites were heated to isotropic state and cooled at the rate of 2°C/min. to room temperature. Two composites of hexadecanethiol functionalized graphene oxide (HDT-GO) and thiophenol functionalized graphene oxide (TP-GO) were prepared. 1% by wt. of HDT-GO in RTAQ (1HDT-GO/AQ), 5% by wt. of HDT-GO in RTAQ (5HDT-GO/AQ), 1% by wt. of TP-GO in RTAQ (1TP-GO/AQ) and 5% by wt. of TP-GO in RTAQ (5TP-GO/AQ) were prepared.

## 3.4. Results and discussions

### 3.4.1. Characterization of functionalized graphene oxide

#### 3.4.1.1. FT-IR spectroscopic analysis of thiolated graphene oxide

The infrared (IR) spectra of hexadecanethiol modified graphene oxide (Figure 1) and thiophenol modified graphene oxide (Figure 2) show C-S stretching vibrations at 723 cm<sup>-1</sup> and 721 cm<sup>-1</sup> respectively indicating the presence of C-S bond, which was absent in IR spectrum of graphene oxide (Figure 3).

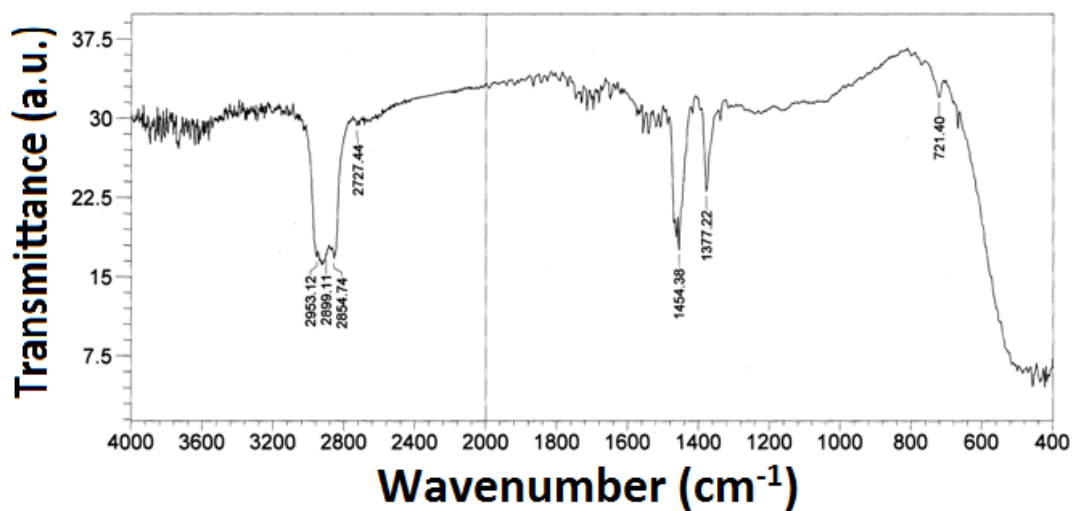


**Figure 1.** IR spectrum of hexadecanethiol functionalized graphene oxide.

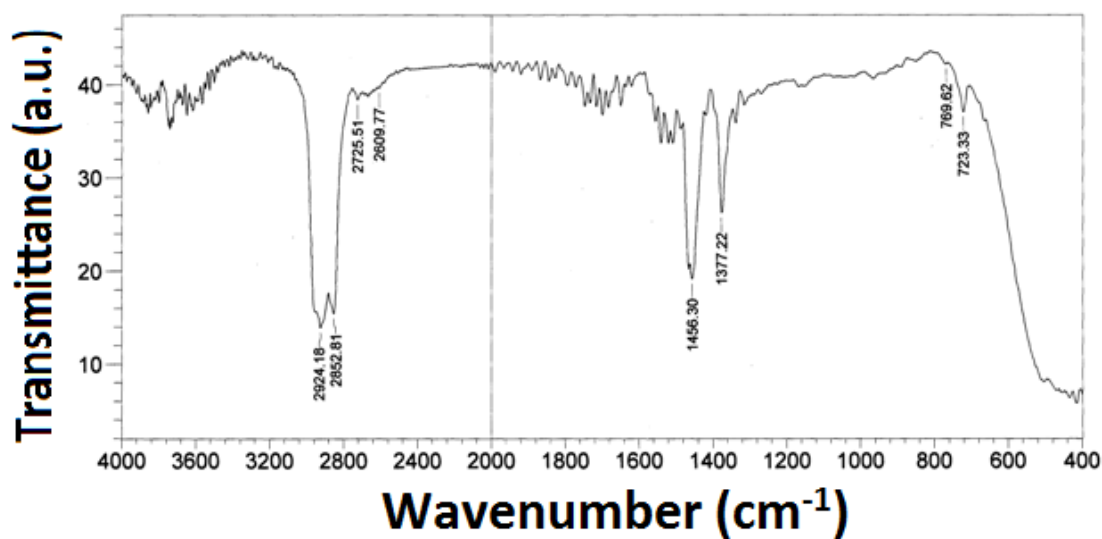


**Figure 2.** IR spectrum of thiophenol functionalized graphene oxide.

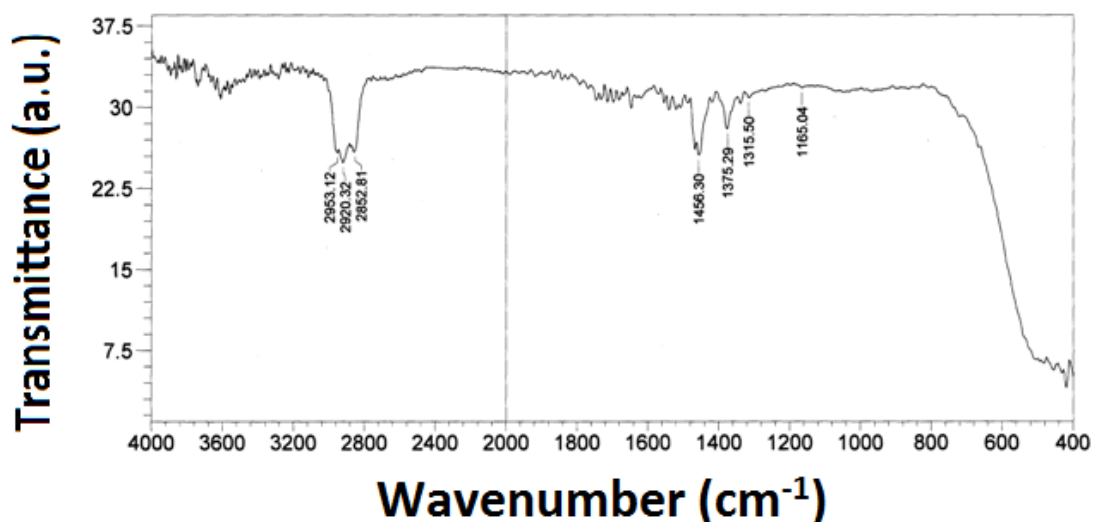


**Figure 3.** IR spectrum of graphene oxide.

#### 3.4.1.2. Solid state <sup>13</sup>C NMR analysis of thiolated graphene oxide

Solid state <sup>13</sup>C NMR spectrum of hexadecanethiol functionalized graphene oxide (Figure 4) shows peaks around 70 ppm which can be attributed to sp<sup>3</sup> carbon attached to oxygen moieties. There are also peaks from 125 ppm to 145 ppm assigned to aromatic carbons; these are typical of graphene oxide.<sup>17, 37</sup> Additionally there are peaks around 30 ppm which can be assigned to methylene groups of hexadecanethiol bonded to graphene oxide.

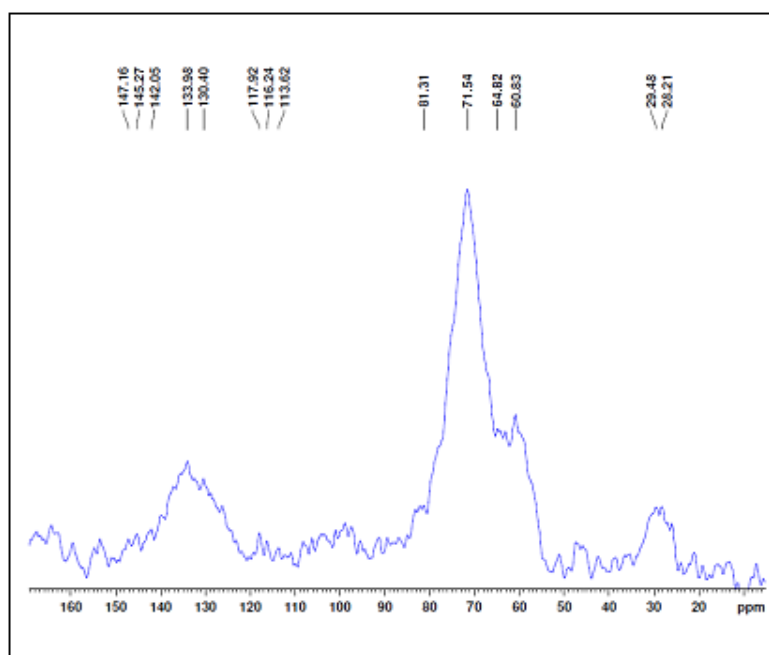


**Figure 4.** Solid state  $^{13}\text{C}$  NMR of hexadecanethiol functionalized graphene oxide.

**Table 1.** Elemental analysis data of graphene oxide (GO), hexadecanethiol functionalized graphene oxide (HDT-GO) and thiophenol functionalized graphene oxide (TP-GO).

Sample	C (%)	H (%)	N (%)	S (%)
GO	46.43	2.12	0	0
HDT-GO	50.316	1.89	0	0.23
TP-GO	51.4305	1.51	0	0.2625

### 3.4.1.3. Elemental analysis of thiolated graphene oxide

Elemental analysis data of all the three samples are given in the Table 1.

The thiolated derivatives show the presence of sulfur in elemental analysis,

while the unmodified graphene oxide does not show any sulphur content. The analysis values of graphene oxide are similar to values observed in literature.<sup>38</sup>

#### 3.4.1.4. X-ray diffraction patterns of functionalized and un-functionalized graphene oxide

XRD patterns of the graphene oxide shows a peak which corresponds to *d*-spacing of 0.877 nm. This *d*-spacing is attributed to distance between two graphene oxide layers having water molecules trapped in between them, which extend hydrogen bonding to oxide functionalities present on graphene oxide. The XRD of graphene oxide carried out at 110 °C show decreased *d*-spacing of 0.63 nm primarily due to removal of these sandwiched water molecules. The XRD patterns of hexadecanethiol and thiophenol modified graphene oxide do not show any similar prominent peak corresponding to the above. This is expected as the hydrophobic alkyl chains present on the surface do not allow water molecule to form hydrogen bonds and the bulky substituents do not allow two graphene sheets to come close. XRD patterns of graphene oxide and modified graphene oxide are shown in Figure 5.<sup>39-40</sup>

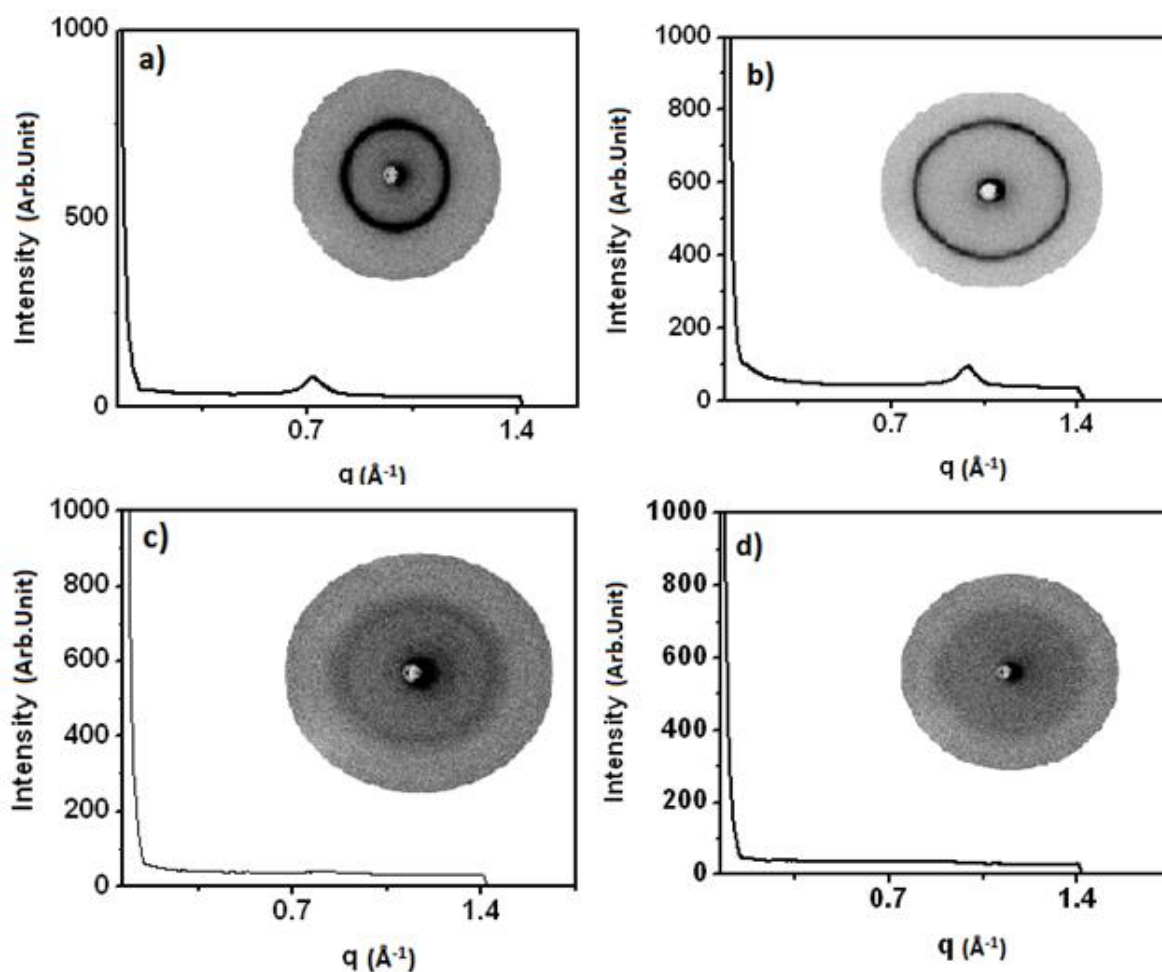


**Figure 5.** XRD patterns of (a) graphene oxide, (b) graphene oxide at 110 °C, (c) hexadecanethiol functionalized graphene oxide, and (d) thiophenol functionalized graphene oxide.

#### 3.4.1.5. TEM analysis

The HRTEM of unmodified graphene oxide (Figure 6) shows graphene sheets with 4-5  $\mu\text{m}$  in dimensions, in some places the layers show folding and overlapping on other sheets. The hexadecanethiol modified graphene oxide images (Figure 7), show the modified graphene oxide are smaller in size, same goes with the thiophenol modified graphene oxide (Figure 8).

Overlapping of sheets is lesser in functionalized graphene oxide sheets.  
(Figure 7 & 8).

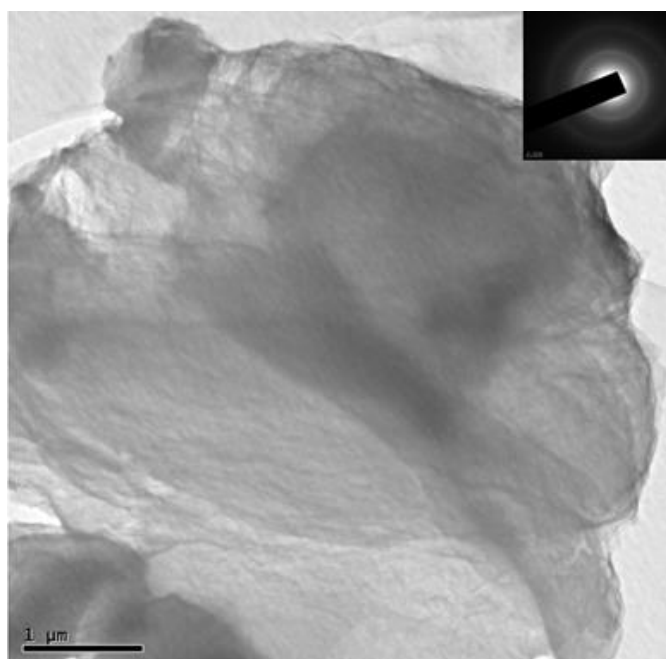


**Figure 6.** TEM image of graphene oxide, inset is a SAED pattern.

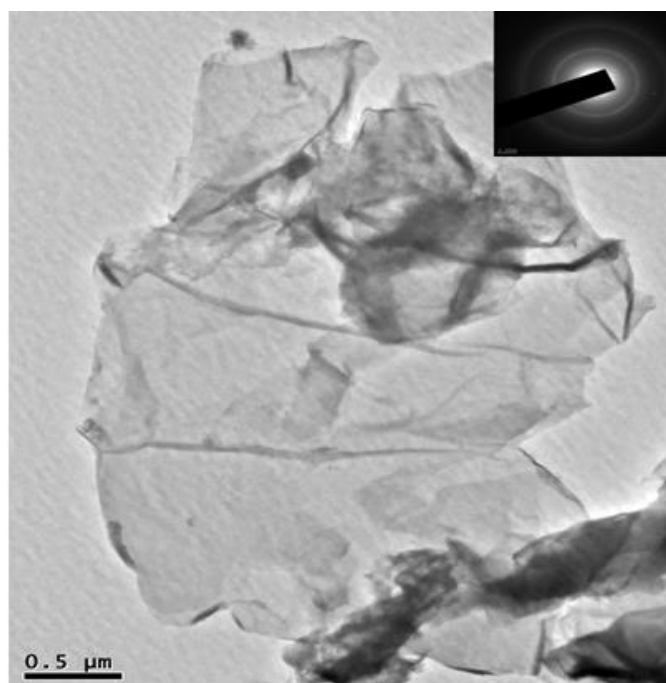


**Figure 7.** TEM image of hexadecanethiol functionalize graphene oxide, inset is a SAED pattern.

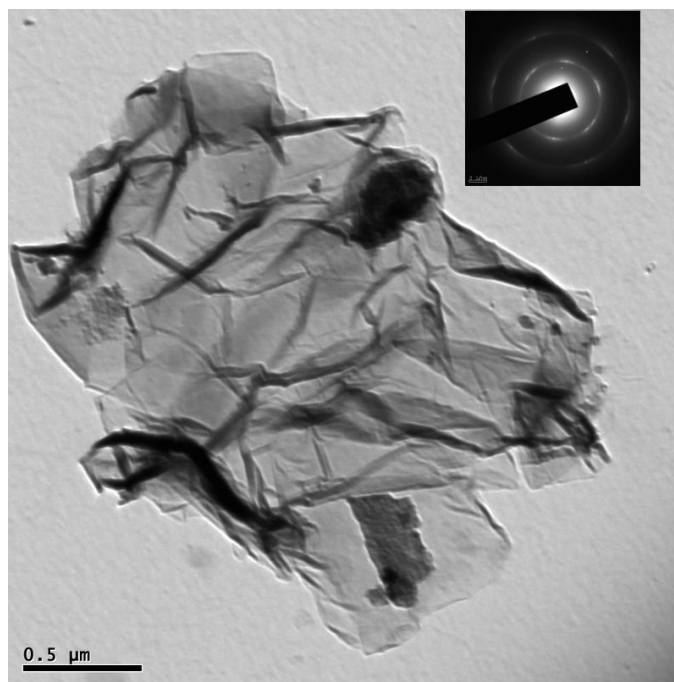


**Figure 8.** TEM image of thiophenol functionalize graphene oxide, inset is a SAED pattern.

#### 3.4.1.6. Raman spectral analysis of modified and unmodified graphene oxide

Raman spectra of unmodified graphene oxide shows D-band at  $1340\text{ cm}^{-1}$  and G-band at  $1584\text{ cm}^{-1}$  (Figure 9). Hexadecanethiol modified graphene oxide shows D-band at  $1340\text{ cm}^{-1}$  and G-band at  $1584\text{ cm}^{-1}$  (Figure 10). Thiophenol modified graphene oxide shows D-band at  $1340\text{ cm}^{-1}$  and G-band at  $1584\text{ cm}^{-1}$  (Figure 11). We observed that chemical functionalization of graphene oxide with thiol molecules, did not change the position of D band and G Band, but the functionalized graphene oxide had a slightly more intense D band, this can be attributed to deformation induced on the surface of graphene oxide by functional groups.

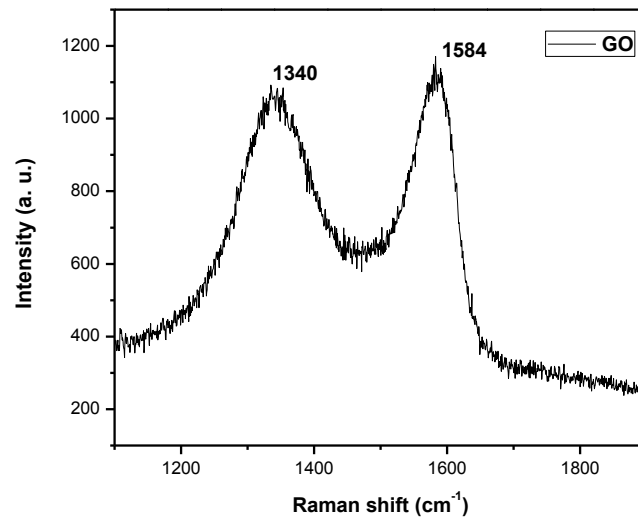


**Figure 9.** Raman spectra of graphene oxide.

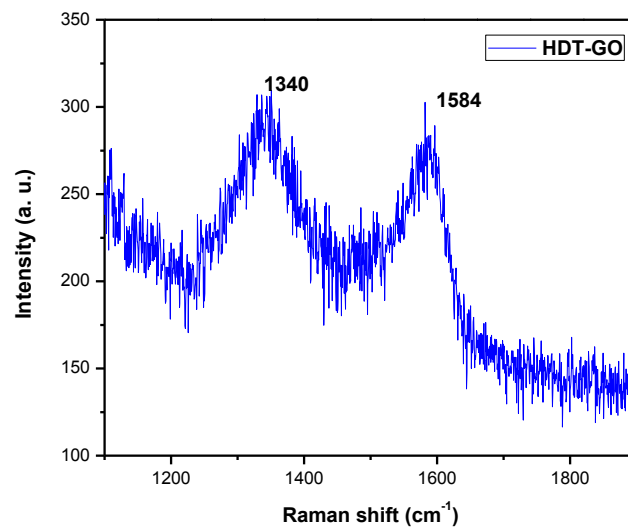


**Figure 10.** Raman spectra of hexadecanethiol functionalized graphene oxide.

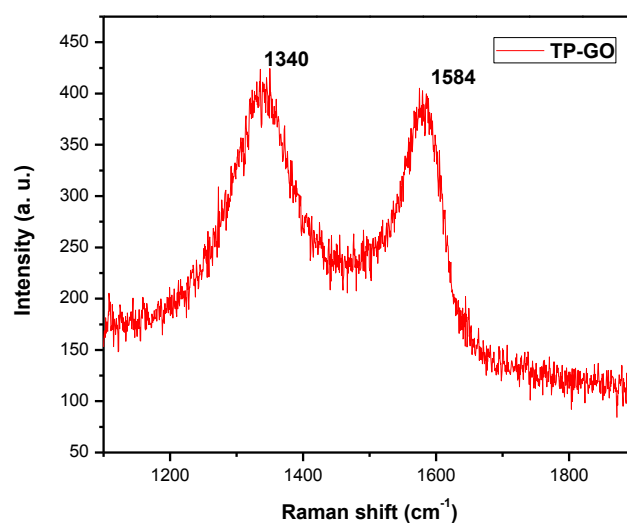


**Figure 11.** Raman spectra of thiophenol functionalized graphene oxide.

### 3.4.2. Characterization of modified gold electrode

#### 3.4.2.1. X-ray photoelectron spectroscopy analysis of gold surface modified with hexadecanethiol functionalized graphene oxide

The XPS was recorded to characterize self-assembled thiolated graphene oxide on gold surface; C1s regions (Figure 12a.) showed three overlapping peaks typical of graphene oxide. The peak at binding energy of 285 eV corresponds to C-C and C-H bonds while the peak at 286.5 eV is due to the C-O bond, while peaks at 289–290 eV can be assigned to C=O and O=C-OH. The O1s spectra show a peak at 532.85 eV which can be assigned to C-OH. The peak at 162.25 eV (Figure 12b.) corresponding to S2p region is that of thiol bound to gold. The absence of any peak at 164 eV suggests the absence of unbound thiol.<sup>19, 39, 41-45</sup>

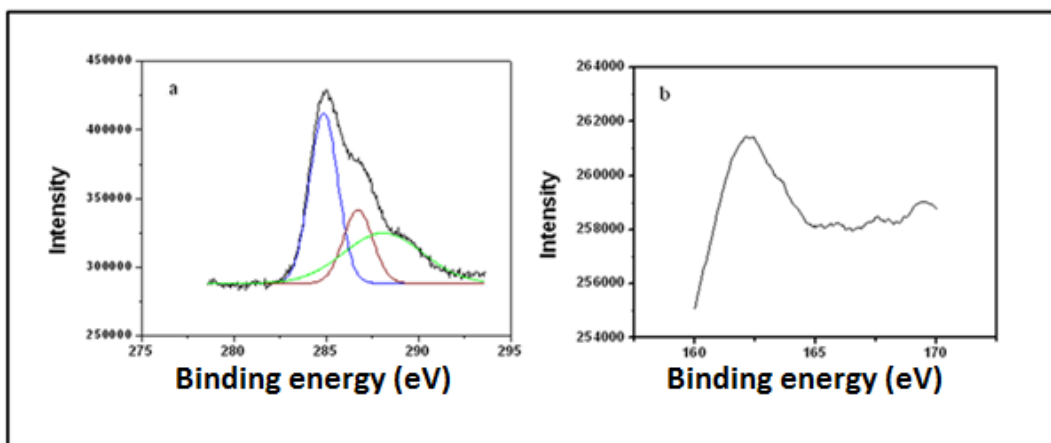


**Figure 12.** XPS spectra of hexadecanethiol functionalized graphene oxide monolayer on gold, (a) C1s region and (b) S2p region.

### 3.4.2.2. Grazing angle IR analysis on gold surface modified with hexadecanethiol functionalized graphene oxide

The hexadecanethiol functionalized graphene oxide monolayer on gold showed peak at  $730\text{ cm}^{-1}$  suggests the presence of C–S bond on gold surface (Figure 13). The thiophenol modified graphene oxide monolayer on gold also showed peak at  $742\text{ cm}^{-1}$  corresponds to the presence of C–S bond on gold surface. Bare gold electrode showed absence of the above mentioned peaks. (Figure 14)

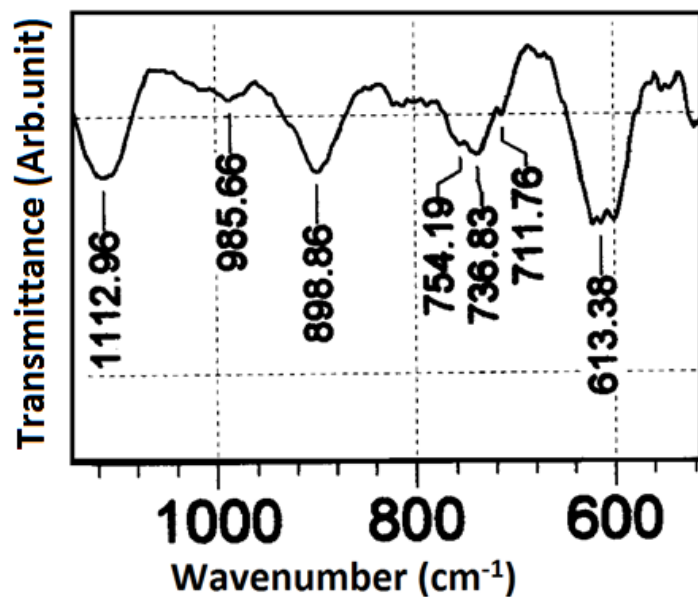


**Figure 13.** Grazing angle IR of hexadecanethiol functionalized graphene oxide on gold showing the sulfur peaks.

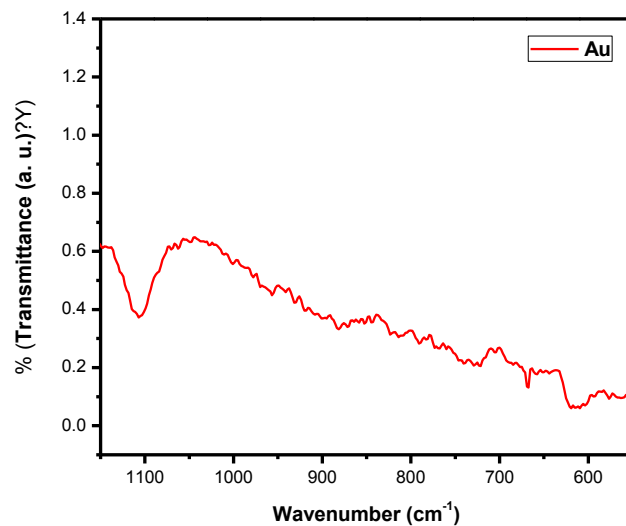


**Figure 14.** Grazing angle IR spectra of bare gold electrode.

### 3.4.2.3. Electrochemical analysis of modified gold electrode with functionalized graphene oxide

Electrochemistry is a well-established method for probing the self-assembled films of organic thiol molecules on noble metal surfaces.<sup>46</sup> In order to confirm the presence of thiolated graphene oxide films on gold electrode we carried out electrochemical studies in 0.1M HClO<sub>4</sub> solution by cycling the potential between 0V – 1.4V. Figure 15 shows the cyclic voltammogram of both unmodified gold electrode (a) and thiolated graphene oxide modified (b). From the CV, it is observed that the peak corresponding to the gold oxidation occurs at 1.1V while the modified electrode has a peak at 1.2V suggesting that there is an inhibition of oxidation due to the presence of graphene oxide layer which causes the oxidation potential to shift to higher potential. The current due to gold oxide reduction peak of modified electrode (Figure 15b) occurs at 0.83V, is almost same as that of the bare gold electrode. This is due to the fact that the thiolated graphene oxide layer is desorbed after the first cycle where the potential is scanned up to 1.2 V. Figure 16 shows different cycles of gold oxide stripping. Desorption of graphene oxide layer is also clear from the fact that during the first cycle, gold oxide stripping (Figure 16a) happens at positive potential of 1.2 V, while during second and third cycles (Figure 16b & 16c) the electrode behaves like bare gold electrode with peak potential at a more negative value of 1.1 V. It is known that application of positive potentials desorb the thiol monolayer due to formation of gold oxide.<sup>46</sup>

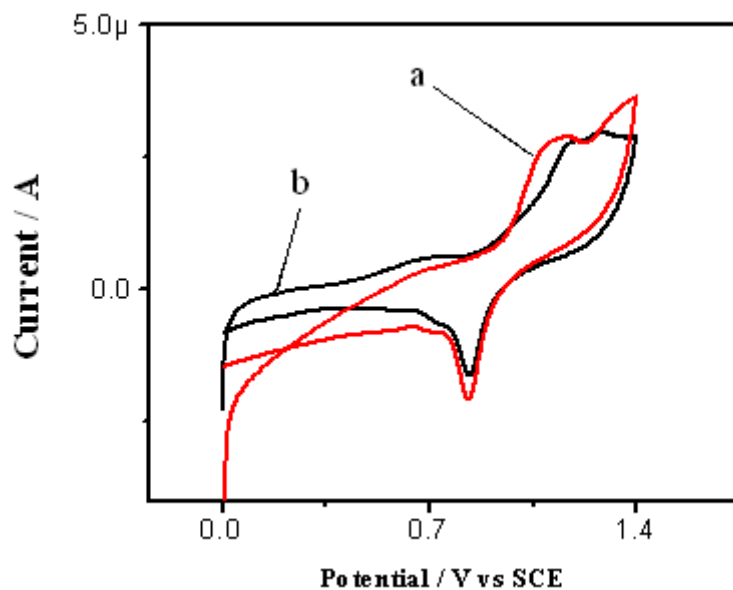


**Figure 15.** Cyclic voltammogram of (a) bare gold (red), and (b) thiophenol substituted graphene oxide (black) in 0.1 M HClO<sub>4</sub>.

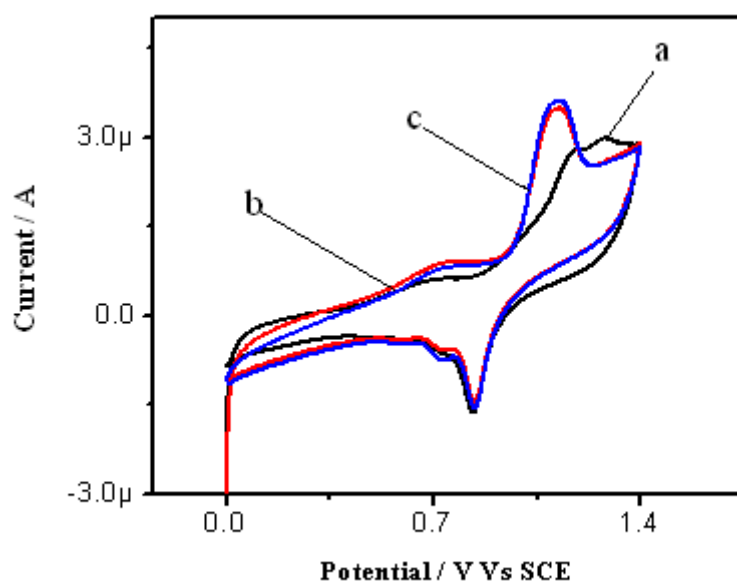


**Figure 16.** Cyclic voltammogram of thiophenol substituted graphene oxide modified gold electrode, (a) first cycle (black), (b) second cycle (red), (c) third cycle (blue) in 0.1 M HClO<sub>4</sub>.

We carried out reductive stripping of thiolated graphene oxide modified gold electrode in 0.5 M KOH solution by cycling the potential between 0V and -1.4V. Figure 17 shows the stripping of modified electrode, first cycle (Figure 17a) shows a broad desorptive stripping with a peak at -0.98V corresponding to reductive stripping which is not seen in second (Figure 17b) and third (Figure 17c) cycles. The broad hump is due to gradual desorption with potential of several thiol groups of graphene oxide on gold electrode. Subsequent cycles do not show any desorption peak confirming the loss of graphene oxide film.

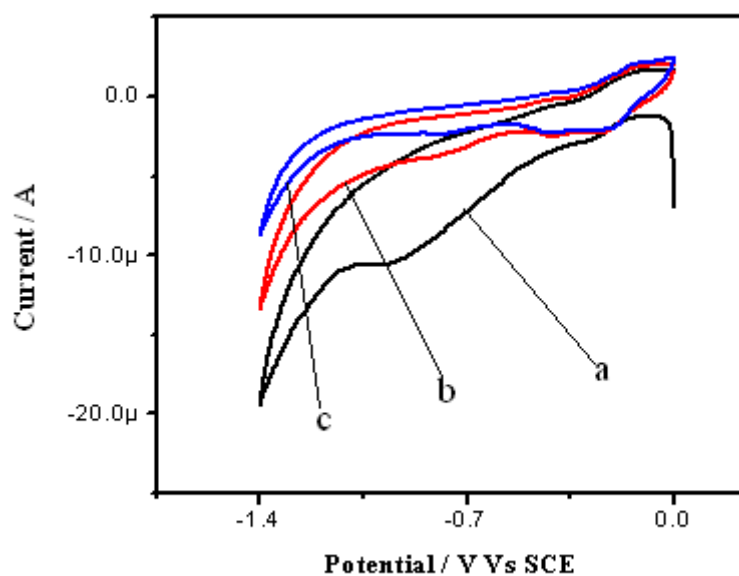


**Figure 17.** Cyclic voltammogram of thiophenol substituted graphene oxide modified gold electrode, (a) first cycle (black), (b) second cycle (red), (c) third cycle (blue) in 0.5 M KOH.

The blocking of thiolated graphene oxide modified gold electrode to electron transfer process was studied using cyclic voltammetry (Figure 18)

and electrochemical impedance spectroscopy (Figure 19). The blocking properties of the self-assembled films of thiolated graphene oxide to electron transfer reactions have been evaluated by using the potassium ferrocyanide /ferricyanide as a redox probe. The CV of bare gold (Figure 18a) shows reversible peaks for the redox couple while the thiolated graphene modified (Figure 18b & 18c) electrodes show quasi reversible behaviour with a larger peak separation ( $\Delta E$ ) of 201 mV for hexadecanethiol substituted graphene oxide and 170 mV for thiophenol substituted graphene oxide and lower peak currents indicating that the self-assembled film hinders the electron transfer process; However the reaction is not completely blocked by the film. This can be due to the thin monolayer film of pi electron rich graphene oxide which to some extent facilitates the electron transfer thereby preventing complete blocking of the redox process. It can also be seen that hexadecanethiol modified electrode shows higher level of blocking compared to thiophenol modified electrode as evidenced by the larger  $\Delta E$  and lower peak current which can be attributed to long alkyl chains partially shielding the access of the redox probe to the graphene oxide surface.

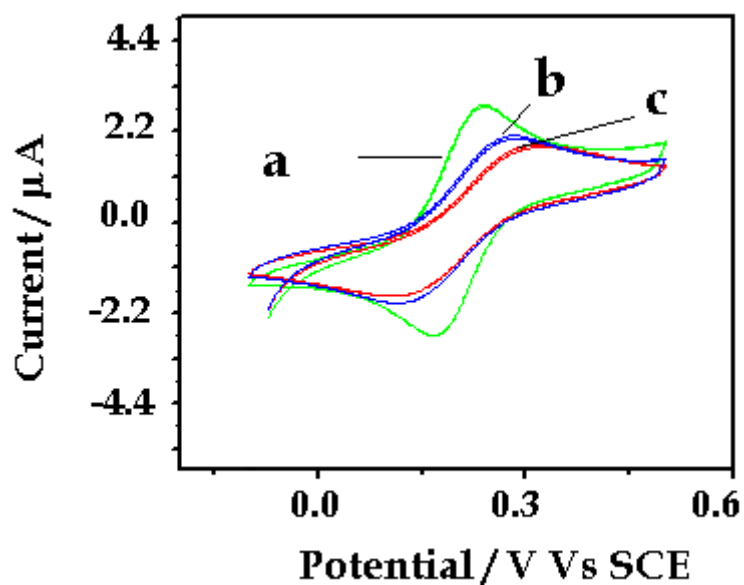


**Figure 18.** Cyclic voltammograms of (a) unmodified gold electrode (green line), (b) thiophenol functionalized graphene oxide modified gold electrode (blue line), and (c) hexadecanethiol functionalized graphene oxide modified electrode (red line) in potassium ferrocyanide / ferricyanide system.

The impedance plots of bare gold shows a straight line over a wide frequency window typical of a reaction which is fully under diffusion control process (Figure 19a). The thiophenol functionalized graphene oxide modified gold electrode shows a semicircle at higher frequencies representing charge transfer process. The width of semicircle further increases in the case of hexadecanethiol functionalized graphene oxide modified gold electrode which is due to blocking nature of the long alkyl chains present on graphene oxide surface.

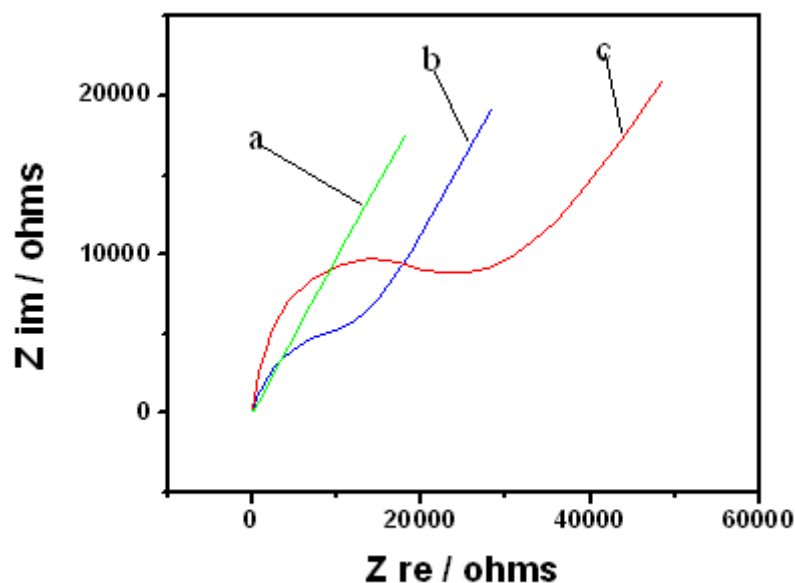


**Figure 19.** Electrochemical impedance analysis and Nyquist plots for (a) bare gold (green), (b) thiophenol functionalized graphene oxide modified gold electrode (blue), (c) hexadecanethiol functionalized graphene oxide modified gold electrode (red)

Randles type equivalent circuit was used to model the impedance plots obtained for the potassium ferrocyanide/potassium ferricyanide redox reaction. Table 2 lists the values of different components, viz.,  $R_u$ ,  $R_{ct}$ ,  $C_{dl}$ ,  $Q$ , and  $W$ , obtained by fitting the impedance data to equivalent circuits (the equivalent circuits are shown at the top of the respective tables). Bare gold fitted well to the equivalent circuit model  $R(C(RW))$ . However, the impedance data of modified electrodes follows the equivalent circuit  $R(Q(RW))$ . As the impedance of the CPE is given by  $Z_{CPE} = 1/Q(j\omega)^n$ , when  $n = 1$ , purely capacitive behavior is expected (i.e.,  $Q = C_{dl}$ ). The values of  $n$  in the case of hexadecanethiol functionalized graphene oxide modified gold electrode and

thiophenol functionalized graphene oxide modified gold electrode are 0.905 and 0.77, respectively, showing deviation from purely capacitive behavior.

**Table 2.** Values of different components of the equivalent circuit R(C(RW)) obtained for gold electrode and the equivalent circuit R(Q(RW)) obtained for thiophenol functionalized graphene oxide and hexadecanethiol functionalized graphene oxide modified gold electrode, from the fitting of impedance data for potassium ferrocyanide/potassium ferricyanide redox reaction in aqueous medium.

Sample	$R_u$ ( $\Omega \text{ cm}^2$ )	$Q$ ( $\Omega^{-1} \text{ cm}^{-2}$ )		$C_{dl}$ ( $\mu\text{F cm}^{-2}$ )	$R_{ct}$ ( $\Omega \text{ cm}^2$ )	$W$ ( $\Omega \text{ cm}^2$ )
		$S^n$	$n$			
Bare gold	0.592	---	--	40.89	1.33	$3.99 \times 10^{-7}$
TP-GO	0.505	$1.93 \times 10^{-4}$	0.77	--	77.57	$2.74 \times 10^{-7}$
HDT-GO	0.632	$4.91 \times 10^{-5}$	0.905	--	177.09	$3.93 \times 10^{-7}$

#### 3.4.2.4. FESEM images of hexadecanethiol functionalized graphene oxide self-assembled on gold surface.

FESEM image of bare gold strip and that of hexadecanethiol functionalized graphene oxide self-assembled to the gold strip are shown in Figure 20a and 20b. The surface of bare gold is featureless as seen in Figure 20a, whereas hexadecanethiol functionalized graphene oxide modified gold electrode

shows layered sheets of graphene oxide present on its surface as seen in Figure 20b.

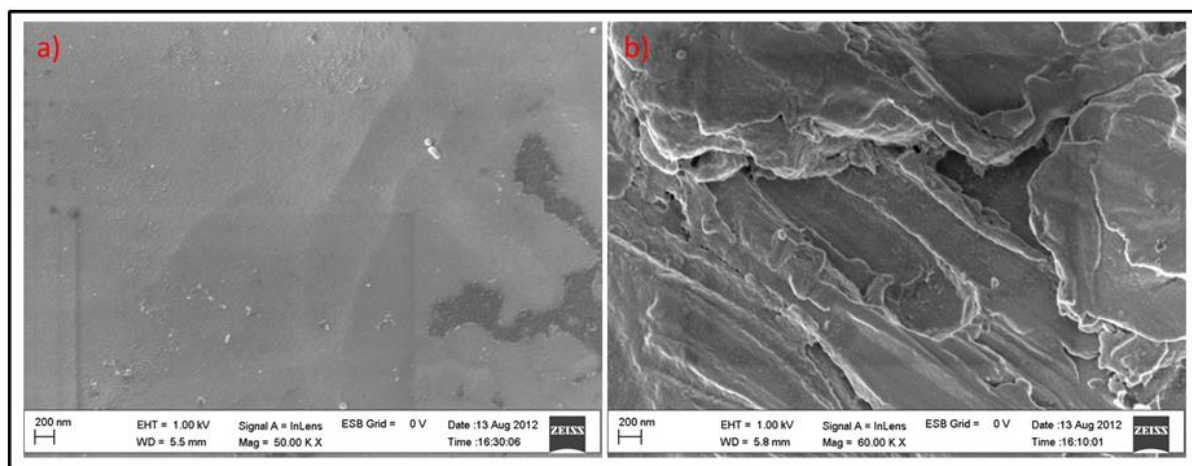


**Figure 20.** FESEM images of (a) bare gold electrode, and (b) bare gold electrode modified with self-assembled layer of hexadecanethiol functionalized graphene oxide.

### 3.4.3. Characterization of nanocomposites of functionalized graphene oxide with anthraquinone discotic liquid crystal.

#### 3.4.3.1. Polarized Optical Microscopy (POM)

The mesomorphic and thermal behaviour of nanocomposites formed by dispersing 1%, 5% HDT-GO and TP-GO in 1,5-dihydroxy-2,3,6,7-tetrakis(3,7-dimethyloctyloxy)-9,10-anthraquinone (RTAQ) was investigated by polarizing optical microscopy (POM) and differential scanning calorimetry (DSC). Figure 21(a-d) shows the typical polarizing optical micrographic textures for the composites 1 HDT-GO/AQ, 5 HDT-GO/AQ and 1TP-GO/AQ, 5TP-GO/AQ respectively. All the samples exhibit classical textures of columnar mesophase at room temperature. These textures are typical of

columnar hexagonal phase and look similar to the POM image of RTAQ (Figure 22). Unlike the pure RTAQ, doped composites cleared to isotropic state at much lower temperatures. 1 HDT-GO/AQ composite melted at 80.1 °C, 5 HDT-GO/AQ composite melted at 82.4 °C, 1TP-GO/AQ composite melted at 72.2 °C, and 5TP-GO/AQ composite melted at 73.6 °C. This decrease in isotropic transition temperatures of the composites points towards disordered mesophase in composites. The surface functionalized graphene oxide induces non stabilizing interactions between the functionalities on the graphene. Hexadecanethiol functionalized graphene oxide melt at higher temperature compared to thiophenol functionalized graphene oxide, this reveals that van der Waals interaction between the alkyl chains of RTAQ and that of HDT-GO induces small amount of stabilization, which is absent in the case of TP-GO composites. Moreover, the steric hindrance of phenyl group could also be responsible for disordering of the mesophase.

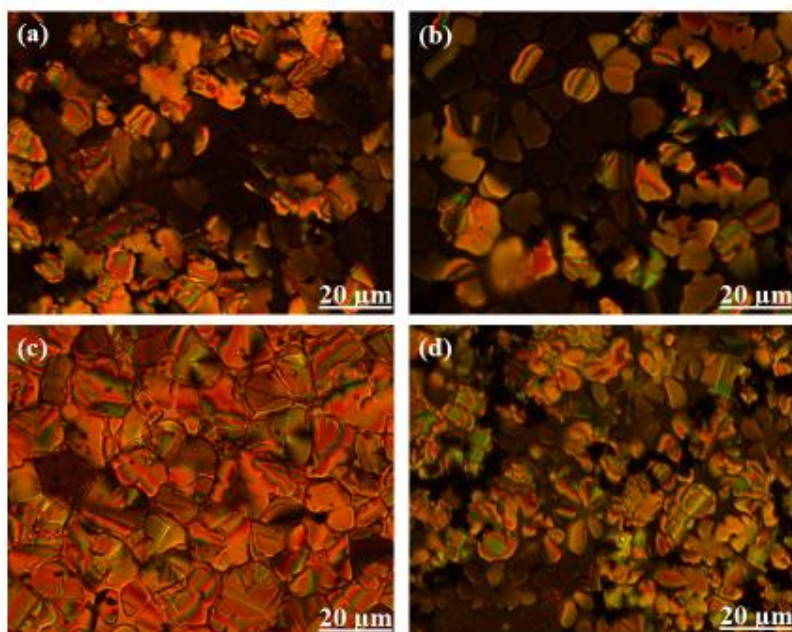


**Figure 21.** Polarizing optical microscope image of the columnar phase of composites (a) 1% HDT-GO/AQ, (b) 5% HDT-GO/AQ, (c) 1% TP-GO/AQ and (d) 5% TP-GO/AQ (at room temperature, crossed polarizers, 50 X magnification).

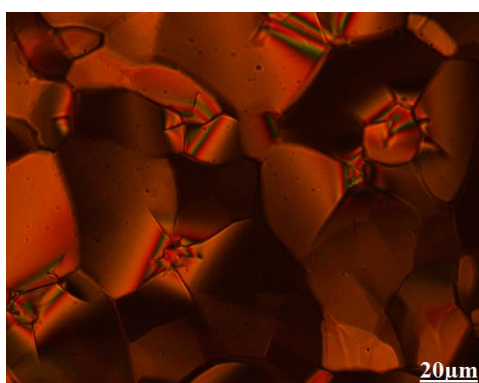


**Figure 22.** Polarized optical microscopy of pure RTAQ discotic liquid crystal (at 50 °C crossed polarizers, 50 X magnification).

### 3.4.3.2. Differential scanning calorimetry (DSC)

Figure 23a and 23b shows the DSC plots for the AQ, 1HDT-GO/AQ, 5HDT-GO/AQ and 1TP-GO/AQ, 5TP-GO/AQ nano-composites recorded at a rate of 10 °C/min. The enthalpy of the phase transition is decreases from 6.38 J/g in pure compound to 0.65 J/g and 0.49 J/g in 1% HDT-GO/AQ and 5% HDT-GO/AQ respectively. Decrease in the enthalpy of transition is due to disorganization in mesophase induced by thiolated graphene oxide. We observe that there is a greater disorganization in the thiophenol functionalized graphene oxide composites, this is due to destabilizing interaction between, thiophenol groups present on graphene oxide surface and alkyl chains of RTAQ. Both the nanocomposites of 1% TP-GO/AQ and 5% TP-GO/AQ show very small enthalpy of transition to isotropic state and thus no observable peak is seen in their DSC traces, which clearly reveals that the thiolated graphene discotic system is disordered. The DSC data obtained are presented in Table 4.

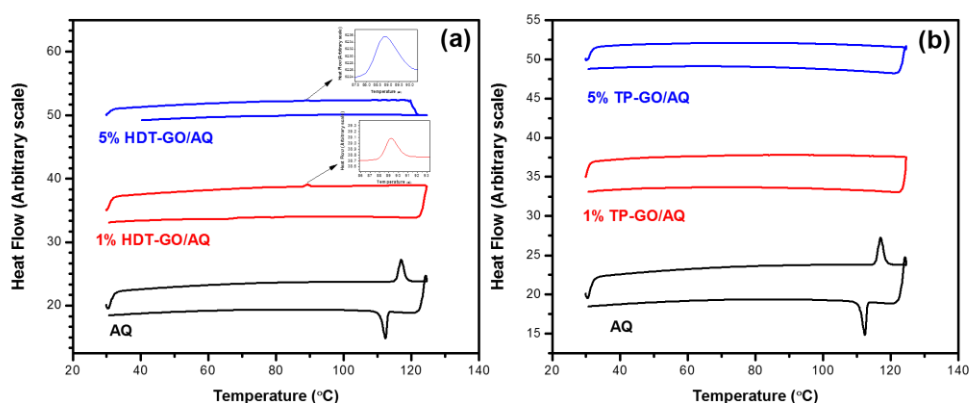


**Figure 23.** DSC curve of nano-composites of: (a) RTAQ (black), 1% HDT-GO/AQ and 5% HDT-GO/AQ (enlarged), and (b) RTAQ, 1% TP-GO/AQ and 5% TP-GO/AQ.

**Table 4.** DSC results of undoped DLC RTAQ and 1% and 5% composites dispersed with hexadecanethiol (HDT-GO). Col<sub>h</sub> = columnar hexagonal mesophase, I = isotropic.

Composites	Thermal Transition (°C)/ Enthalpy (J/g)	
	Heating Scan	Cooling Scan
RTAQ	Col <sub>h</sub> 116.86(6.38) I	I 112.38(6.01) Col <sub>h</sub>
HDT-GO/AQ 1%	Col <sub>h</sub> 89.20(0.65) I	I 79.39(0.065) Col <sub>h</sub>
5%	Col <sub>h</sub> 88.69(0.49) I	I 79.55(0.047) Col <sub>h</sub>

#### 3.4.3.3. Small angle X-ray scattering (SAXS)

The liquid crystalline phases of the nanocomposites were further studied by SAXS. The SAXS pattern of composite and pure RTAQ are recorded at room temperature and the intensity vs  $2\theta$  diffraction pattern for HDT-GO/AQ and TP-GO/AQ nano-composites are shown in Figure 24a and Fig. 24b. The diffraction peaks of nanocomposites in the small angle region follow the ratio of  $1: 1/\sqrt{3}: 1/2:1/\sqrt{7}$ , typical of hexagonal arrangement. In the wide angle region they show a broad halo around 4.3 Å (fluidic alkyl chains) and a broad peak at 3.4 Å (core-core separation). The results suggest that the columnar hexagonal order of discotics is not affected on dispersion of thiolated graphene oxide into the columnar matrix.

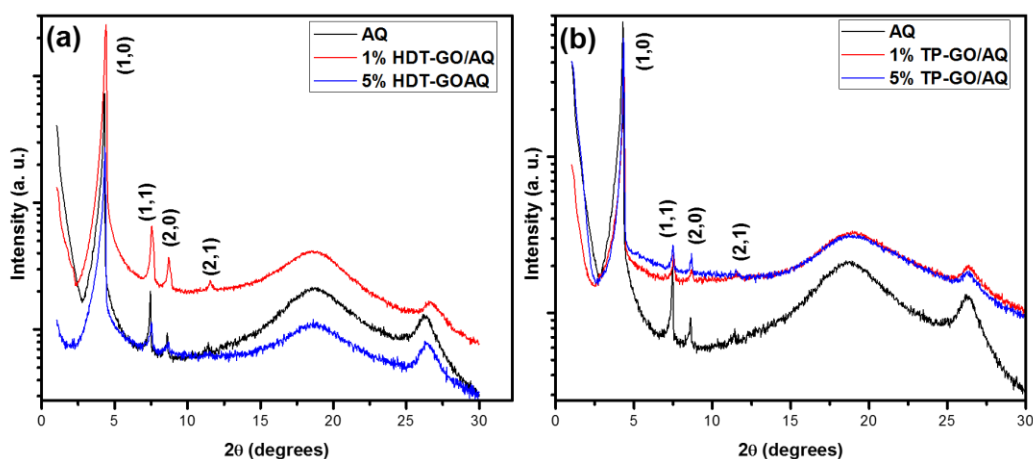


**Figure 24.** Intensity vs  $2\theta$  plots for: (a) RTAQ, 1% HDT-GO/AQ and 5% HDT-GO/AQ and (b) RTAQ, 1% TP-GO/AQ and 5% TP-GO/AQ (SAXS pattern were recorded at room temperature)

#### 3.4.3.4. Cryo-SEM analysis of self-assembled discotics with thiolated graphene oxide

Cryo-SEM images of the composites and pure liquid crystals were acquired to study the ordering of nanocomposites. We observe spherical aggregates in pure liquid crystalline system (Figure 25a). Both the doped composites showed layered structure owing to functionalized graphene oxide sheets, one could observe the presence of liquid crystalline domains on these layered structures. The ordering of liquid crystals on the sheet is not very clear from these images. Cryo-SEM reveals the layered structures which are absent in pure liquid crystal (Figure 25b-e). The layered structures observed in Cryo-SEM images of all the composites can be pictured as in the given model (Figure 26a and 26b).

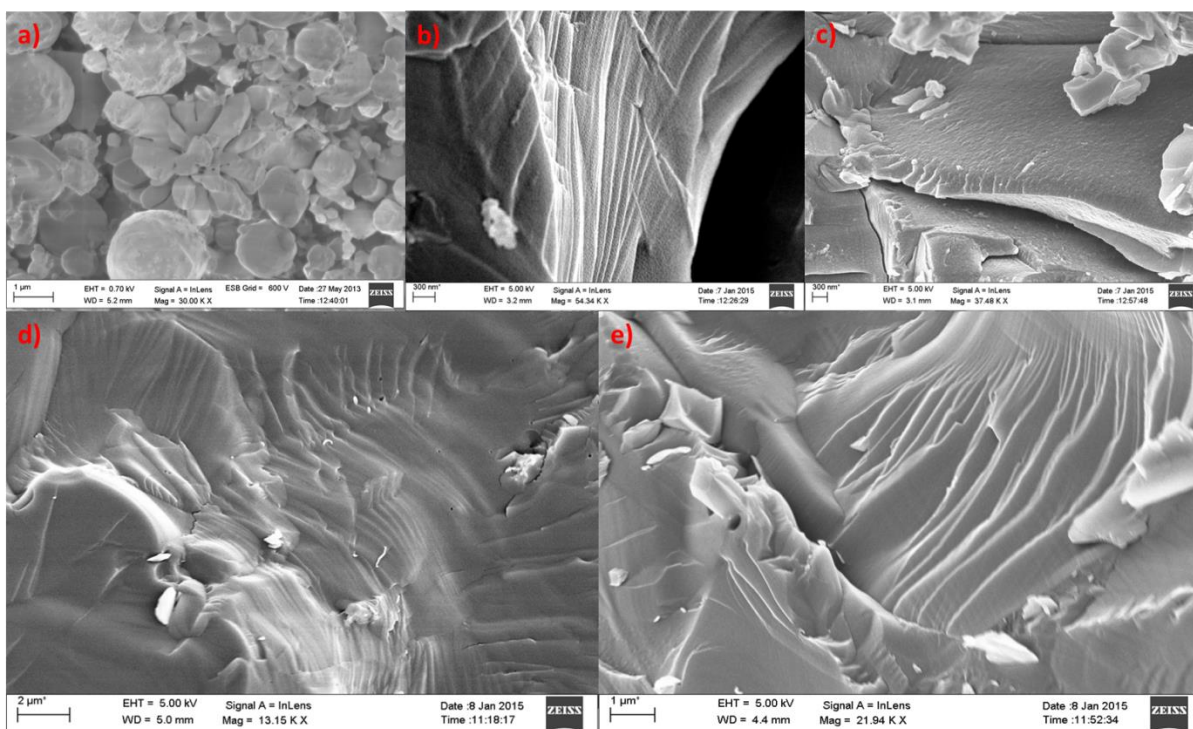


**Figure 25.** Cryo-SEM images of a) RTAQ b) 1% HDT-GO/AQ, c) 1% TP-GO/AQ, d) 5% HDT-GO/AQ and e) 5% TP-GO/AQ

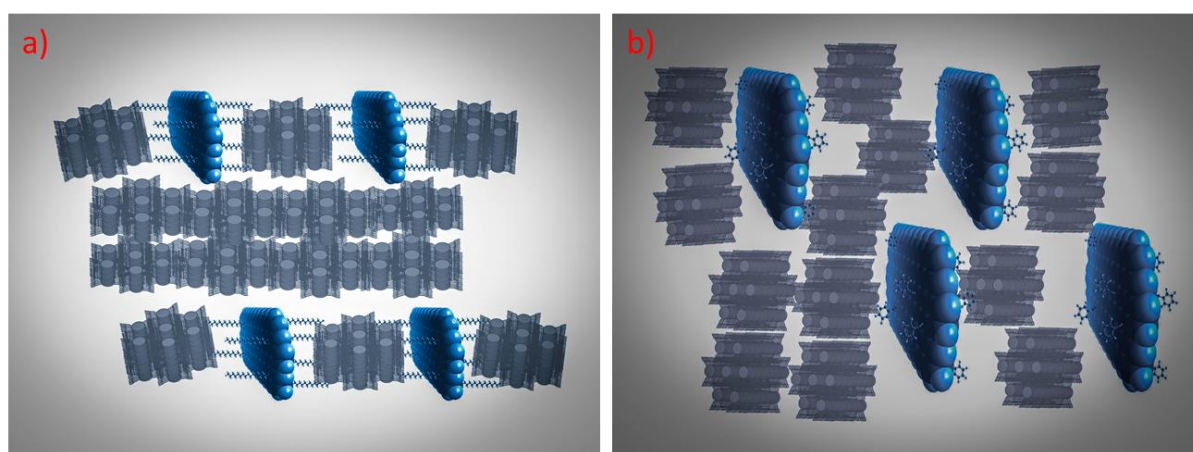


**Figure 26.** Schematic interpretation of self-assembly of a) hexadecanethiol functionalized graphene oxide in RTAQ, b) thiophene functionalized graphene oxide in RTAQ

### 3.5. Conclusions

In conclusion we have shown for the first time that graphene oxide can be functionalized with thiol which can self-assemble onto gold surface. The SEM images show presence of layered graphene oxide sheets on the gold strip. This monolayer film acting as blanket on the gold surface has potential application in various devices applications such as sensors, organic electronic devices etc. We have also studied the self-assembly of thiolated graphene oxide in supra-molecular structures of discotic liquid crystals, the observation reveals that thiolated graphene oxide due to its functionalization on the surface induces destabilization in columnar arrangement.

### 3.6. References:

1. Geim, A. K.; Novoselov, K. S., The Rise of Graphene. *Nat. Mater.* 2007, 6(3), 183–191.
2. Li, D.; Mueller, M. B.; Gilje, S.; Kaner, R. B.; Wallace, G. G., Processable Aqueous Dispersions of Graphene Nanosheets. *Nat. Nanotechnol.* 2008, 3(2), 101–105.
3. Novoselov, K. S.; Geim, A. K.; Morozov, S. V.; Jiang, D.; Zhang, Y.; Dubonos, S. V.; Grigorieva, I. V.; Firsov, A. A., Electric Field Effect in Atomically Thin Carbon Films. *Science* 2004, 306(5696), 666–669.
4. Zhang, Y.; Tan, Y. W.; Stormer, H. L.; Kim, P., Experimental Observation of the Quantum Hall Effect and Berry's Phase in Graphene. *Nature* 2005, 38(7065), 201–204.

5. Zimney, E. J.; Piner, R. D.; Dommett, G. H. B.; Evmenenko, G., Preparation and Characterization of Graphene Oxide Paper. *Nature* 2007, 448(7152), 457-460.
6. Allen, M. J.; Tung, V. C.; Kaner, R. B., Honeycomb Carbon: A Review of Graphene. *Chem. rev.* 2009, 110(1), 132-145.
7. Rao, C. N. R.; Sood, A. K.; Subrahmanyam, K. S., Graphene: The New Two Dimensional Nanomaterial. *Angew. Chem. Int. Ed.* 2009, 48, 7752 – 7777.
8. Bao, Z.; Liu, Z.; Chen, Y.; Peumans, P., Organic Solar Cells with Solution-Processed Graphene Transparent Electrodes. *Appl. Phys. Lett.* 2008, 92, 263302.
9. Eda, G.; Lin, Y. Y.; Miller, S.; Chen, C. W.; Su, W. F., Transparent and Conducting Electrodes for Organic Electronics from Reduced Graphene Oxide. *Appl. Phys. Lett.* 2008, 92, 233305.
10. Wu, J.; Agrawal, M.; Becerril, H. A.; Bao, Z.; Liu, Z.; Chen, Y.; Peumans, P., Organic Light-Emitting Diodes on Solution-Processed Graphene Transparent Electrodes. *ACS nano* 2010, 4, 43-48.
11. Dong, H.; Gao, W.; Yan, F.; Ji, H.; Ju, H., Fluorescence Resonance Energy Transfer between Quantum Dots and Graphene Oxide for Sensing Biomolecules. *Anal. chem.* 2010, 82(13), 5511-5517.
12. He, S.; Song, B.; Li, D.; Zhu, C.; Qi, W.; Wen, Y., A Graphene Nanoprobe for Rapid, Sensitive, and Multicolor Fluorescent DNA Analysis. *Adv. Fun. Mat.* 2010, 20(3), 453-459.

13. Li, S. S.; Tu, K. H.; Lin, C. C.; Chen, C. W.; Chhowalla, M., Solution-Processable Graphene Oxide as an Efficient Hole Transport Layer in Polymer Solar Cells. *ACS nano* 2010, 4(6), 3169-3174.
14. Loh, K. P.; Bao, Q.; Eda, G.; Chhowalla, M., Graphene Oxide as a Chemically Tunable Platform for Optical Applications. *Nat. chem.* 2010, 2, 1015-1024.
15. Zhang, C.; Yuan, Y.; Zhang, S.; Wang, Y., Biosensing Platform Based on Fluorescence Resonance Energy Transfer from Upconverting Nanocrystals to Graphene Oxide. *Angew. Chem. Int. Ed.* 2011, 50(30), 6851-6854.
16. Dreyer, D. R.; Park, S.; Bielawski, C. W., The Chemistry of Graphene Oxide. *Chem. Soc. Rev.* 2010, 39(1), 228-24.
17. Lerf, A.; He, H.; Forster, M.; Klinowski, J., Structure of Graphite Oxide Revisited. *J. Phys. Chem. B*, 1998, 102 (23), pp 4477-4482.
18. Stankovich, S.; Piner, R. D.; Nguyen, S. B. T.; Ruoff, R. S., Synthesis and Exfoliation of Isocyanate-Treated Graphene Oxide Nanoplatelets. *Carbon* 2006, 44(15), 3342-3347.
19. Yang, D.; Velamakanni, A.; Bozoklu, G.; Park, S.; Stoller, M., Chemical Analysis of Graphene Oxide Films after Heat and Chemical Treatments by X-Ray Photoelectron and Micro-Raman Spectroscopy. *Carbon* 2009, 47(1), 145-152.
20. Zhu, Y.; Murali, S.; Cai, W.; Li, X.; Suk, J. W., Graphene and Graphene Oxide: Synthesis, Properties, and Applications. *Adv. mat.* 2010, 22(35), 3906-3924.

21. Zhu, Y.; Murali, S.; Stoller, M. D.; Velamakanni, A.; Piner, R. D., Microwave Assisted Exfoliation and Reduction of Graphite Oxide for Ultracapacitors. *Carbon* 2010, 48(7), 2118-2122.
22. Tozzini, V.; Pellegrini, V., Prospects for Hydrogen Storage in Graphene. *Phys. Chem. Chem. Phys.*, 2013, 15, 80-89.
23. Wang, L.; Lee, K.; Sun, Y. Y.; Lucking, M.; Chen, Z.; Zhao, J. J., Graphene Oxide as an Ideal Substrate for Hydrogen Storage. *ACS Nano* 2009, 3 (10), pp 2995–3000.
24. Lee, J. K.; Smith, K. B.; Hayner, C. M.; Kung, H. H., Silicon Nanoparticles–Graphene Paper Composites for Li Ion Battery Anodes. *Chem. Commun.* 2010, 46, 2025-2027.
25. Wang, H.; Cui, L. F.; Yang, Y., Mn<sub>3</sub>O<sub>4</sub>– Graphene Hybrid as a High-Capacity Anode Material for Lithium Ion Batteries. *J. Am. Chem. Soc.*, 2010, 132 (40), pp 13978–13980.
26. Yang, X.; Zhang, X.; Ma, Y.; Huang, Y.; Wang, Y., Superparamagnetic Graphene Oxide–Fe<sub>3</sub>O<sub>4</sub> Nanoparticles Hybrid for Controlled Targeted Drug Carriers. *J. Mater. Chem.*, 2009, 19, 2710-2714.
27. Zhang, M.; Lei, D.; Yin, X.; Chen, L.; Li, Q.; Wang, Y., Magnetite/Graphene Composites: Microwave Irradiation Synthesis and Enhanced Cycling and Rate Performances for Lithium Ion Batteries. *J. Mater. Chem.*, 2010, 20, 5538-5543.
28. Zhou, G.; Wang, D. W.; Li, F.; Zhang, L.; Li, N., Graphene-Wrapped Fe<sub>3</sub>O<sub>4</sub> Anode Material with Improved Reversible Capacity and Cyclic Stability for Lithium Ion Batteries. *Chem. Mater.*, 2010, 22 (18), pp 5306–5313.

29. Zhu, Y.; Murali, S.; Stoller, M. D.; Ganesh, K. J.; Cai, W., Carbon-Based Supercapacitors Produced by Activation of Graphene. *Science* 2011, Vol. 332 no. 6037 pp. 1537-1541.
30. Yang, S.; Xu, B.; Zhang, J.; Huang, X.; Ye, J., Controllable Adsorption of Reduced Graphene Oxide onto Self-Assembled Alkanethiol Monolayers on Gold Electrodes: Tunable Electrode Dimension and Potential. *J. Phys. Chem. C*, 2010, 114 (10), pp 4389–4393.
31. Ramesha, G. K.; Sampath, S., Electrochemical Reduction of Oriented Graphene Oxide Films: An in Situ Raman Spectroelectrochemical Study. *J. Phys. Chem. C*, 2009, 113 (19), pp 7985–7989.
32. Wang, H.; Wang, X.; Li, X.; Dai, H., Chemical Self-Assembly of Graphene Sheets. *Nano Research* 2009, 2, 336.
33. Yang, Q. H.; Yang, Y. G.; Lv, W.; Wen, Y. F.; Hou, P. X., Self-Assembled Free-Standing Graphite Oxide Membrane. *Adv. Mater*, 2009,21(29), 3007-3011.
34. Shivanandareddy, A. B.; Krishnamurthy, S.; Lakshminarayanan, V.; Kumar, S., Mutually Ordered Self-Assembly of Discotic Liquid Crystal-Graphene Nanocomposites. *Chem, Commun.* 2014, 50, 710-712.
35. Ganesh, V.; Lakshminarayanan, V., Scanning Tunneling Microscopy, Fourier Transform Infrared Spectroscopy, and Electrochemical Characterization of 2-Naphthalenethiol Self-Assembled Monolayers. *J. Phys. Chem. B*, 2005, 109 (34), pp 16372–16381.
36. Bisoyi, H. K.; Kumar, S., Carbon Nanotubes in Triphenylene and Rufigallol-Based Room Temperature Monomeric and Polymeric Discotic Liquid Crystals. *J. Mater. Chem.*, 2008, 18, 3032-3039.

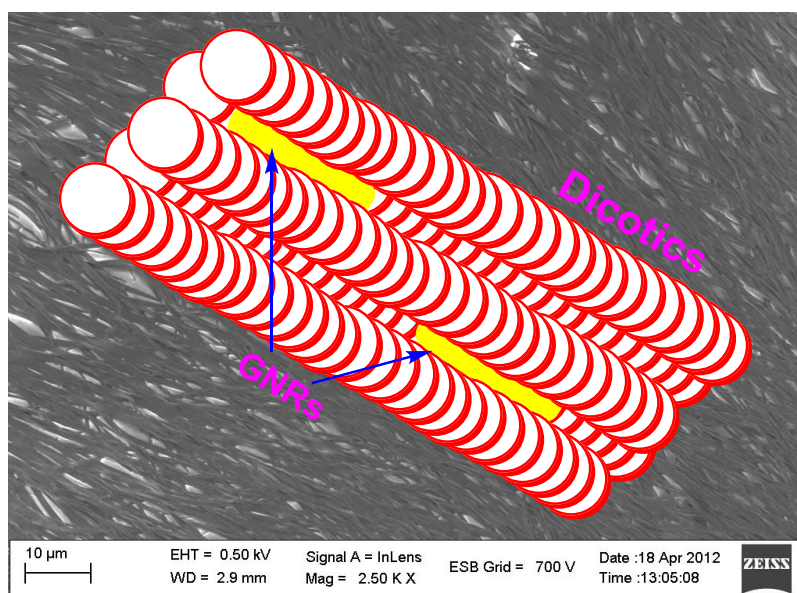
37. Stankovich, S.; Dikin, D. A.; Piner, R. D.; Kohlhaas, K. A., Synthesis of Graphene-Based Nanosheets Via Chemical Reduction of Exfoliated Graphite Oxide. *Carbon* 2007, 45, 1558–1565.
38. Seredych, M.; Bandosz, T. J., Mechanism of Ammonia Retention on Graphite Oxides: Role of Surface Chemistry and Structure. *J. Phys. Chem. C*, 2007, 111 (43), pp 15596–15604.
39. Dikin, D. A.; Stankovich, S.; Zimney, E. J.; Piner, R. D., Preparation and Characterization of Graphene Oxide Paper. *Nature* 2007, 448, 457.
40. Stankovich, S.; Dikin, D. A.; Compton, O. C., Systematic Post-Assembly Modification of Graphene Oxide Paper with Primary Alkylamines. *Chem. Mater.*, 2010, 22 (14), pp 4153–4157.
41. Beulen, M. W. J.; Huisman, B. H.; van der Heijden, P. A., Evidence for Nondestructive Adsorption of Dialkyl Sulfides on Gold. *Langmuir* 1996, 12(26), 6170-6172.
42. Castner, D. G.; Hinds, K.; Grainger, D. W., X-Ray Photoelectron Spectroscopy Sulfur 2p Study of Organic Thiol and Disulfide Binding Interactions with Gold Surfaces. *Langmuir* 1996, 12(21), 5083-5086.
43. Kim, J. Y.; Jin, M. H.; Park, C. Y.; Lee, Y. H., X-Ray Absorption Spectroscopy of Graphite Oxide. *EPL (Europhysics Letters)* 2008, 82, Number 6.
44. Ou, J.; Wang, J.; Liu, S.; Mu, B.; Ren, J.; Wang, H.; Yang, S., Tribology Study of Reduced Graphene Oxide Sheets on Silicon Substrate Synthesized Via Covalent Assembly. *Langmuir* 2010, 26 (20), pp 15830–15836.

45. Park, S.; An, J.; Piner, R. D.; Jung, I.; Yang, D., Aqueous Suspension and Characterization of Chemically Modified Graphene Sheets. *Chem. Mater.* 2008, 20 (21), pp 6592–6594
46. Ko, H.; Singamaneni, S.; Tsukruk, V. V., Nanostructured Surfaces and Assemblies as Sens Media. *Small* 2008, 4, 1576-1599.

# CHAPTER 4

---

## Gold Nanorods Embedded Discotic Nanoribbons



We have shown that gold nanorods (GNRs) can be easily inserted in the supramolecular order of discotic liquid crystals (DLCs) along the director without disturbing their mesomorphism. GNRs embedded discotic ribbons, useful for constructing devices like thin film transistors, sensors, etc., are prepared by simple solution processing of GNRs-DLC nanocomposites.

## 4.1 Introduction.

Nanoparticles are typically less than 100 nm in one dimension, they show properties that are very different from bulk Gold have gained great deal of attention in last two decades owing to ease of synthesis and reproducibility. Gold nanoparticles show number of interesting properties due to their plasmonic and optical properties, such as surface plasmon resonance (SPR), surface-enhanced Raman scattering (SERS), enhanced IR absorption, and nonlinear optical, electronic and magnetic properties. Plasmonic properties of gold nanoparticles vary as a function of their shape and size. Dielectric permittivity also plays an important role in plasmonic responses. gold nanoparticles have found applications in catalysis, optics, sensors, biological imaging, etc.<sup>1-3</sup>

Michael Faraday, an electrochemist, reported the synthesis of colloidal gold<sup>4</sup> in 1857 and after that the scientific research of gold nanoparticles received increased attention. During the past few years, a large number of methods have been developed to prepare gold nanoparticles with various shapes and sizes. Among various methods such as, electrochemical, gas phase and liquid phase synthesis, the preparation of gold nanoparticles in the liquid phase has received much attention due to its many advantages, such as large-scale production, reproducibility and good yield. These NPs are typically prepared via the reduction of gold salts in aqueous or organic media in the presence of surface stabilizers. Though the synthesis of alkanethiols protected GNPs has been reported by Mulvaney and Giersig in 1993,<sup>5</sup> the Brust–Schiffrin methods of monolayer-protected gold

nanoparticles in organic solvent appeared in 1994 have become the most popular methods for the synthesis of smaller gold particles.<sup>6-7</sup>

#### 4.1.1 Spherical or quasi-spherical metallic nanoparticles

Spherical nanoparticles are likely the best understood nanoparticles from chemical properties and stabilizing techniques point of views, and therefore, by far the most extensively investigated nanoparticles. The nanoparticles obtained from Brust–Schiffrin methods are commonly referred to as monolayer-protected gold nanoparticles. Usually, sodium borohydride a strong reducing agent is used to reduce gold(III) salt in the presence of an alkanethiol capping agent to produce 1–3 nm gold nanoparticles. The sizes of nanoparticles can be controlled between 2 and 5 nm by varying the thiol concentration.<sup>6-8</sup> Sodium borohydride being a strong reducing agent causes more nucleation and alkanethiol being a strong capping agent drastically inhibits the growth of nanoparticles. Subsequently, several other reducing agents, capping ligands and reaction conditions (e.g., single phase, biphasic reactions, low temperature) have been used to prepare a variety of GNPs. Additionally, several other methodologies such as photochemical, electrochemical, radiolytic, microwave and sonochemical methods have been developed to prepare gold nanoparticles.<sup>3</sup> Moreover, the ligand-exchange methodology allows incorporation of various surface functionalities on nanoparticles. These monolayer-protected gold metal clusters are promising materials, since they can be handled in a similar manner as general organic compounds due to their high stability under ambient conditions and

solubility in conventional organic solvents. Further, a variety of chemical reactions can be performed on functionalized gold nanoparticles.

#### 4.1.2 Liquid crystal-GNP hybrids

Though homogeneous mixing of anisotropic liquid crystals with isotropic spherical or quasi spherical NPs seems difficult, several efforts have been made to disperse these NPs in various liquid crystals in small amount. Efforts have also been made to create liquid crystalline nanoparticles via attaching anisotropic mesogens on the surface of nanoparticles, with the idea that if the anisotropic ligands impart sufficient anisotropy into the hybrid system, these nanoparticles may display mesomorphism. A number of liquid crystal-gold nanoparticles hybrids have been prepared to study their physical properties.<sup>9</sup> Primarily three methods have been used to prepare liquid crystal-gold nanoparticle hybrid systems. The simplest one is mixing of gold nanoparticles and liquid crystals in a solvent followed by removal of the solvent. To ensure good mixing of nanoparticles in liquid crystal media, usually organic soluble monolayer-protected metallic nanoparticles are used (often alkanethiol-protected gold nanoparticles) to prepare nanocomposites. Because of the non-compatibility of systems, only a very small amount of spherical nanoparticles can be homogeneously mixed in liquid crystals.

The ligand exchange of alkanethiol-protected GNPs with desired thiol-terminated mesogens provides mixed monolayer-protected gold nanoparticles having both alkane thiols and mesogens attached to the gold

surface. Such mixed monolayer-protected gold nanoparticles may have better compatibility with liquid crystalline media and can be obtained easily without using huge excess of thiol-terminated mesogen which is usually difficult to prepare. On the other hand, reduction of gold salt in the presence of an excess of thiol-terminated mesogens afford gold nanoparticles passivated with mesogens only. A flexible spacer is commonly used to attach mesogenic ligand with gold nanoparticles. A few such systems have been reported to be liquid crystalline in their pure state.<sup>10</sup>

Ensuring the purity of final isolated gold nanoparticles is very important. As the ligand is used in huge excess in the reaction, the unreacted ligand must be completely removed. If the ligand is not removed completely, the system may act as monolayer-protected gold nanoparticles dispersed in the ligand and if the ligand is itself liquid crystalline, it may give spurious results. Further, it is noteworthy that though the thiol-terminated ligand may not be liquid crystalline itself but its dimer (disulphide), formed in the reaction, could be liquid crystalline. Therefore, ascertaining the purity of liquid crystalline nanoparticles through the use of spectral and analytical techniques is quite important. Purification of the monolayer-protected gold nanoparticles is usually carried out through repeated precipitation (taking the nanoparticles in nonpolar solvent like dichloromethane and then adding an excess of a polar solvent like ethanol followed by centrifugation) or via chromatography or through a combination of these methods. However, unlike any organic material, it is generally difficult to get monolayer-protected nanoparticles of very high purity.

Metallic nanoparticles of gold, silver and palladium have been dispersed in various calamitic liquid crystals to study the effects of these nanoparticles on various physical properties of liquid crystals.<sup>9-12</sup> While studying physical properties of liquid crystal nanocomposites, care should be taken in selecting the liquid crystals having low isotropic temperature (preferably below 160 °C) as alkanethiol-coated nanoparticles often start decomposing above this temperature. Further, nanocomposites should be prepared by mixing two components (liquid crystals and nanoparticles) in a low boiling solvent such as dichloromethane or diethyl ether which can be removed easily at room temperature. Treatment of small nanoparticles at high temperature may increase their size significantly via migration of alkanethiols on the nanoparticles.

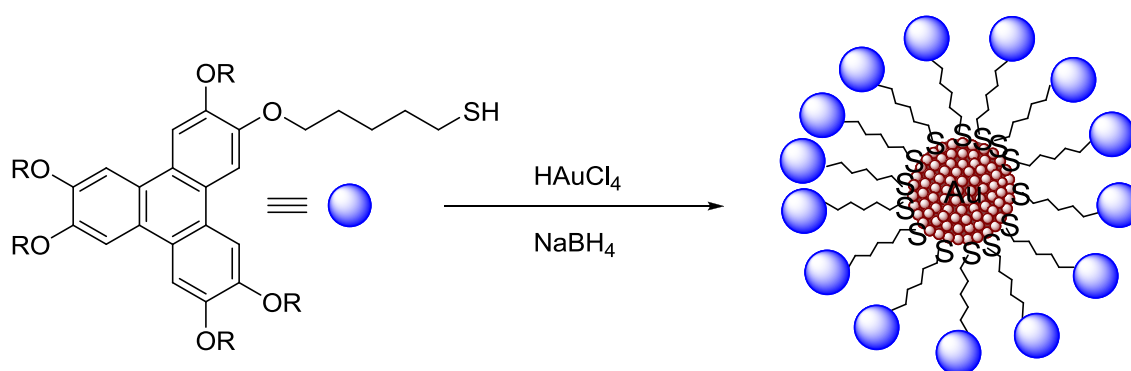
#### **4.1.3 Gold nanoparticles in discotic liquid crystals**

Dispersion of gold nanoparticles in discotic liquid crystals was done by doping simple hexanethiol-passivated gold nanoparticles in triphenylene and benzene-based discotic liquid crystals.<sup>13</sup> Gold nanoparticles with a core diameter of about 1.6 nm were prepared by reduction of gold salt ( $\text{HAuCl}_4$ ) with sodium borohydride in the presence of hexanethiol. These nanoparticles were dispersed in three different discotic liquid crystals, namely hexakis(hexylthio)triphenylene (HHTT), hexakis(pentyloxy)triphenylene (HPT) and hexakis(4-nonylphenylethynyl)benzene, by mixing (sonication) the two components, i.e., discotic liquid crystal and gold nanoparticles, in dichloromethane

followed by removal of the solvent and drying under vacuum at room temperature. While the dispersion of gold nanoparticles in calamitic nematic liquid crystals has been extensively studied,<sup>9-12</sup> discotic nematic phases have not yet received much attention. In a single experiment, hexakis(4-nonylphenylethynyl)benzene and gold nanoparticles were mixed in 1:1 ratio which resulted in the macroscopic phase separation of two components. This is not surprising as nanoparticles in such a high concentration cannot be dispersed homogeneously in any liquid crystal. Therefore, it is of paramount importance to look the dispersion of gold nanoparticles in small amounts and particularly in a room temperature discotic nematic liquid crystal.

On the other hand, smooth dispersion of hexanethiol-passivated gold nanoparticles in columnar phases of discotic liquid crystals could be realized.<sup>13</sup> Several binary mixtures of gold nanoparticles and HHTT were prepared and characterized from their spectral and thermal analysis. Increasing the amount of nanoparticles in discotic liquid crystals decreases the mesophase to isotropic temperature but the crystals to mesophase or mesophase to mesophase (helical phase to columnar phase) temperatures do not change significantly. Investigations performed by X-ray diffraction (XRD) studies on a gold nanoparticles-doped HHTT system described the formation of self-assembled superlattices of gold nanoparticles in the helical phase of HHTT.<sup>14</sup> An increase in the electrical conductivity of the nanocomposite was observed due to the presence of gold nanoparticles in the matrix.

Subsequently, gold nanoparticles fully covered with triphenylene discotics were synthesized with the idea that such a functionalization could yield liquid-crystalline nanoparticles.<sup>15</sup> These triphenylene-capped gold nanoparticles were prepared by reduction of  $\text{HAuCl}_4$  in the presence of a thiol-functionalized triphenylene derivative as shown in Scheme 1. Transmission electron microscopy (TEM) studies revealed that on surfaces the discotic functionalized nanoparticles self-assemble into hexagonal patterns believed to arise from the strong  $\pi$ - $\pi$  interactions between the triphenylene ligands of adjacent nanoparticles. Shen *et al.* prepared triphenylene-protected gold nanoparticles with different spacer lengths and investigated the self-assembled 1-D stripes and hexagonal close packed or disordered organization of gold nanoparticles as a function of the size of gold nanoparticles, alkyl chain lengths, interparticle  $\pi$ - $\pi$  interaction and solvent hydrophilicity.<sup>16</sup> It is interesting that the self-assembled structure of these nanoparticles could be controlled (hexagonal or 1D nanochain) just by altering the ratio of methanol to toluene in the solvent.



**Scheme 1.** Synthesis of discotic-decorated gold nanoparticles

Though mesomorphism was not observed in these discotic decorated gold nanoparticles, they could be dispersed in large quantities into the columnar phase of a related triphenylene derivative, owing to their chemical compatibility with one another. X-ray diffraction studies of the bulk composites suggested random distribution of gold nanoparticles between the domain gaps of the columnar phase in a disordered fashion (Figure 1). The dispersion of just 1% hexaalkoxytriphenylene-capped gold nanoparticles in a hexagonal columnar phase forming triphenylene discotic liquid crystals exhibits remarkable six orders of magnitude enhancement in the electrical conductivity of the system. Similar enhancement in the conductivity has also been observed when a triphenylene-based discotic liquid crystals was doped with about 1% of an electron-deficient molecule, trinitrofluorenone (TNF).<sup>17</sup> In the case of H7TP- gold nanoparticle composites, gold nanoparticles can act as electron deficient moiety. The large electrical conductivity of the nanocomposites could be due to the highly delocalized pi electron density of triphenylene molecules covalently bonded to gold nanoparticles which provide a facile path for electronic conduction. Holt *et al.* confirmed the six orders of magnitude enhancement in electrical conductivity in the hexagonal columnar phase of a triphenylene-based discotic liquid crystals doped with 1% methylbenzene thiol-covered gold nanoparticles.<sup>18</sup> The formation of small chain-like aggregates of gold nanoparticles upon applying DC field was proposed.

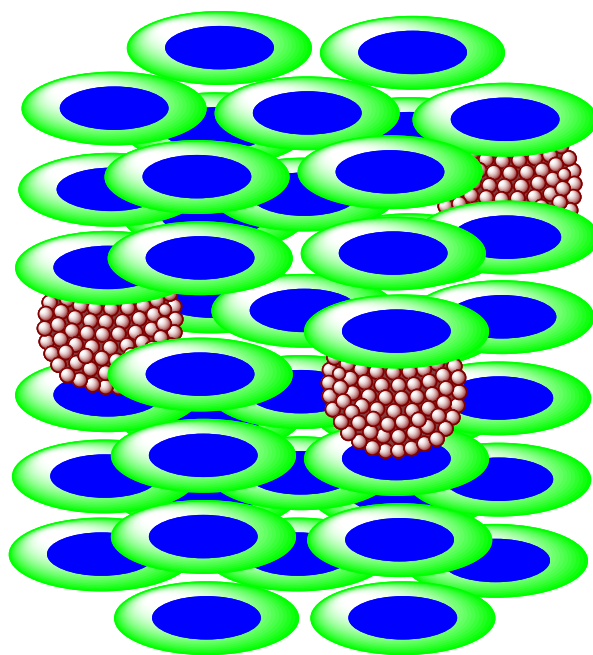


**Figure 1.** A simplified illustration of the NPs dispersion in a hexagonal columnar matrix.

Very recently, Basova *et al.*<sup>19</sup> reported nanocomposites of discotic tetra-substituted nickel phthalocyanine with hexadecylamine coated gold nanoparticles. Four composites containing 0.1, 1, 2 and 5 wt.% of hexadecylamine coated gold nanoparticles in phthalocyanine were prepared and studied for their mesomorphic and electrical properties. All composites containing 0.1-5 wt.% of gold nanoparticles were found to be liquid-crystalline in nature. Nanocomposites exhibit two orders of magnitude higher conductivity compared to pure discotic liquid crystal. The lateral conductivity tends to increase with the increase in gold nanoparticles concentration.

Supreet *et al.* studied the effect of dispersion of gold nanoparticles on optical and electrical properties of a polar nitro-functionalized triphenylene discotic liquid crystal.<sup>20</sup> Dispersions of hexanethiol-passivated gold nanoparticles of core diameter in range 1.2–2 nm in nitro-functionalized

triphenylene discotic liquid crystal were prepared with 0.25% to 1% gold nanoparticles in discotic liquid crystal. A decrease in orientational order parameter (S), an increase in relaxation time ( $\tau$ ) for disc motion with gold nanoparticles in Col<sub>p</sub> and enhancement in DC electrical conductivity by several orders of magnitude at ambient conditions was observed upon doping gold nanoparticles.

#### 4.1.4 Gold nanorods

Gold nanorods can be prepared by following two different approaches, top down method and bottom up method. Top down method requires physical lithography processes and gold deposition. In bottom up method the gold nanorods are grown in a medium containing gold salts, surfactants and reducing agent. Nucleation is initiated by a seed particle, over which the growth happens, shape anisotropy is often obtained due to templates.

Bottom up method of synthesis of gold nanorods, have been explored in great detail due to ease of the synthesis, some of the well-established synthetic routes are wet-chemical,<sup>21-23</sup> electrochemical,<sup>24</sup> microwave-assisted,<sup>25</sup> photochemical reduction techniques,<sup>26</sup> sonochemical,<sup>27</sup> and solvothermal.<sup>28</sup> Anodic aluminium oxide has been used as hard template to grow anisotropic gold nanorods. They possess cylindrical, monodisperse perpendicular pores with high densities and controllable pore sizes, gold salts are reduced in these pores by using reducing agents, external stimuli is used to trigger the reduction process.<sup>29-31</sup> Cationic ammonium surfactants are used as soft template to grow gold nanorods, among these surfactants

cetyltrimethylammonium bromide (CTAB) is the most common one. Surfactants also act as stabilizing agent and stops the nanorods from aggregating.<sup>32</sup>

Seed mediated method of growing gold nanorods makes use of soft template formed by CTAB. This method was developed independently by El-Sayed *et al.* and Murphy *et al.*<sup>21-22, 32</sup> In a typical growth, chloroauric acid (HAuCl<sub>4</sub>) is reduced using sodium borohydride (NaBH<sub>4</sub>) in an aqueous CTAB solution, to yield small Au nanoparticle seeds of 1.5 nm in size. A certain amount of the seed solution is then introduced into the growth solution. Growth solution is obtained by reducing Au(III) complex ions to Au(I) complex ions with ascorbic acid (mild reducing agent) in an aqueous CTAB solution. The added seeds thereafter catalyse the further reduction of Au(I) complex ions to form Au nanorods. Au nanorods in high yields can be obtained by adding small amount of AgNO<sub>3</sub> to the growth solution. In the absence of Ag<sup>+</sup> ions, the obtained product consists of nanocrystals having many different shapes, including spheres, triangular plates, and rods.<sup>32-33</sup>

Gold nanorods are very different when compared to gold nanoparticles, they possess very different physical properties, they have broad absorption band in visible region which in some cases can span up to near infra-red region, and the absorption band in gold nanorods can be tuned by varying the size of nanorods.<sup>34-35</sup> The shape of nanorods also contributes to surface enhanced Raman scattering, gold nanorods showed an enhancement of 10<sup>4</sup>-10<sup>5</sup> times for molecules absorbed on them, under similar conditions gold nanoparticles failed to show any enhancement.<sup>36</sup> Self-assembled gold

nanorods have been shown to enhance local electric field  $10^5$  times, this effect has been utilized to develop sensors.<sup>37-38</sup>

Liu *et al.* have explored dispersing and aligning gold nanorods in lyotropic nematic and lyotropic hexagonal phases.<sup>39</sup> Li *et al.* functionalized gold nanorods with discotic perylene and porphyrin molecules, they observed that functionalized gold nanorods aligned in a side by side arrangement due to intermolecular pi-pi attraction between discotic cores.<sup>40-42</sup>

#### 4.1.5 Organic nanoribbons.

The self-assembling property of discotic liquid crystal can be made use of to prepare nanofibers. The formation of 1-D nanostructures composed of discotic molecules with the pi planes stacking in the direction of the long axis of the nanofiber has received considerable interest because of the potential of such systems for electronic devices. Xiao *et al.*<sup>43</sup> reported that a discotic hexabenzocoronene derivative self-assemble into molecular stacks and that these stacks organize into cables or fibers. Wang *et al.* have formed nanowires of triphenylene by vapour deposition of triphenylene,<sup>44</sup> similarly Ji *et al.* prepared nanowires of perylenediimide and naphthalenediimide.<sup>45</sup> Nanowires derived from triphenylene, perylene and decacyclene discotics have been used for the sensing of chemical explosives.<sup>46-47</sup>

## 4.2 Objectives.

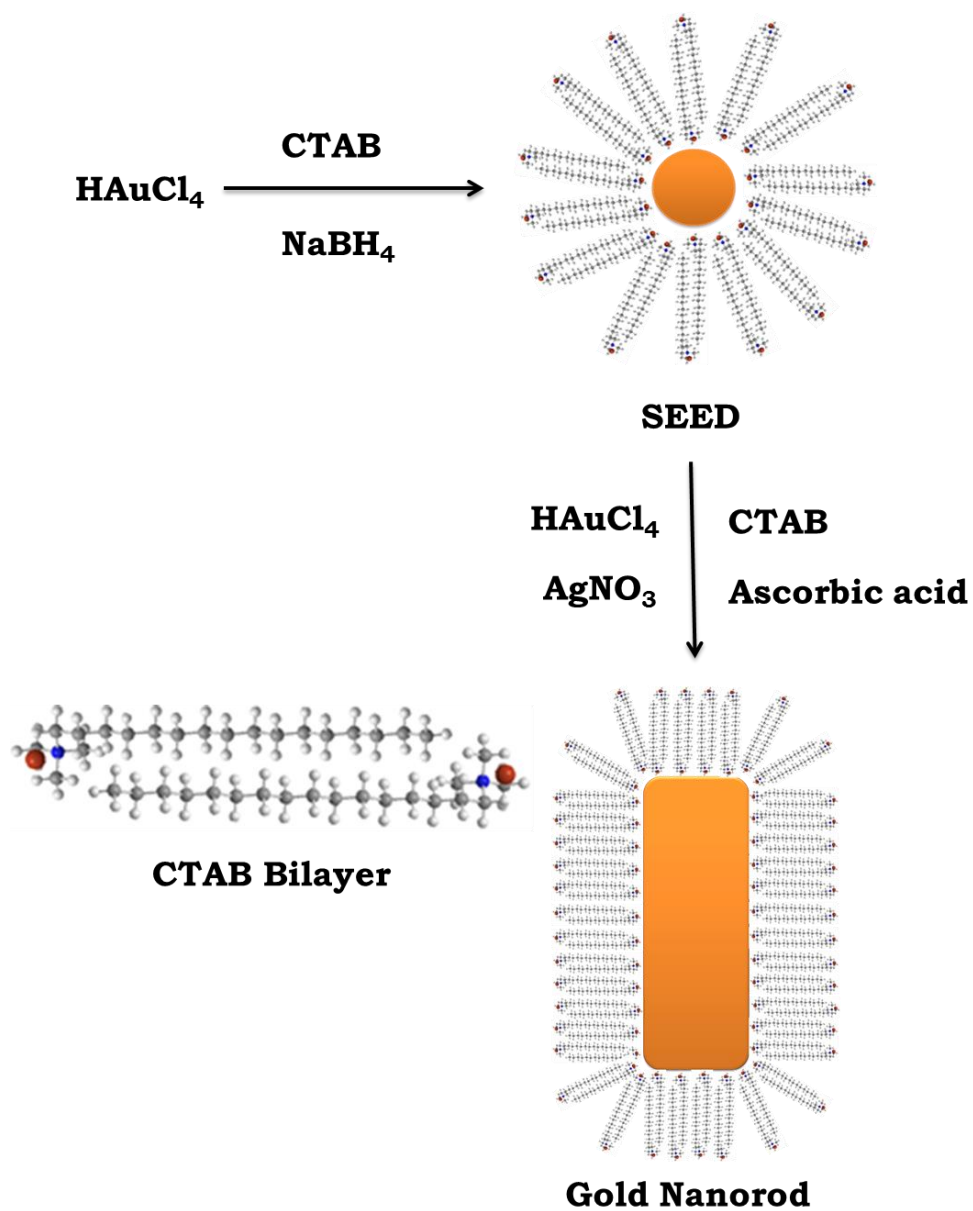
Columnar liquid crystals are excellent example of molecular wires thanks to the anisotropy in their conducting properties, which shows a higher conductivity along the length of the column compared to across it. This one dimensional conductivity was further enhanced by doping a small amount of nanoparticles in the liquid crystal. In this work we have tried to introduce another anisotropic nanomaterial, gold nanorods and try to align it with that of columnar liquid crystal. Presence of these nanorods would enhance the conductivity of the molecular wires. We have tuned the surface of gold nanorods such that they self-assemble into columnar mesophase with gold nanorods long axis aligned parallel to the long axis of columnar liquid crystal. This can be achieved by replacing the CTAB ligands from the gold nanorods with dodecanethiol. Dodecanethiol functionalized gold nanorods align in between columns where alkyl chains of columnar liquid crystal are present, due to van der Waals attraction between the alkyl chains on gold nanorods and that surrounding triphenylene nanoribbons.

## 4.3 Experimental Methods

### 4.3.1 Synthesis of gold nanorods.

Gold nanorods are prepared via seed-mediated growth method following the procedure of El-Sayed *et al.*<sup>22</sup> First step in this procedure involves

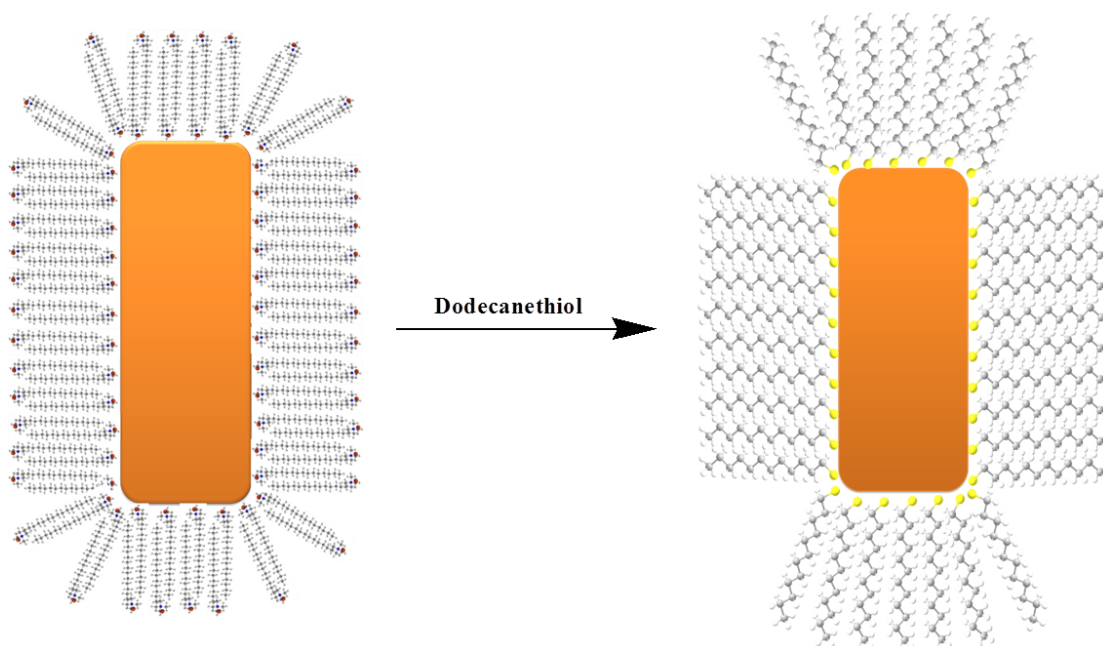
preparation of seed solution. 5mL, 0.20M CTAB solution was mixed with 5.0mL of 0.0005 M HAuCl<sub>4</sub>. This solution was stirred well to ensure proper dissolution. To the stirred solution 0.6 mL of ice cold 0.01M NaBH<sub>4</sub> was added. This resulted in the formation of a brownish yellow solution. Vigorous stirring of the seed solution was continued for 2 minutes and then stored at 25 °C, to be used for the growth of nanorods. 150 μL of 0.004M AgNO<sub>3</sub> was added to 5mL of 0.2M CTAB solution (aqueous) at 25 °C. To this solution, 5mL of 0.001M HAuCl<sub>4</sub> solution was added and after gentle mixing of the solution 70 μL of 0.0788M ascorbic acid was added. Ascorbic acid acts as a mild reducing agent and changes the growth solution from dark yellow to colourless. In the final step 12 μL of the seed solution is added to the growth solution at 27 - 30 °C. The colour of the solution gradually changed within ten minutes. The resultant solution can be retained for long times, as the gold nanorods are stable in this solution, for doping studies the resultant solution was centrifuged at 6000 rpm for 15 minutes and supernatant solution was pipetted out, gold nanorods settle down as precipitate, this precipitate is re-dispersed in Millipore water by sonication and centrifuged again, re-dispersing and centrifuging is done two more times, to remove all the non-ligated surfactants molecules from gold nanorods, they were then dispersed in Millipore water at a concentration of 10 mg/mL and used for further studies. The characterization of synthesized gold nanorods is included in results and discussion.



**Scheme 2.** Steps involved in synthesizing gold nanorods.

### 4.3.2 Ligand exchange of gold nanorods.

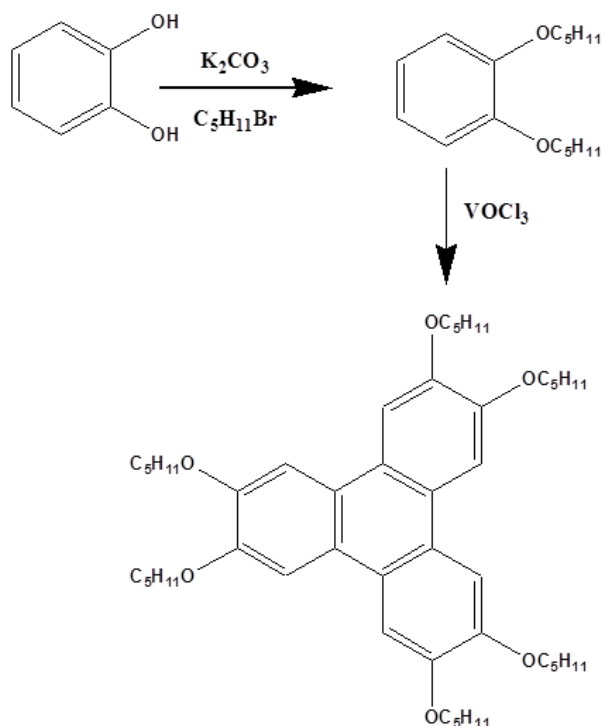
To prepare organic soluble gold nanorods, the gold nanorods solution obtained from the above procedure was taken. 10 ml of 100 mg gold nanorods solution taken and solvent was removed under vacuum (care should be taken to ensure temperature doesn't increase above 40°C), 100mg of gold nanorods is mixed with THF to which 2ml (in excess) of dodecanethiol was added. The mixture was sonicated in the beginning and stirred for 3 days (stirring was accompanied with sonication for 10 minutes every 2 hours, to ensure gold nanorods don't settle down) at room temperature. The dodecanethiol present in the solution displaces part of the CTAB from gold nanorods owing to the strong gold thiol interactions,<sup>48-49</sup> the resultant dodecanthiol functionalized gold nanorods (d-GNR) are dispersed in chloroform (1mg/ml).



**Scheme 3.** Ligand exchange on the surface of gold nanorods.

### 4.3.3 Synthesis of 2,3,6,7,10,11-hexakis(pentyloxy)triphenylene.

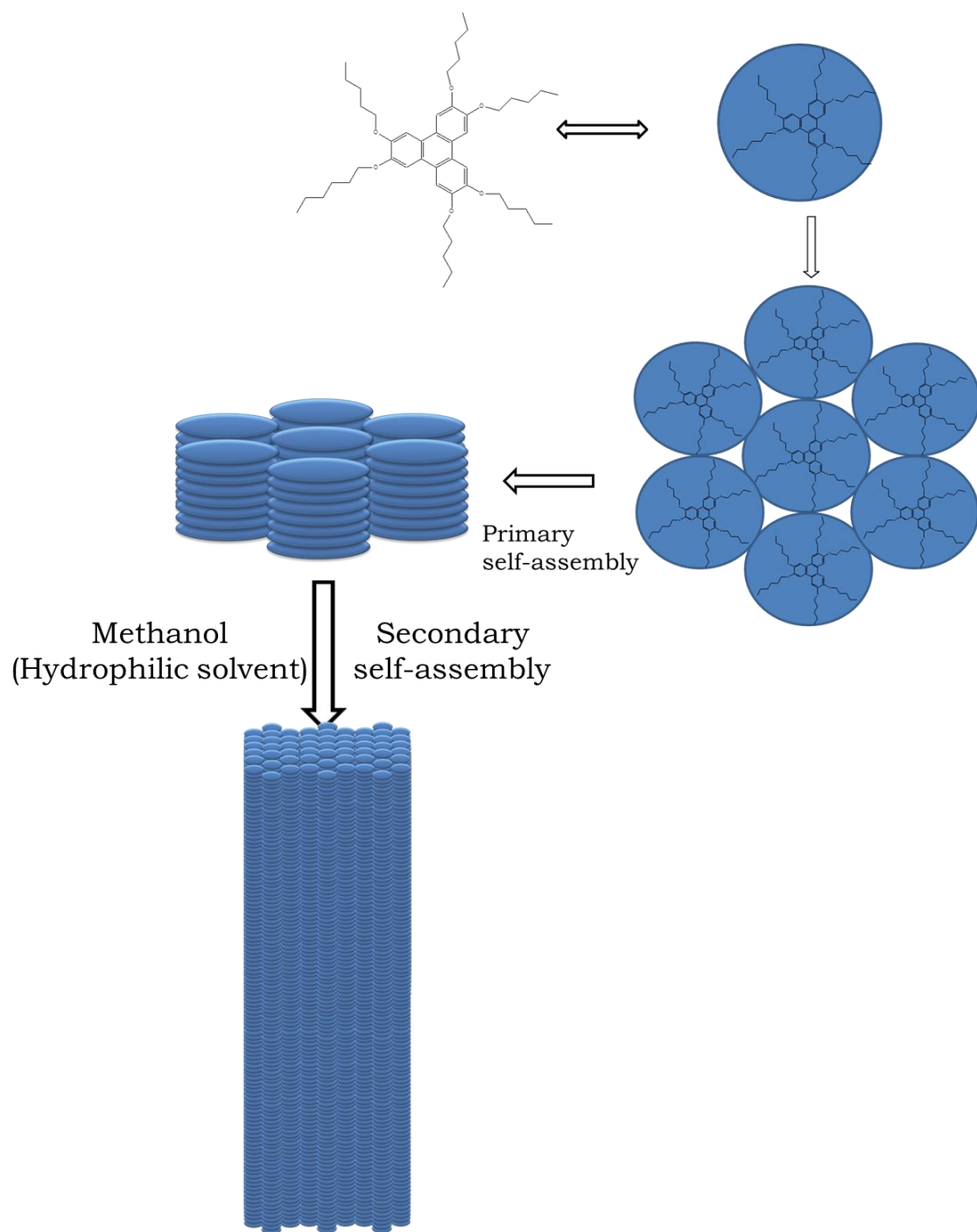
2,3,6,7,10,11-hexakis(pentyloxy)triphenylene (HPT) was synthesized by oxidative trimerization of 1,2-dipentyloxybenzene with  $\text{VOCl}_3$ . To a solution of 1,2-dipentyloxybenzene (0.01 mol) in dry  $\text{CH}_2\text{Cl}_2$  (10 mL),  $\text{VOCl}_3$  (0.026 mol) was added dropwise. The reaction mixture was stirred at r.t. for 5-10 min under  $\text{N}_2$  atm. The reaction was quenched with MeOH (10 mL), and extracted with  $\text{CH}_2\text{Cl}_2$  (4 \ 20 mL). The crude product was purified by repeated column chromatography over silica gel (hexane- $\text{CH}_2\text{Cl}_2$  mixtures). The characterization of synthesized HPT is included in results and discussion.



**Scheme 4.** Schematic diagram showing synthesis of 2,3,6,7,10,11-hexakis(pentyloxy)triphenylene.

#### 4.3.4 Preparation of Triphenylene Nanoribbons.

2,3,6,7,10,11-hexakis(pentyloxy)triphenylene (0.5 mg -1 mg) is taken in small test tube and dissolved in a minimal amount of  $\text{CHCl}_3$  (100-500  $\mu\text{L}$ ), alternatively one could take little excess of  $\text{CHCl}_3$  and carefully remove solvent to get concentrated solution. To the above prepared solution an excess of methanol/ethanol (1-2 mL) is added, the resultant solution contains triphenylene nanoribbons suspended in the solvent. One can instantly pipette it out and drop cast it on any substrate. If nanoribbons settle down after 10-15 min, one can sonicate it and re-suspend the nanoribbons in the solution.



**Scheme 5.** Preparation of triphenylene nanoribbons.

#### 4.3.5 Preparation of Composites.

2,3,6,7,10,11-hexakis(pentyloxy)triphenylene is used as the host liquid crystal. Three composites 1GNRTP, 2GNRTP and 5GNRTP are prepared for studies. 1GNRTP is prepared by taking 99 mg of HPT and adding 1mg of d-GNR, both are dissolved in chloroform and sonicated for one hour, after which solvent is removed by heating (under sonication). 2GNRTP is prepared by mixing 98mg of HPT and 2mg of d-GNR and 5GNRTP is prepared by mixing 95mg of HPT and 5mg of d-GNR.

**Table 1.** Describes the composition of 1GNRTP, 2GNRTP and 5GNRTP.

Sample	HPT (mg)	d-GNR (mg)	Doping percentage
1GNRTP	99	1	1%
2GNRTP	98	2	2%
5GNRTP	95	5	5%

#### 4.4 Results and discussion.

Gold nanorods prepared were characterized by transmission electron microscopy (TEM) (Figure 2) and UV-Vis spectroscopy (Figure 3). TEM image of gold nanorods (Figure 2a) shows that the nanorods prepared have an aspect ratio of 2.7, it has dimensions of 40 nm in length and 15 nm in breadth. UV-Vis Spectra of gold nanorods in aqueous medium, has two peaks, a small peak at 515 nm and a peak at 733nm. These are transverse

and longitudinal plasmon bands respectively, typical of gold nanorods (Figure 3).<sup>22</sup> The band at 515 nm has a shoulder band 581 nm this is due to dog bone shape of gold nanorods which have slightly thicker edges compared to middle portion.<sup>50</sup>

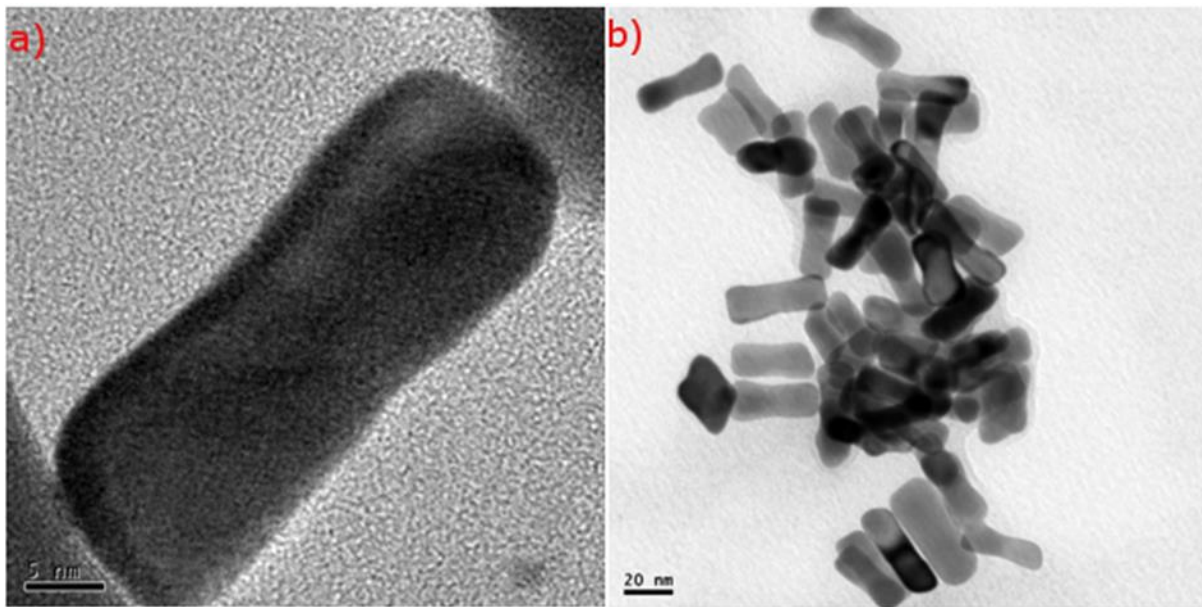


**Figure 2.** (a&b) TEM image of gold nanorod.

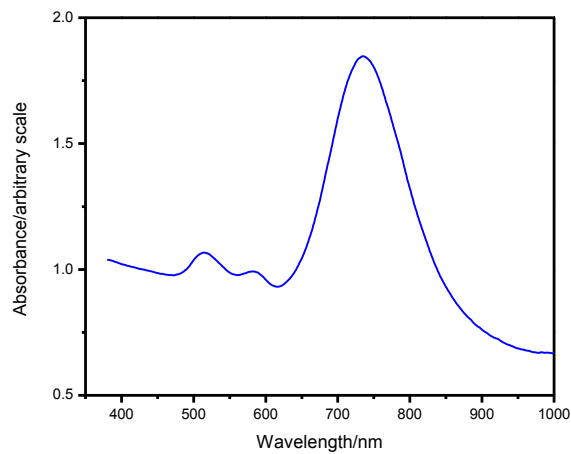


**Figure 3.** UV-Vis Spectra of gold nanorods in aqueous medium.

2,3,6,7,10,11-hexakis(pentyloxy)triphenylene, was characterized using proton-NMR, POM, X-ray diffraction and DSC studies. The  $^1\text{H}$  NMR (500 MHz;  $\text{CDCl}_3$ ) shows following signals, which were in accordance with that reported for pure compound.  $\delta_{\text{H}}$  7.7 (6H, Ar-H), 4.16 (12H,  $\text{ArOCH}_2$ ), 1.88 (12H, aliphatic  $\text{CH}_2$ ), 1.37 (24H, aliphatic  $\text{CH}_2$ ), 0.9 (18H, aliphatic  $\text{CH}_3$ ). HPT showed melting transition into mesophase at 64.8  $^\circ\text{C}$ , the mesophase lasted up to 122.5  $^\circ\text{C}$ . At this temperature it clears to isotropic liquid. The POM images showed the columnar hexagonal texture typical of HPT, this observation of columnar hexagonal phase was also confirmed by XRD.

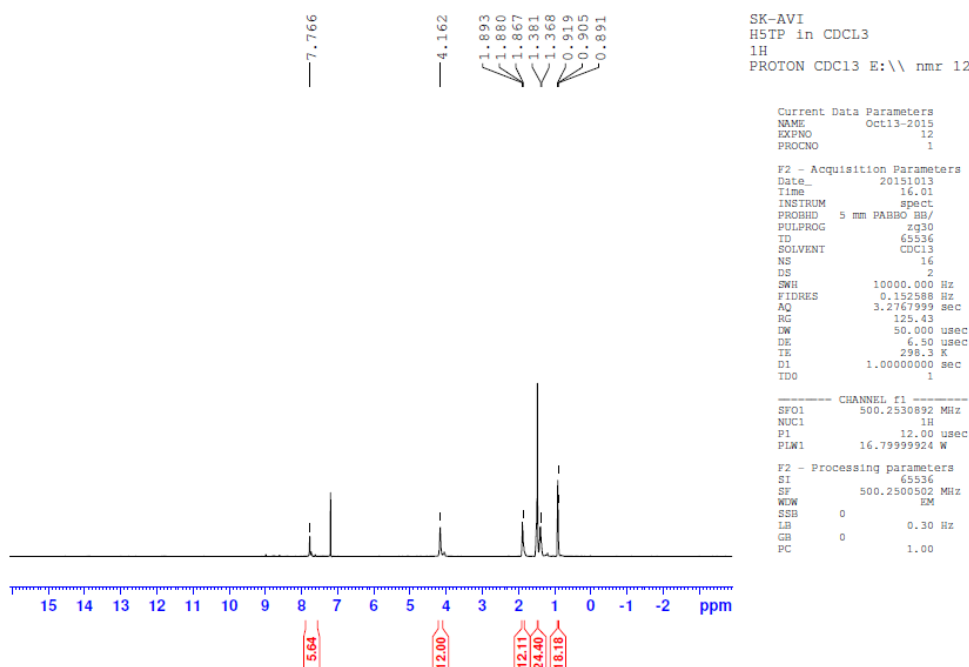


**Figure 4.**  $^1\text{H}$  NMR spectra of 2,3,6,7,10,11-hexakis(pentyloxy)triphenylene.

The UV-vis spectra of pure HPT and doped samples 1GNRTP, 2GNRTP, and 5GNRTP showed similar peaks typical of HPT (Figure 5), indicating that the addition of gold nanorods does not change absorption band of triphenylene systems. Plasmon resonance band of gold nanorods are not observed in the spectra of composites, as their concentration was very low.

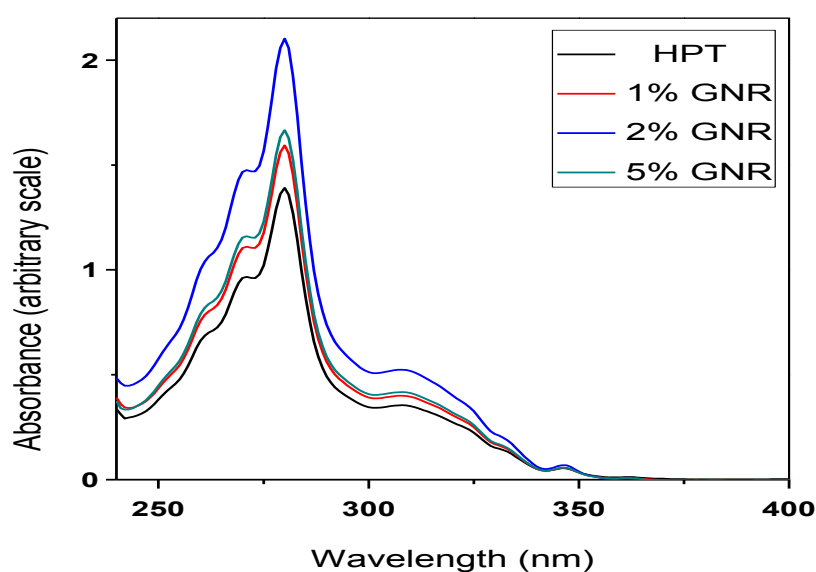


**Figure 5.** UV-Vis Spectra of HPT (black), 1GNRTP (red), 2GNRTP (blue), 5GNRTP (green) in chloroform.

The mesophase behaviour of the HPT and its composites 1GNRTP, 2GNRTP, and 5GNRTP was deduced by POM, DSC and XRD analysis. All the composites showed liquid crystalline behaviour. POM textures of the pure HPT as well as gold nanorods composites (Figure 6) show columnar hexagonal textures, none of the composites showed any phase segregation indicating that gold nanorods are evenly dispersed in the mesophase. Dodecanethiol functionalization of gold nanorods helps them to evenly

disperse in the mesophase along with the alkyl chains of columnar liquid crystal.

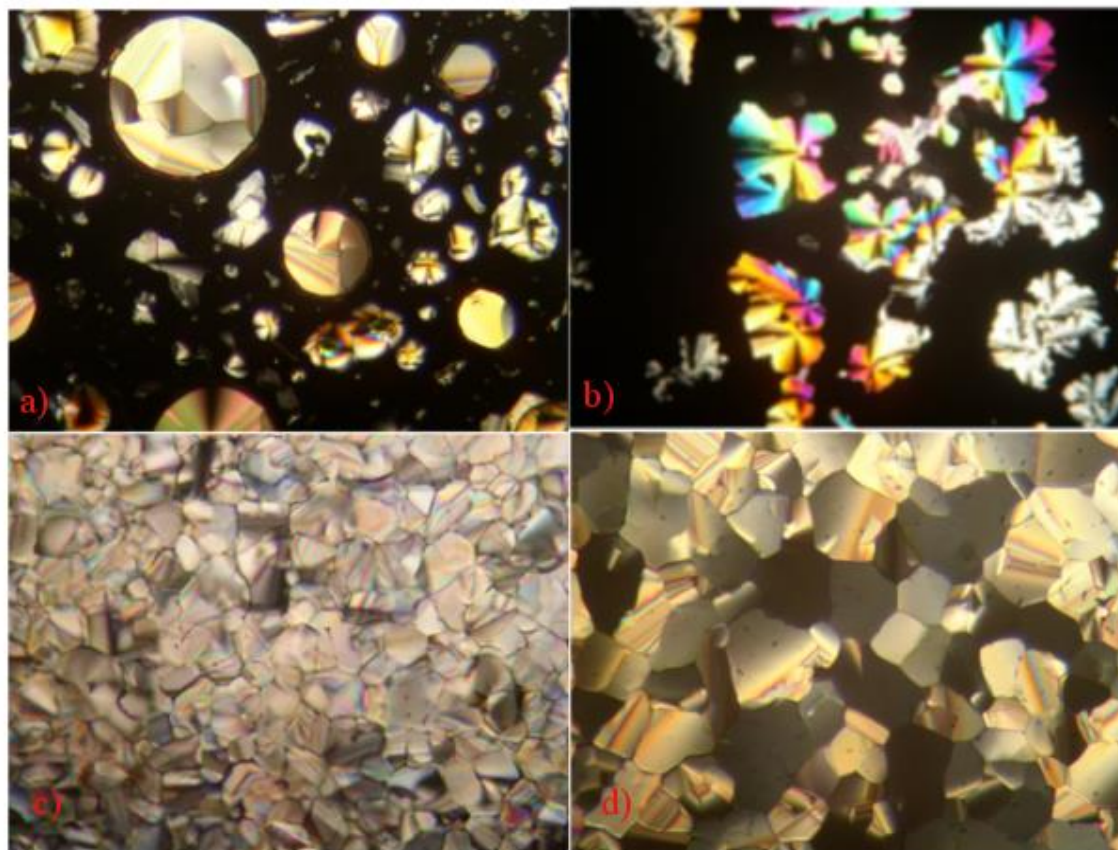


**Figure 6.** POM textures of (a) HPT, (b) 1GNRTP, (c) 2GNRTP and (d) 5GNRTP. The photographs were taken under crossed polarisers at 90 °C; 50 X magnification.

Differential scanning calorimetry (DSC) of composites 1GNRTP, 2GNRTP, and 5GNRTP were recorded and compared with HPT to analyse the transition temperatures and enthalpy associated with it (Figure 7). Table 2 shows the melting and clearing temperatures of HPT and its gold nanorod composites. The doped samples show a small increase in melting temperature compared to the pure HPT, while the clearing temperatures are

not affected much. This observation shows that gold nanorods stabilize the peripheral alkyl chain melting without imparting any significant effect on core-core packing. Enhanced stability in melting transition could be due to van der Waals interaction between alkyl chains surrounding the discotics and dodecanethiol alkyl chains present on gold. Interestingly we observed that mesophase to crystal transition during cooling cycle, appeared to happen at relatively higher temperature compared to pure HPT this behaviour is due to the fact that gold nanorods in the mesophase act as seeding agents and thus initiates the crystallization of the mesophase prior to that of HPT.

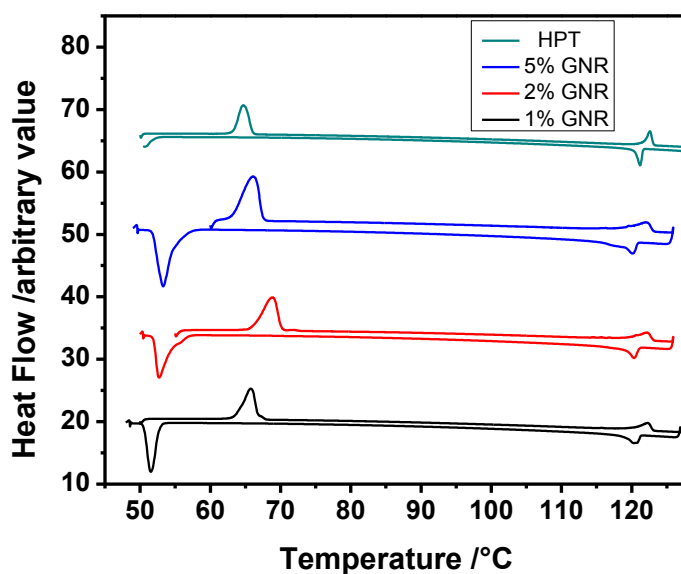


**Figure 7.** DSC curves of HPT (green), 1GNRTP (black), 2GNRTP (red) and 5GNRTP (blue)

**Table 2.** Transition temperatures and enthalpy associated with it, of pure HPT and the gold nanorod composites.

Sample	Cr $\rightarrow$ Col <sub>h</sub>	Col <sub>h</sub> $\rightarrow$ I
HPT	64.8 °C (42.92 J/g)	122.5 °C (11.26 J/g)
1GNRTP	65.8 °C (42.46 J/g)	122.1 °C (10.81 J/g)
2GNRTP	68.8 °C (41.04 J/g)	122.1 °C (8 J/g)
5GNRTP	66.1 °C (42.12 J/g)	122 °C (9.06 J/g)

The X-ray diffraction patterns were recorded for HPT and composites 1GNRTP, 2GNRTP, and 5GNRTP under the same conditions at 90 °C. One-dimensional intensity vs.  $2\theta$  and diffraction patterns for pure HPT and composites are shown in (Figure 8), all the samples showed similar plot with  $d$  spacings of first two reflection having a ratio of 1:  $1/\sqrt{3}$  typical of Columnar hexagonal phase. There is not much difference found between HPT and composites indicating that the insertion of GNRs does not destroy columnar arrangement of discs.

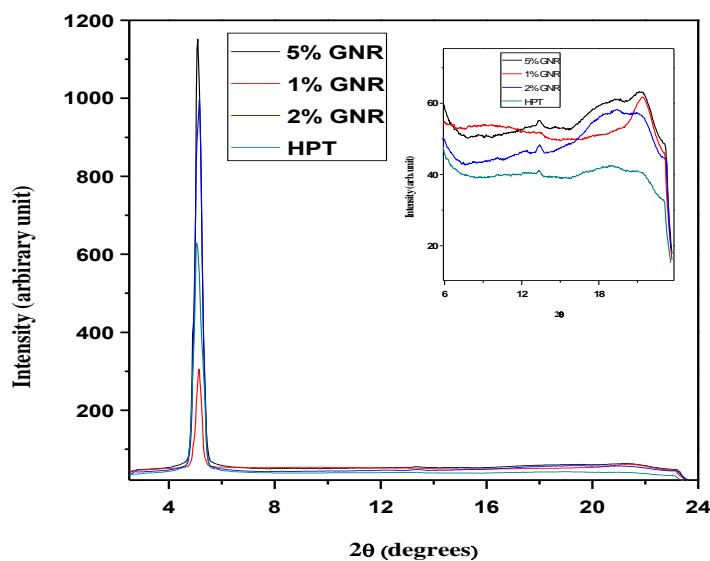


**Figure 8.** One dimensional intensity vs.  $2\theta$  and diffraction patterns for pure HPT (green), 1GNRTP (red), 2GNRTP (blue), 5GNRTP (black). Inset shows the expanded portion.

The undoped HPT sample shows a conductivity of  $7.2 \times 10^{-9} \text{ Sm}^{-1}$  at  $132 \text{ }^\circ\text{C}$ , conductivity of the sample increased with increase in temperature. Mesophase conductivity of HPT varies from  $4.7 \times 10^{-10} \text{ Sm}^{-1}$  at  $65 \text{ }^\circ\text{C}$  to  $4.5 \times 10^{-9} \text{ Sm}^{-1}$  at  $122 \text{ }^\circ\text{C}$ . The doped samples show much higher conductivity, 1GNRTP shows conductivity of  $1.22 \times 10^{-6} \text{ Sm}^{-1}$  at  $121 \text{ }^\circ\text{C}$  but above isotropic phase conductivity decreased to  $6 \times 10^{-7} \text{ Sm}^{-1}$ . 2GNRTP shows conductivity of  $8.95 \times 10^{-6} \text{ Sm}^{-1}$  at  $120.5 \text{ }^\circ\text{C}$  but above isotropic phase which decreases to  $2.5 \times 10^{-6} \text{ Sm}^{-1}$ . 5GNRTP shows conductivity of  $9.27 \times 10^{-6} \text{ Sm}^{-1}$  at  $115 \text{ }^\circ\text{C}$  but above isotropic phase conductivity decreased to  $2.1 \times 10^{-6} \text{ Sm}^{-1}$ . In all the cases the conductivity in the mesophase increases with increases in temperature (Figure 9).

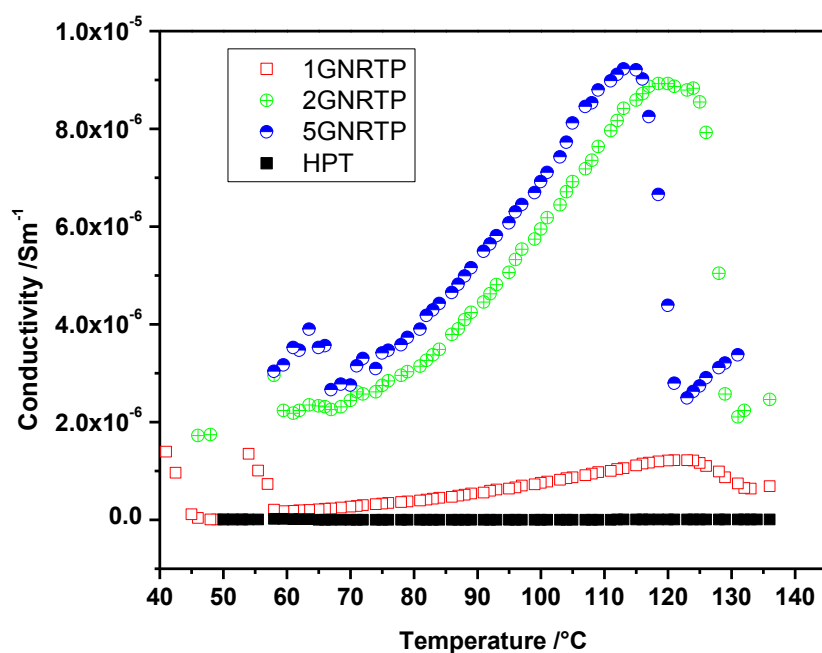


**Figure 9.** Conductivity of the samples HPT (black), 1GNRTP (red), 2GNRTP (green), 5GNRTP (blue).

Discotic nanoribbons are formed when a solution of HPT or HPT-GNR composites in chloroform was added to methanol. The resultant material was drop casted on silicon substrate and copper grid for SEM and STEM analysis respectively. Both HPT and gold nanorod composites showed long ribbon like structures (Figure 10) formed by coming together of many hexagonal columns. The non-polar alkyl chains surrounding the discs, in a polar solvent drive the columnar structure formed by individual discs to come together and form supramolecular aggregates. This leads columnar structures to form supramolecular ribbon like structure.

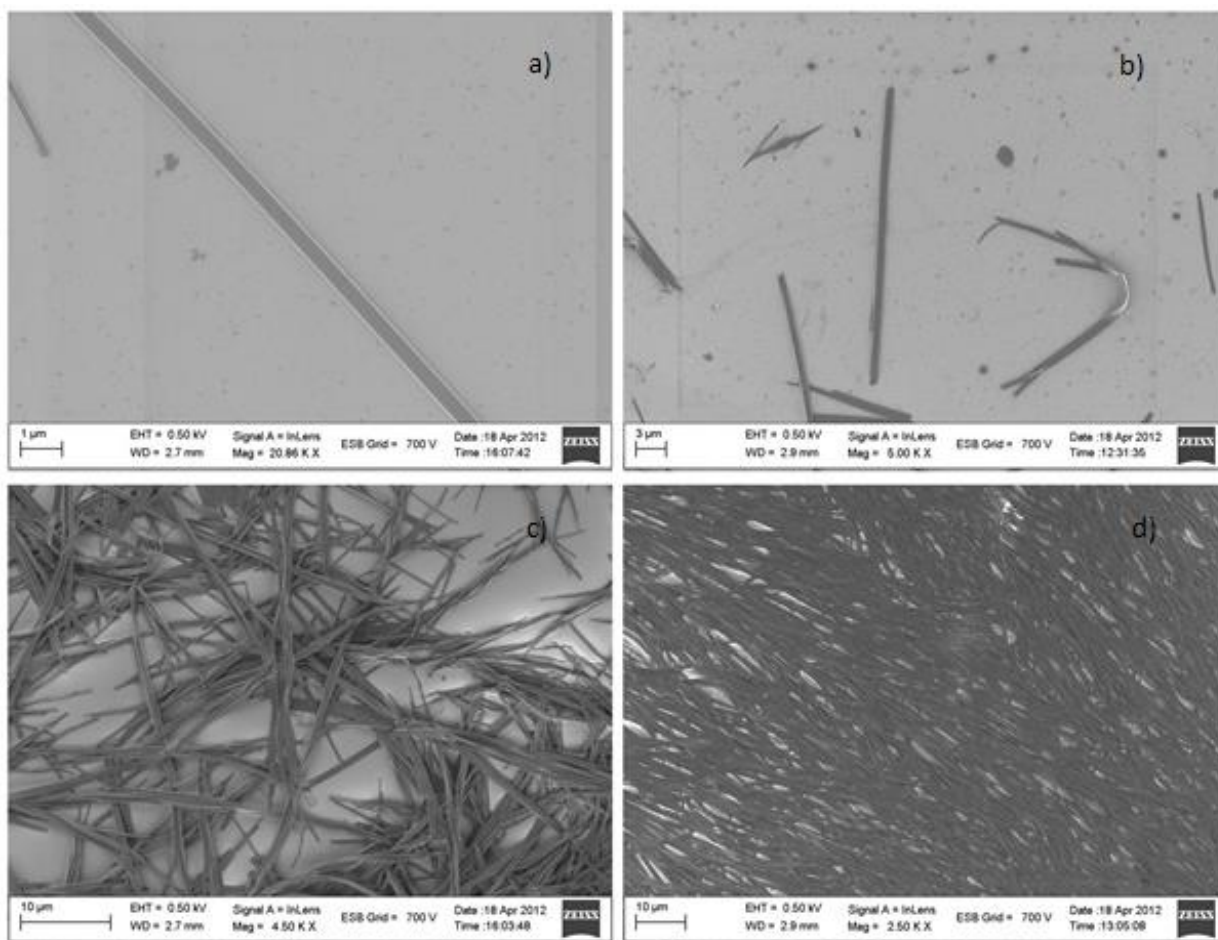


**Figure 10.** SEM images of (a) single ribbon of HPT, (b) ribbons formed by 1 GNRTTP, (c) randomly oriented ribbons of HPT and (d) bundles of ribbons formed by 1GNRTTP.

Dark field STEM images of 5GNRTTP ribbons (Figure 11) confirm the presence of gold nanorods in the supramolecular order. The image clearly shows that gold nanorods are aligned with its long axis parallel to length of the ribbon. This can be represented by the model shown in Figure 12.

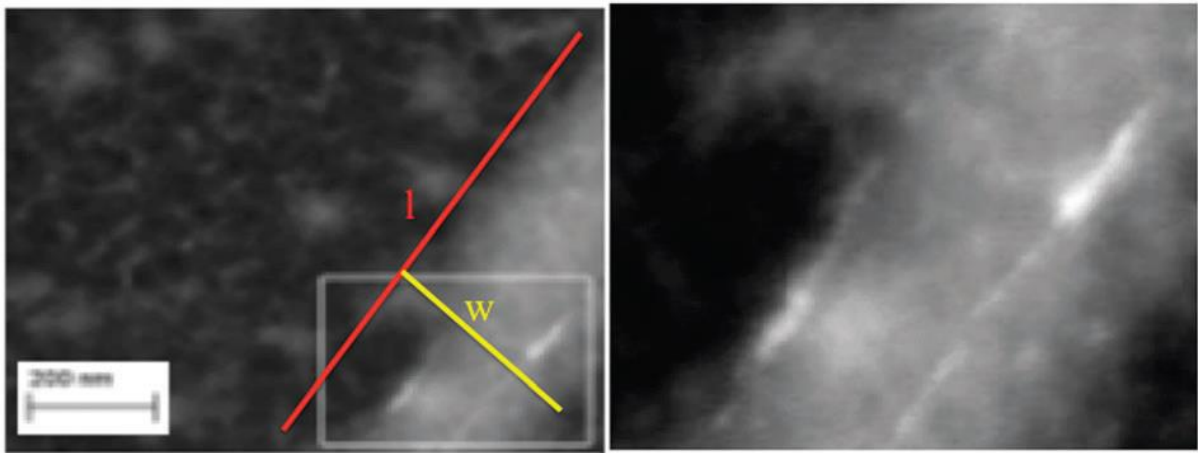


**Figure 11.** Dark field STEM images of gold nanorods embedded in HPT ribbons; (a) bright spots in the fibres are due to gold nanorods embedded in the ribbon with their longitudinal axis parallel to length of ribbon, (b) magnified portion of figure (a) showing gold nanorods of length  $\sim 40$  nm in ribbons.

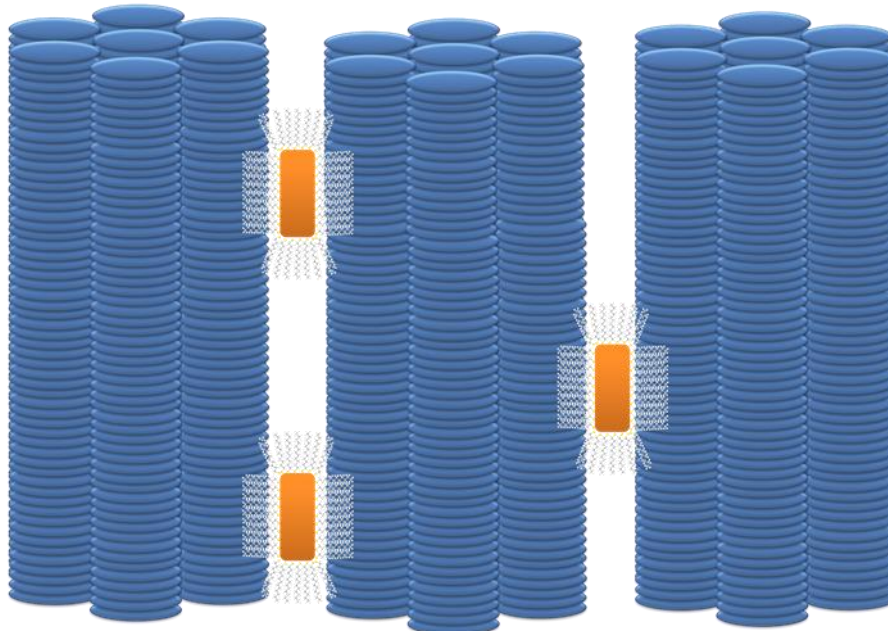


**Figure 12.** Schematic representation of GNRs embedded discotic ribbons.

## 4.5 Conclusion.

We have shown that hexpentyloxytriphenylene primarily self-assembles into hexagonal structures, which on proper solution processing can be made to grow into ribbon like secondary structures. During the growth, these supramolecular structures can trap the gold nanorods present in the solution, thus forming supramolecular nanocomposites. These nanocomposites show enhanced conductivity owing to insertion of nanorods in ribbon like structures.

## 4.6 References

1. Daniel, M.-C.; Astruc, D., Gold Nanoparticles: Assembly, Supramolecular Chemistry, Quantum-Size-Related Properties, and Applications toward Biology, Catalysis, and Nanotechnology. *Chem. Rev.* 2004, 104, 293–346.
2. Zhao, P.; Li, N.; Astruc, D., State of the Art in Gold Nanoparticle Synthesis. *Coord. Chem. Rev.* 2013, 257, 638
3. Louis, C.; Pluchery, O., Gold Nanoparticles for Physics, *Chemistry and Biology.* 2012.
4. Faraday, M., The Bakerian Lecture: Experimental Relations of Gold (and Other Metals) to Light. *Transactions of the Royal Society of chemistry,* 1857.
5. Giersig, M.; Mulvaney, P., Preparation of Ordered Colloid Monolayers

- by Electrophoretic Deposition. *Langmuir* 1993, 9 (12), pp 3408–3413.
6. Brust, M.; Fink, J.; Bethell, D.; Schiffrin, D. J., Synthesis and Reactions of Functionalised Gold Nanoparticles. *J. Chem. Soc., Chem. Commun.*, 1995, 1655-1656.
  7. Brust, M.; Walker, M.; Bethell, D.; Schiffrin, D. J., Synthesis of Thiol-Derivatised Gold Nanoparticles in a Two-Phase Liquid–Liquid System. *J. Chem. Soc., Chem. Commun.*, 1994, 801-802.
  8. Michael, J. H., et al., Alkanethiolate Gold Cluster Molecules with Core Diameters from 1.5 to 5.2 Nm: Core and Monolayer Properties as a Function of Core Size. *Langmuir* 1998, 14 (1), pp 17–30.
  9. Goodby, J. W., *Handbook of Liquid Crystals*. Vol. 6, Vol. 6; Wiley-VCH: Weinheim, 2014.
  10. Nealon, G. L.; Greget, R.; Dominguez, C., Liquid-Crystalline Nanoparticles: Hybrid Design and Mesophase Structures. *Beilstein J. Org. Chem.* 2012, 8, 349–370.
  11. Lagerwall, J. P. F.; Scalia, G., A New Era for Liquid Crystal Research: Applications of Liquid Crystals in Soft Matter Nano-, Bio-and Microtechnology. *Current Applied Physics* 2012, 12, 1387.
  12. Stamatoiu, O.; Mirzaei, J.; Feng, X.; Hegmann, T., Nanoparticles in Liquid Crystals and Liquid Crystalline Nanoparticles. *Liquid Crystals* 2012, 318, 331.
  13. Kumar, S.; Lakshminarayanan, V., Inclusion of Gold Nanoparticles into a Discotic Liquid Crystalline Matrix. *Chem. commun.* 2004, 1600-1601.
  14. Vijayaraghavan, D.; Kumar, S., Self-Assembled Superlattices of Gold Nanoparticles in a Discotic Liquid Crystal. *Mol. Cryst. Liq. Cryst.* 2009, 508,

101.

15. Kumar, S.; Pal, S. K.; Kumar, P. S.; Lakshminarayanan, V., Novel Conducting Nanocomposites: Synthesis of Triphenylene-Covered Gold Nanoparticles and Their Insertion into a Columnar Matrix. *Soft Matter* 2007,3, 896-900.

16. Shen, Z.; Yamada, M.; Miyake, M., Control of Stripelike and Hexagonal Self-Assembly of Gold Nanoparticles by the Tuning of Interactions between Triphenylene Ligands. *J. Am. Chem. Soc.* 2007, 129 (46), pp 14271–14280.

17. Balagurusamy, V. S. K.; Prasad, K. S., Quasi-One Dimensional Electrical Conductivity and Thermoelectric Power Studies on a Discotic Liquid Crystal. *Pramana-J. of Phy.* 1999, 53, 3-11.

18. Holt, L. A.; Bushby, R. J.; Evans, S. D.; Burgess, A., A 106-Fold Enhancement in the Conductivity of a Discotic Liquid Crystal Doped with Only 1%(W/W) Gold Nanoparticles. *J. Appl. Phys.* 2008, 103, 063712.

19. Basova, T. V.; Parkhomenko, R. G.; Igumenov, I. K., Composites of Liquid Crystalline Nickel Phthalocyanine with Gold Nanoparticles: Liquid Crystalline Behaviour and Optical Properties. *Dyes and Pigments* 2014, 111, 58-63.

20. Supreet; Pratibha, R.; Kumar, S.; Raina, K. K., Effect of Dispersion of Gold Nanoparticles on the Optical and Electrical Properties of Discotic Liquid Crystal. *Liquid Crystals* 2014, 41, 933.

21. Gole, A.; Murphy, C. J., Seed-Mediated Synthesis of Gold Nanorods: Role of the Size and Nature of the Seed. *Chem. Mater.* 2004, 16 (19), pp 3633–3640.

22. Nikoobakht, B.; El-Sayed, M. A., Preparation and Growth Mechanism of Gold Nanorods (Nrs) Using Seed-Mediated Growth Method. *Chem. Mater.* 2003, 15 (10), pp 1957–1962.
23. Ye, X.; Jin, L.; Caglayan, H.; Chen, J.; Xing, G.; Zheng, C., Improved Size-Tunable Synthesis of Monodisperse Gold Nanorods through the Use of Aromatic Additives. *ACS Nano* 2012, 6 (3), pp 2804–2817.
24. Yu, Y. Y.; Chang, S. S.; Lee, C. L., Gold Nanorods: Electrochemical Synthesis and Optical Properties. *J. Phys. Chem. B* 1997, 101 (34), pp 6661–6664.
25. Zhu, Y. J.; Hu, X. L., Microwave-Polyol Preparation of Single-Crystalline Gold Nanorods and Nanowires. *Chemistry Letters* 2003, 32, 1140.
26. Kim, F.; Song, J. H.; Yang, P., Photochemical Synthesis of Gold Nanorods. *J. Am. Chem. Soc.* 2002, 124 (48), pp 14316–14317.
27. Okitsu, K.; Sharyo, K.; Nishimura, R., One-Pot Synthesis of Gold Nanorods by Ultrasonic Irradiation: The Effect of Ph on the Shape of the Gold Nanorods and Nanoparticles. *Langmuir* 2009, 25 (14), pp 7786–7790.
28. Cao, J.; Ma, X.; Zheng, M.; Liu, J.; Ji, H., Solvothermal Preparation of Single-Crystalline Gold Nanorods in Novel Nonaqueous Microemulsions. *Chemistry Letters* 2005, 34, 730.
29. Bachtold, A.; Huber, R.; Birk, H.; Stauer, U., Template Synthesis of Nanowires in Porous Polycarbonate Membranes: Electrochemistry and Morphology. *J. Phys. Chem. B* 1997, 101 (28), pp 5497–5505.
30. Cepak, V. M.; Martin, C. R., Preparation and Stability of Template-Synthesized Metal Nanorod Sols in Organic Solvents. *J. Phys. Chem. B.*

1998, 102 (49), pp 9985–9990.

31. van der Zande, B. M. I.; Böhmer, M. R.; Fokkink, L. G. J., Colloidal Dispersions of Gold Rods: Synthesis and Optical Properties. *Langmuir* 2000, 16 (2), pp 451–458.

32. Jana, N. R.; Gearheart, L.; Murphy, C. J., Seed-Mediated Growth Approach for Shape-Controlled Synthesis of Spheroidal and Rod-Like Gold Nanoparticles Using a Surfactant Template. *Adv. Mater.* 2001, 13, 1389.

33. Busbee, B. D.; Obare, S. O.; Murphy, C. J., An Improved Synthesis of High Aspect Ratio Gold Nanorods. *Adv. Mater.* 2003, 15, 414.

34. Link, S.; El-Sayed, M. A., Spectral Properties and Relaxation Dynamics of Surface Plasmon Electronic Oscillations in Gold and Silver Nanodots and Nanorods. *J. Phys. Chem. B*, 1999, 103 (40), pp 8410–8426.

35. Murphy, C. J.; Sau, T. K.; Gole, A. M., Anisotropic Metal Nanoparticles: Synthesis, Assembly, and Optical Applications. *J. Phys. Chem. B*, 2005, 109 (29), pp 13857–13870.

36. Nikoobakht, B.; Wang, J.; El-Sayed, M. A., Surface-Enhanced Raman Scattering of Molecules Adsorbed on Gold Nanorods: Off-Surface Plasmon Resonance Condition. *Chemical Physics Letters* 2002, 366, 17-23.

37. Funston, A. M.; Novo, C.; Davis, T. J.; Mulvaney, P., Plasmon Coupling of Gold Nanorods at Short Distances and in Different Geometries. *Nano Lett.*, 2009, 9 (4), pp 1651–1658.

38. Jain, P. K.; El-Sayed, M. A., Plasmonic Coupling in Noble Metal Nanostructures. *Chemical Physics Letters* 2010, 153, 487.

39. Liu, Q.; Cui, Y.; Gardner, D.; Li, X.; He, S.; Smalyukh, II, Self-Alignment of Plasmonic Gold Nanorods in Reconfigurable Anisotropic Fluids

for Tunable Bulk Metamaterial Applications. *Nano Lett.*, 2010, 10 (4), pp 1347–1353.

40. Xue, C.; Birel, O.; Gao, M.; Zhang, S.; Dai, L., Perylene Monolayer Protected Gold Nanorods: Unique Optical, Electronic Properties and Self-Assemblies. *J. Phys. Chem. C* 2012, 116 (18), pp 10396–10404.

41. Xue, C.; Birel, O.; Li, Y.; Ma, X.; Gao, M.; Urbas, A., Porphyrin Metal Complex Monolayer-Protected Gold Nanorods: A Parallel Facile Synthesis and Self-Assembly. *Journal of colloid and interference science* 2013, 398, 1-6.

42. Xue, C.; Xu, Y.; Pang, Y.; Yu, D.; Dai, L.; Gao, M.; Urbas, A., Organo-Soluble Porphyrin Mixed Monolayer-Protected Gold Nanorods with Intercalated Fullerenes. *Langmuir* 2012, 28 (14), pp 5956–5963.

43. Xiao, S.; Tang, J.; Beetz, T.; Guo, X., Transferring Self-Assembled, Nanoscale Cables into Electrical Devices. *J. Am. Chem. Soc.* 2006, 128 (33), pp 10700–10701.

44. Wang, H.; Xu, X.; Kojtari, A.; Ji, H. F., Triphenylene Nano/Microwires for Sensing Nitroaromatics. *J. Phys. Chem. C* 2011, 115 (41), pp 20091–20096.

45. Ji, H.-F. F.; Majithia, R.; Yang, X.; Xu, X.; More, K., Self-Assembly of Perylenediimide and Naphthalenediimide Nanostructures on Glass Substrates through Deposition from the Gas Phase. *J. Am. Chem. Soc.*, 2008, 130 (31), pp 10056–10057.

46. Che, Y.; Yang, X.; Liu, G.; Yu, C.; Ji, H.; Zuo, J., Ultrathin N-Type Organic Nanoribbons with High Photoconductivity and Application in Optoelectronic Vapor Sensing of Explosives. *J. Am. Chem. Soc.* 2010, 132

(16), pp 5743–5750.

47. Wang, H.; Xu, X.; Li, L.; Yang, C.; Ji, H. F., Optoelectronic Property and Sensing Applications of Crystalline Nano/Microwires of Decacyclene.

*Micro & Nano Letters* 2011, 6, 763.

48. Jebb, M.; Sudeep, P. K.; Pramod, P.; Thomas, K. G.; Kamat, P. V., Ruthenium(II) Trisbipyridine Functionalized Gold Nanorods. Morphological

Changes and Excited-State Interactions. *J. Phys. Chem. B*, 2007, 111 (24), pp 6839–6844.

49. Vigdeman, L.; Manna, P.; Zubarev, E. R., Quantitative Replacement of Cetyl Trimethylammonium Bromide by Cationic Thiol Ligands on the

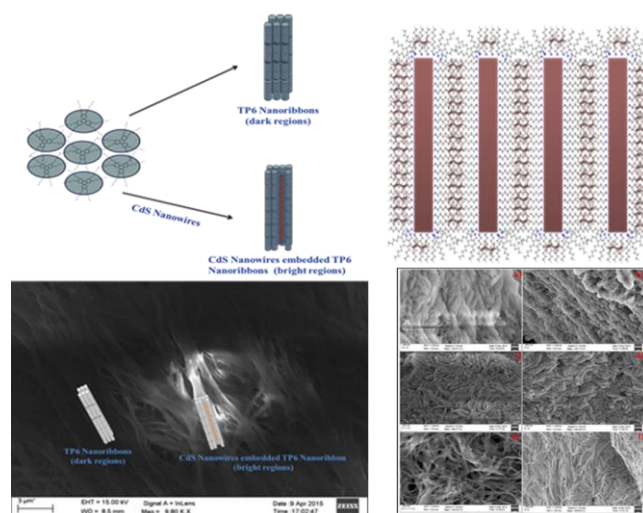
Surface of Gold Nanorods and Their Extremely Large Uptake by Cancer Cells. *Angew. Chem* 2012, 51, 636-641.

50. Gou, L.; Murphy, C. J., Fine-Tuning the Shape of Gold Nanorods.

*Chem. Mater.* 2005, 17 (14), pp 3668–3672.

# Chapter 5

## Self-assembly of CdS Nanowires into Lyotropic Lamellar Phase, and in Supramolecular Organic Nanoribbons



### Abstract

We demonstrate the incorporation of Cadmium sulphide nanowires in the supramolecular order of discotic liquid crystal. This was studied by polarized optical microscopy, differential scanning calorimetry, X-ray diffraction, FE-SEM and EDAX. Results indicate that CdS nanowires were trapped in ribbon like structures of hexahexyloxytriphenylene discotic liquid crystals. We have also shown formation of lyotropic lamellar phase in CdS nanoribbons in cyclohexane, and we have characterized this self-organization by polarized optical microscopy, differential scanning calorimetry, X-ray diffraction, Cryo-SEM techniques.

## 5.1 Introduction

Many one-dimensional (1-D) nanomaterials have attracted much attention of researchers due to their unique properties and potential uses in both mesoscopic research and in the development of nanodevices.<sup>1-6</sup> Nanoparticles made of semiconductor materials have been extensively studied during the past decade because of their potential applications in the life sciences and materials science.<sup>7-9</sup> Semiconductor nano-structures like quantum dots, and nanowires belonging to group II-VI have been prepared and extensively studied for various applications. CdS is one of the very important mid band gap II-VI group semiconductors. Recently the chemical synthesis of 2-D colloidal nanostructures has been perfected. These chemical synthesis methods provide an alternate to more expensive method like molecular beam epitaxy. These synthesized 2-D colloidal nanostructures act as quantum wells where photogenerated excitons undergo strong 1-D spatial confinement due to the finite thickness of the nanostructures.<sup>10</sup> Because of their bandgap (direct wide band gap 2.42 eV), which covers a wide range of wavelengths,<sup>11</sup> their applications in solar cells, optoelectronics and electronic devices, LED's, laser diodes and thin film transistors, have been sought.

### 5.1.1 Semiconducting NPs in discotic liquid crystals

#### 5.1.1.1 CdSe Quantum dots in discotic liquid crystals

Nanoparticles made of semiconductor materials, often referred to as quantum dots have been extensively studied during the past decade because

of their potential applications in the life sciences and materials science.<sup>7, 9</sup> Compared to pure metallic nanoparticles, much larger variety of quantum dots can be prepared via the combination of various elements, for example, quantum dots belonging to group II and VI elements (e.g., CdSe, CdS, CdTe, ZnO, ZnSe and so on), group IV and VI elements (e.g., PbS, PbSe, SnS and so on), and group III and V elements (e.g., InP, InS, InN and so on) have been prepared and extensively studied for various properties. Among all the quantum dots, CdSe quantum dots have received much attention in materials science due to their interesting photoluminescence properties.

High-quality monodisperse Cd-based quantum dots can be easily prepared by several methods.<sup>12-14</sup> Liquid crystalline medium can also be used to prepare these nanoparticles.<sup>15</sup> With the hope that excellent optical and electronic properties of CdSe quantum dots can be coupled with the self-organizing behavior of liquid crystals and such liquid crystal-quantum dot nanocomposites may exhibit mutually beneficial effects on various electro-optical properties. A number of quantum dots have been dispersed in various calamitic liquid crystals.<sup>16</sup>

Kumar *et al.* looked the dispersion of CdSe quantum dots in discotic liquid crystals.<sup>17</sup> Organic soluble, octadecylamine passivated CdSe quantum dots of two different sizes, 2.4 and 3.5 nm, were prepared and dispersed in a columnar matrix of hexabutyloxytriphenylene (H4TP) discotic liquid crystal. The formation of spherical particles with uniform sizes and shapes was confirmed by transmission electron microscopy (TEM). The narrow size distribution of the particles was inferred from the photoluminescence spectra of the quantum dots. The absorption and emission spectra show an

apparent red-shift, as expected, with the increase in the size of the particle. Nanocomposites of discotic liquid crystal and CdSe quantum dots were prepared by mixing the two components in a low boiling solvent via sonication followed by removal of the solvent and drying in vacuum. Several composites with 1%, 2%, 3% and 5% of CdSe quantum dots in H4TP were prepared and analyzed using POM, DSC and XRD. Like metallic gold nanoparticles dispersion in discotic liquid crystals, CdSe quantum dots also get dispersed in columnar matrix of discotic liquid crystals. The hexagonal columnar lattice of the discotic liquid crystal remains unaffected by the insertion of quantum dots. Similar to gold nanoparticles, a random distribution of quantum dots in the columnar phase was visualized. The electrical conductivity of the composites was found to be enhanced by two orders of magnitude. The enhancement in the conductivity could be a result of the formation of electron donor–acceptor interactions between the electron-rich organic triphenylene and the inorganic semiconductor.

#### 5.1.1.2 ZnO nanoparticles in discotic liquid crystals

Zinc oxide (ZnO) is a wide band gap semiconductor of the II–VI semiconductor group. It possesses a direct band gap of 3.37 eV and large excitonic binding energy of about 60 meV at room temperature.<sup>18</sup> ZnO nanoparticles can be employed as a non-toxic alternative to metal chalcogenides. They have potential application in devices like, light-emitting

diodes, field-effect transistors, photo diodes, ultraviolet photo detectors, solar cells, UV light emitters, sensors and lasers.<sup>19</sup> The dispersion of ZnO nanoparticles into calamitic ferroelectric liquid crystal and nematic liquid crystal have been investigated.<sup>20-21</sup> The addition of ZnO nanoparticles in the SmC\* phase improves the optical contrast and reduces the threshold voltage of liquid crystal display devices. A physical model describing an interaction of ZnO nanoparticles with the surrounding ferroelectric liquid crystal molecules was proposed.<sup>22</sup> Doping of ZnO nanoparticles in surface-stabilized ferroelectric liquid crystals was found to improve the alignment of the ferroelectric liquid crystal molecules, and a field-induced reorientation process was also observed.<sup>23</sup> The role of ZnO nanoparticles in ordering the liquid crystalline systems that can be used for photovoltaic applications was studied by Martinez-Miranda *et al.*<sup>24</sup> An improvement in the alignment of the liquid crystal with increasing weight percentage of ZnO nanoparticle was observed and a three orders of magnitude enhancement in the current generated was reported.

Supreet *et al.* studied the dispersions of ZnO nanoparticles in the columnar matrix of discotic liquid crystals for the first time.<sup>25</sup> The inclusion of ZnO nanoparticles into the columnar matrix enhances the orientational order in the columnar phase without affecting the two-dimensional hexagonal lattice of the mesophase. The homeotropic alignment in samples was also found to be better with the addition of the nanoparticles. The real ( $\epsilon'$ ) and imaginary parts ( $\epsilon''$ ) of the permittivity increase by a small amount in these dispersions. The order parameter measured using the IR dichroism technique in the face-on geometry (homeotropic alignment) shows an

enhancement for the composite system. The DC conductivity was also found to increase, albeit only by an order of magnitude, on addition of the nanoparticles.

Chen *et al.* reported the preparation of self-assembled ZnO nanoparticles modified with a triphenylene-based discotic liquid crystal ligands (TP-S@ZnO).<sup>26</sup> The bulk heterojunction devices based on P3HT/ZnO film showed a PCE of 0.46% which improves to 0.51% on annealing the sample at 130 °C. The device based on TP-S@ZnO/P3HT showed an improvement with a PCE of 0.70%, which further improves to 0.95% on annealing the sample at 130 °C.

## 5.1.2 Mineral based liquid crystals

### 5.1.2.1 Rod like particles

Buining *et al.*<sup>27</sup> prepared colloidal boehmite rods by hydrothermal treatment of aluminium alkoxide precursors. Colloidal boehmite rods with an average length 100-400nm with aspect ratio varying from 10 to 30 were prepared. Later, these rod like particles were sterically stabilized by grafting a layer of low-molecular-weight poly(isobutene) molecules on their surface.<sup>28</sup> The particles were then dispersed in cyclohexane, the sterically stabilized boehmite rods repel each other as a result of steric hindrance of the grafted polymer chains. As the concentration of these particles increased, the sterically stabilized boehmite rods show a fast isotropic to nematic phase

transition. A second nematic phase emerged in the biphasic dispersion when the same dispersion was aged for several months.

Maeda & Hachisu<sup>29-30</sup> proved by optical microscopy and electron microscopy that in low-salt ( $10^{-4}$  mol l<sup>-1</sup> or less monovalent salt) aqueous suspensions of  $\beta$ -FeO(OH) colloids a biphasic equilibrium is observed between an isotropic and a smectic phase. The length of the rod like particle was 350 nm, and had an aspect ratio of six. The work of Maeda and Hachisu was further explored by Maeda and Maeda. They used atomic force microscopy to investigate the smectic structures of  $\beta$ -FeO(OH)rods.<sup>31-32</sup>

Rod-like silica colloids were synthesized by Kuijk *et al.*<sup>33</sup> These rods were 200 nm in diameter and up to 10  $\mu$ m long. The growth mechanism of these rods involves emulsion droplets inside which silica condensation takes place. At higher concentration, these rods self-assemble into liquid crystalline phases. The silica rods with aspect ratio of five form a multi-phase equilibrium involving an isotropic, nematic, smectic and SmB phase.<sup>34</sup>

Jana *et al.*<sup>35</sup> observed that the high aspect ratio gold nanorods form of a nematic phase at higher concentration. Additionally, nematic like and smectic like structures were formed by drying induced self-assembly have been observed in transmission electron microscopy images.<sup>36-37</sup>

Peng *et al.*<sup>38</sup> showed that shapes of the cadmium selenide nanoparticles could be tuned to vary from a spherical particle to a rod-like one, with aspect ratios as large as 1 to 10 by controlling the growth kinetics. Li *et al.*<sup>39-40</sup> observed a nematic liquid crystal phase in suspensions of CdSe

semiconductor nanorods. Smectic like liquid crystal structures were observed by drying induced self-assembly in transmission electron microscopy images for CdSe nanorods by Li & Alivisatos<sup>41</sup> and for CdSe/CdS heteronanorods by Carbone *et al.*<sup>42</sup>, while Talapin *et al.*<sup>43</sup> took the drying-induced self-assembly method one step further to produce highly luminescent smectic three-dimensional structures of CdSe and CdSe/CdS. More recently, Baranov *et al.*<sup>44</sup> succeeded in producing two-dimensional smectic monolayers of close-packed hexagonally ordered arrays of nanorods directly in solution by tuning the depletion attraction forces between CdSe/CdS nanorods with surfactant micelles.

Dessombz *et al.*<sup>45</sup> synthesized rutile (TiO<sub>2</sub>) nanorods of length 160 nm and diameter 15nm that displayed an isotropic to nematic phase separation in aqueous solution. These liquid crystal suspensions were spin-coated into well-aligned rutile films, the photocatalytic properties of which were examined by monitoring the decomposition of methylene blue under UV light.

#### 5.1.2.2 Plate like particles

Wierenga *et al.*<sup>46</sup> discovered a synthesis route which yields well-formed hexagonal plate-like gibbsite crystals ( $\gamma$ -Al(OH)<sub>3</sub>). These crystals had a diameter of 100 to 200 nm and thickness in between 5 to 15 nm). van der Kooij & Lekkerkerker<sup>47</sup> succeeded in stabilizing these gibbsite platelets by

attaching a layer of low-molecular-weight poly(isobutene) molecules. This novel model system of hard colloidal platelets was observed to phase-separate into an isotropic and a nematic liquid crystalline phase.<sup>47</sup> On increasing the concentration, van der Kooij *et al.*<sup>48</sup> observed that suspensions of these sterically stabilized plate-like gibbsite colloids also display a columnar phase. Gibbsite particles are charged in suspension, these particles interact through double-layer repulsions. The liquid crystalline phase behavior now depends on the ionic strength.<sup>49-51</sup> Decreasing the salt concentration and/or increasing gibbsite concentration, the nematic phase gradually changes to discotic nematic into a columnar nematic phase with stronger side-to-side inter-particle correlations. Kleshchanok *et al.*<sup>52</sup> studied colloidal gibbsite platelets suspended in dimethyl sulphoxide, it failed to show nematic and columnar phase but it formed a layered liquid crystal phase consisting of hexagonally ordered particles, which is Smectic B in nature. The use of dimethyl sulphoxide, a polar aprotic solvent, lead to electrostatic repulsion between platelets, leading to formation of the Smectic B phase.

Brown *et al.*<sup>53-54</sup> synthesized monodisperse plate-like particles of Ni(OH)<sub>2</sub>, they were sterically stabilized by adsorbing a sodium polyacrylate layer on the surface. These plate-like particles of Ni(OH)<sub>2</sub> form a highly ordered phase in a concentrated dispersion, this phase was identified as a columnar phase using neutron scattering.

Hydrotalcite is the layered double hydroxide that contains Mg<sup>2+</sup> and Al<sup>3+</sup>. Colloidal platelets of hydrotalcite having a diameter of 100–200 nm and thickness of 10 nm have been prepared by co-precipitation of magnesium

salts and aluminium salts.<sup>55-57</sup> Different ratios of magnesium to aluminium can change the charge on these particles. Liu *et al.* and Wang *et al.* observed that hydrotalcite suspensions with Mg/Al molar ratios 2 : 1 and 1 : 1 show different liquid crystal phase behaviour. The former shows a nematic phase [69] while, in the latter, a lamellar phase is observed.<sup>58-59</sup>

#### 5.1.2.3 Lath like particles

Vanadium pentoxide ribbons of approximate thickness 1 nm, width 25 nm and persistence length of 300 nm (i.e. the length over which the ribbons are rigid and straight) synthesized by Zocher *et al.* from 0.5 to 0.7 percent volume fraction dispersions display an isotropic–nematic coexistence, which extends into a nematic phase and forms a nematic gel beyond 1.5 per cent volume fraction.

Biaxial nematic mineral liquid crystal is observed for goethite ( $\alpha$ -FeOOH).<sup>58-59</sup> In basic conditions goethite crystallites slowly grow and form approximately rectangular board-like particles, which can subsequently be electrostatically stabilized at pH=3. Samples of different volume fractions underwent an isotropic to nematic phase separation, which through sedimentation and fractionation (over months to years) formed clear isotropic, nematic<sup>60</sup> and smectic<sup>61</sup> phases (at polydispersities above 20% in combination with columnar phases).<sup>62</sup>

## 5.2 Objectives

In the work discussed in previous chapter, we dispersed gold nanorods in supramolecular order of discotic liquid crystal. Here we tried to insert anisotropic CdS nanowires of much higher aspect ratio, this is quite a challenging task, as the ability to self-assemble long nanowires in equally long nanoribbons will need tuning of the functional groups on both CdS nanowires and as well as of discotic liquid crystal. Another challenging task would be to find appropriate solvent and technique to insert nanowires in discotic nanoribbons while they are being grown. Once the composites are obtained it is an equally challenging task to characterize them and study the orientation of nanowires in nanoribbons.

We also wish to explore the lyotropic mesophase behavior shown by CdS nanowires. The last report of semiconducting nanostructures showing lyotropic behavior was explored by allivasatos *et al.* We in this chapter have shown that CdS nanowires of various sizes can self-assemble into interesting supramolecular structures in cyclohexane. We have characterized the self-assembly through polarizing optical microscopy, X-ray diffraction studies and Cryo-SEM. We have provided a model explaining the self-assembly and lyotropic mesophase behavior.

## 5.3 Experimental section

### 5.3.1 Synthesis of 2,3,6,7,10,11-hexakis(hexyloxy)triphenylene

2,3,6,7,10,11-hexakis(hexyloxy)triphenylene (HAT6) was synthesized by oxidative trimerization of 1,2-dihexyloxybenzene with  $\text{MoCl}_5$ .<sup>63</sup> In a typical reaction,  $\text{MoCl}_5$  (0.0051 mol) was added to a solution of 1,2-dihexyloxybenzene (0.005 mol) in 10 ml of dry  $\text{CH}_2\text{Cl}_2$ . The reaction mixture was maintained in an ice bath and stirred for 30 min under anhydrous conditions. Reaction mixture was then poured over cold MeOH (15 ml) and extracted with dichloromethane (4 X 20 ml). The combined extracts were repeatedly washed with water and brine, solvent was removed under vacuum, dried over anhydrous sodium sulfate, and the crude product was purified by column chromatography over silica gel.

### 5.3.2 Synthesis of CdS nanowires

Synthesis of the CdS nanowires were followed by previously reported method by Son *et al.*<sup>64</sup> CdS nanowires were prepared by reaction of  $\text{CdCl}_2(\text{octylamine})$  complex and sulfur-octylamine complex with octylamine as solvent. First  $\text{CdCl}_2$  (1.5 mmol) was complexed with octylamine (10 ml) by aging the mixture at 120 °C for 2 hrs. Sulfur (4.5 mmol) was complexed with octylamine (5ml) to obtain reddish brown solution, Sulfur octylamine complex was injected into  $\text{CdCl}_2(\text{octylamine})$  complex at room temperature, the resultant solution was slowly heated at rate of  $2\text{K min}^{-1}$  to 50 °C and maintained at that temperature for 48 hrs. The obtained product was precipitated out by adding excess ethanol. It was further purified by

repeated centrifugation and washing with ethanol. The product CdS-50 obtained was then dried under vacuum. To prepare CdS nanowires CdS-60 and CdS-70 same procedure was followed, but after Sulfur octylamine complex was injected into CdCl<sub>2</sub>(octylamine) complex at room temperature the mixtures were heated at rate of 2K min<sup>-1</sup> to 60 °C and 70 °C to obtain CdS-60 and CdS-70 respectively.

### **5.3.3 Preparation of nanocomposites.**

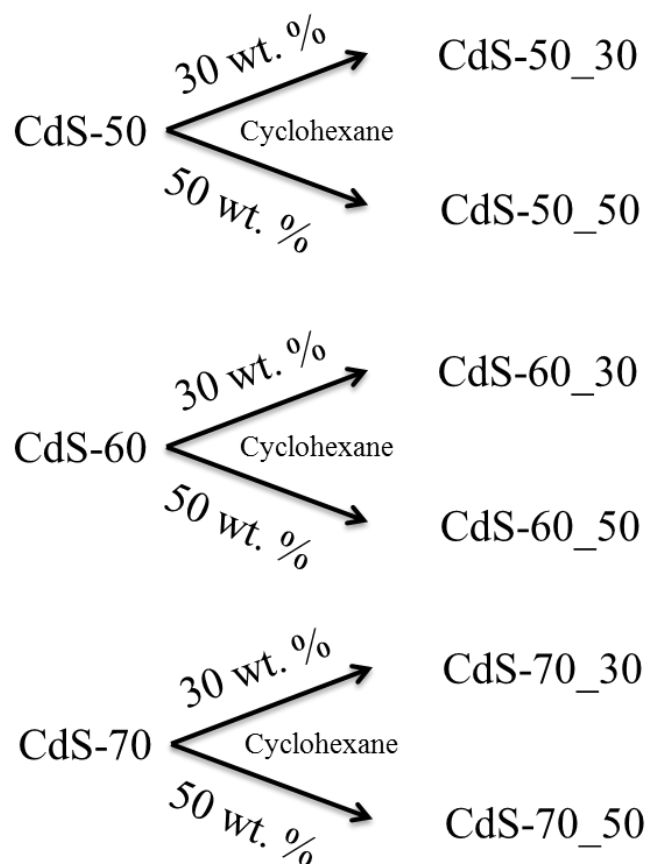
Nanocomposites having weight percentage of 0.5 and 1 of CdS nanowires in HAT6 were prepared by mixing two components in chloroform. For 0.5% CdS-70/HAT6 composite (0.5CdS-70/HAT6), CdS nanowires (0.5 mg) were taken in chloroform (5 mL) and sonicated for 2 hrs. To this solution, triphenylene derivative HAT6 (99.5mg) was added and the mixture was further sonicated for 2 hrs to ensure homogenous dispersion. After that the solvent was removed by evaporation under N<sub>2</sub> flow. Similarly 1% CdS-70/HAT6 composite (1CdS-70/HAT6) was prepared by adding CdS nanowires (1mg) in HAT6 discotic liquid crystal (99mg).

### **5.3.4 Preparation of CdS based lyotropic liquid crystals.**

Cyclohexane was chosen as the solvent that forms lyotropic liquid crystals with CdS nanowires on the basis of trial and error method. Two weight percentages, for each CdS nanowire (CdS-50, CdS-60 and CdS-70) were prepared, 50 weight percentage (50 wt.%) samples were obtained by dissolving 50mg of CdS nanowire in 64 µl of cyclohexane, similarly 30 weight percentage (30 wt.%) samples were obtained by dissolving 30mg of

CdS nanowire in 90  $\mu\text{l}$  of cyclohexane. Thus six samples were prepared (Scheme 1), two samples of CdS-50, 50 wt.% (CdS-50\_50) and 30 wt.% (CdS-50\_30). Two samples of CdS-60, 50 wt.% (CdS-60\_50) and 30 wt.% (CdS-60\_30). Two samples of CdS-70, 50 wt.% (CdS-70\_50) and 30 wt.% (CdS-70\_30).

### Preparation of CdS based lyotropic liquid crystals



**Scheme 1.** Six samples prepared for characterizing lyotropic mesophase of CdS nanowires.

## 5.4 Results and Discussion

The UV-vis absorption spectras of CdS-50, CdS-60 and CdS-70 nanowires is shown in Figure 1. CdS-50 nanowires shows a peak at 377 nm with a shoulder at 380 nm, this double peak is typical of CdS nanowires. This double peak is caused by electron-light hole and electron-heavy hole transitions. These peaks don't change much as long as growth temperature is below 60 °C. At higher temperatures these peaks get red shifted due to increase in thickness, thus CdS-70 nanowires show absorption maxima at 407 nm.<sup>64</sup> All CdS nanowire samples were dispersed in chloroform with the concentration of 0.1 mg/mL.

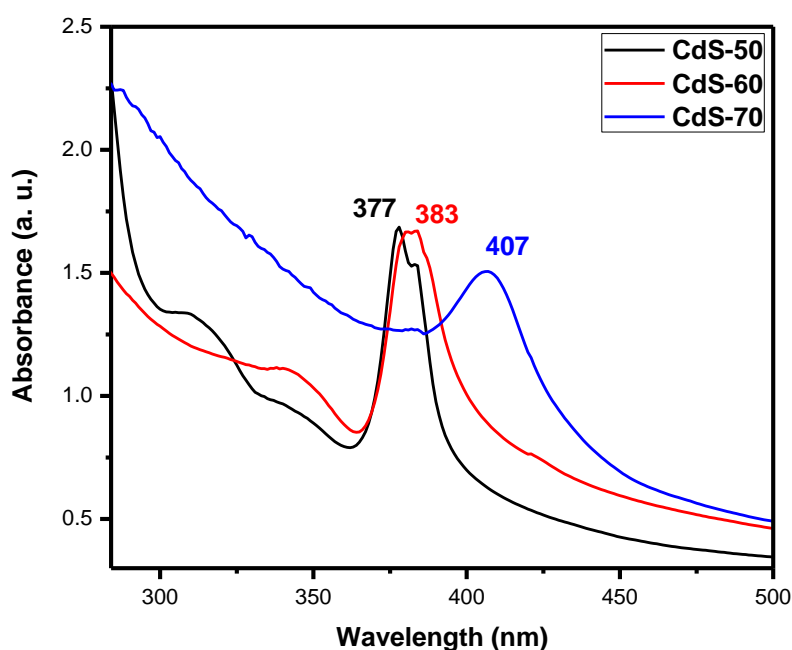


**Figure 1.** (a) UV-vis spectroscopy of CdS-50 (black), of CdS-60 (red) and of CdS-70 (blue).

The crystallographic characterizations of as-prepared CdS nanowires were studied by X-ray powder diffraction (Figure 2). Spectra shows that as prepared CdS-70 consist of the characteristics of bulk hexagonal CdS pattern with diffractive peaks ( $2\theta$ ) at  $25.46^\circ$ ,  $26.80^\circ$  and  $28.78^\circ$  which is also the dominant crystal phase of bulk CdS. All the three broad peaks correspond to (100), (002), and (101) planes matched quiet well with the reported hexagonal wurtzite structure (JCPDS, File No. 41-1049, CdS). The narrow and strong diffraction peak (002), the second strongest peak in bulk hexagonal CdS nanowires indicating a preferential growth along the c-axis in the product. The small angle region of the spectra point towards lamellar ordering of nanowires. CdS-50 and CdS-60 showed similar crystalline structure.

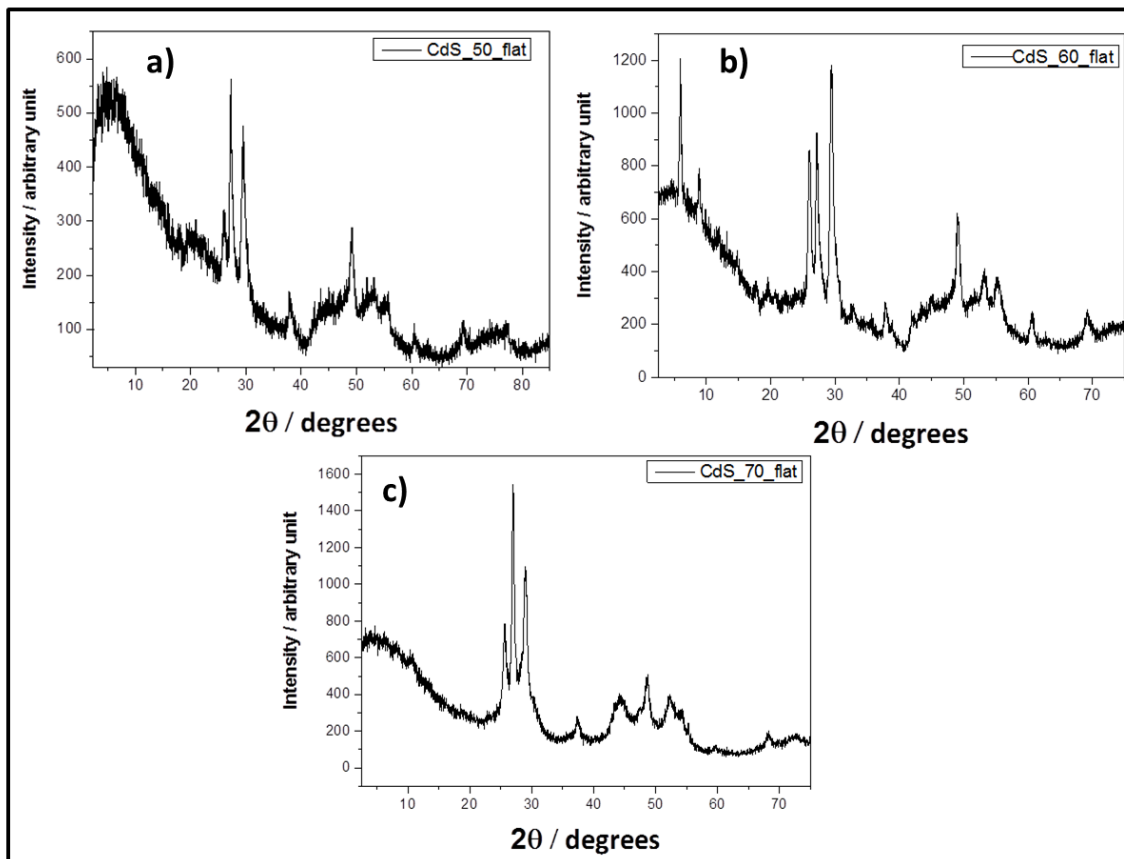


**Figure 2.** XRD pattern of a) CdS-50 nanowires, b) CdS-60 nanowires, c) CdS-70 nanowires.

We acquired high resolution transmission electron microscopy (HR-TEM) images of CdS-70. The samples were dispersed by intense ultra-sonication in chloroform containing very small amount of hexadecylamine and drop casted on copper grids. The Figure 3 shows the HR-TEM images of CdS-50, CdS-60, and CdS-70 nanowires. The CdS-70 nanowires were 1.4-2.1 nm in thickness and 800 nm to 1  $\mu\text{m}$  in length. These nanowires show very high van der Waals attraction between individual nanowires and in the absence of hexadecylamine form aggregates.<sup>64</sup>

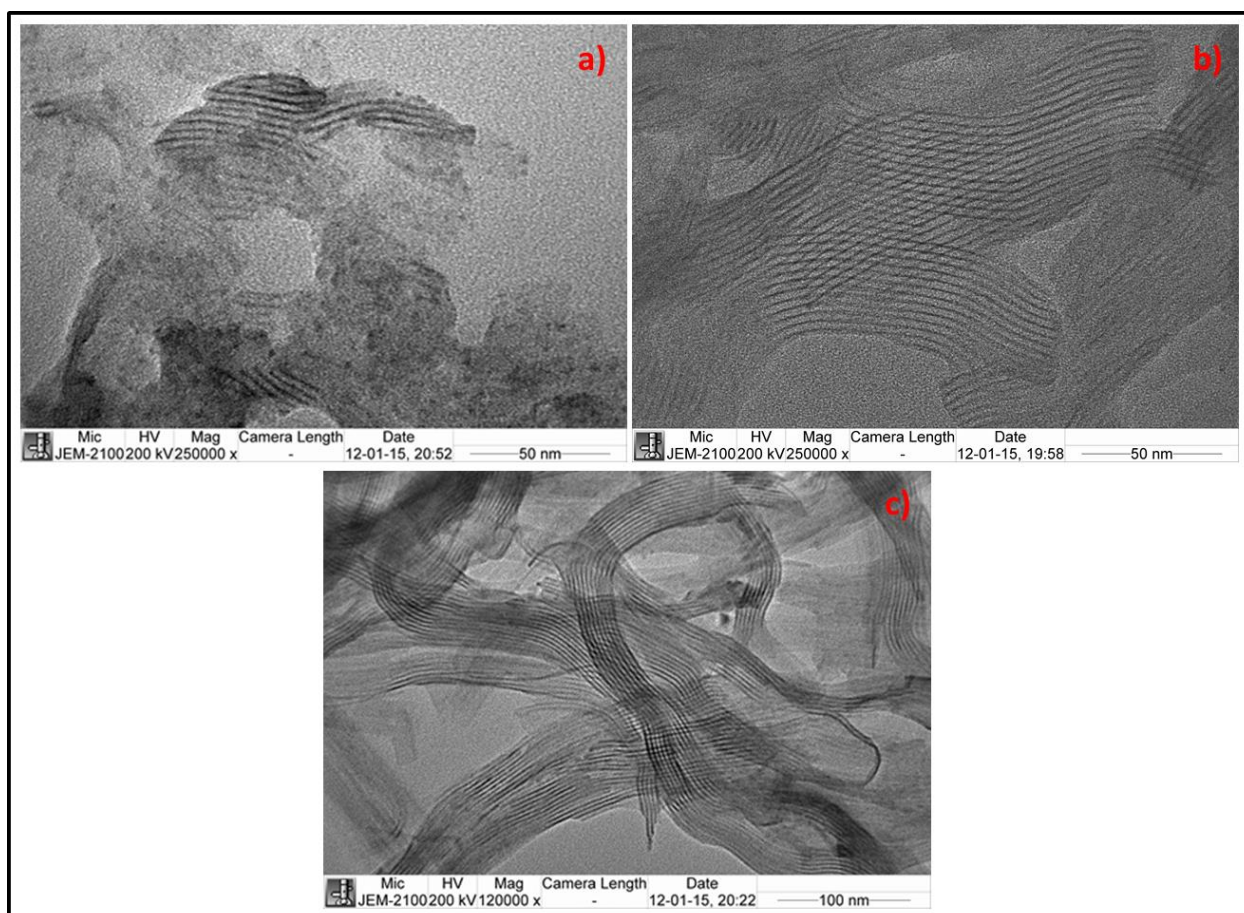


**Figure 3.** HR-TEM of a) CdS-50 nanowires, b) CdS-60 nanowires, c) CdS-70 nanowires.

2,3,6,7,10,11-hexakis(hexyloxy)triphenylene, was characterised using Proton-NMR, POM, X-ray diffraction and DSC studies, compound showed melting transition into mesophase at 70 °C, the mesophase lasted up to 98.8 °C at this temperature it clears to isotropic liquid. The POM images showed the columnar hexagonal texture at 90 °C, this observation of columnar hexagonal phase was further confirmed by XRD analysis. The <sup>1</sup>H NMR (500 MHz; CDCl<sub>3</sub>) shows following signals which are in accordance to that obtained for pure compound δ<sub>H</sub> 7.86 (6H, Ar-H), 4.26 (12H, ArOCH<sub>2</sub>), 1.96 (12H, aliphatic CH<sub>2</sub>), 1.6 (24H, aliphatic CH<sub>2</sub>), 1.42 (12H, aliphatic CH<sub>2</sub>), 0.96 (18H, aliphatic CH<sub>3</sub>).

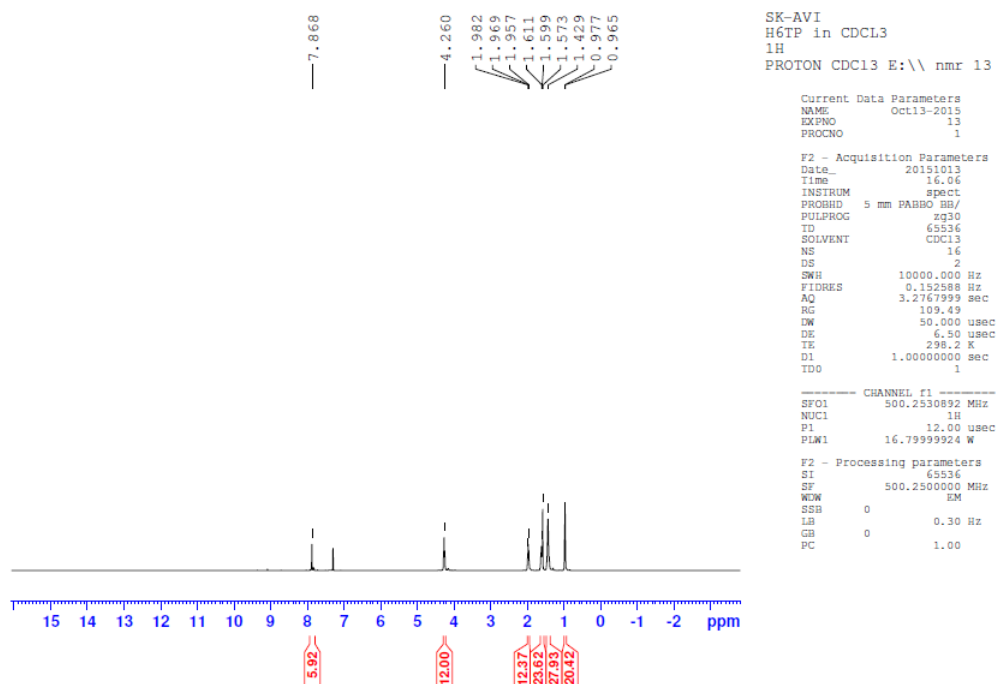


**Figure 4.** <sup>1</sup>H NMR spectra of 2,3,6,7,10,11-hexakis(hexyloxy)triphenylene.

The mesomorphic and thermal behaviour of nanocomposites 0.5CdS-70/HAT6 and 1CdS-70/HAT6 were investigated by polarizing optical microscopy (POM) and differential scanning calorimetry (DSC). Figure 5a, and 5b shows the typical columnar hexagonal textures upon cooling from the isotropic phase for the composites of 0.5CdS-70/HAT6 and 1CdS-70/HAT6, respectively. The textures are similar to the POM texture of pure HAT6 (Figure 5c). POM studies clearly indicate the homogeneous dispersion of semiconductor nanowires in discotic liquid crystal matrix.

The small angle X-ray diffraction pattern were recorded for pure HAT6, 0.5CdS-70/HAT6 and 1CdS-70/HAT6 composites under the same conditions at 85 °C for further characterization of liquid crystalline phase. One dimensional intensity vs  $2\theta$  plot for composites are shown in Figure 5d. It is revealed from the SAXS analysis that there is a small decrease in core-core separation of the composites compared to the pure HAT6. In HAT6 it is 3.63 Å, and in 0.5CdS-70/HAT6 is 3.57 and in 1CdS-70/HAT6 is 3.57 Å. Presence of the nanowires appears to induce a comparatively closer core to core packing. The first two peaks in the small angle region of pure HAT6 and the composites showed a ratio of 1:  $1/\sqrt{3}$ , pointing towards columnar hexagonal ordering in the mesophase which is in line with columnar hexagonal texture observed in the POM of pure HAT6 and composites.

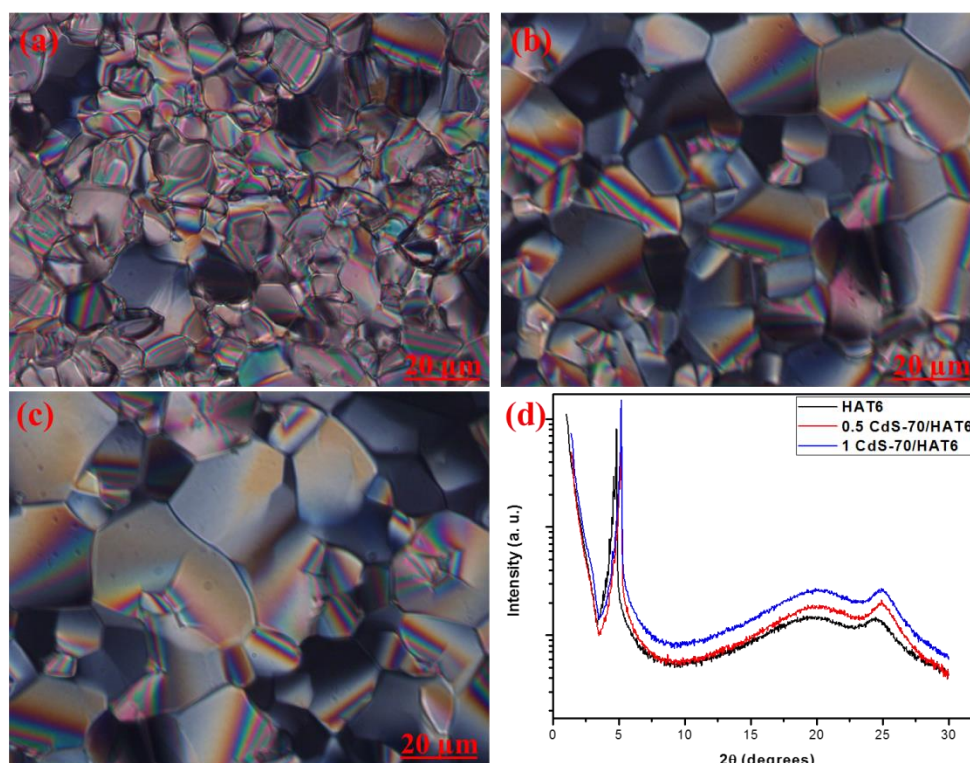


**Figure 5.** Polarizing optical microscope image of the columnar phase of (a) 0.5CdS-70/HAT6, (b) 1CdS-70/HAT6, and (c) HAT6 (at 75 °C crossed polarizers, 50 X magnification). (d) SAXS pattern of composites at 85 °C.

The DSC plots for the HAT6, 0.5CdS-70/HAT6 and 1CdS-70/HAT6 composites recorded at a rate of 10 °C/min (Figure 6). There is no decrease in melting temperature of composites at smaller loading compared to pure HAT6, on higher loading there is a small decrease in melting temperature of 0.38 °C (Table 1). The presence of the CdS nanowires amongst the hexagonal self-assembly of triphenylene appears to induce slight disorder in alkyl chains of discotics at higher loading, and this contributes to decrease in the melting temperatures. The enthalpy of transition also decreases significantly at higher loading, this again can be associated to nanoribbon induced disorder of alkyl chains. There is also an increase in clearing

temperature of the composites compared to HAT6, for 0.5CdS-70/HAT6 it is 1.18 °C and in 1CdS-70/HAT6 is 0.84 °C. The presence of nanowire like structures appears to weakly stabilize the mesophase ordering.

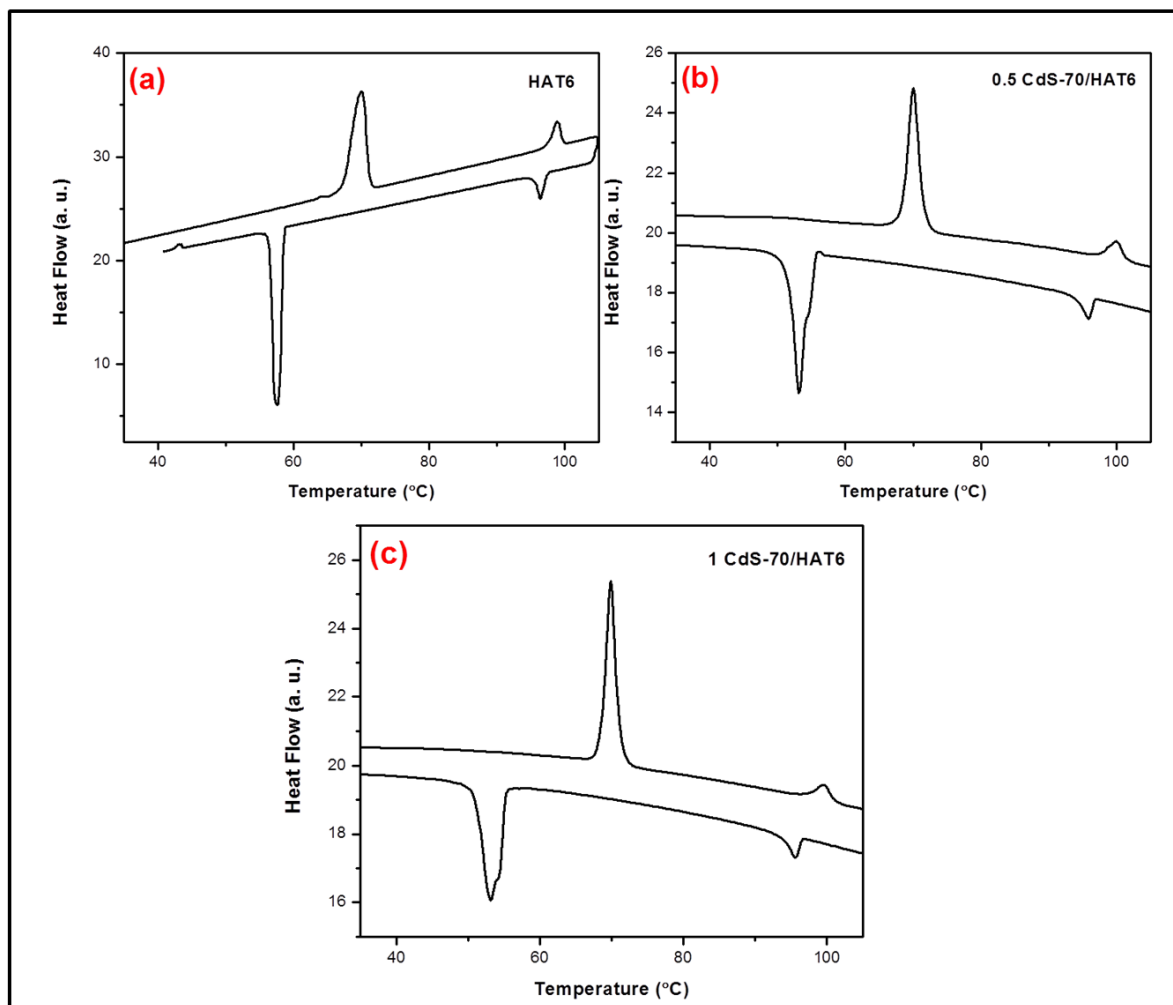
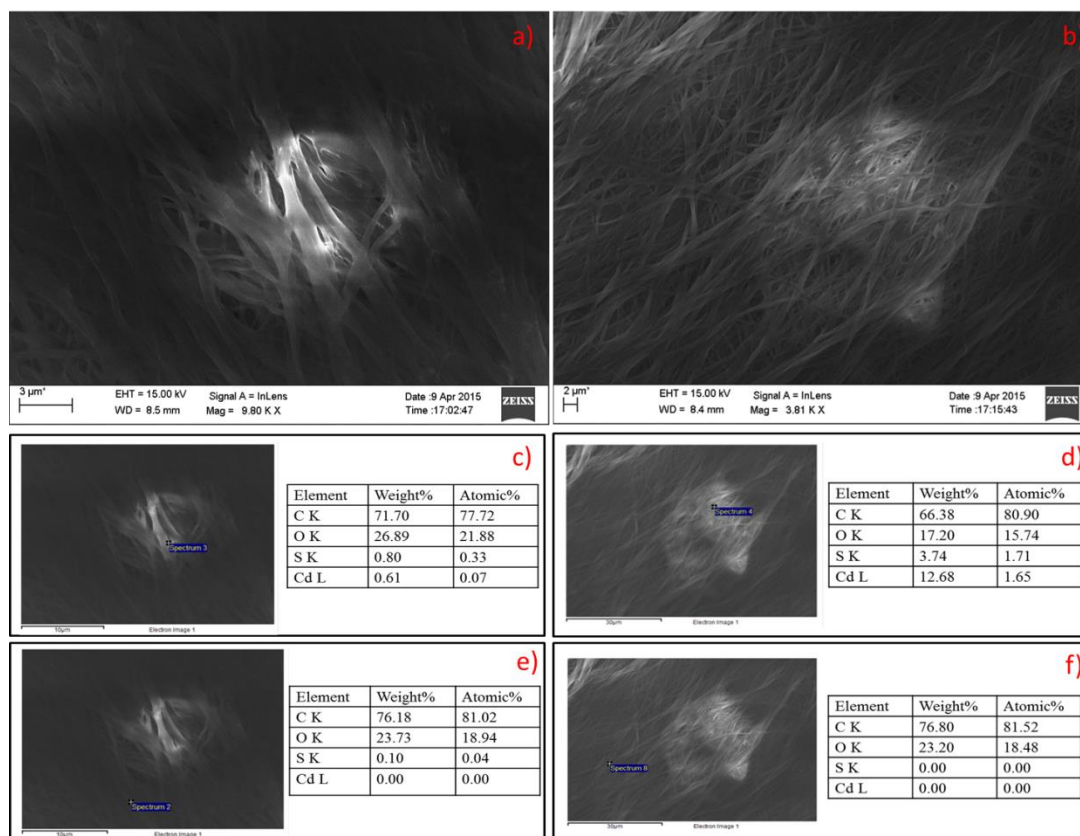


**Figure 6.** DSC images of (a) HAT6, (b) 0.5 CdS-70/HAT6, and (c) 1 CdS-70/HAT6 composites.

**Table 1.** DSC results of HAT6, 0.5CdS-70/HAT6 and 1CdS-70/HAT6. Cr= crystal, Colh = columnar hexagonal mesophase, I = isotropic.

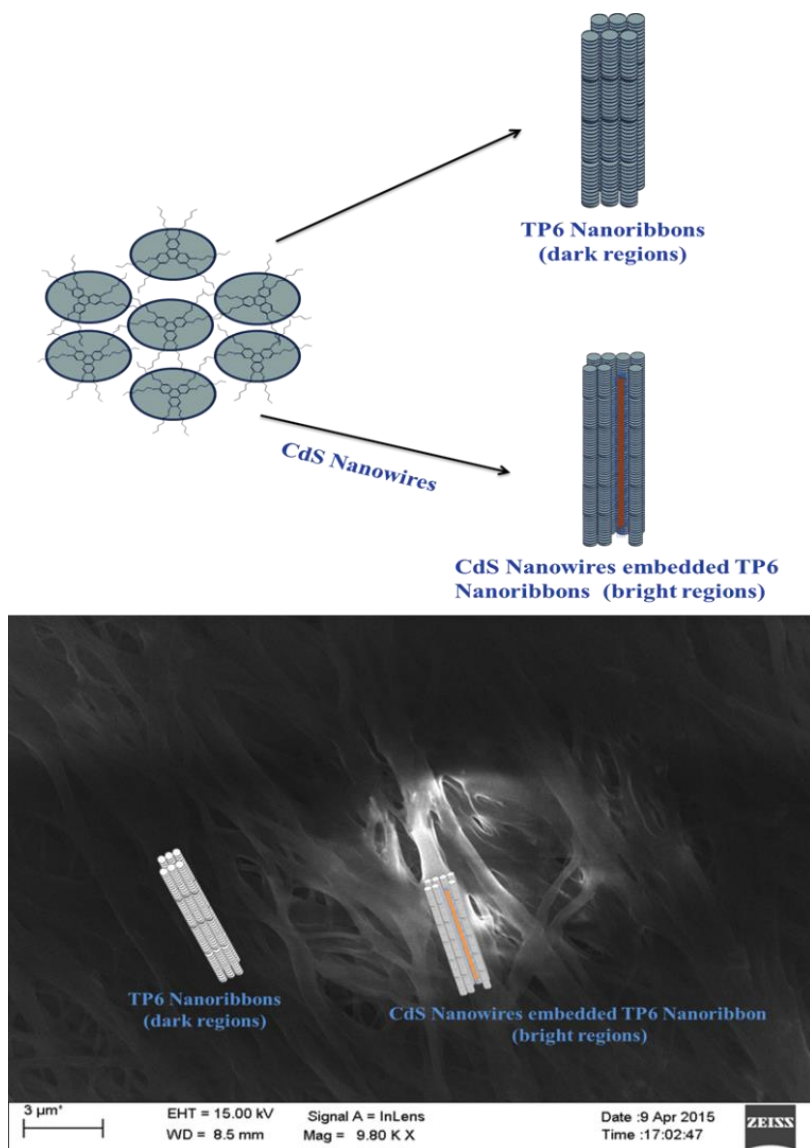
Composites	Thermal Transition (peak values) (°C) / Enthalpy (J/g)	
	Heating Scan	Cooling Scan
HAT6	Cr 70(49) Col <sub>h</sub> 98.79(6.08) I	I 96.39(6.01) Col <sub>h</sub> 57.52(51.42) Cr
0.5CdS- 70/HAT6	Cr 70.09(40.65) Col <sub>h</sub> 99.97(5.82) I	I 95.98(5.07) Col <sub>h</sub> 53.31(42.52) Cr
1CdS- 70/HAT6	Cr 69.62(27.99) Col <sub>h</sub> 99.63(3.19) I	I 95.65(3.18) Col <sub>h</sub> 53.31(27.41) Cr

Figure 7a and 7b shows the SEM images of 0.5CdS-70/HAT6 and 1CdS-70/HAT6 composites, respectively. Interestingly there were bright spots present in certain regions of these nanocomposites. On further EDAX analysis we observed that the bright spots showed presence of Cd and S (Figure 7c, and 7d), and the dark regions were devoid of Cd and S. (Figure 7e, and 7f). The SEM samples were prepared by dissolving composites in a minimal amount of chloroform followed by sonication for 2 hrs. to ensure that the CdS nanowires are not aggregated. To this resultant mixture an excess of polar solvent like ethanol was added. In the presence of this polar solvent the HAT6 start aggregating to form ribbon like structures and in this process the CdS nanowires gets trapped in the HAT6 ribbons.



**Figure 7.** FE-SEM images of (a) 0.5CdS-70/HAT6, (b) 1CdS-70/HAT6 composites, and EDAX analysis of bright regions of (c) 0.5CdS-70/HAT6 and (d) 1CdS-70/HAT6 composites, dark regions of (e) 0.5CdS-70/HAT6 and (f) 1CdS-70/HAT6 composites.

Based on these observations of SEM, EDAX, SAXS and DSC, we have prepared a model shown in Figure 8 of the trapping of nanowires in certain regions. Since the doping percentage in the above studies is very small we observed that CdS nanowires were trapped in only in certain regions of HAT6 nanoribbons. In the given model, we have shown the organization of HAT6 nanoribbons with and without CdS nanowires.



**Figure 8.** Schematic illustration of trapping of CdS nanowires in nanoribbons of triphenylene.

The formation of lyotropic mesophase in CdS nanowires and their ordering was characterized by polarizing optical microscopy, X-ray diffraction studies, and cryo-SEM images. Polarizing optical microscopy images of all the lyotropic mixtures are shown in Figure 9, all the mixtures showed patterns similar to oily streaks which are typical of lamellar phases. These type mesophase textures are absent in samples of weight percentage

25 or below. This behavior is expected, as at higher cyclohexane loading CdS nanowires dissolves in the medium, leading to loss of anisotropic order in these samples. We observed that due to volatile nature of cyclohexane, it was hard to prepare and handle samples of weight percentage larger than 50. The similar lamellar textures are observed at both 50 wt.% as well as 30 wt.%.

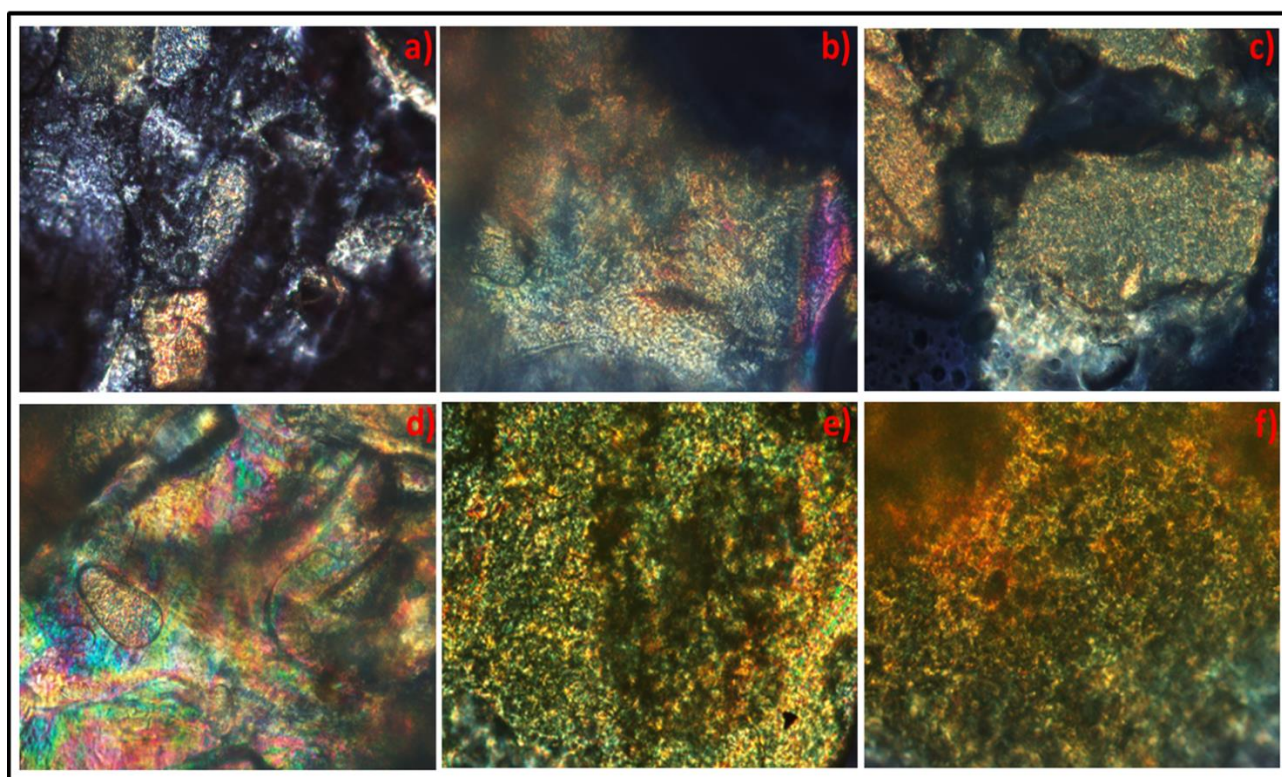


**Figure 9.** Polarized optical microscope images of; a) CdS-50\_30, b) CdS-50\_50, c) CdS-60\_30, d) CdS-60\_50, e) CdS-70\_30, f) CdS-70\_50 (crossed polarizers, 50 X magnification)

X-ray powder diffraction (Figure 10), shows that all samples had first three peaks (small angle region) in a ratio of  $1:1/2:1/3$  pointing towards a lamellar ordering of the CdS nanowires in the lyotropic phase. The small

angle region of the spectra retained the peaks shown by CdS nanowires. This shows the hexagonal wurtzite structure of CdS nanowires remain undisturbed. The region in the spectra between  $15^\circ$  ( $2\theta$ ) and  $22^\circ$  ( $2\theta$ ) shows a very broad peak, this can be attributed to melting of the alkyl chains in the presence of cyclohexane solvent.

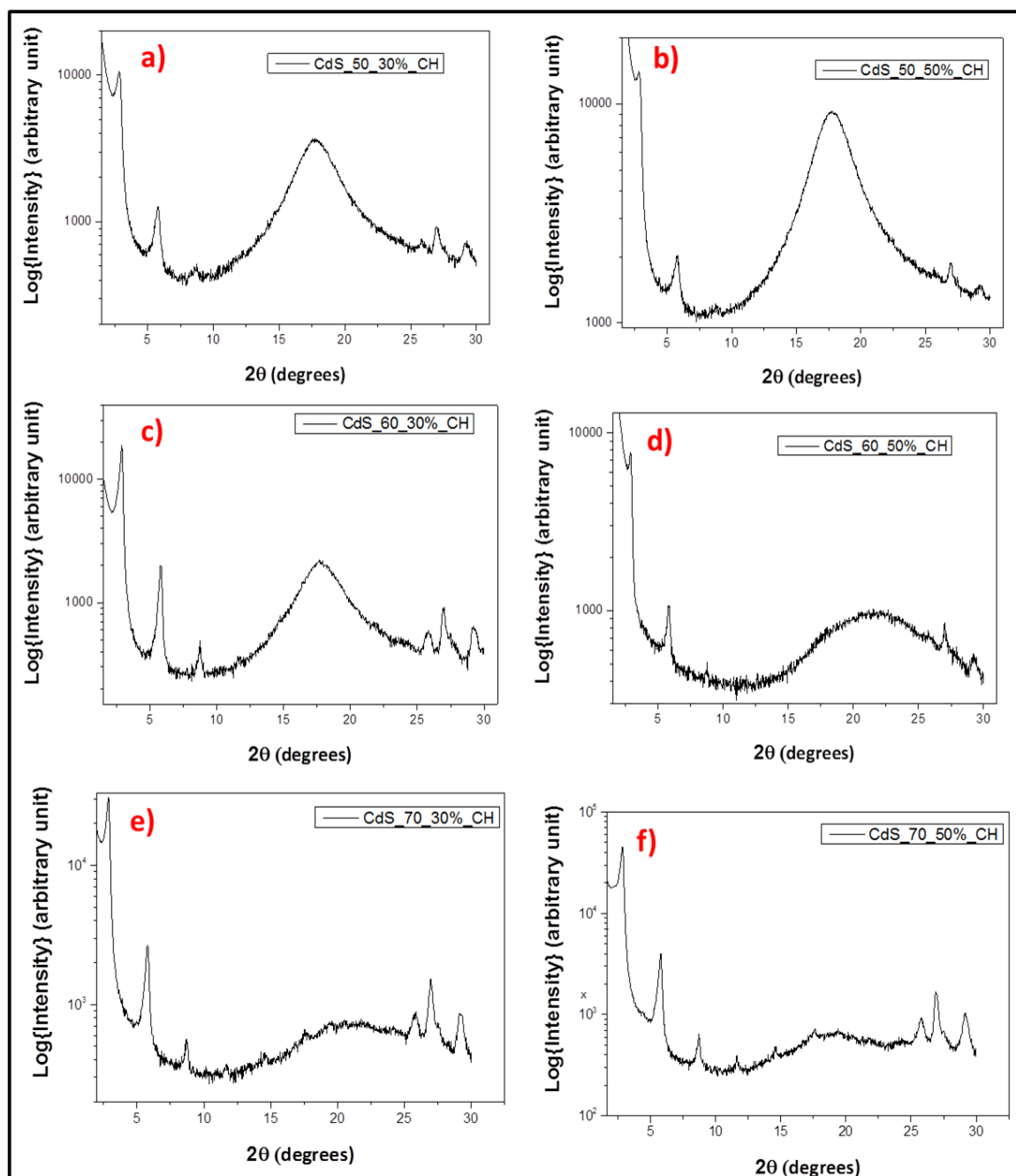


**Figure 10.** SAXS pattern of; a) CdS-50\_30, b) CdS-50\_50, c) CdS-60\_30, d) CdS-60\_50, e) CdS-70\_30, and f) CdS-70\_50.

The cryo-SEM images (Figure 11) of CdS-50\_30 show a bundling of nanowires into small rod like clusters. On increasing their concentration in CdS-50\_50, we observe that the clusters arrange in highly ordered structures. The sample CdS-60\_30 also shows aggregation of nanowires; here the bundles are much longer compared to CdS-50\_30 due to the fact that CdS-60 samples are longer. CdS-60\_50 shows that bundles are much thicker as the concentration of nanowires are higher. CdS-70\_30 shows a ribbon like intercalated structure by coming together of many wires their length spanning more than 1 micron, CdS-70\_50 due to the higher loading, form a rope like structure spanning lengths of more than 1 micron. Cyclohexane in all the cases acts as glue bringing together many molecular wires to form very interesting supramolecular structures. These supramolecular structures are arranged in an ordered assemblies spanning over several 100 nanometers.

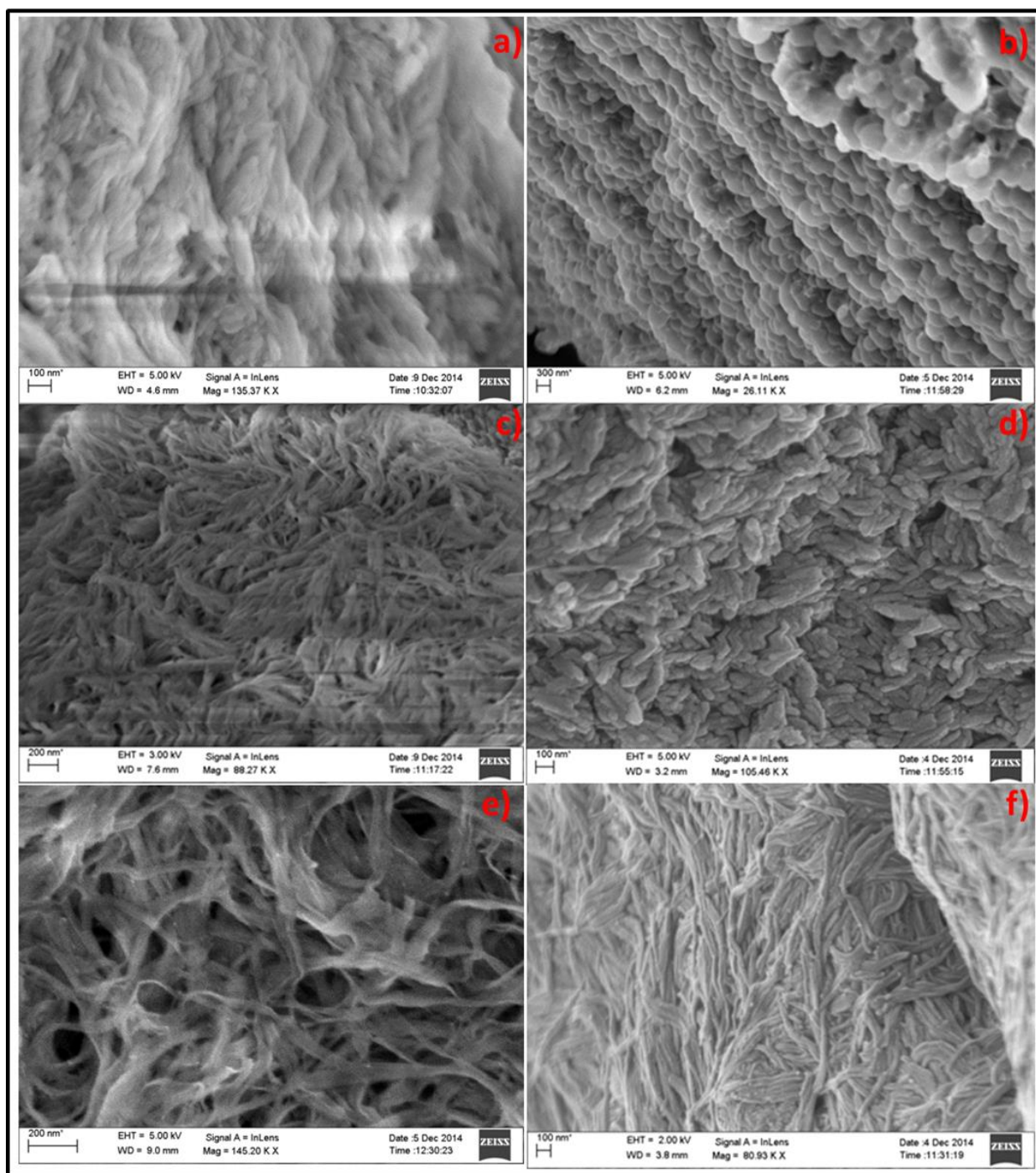


**Figure 11.** Cryo-SEM images of; a) CdS-50\_30, b) CdS-50\_50, c) CdS-60\_30, d) CdS-60\_50, e) CdS-70\_30, and f) CdS-70\_50.

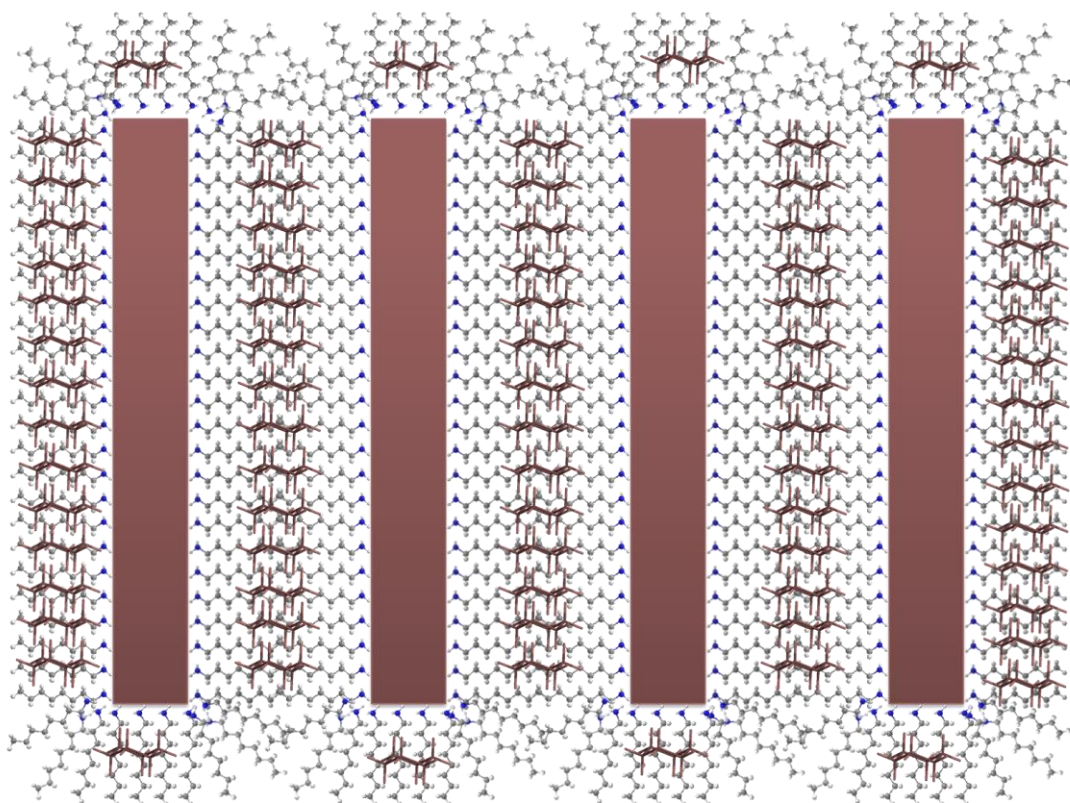


**Figure 12.** Model describing the ordering of CdS nanowires in lyotropic mesophase, the space between nanowires which contains octylamine alkyl chains are solvated by cyclohexane, leading to formation of the mesophase.

Based on the polarizing optical microscopy images, X-ray diffraction studies and cryo-SEM images analysis we have prepared a model in which CdS nanowires are arranged in lamellar fashion. The octylamine alkyl chains coming out of CdS nanowires are solvated by cyclohexane (Figure 12).

## 5.4 Conclusion

In conclusion, we have observed the dispersion of CdS nanowires in discotic liquid crystals. The POM, DSC and SAXS studies reveals that the doping of CdS nanowires into discotic liquid crystals does not disturb the nature of mesophase with different concentration variations on the length scale but minor shift in the transition temperature is observed. These hybrids of two different class of semiconductors makes themselves a potential candidate for devices like thin film transistors, LED's, and organic solar cell.

We have also shown that CdS nanowires of various lengths form a lyotropic liquid crystalline phase in cyclohexane, which show a lamellar ordering. We have characterized the mesophase using POM, XRD and Cryo-SEM analysis and observed that these CdS nanowires aggregate in presence of cyclohexane to form rod like (Cds-50 and CdS-60) to rope like (CdS-70) supramolecular structures.

## 5.5 References

1. Dai, H.; Wong, E. W.; Lu, Y. Z.; Fan, S.; Lieber, C. M., Synthesis and Characterization of Carbide Nanorods. *Nature* 1995, 375, 769 - 772.
2. Han, W.; Fan, S.; Li, Q.; Hu, Y., Synthesis of Gallium Nitride Nanorods through a Carbon Nanotube-Confined Reaction. *Science* 1997, 277, 1287.
3. Alivisatos, A.P., Semiconductor Clusters, Nanocrystals, and Quantum Dots. *Science* 1996, 271, 5221.
4. Morales, A. M.; Lieber, C. M., A Laser Ablation Method for the Synthesis of Crystalline Semiconductor Nanowires. *Science* 1998, 279, 208-211.
5. Saito, S., Carbon Nanotubes for Next-Generation Electronics Devices. *Science* 1997, 278, 77.
6. Suenaga, K.; Colliex, C.; Demoncey, N.; Loiseau, A., Synthesis of Nanoparticles and Nanotubes with Well-Separated Layers of Boron Nitride and Carbon. *Science* 1997, 278, 653.
7. Bera, D.; Qian, L.; Tseng, T. K.; Holloway, P. H., Quantum Dots and Their Multimodal Applications: A Review. *Materials* 2010, 3(4), 2260-2345.

8. Michalet, X.; Pinaud, F. F.; Bentolila, L. A.; Tsay, J. M.; Doose, S., Quantum Dots for Live Cells, in Vivo Imaging, and Diagnostics. *science* 2005, 307, 538.
9. Semonin, O. E.; Luther, J. M.; Beard, M. C., Quantum Dots for Next-Generation Photovoltaics. *Materials Today* 2012, 15, 508.
10. Nag, B. R., *Physics of Quantum Well Devices*. 2002.
11. Ruyter, A.; O'Mahoney, H., *Quantum Wells Theory, Fabrication and Applications*. Nova Science Publishers, 2009.
12. Cushing, B. L.; Kolesnichenko, V. L.; O'Connor, C. J., Recent Advances in the Liquid-Phase Syntheses of Inorganic Nanoparticles. *Chem. Rev.* 2004, 104, 3893–3946.
13. Murray, C. B.; Norris, D. J.; Bawendi, M. G., Synthesis and Characterization of Nearly Monodisperse Cde (E= Sulfur, Selenium, Tellurium) Semiconductor Nanocrystallites. *J. Am. Chem. Soc.*, 1993, 115 (19), pp 8706–8715.
14. Rao, C. N. R.; Vivekchand, S. R. C.; Biswas, K., Synthesis of Inorganic Nanomaterials. *Dalton Trans.*, 2007, 3728-3749.
15. Karanikolos, G. N.; Alexandridis, P., Block Copolymer-Templated Synthesis and Organization of Semiconductor Nanocrystals. *Macromolecular Symposia* 2010, 289, 43.

16. Mirzaei, J.; Reznikov, M.; Hegmann, T., Quantum Dots as Liquid Crystal Dopants. *J. Mater. Chem.*, 2012, 22, 22350-22365.
17. Kumar, S.; Sagar, L. K., Cdse Quantum Dots in a Columnar Matrix. *Chem. Commun.*, 2011, 47, 12182-12184.
18. Özgür, Ü.; Alivov, Y. I.; Liu, C.; Teke, A., A Comprehensive Review of Zno Materials and Devices. *J. Appl. Phys.* 2005, 98, 041301.
19. Gomez, J. L.; Tigli, O., Zinc Oxide Nanostructures: From Growth to Application. *Journal of Materials Science* 2013, 48, 612.
20. Jiang, H.; Toshima, N., Low Driving Voltage of a Liquid Crystal Device Fabricated from 4'-Pentyl-4-Biphenylcarbonitrile Doped with Environmentally Friendly Zno Nanoparticles. *Chemistry Letters* 2009, 38, 566.
21. Joshi, T.; Kumar, A.; Prakash, J.; Biradar, A. M., Low Power Operation of Ferroelectric Liquid Crystal System Dispersed with Zinc Oxide Nanoparticles. *Appl. Phys. Lett.* 2010, 96, 253109.
22. Li, L. S.; Huang, J. Y., Tailoring Switching Properties of Dipolar Species in Ferroelectric Liquid Crystal with Zno Nanoparticles. *Journal of Physics D: Applied Physics* 2009, 42, 12.
23. Huang, J. Y.; Li, L. S.; Chen, M. C., Probing Molecular Binding Effect from Zinc Oxide Nanocrystal Doping in Surface-Stabilized Ferroelectric Liquid Crystal with Two-Dimensional Infrared Correlation Technique. *J. Phys. Chem. C* 2008, 112 (14), pp 5410–5415.

24. Martínez-Miranda, L. J.; Traister, K. M., Liquid Crystal-Zno Nanoparticle Photovoltaics: Role of Nanoparticles in Ordering the Liquid Crystal. *Appl. Phys. Lett.* 2010, 97, 223301.
25. Supreet; Kumar, S.; Raina, K. K.; Pratibha, R., Enhanced Stability of the Columnar Matrix in a Discotic Liquid Crystal by Insertion of Zno Nanoparticles. *Liquid Crystals* 2013, 40, 228.
26. Chen, X.; Chen, L.; Chen, Y., Self-Assembly of Discotic Liquid Crystal Decorated Zno Nanoparticles for Efficient Hybrid Solar Cells. *RSC Adv.* 2014, 4, 3627-3632.
27. Buining, P. A.; Pathmamanoharan, C., Preparation of Colloidal Boehmite Needles by Hydrothermal Treatment of Aluminum Alkoxide Precursors. *Journal of the American Ceramic Society*, 1991, 74, 1303.
28. Buining, P. A.; Lekkerkerker, H. N. W., Isotropic-Nematic Phase Separation of a Dispersion of Organophilic Boehmite Rods. *J. Phys. Chem.* 1993, 97 (44), pp 11510–11516.
29. Maeda, Y.; Hachisu, S., Structure of Schiller Layers in B-Feooh Sols: Observation by Scanning Electron Microscope. *Colloids and surfaces* 1983, 7, 357.
30. Maeda, Y.; Hachisu, S., Schiller Layers in B-Ferric Oxyhydroxide Sol as an Order—Disorder Phase Separating System. *Colloids and Surfaces* 1983, 6, 1-16.

31. Maeda, H.; Maeda, Y., Atomic Force Microscopy Studies for Investigating the Smectic Structures of Colloidal Crystals of B-Feooh. *Langmuir* 1996, 12 (6), pp 1446–1452.
32. Maeda, H.; Maeda, Y., An Atomic Force Microscopy Study of Surface Structures of Colloidal B-Feooh Particles Forming Smectic Layers. *Nano Letters* 2002, 2 (10), pp 1073–1077.
33. Kuijk, A.; van Blaaderen, A.; Imhof, A., Synthesis of Monodisperse, Rodlike Silica Colloids with Tunable Aspect Ratio. *J. Am. Chem. Soc.*, 2011, 133 (8), pp 2346–2349.
34. Kuijk, A., Fluorescent Colloidal Silica Rods-Synthesis and Phase Behavior. 2012.
35. Jana, N. R.; Gearheart, L. A.; Obare, S. O.; Johnson, C. J., Liquid Crystalline Assemblies of Ordered Gold Nanorods. *J. Mater. Chem.* 2002,12, 2909-2912.
36. Nikoobakht, B.; Wang, Z. L., Self-Assembly of Gold Nanorods. *J. Phys. Chem. B* 2000, 104 (36), pp 8635–8640.
37. Sharma, V.; Park, K.; Srinivasarao, M., Colloidal Dispersion of Gold Nanorods: Historical Background, Optical Properties, Seed-Mediated Synthesis, Shape Separation and Self-Assembly. *Materials Science and Engineering: R: Reports* 2009, 65, 1-38.
38. Peng, X.; Manna, L.; Yang, W.; Wickham, J.; Scher, E., Shape Control of Cdse Nanocrystals. *Nature* 2000, 404, 59-61.

39. Li, L.; Walda, J.; Manna, L.; Alivisatos, A. P., Semiconductor Nanorod Liquid Crystals. *Nano Letters* 2002, 2 (6), pp 557–560.
40. Li, L.; Marjanska, M.; Park, G. H. J.; Pines, A., Isotropic-Liquid Crystalline Phase Diagram of a Cdse Nanorod Solution. *Journal of Chemical Physics* 2004, 120, 1149.
41. Li, L.; Alivisatos, A. P., Semiconductor Nanorod Liquid Crystals and Their Assembly on a Substrate. *Adv. Mater.* 2003, 15, 408.
42. Carbone, L.; Nobile, C.; Giorgi, D. M.; Sala, F. D., Synthesis and Micrometer-Scale Assembly of Colloidal Cdse/Cds Nanorods Prepared by a Seeded Growth Approach. *Nano Lett.*, 2007, 7 (10), pp 2942–2950.
43. Talapin, D. V.; Shevchenko, E. V.; Murray, C. B., Cdse and Cdse/Cds Nanorod Solids. *J. Am. Chem. Soc.*, 2004, 126 (40), pp 12984–12988.
44. Baranov, D.; Fiore, A.; van Huis, M.; Giannini, C., Assembly of Colloidal Semiconductor Nanorods in Solution by Depletion Attraction. *Nano Lett.*, 2010, 10 (2), pp 743–749.
45. Dessombz, A.; Chiche, D.; Davidson, P., Design of Liquid-Crystalline Aqueous Suspensions of Rutile Nanorods: Evidence of Anisotropic Photocatalytic Properties. *J. Am. Chem. Soc.*, 2007, 129 (18), pp 5904–5909.
46. Wierenga, A. M.; Lenstra, T. A. J.; Philipse, A. P., Aqueous Dispersions of Colloidal Gibbsite Platelets: Synthesis, Characterisation and

Intrinsic Viscosity Measurements. *Colloids and Surfaces A: Physicochemical and Engineering Aspects*, 1998, 134, 359.

47. van der Kooij, F. M., Formation of Nematic Liquid Crystals in Suspensions of Hard Colloidal Platelets. *J. Phys. Chem. B*, 1998, 102 (40), pp 7829–7832.

48. van der Kooij, F. M.; Kassapidou, K.; Lekkerkerker, H. N. W., Liquid Crystal Phase Transitions in Suspensions of Polydisperse Plate-Like Particles. *Nature* 2000, 406, 868.

49. Mourad, M. C. D.; Byelov, D. V.; Petukhov, A. V., Structure of the Repulsive Gel/Glass in Suspensions of Charged Colloidal Platelets. *J. Phys. Chem. B*, 2009, 113 (34), pp 11604–11613.

50. Mourad, M. C. D.; Byelov, D. V.; Petukhov, A. V., Sol– Gel Transitions and Liquid Crystal Phase Transitions in Concentrated Aqueous Suspensions of Colloidal Gibbsite Platelets. *J. Phys. Chem. B*, 2009, 113 (34), pp 11604–11613.

51. van der Beek, D.; Lekkerkerker, H. N. W., Liquid Crystal Phases of Charged Colloidal Platelets. *Langmuir*, 2004, 20 (20), pp 8582–8586.

52. Kleshchanok, D.; Holmqvist, P.; Meijer, J. M., Lyotropic Smectic B Phase Formed in Suspensions of Charged Colloidal Platelets. *J. Am. Chem. Soc.*, 2012, 134 (13), pp 5985–5990.

53. Brown, A. B. D.; Clarke, S. M.; Rennie, A. R., Ordered Phase of Platelike Particles in Concentrated Dispersions. *Langmuir*, 1998, 14 (11), pp 3129–3132.

54. Brown, A. B. D.; Ferrero, C.; Narayanan, T., Phase Separation and Structure in a Concentrated Colloidal Dispersion of Uniform Plates. *The European Physical Journal B - Condensed Matter and Complex Systems*, 1999, Volume 11, Issue 3, pp 481-489.

55. Hickey, L.; Klopogge, J. T.; Frost, R. L., The Effects of Various Hydrothermal Treatments on Magnesium-Aluminium Hydrotalcites. *Journal of Materials Science* 2000, 35, 4347.

56. Lagaly, G.; Mecking, O.; Penner, D., Colloidal Magnesium Aluminum Hydroxide and Heterocoagulation with a Clay Mineral. I. Properties of Colloidal Magnesium Aluminum Hydroxide. *Colloid and Polymer Science* 2001, 279, 1090.

57. Vaccari, A., Preparation and Catalytic Properties of Cationic and Anionic Clays. *Catalysis Today* 1998.

58. Liu, S.; Zhang, J.; Wang, N.; Liu, W.; Zhang, C., Liquid-Crystalline Phases of Colloidal Dispersions of Layered Double Hydroxides. *Chem. Mater.*, 2003, 15 (17), pp 3240–3241.

59. Wang, N.; Liu, S.; Zhang, J.; Wu, Z.; Chen, J.; Sun, D., Lamellar Phase in Colloidal Suspensions of Positively Charged Ldhs Platelets. *Soft Matter*, 2005,1, 428-430.

60. Lemaire, B. J.; Davidson, P.; Ferré, J.; Jamet, J. P.; Panine, P., Outstanding Magnetic Properties of Nematic Suspensions of Goethite (A-Feooh) Nanorods. *Phys. Rev. Lett.* 2002,88, 125507.
61. Vroege, G. J.; Thies-Weesie, D. M., Smectic Liquid-Crystalline Order in Suspensions of Highly Polydisperse Goethite Nanorods. *Adv. Mater.* 2006, 18, 2565–2568.
62. den Pol, V. E.; Thies-Weesie, D. M. E., Influence of Polydispersity on the Phase Behavior of Colloidal Goethite. *J. Chem. Phys.* 2008,129, 164715.
63. Kumar, S.; Manickam, M., Oxidative Trimerization of O-Dialkoxybenzenes Tohexaalkoxytriphenylenes: Molybdenum (V) Chloride as a Novel Reagent. *Chem. Commun.*, 1997, 1615-1666.
64. Yang, J.; Choi, M. K.; Kim, J.; Yu, J. H.; Joo, J.; Hyeon, T., Dimension Controlled Synthesis of Cds Nanocrystals: From 0d Quantum Dots to 2d Nanoplates. *Small* 2012, 8, 2394.

# Chapter 6

---

## 6.1 Summary

In this chapter, we summarize some the important results and conclusions derived from this thesis work, which deals with '**Synthesis, Characterization and Properties of Some Novel Discotic Nanocomposites**'. Broadly, the research work that has been reported in this thesis can be classified as follows:

Chapter 1 is an introductory chapter and mainly deals with the classification of liquid crystals, and discussion about columnar liquid crystals. Phases shown by the discotic molecules have been discussed, there is also discussions about structure discotic mesogens and chemistry involved in synthesis of these molecules. Techniques used for characterization of columnar mesophase have been dealt in short. The potential of columnar molecules in applications like organic electronics are discussed. This chapter also contains discussion about lyotropic liquid crystals. There is a brief of discussion about nanomaterials, which are later elaborated in specific discussions in following chapters.

Chapter 2 describes the mutual self-assembly of f-graphene and anthraquinone based discotic liquid crystal. We have shown that f-graphene can be efficiently dispersed in the supramolecular order of DLCs. These composites show higher transition temperatures compared to pure DLC due to enhanced ordering of discotics on the surface of reduced graphene oxide owing to strong pi-pi attraction. Cryo-SEM images of the composites show

us that discotics and graphene are mutually ordered into sandwich like structures. We have also found that the composites show higher conductivity compared to pure DLC. The f-graphene fillers act as bridges across grain boundaries resulting in efficient charge transport. The creation of sandwich like self-assembly with DLCs may widen the applicability of these graphene derivatives in materials science. Ordered structures can be simply achieved through self-organization of a variety of interacting molecular components. The creation of such molecular buildings via self-assembly of LCs may lead to the induction of dynamically functional properties such as facile charge and energy migration in self-organized systems. The construction of such ordered molecular architectures is essential for the realization of next-generation electronic devices.

In Chapter 3 we have studied the self-assembly of thiolated graphene oxide in supra-molecular structures of discotic liquid crystals. These supramolecular nanocomposites were characterized using SAXS, POM, DSC and Cryo-SEM. The observation reveals that thiolated graphene oxide due to its functionalization on the surface induces destabilization in columnar mesophase. Unlike the results obtained previous chapter (edge functionalized graphene, which showed stabilizing behaviour) the surface functionalized graphene oxide, causes a steric hindrance for discotic self-assembly onto graphene oxide surface.

Second part of this chapter explored self-assembly of thiolated graphene oxide onto gold surface. The formation of self-assembled layers on the gold surface was confirmed by electrochemical, XPS, SEM, grazing angle IR studies. All the studies confirmed presence of layered graphene oxide sheets

on the gold strip. This monolayer film acting as blanket on the gold surface has potential application in various devices applications such as sensors, organic electronic devices etc.

Chapter 4 discusses the insertion of gold nanorods in supramolecular structures of discotics. The self-assembly of gold nanorods in discotics was probed using SAXS, POM, DSC, conductivity, SEM and STEM studies. We have shown that hexpentyloxytriphenylene primarily self-assembles into hexagonal structures, which on proper solution processing can be made to grow into ribbon like secondary structures. During the growth, these supramolecular structures can trap the gold nanorods present in the solution. These nanocomposites show enhanced conductivity owing to insertion of nanorods in ribbon like structures.

First part of Chapter 5 discusses incorporation of Cadmium sulphide nanowires in the supramolecular order of discotic liquid crystal. This was studied by polarized optical microscopy, differential scanning calorimetry, X-ray diffraction, FE-SEM and EDAX. Results indicate that CdS nanowires were trapped in ribbon like structures of hexahexyloxy-triphenylene discotic liquid crystals. The doping of CdS nanowires into discotic liquid crystals does not disturb the nature of mesophase with different concentration variations on the length scale but minor shift in the transition temperature is observed. This hybrid of two different classes of semiconductors makes themselves a potential candidate for devices like thin film transistors, LED's, and organic solar cells.

Second part of this chapter discusses formation of lyotropic mesophase in inorganic CdS based nanowires in cyclohexane. We have also shown that CdS nanowires of various lengths form a lyotropic liquid crystalline phase, which show a lamellar ordering. We have characterized the mesophase using POM, XRD and Cryo-SEM analysis and observed that these CdS nanowires aggregate in presence of cyclohexane to form rod like (CdS-50 and CdS-60) to rope like (CdS-70) supramolecular structures.

Overall in this thesis we have tried to functionalize one-dimensional and two-dimensional nanomaterials so that they self-assemble in supramolecular order of columnar liquid crystal, we have characterized the influence of these dopants on mesophase and physical properties of columnar liquid crystal. We have also explored the self-assembly of thiolated graphene oxide onto gold electrodes, and characterized the thiolated graphene oxide modified gold electrodes. We have shown that CdS nanowires form lyotropic lamellar phase, and have probed the supramolecular organization of these aggregates.

Some of the findings of this thesis have been published/communicated in the following international journals.

## 6.2 Publications

1) Gold Nanorods Embedded Discotic Nanoribbons,  
Bangalore Shivanadareddy Avinash, V Lakshminarayanan, Sandeep Kumar,  
JK Vij,  
Chemical Communications 49 (10), 978-980, 2013.

2) Mutually ordered self-assembly of discotic liquid crystal-graphene  
nanocomposites,  
Avinash B Shivanandareddy, Suvratha Krishnamurthy, V  
Lakshminarayanan, Sandeep Kumar,  
Chemical Communications 50 (6), 710-712, 2014.

3) Self-assembly of thiolated graphene oxide onto gold surface and in the  
supramolecular order of discotic liquid crystals,  
Avinash B Shivanandareddy, M Kumar, V Lakshminarayanan, Sandeep  
Kumar,  
RSC Advances, 5, 47692-47700, 2015.

4) Photoconductivity of doped hexa-alkoxy triphenylene nano composite  
structures,

C Kavitha, Avinash B Shivanandareddy, Sandeep Kumar, V

Lakshminarayanan,

Materials Chemistry and Physics 133 (2), 635-641, 2012.

5) Triphenylene-based discotic liquid crystals: recent advances, Santanu K

Pal, Shilpa Setia, Avinash B Shivanandareddy, Sandeep Kumar, Liquid

Crystals 40 (12), 1769-1816, 2013.

6) Lyotropic liquid crystals of CdS nanoribbons

Manuscript under preparation.

7) Mutual self-assembly of inorganic CdS and organic triphenylene

nanoribbons.

Manuscript under preparation.